Univeristé de Montréal

Molecular Tectonics: Functional Materials for Crystal Engineering

par

Michael Lautman

Département de Chimie
Faculté des Arts et des Sciences

Thèse présentée à la Faculté des études supérieures
en vue de l'obtention du grade de
Philisophiae Doctor (Ph.D.)
en chimie

Mai 2007

Univeristé de Montréal
Faculté des études supérieures

Cette thèse intitulée :

Molecular Tectonics: Functional Materials for Crystal Engineering

présenté par:

Michael Lautman

a été évaluée par un jury composé des personnes suivantes :

Professeur William D. Lubell	président-rapporteur
Professeur James D. Wuest	directeur de recherché
Professeur André L. Beauchamp	membre du jury
Professeur Dimitrii F. Perepichka	examinateur externe
Professeur William D. Lubell	représentant du doyen de la FES

Sommaire

La chimie supramoléculaire et l'exploitation des interactions non covalentes sont des outils indispensables pour le développement de nouveaux matériaux. La *tectonique moléculaire* est une stratégie qui exploite l'auto-association de composés soigneusement choisis pour construire de nouvelles architectures supramoléculaires. Les *tectons* agissent comme des unités de base pour la construction d'un réseau cristallin plus complexe. La tectonique moléculaire est particulièrement efficace pour la préparation de matériaux fonctionnels poreux.

Des études précédentes ont démontré que les dérivés de la triphénylamine sont de bons candidats pour explorer la construction de réseaux supramoléculaires. Ce type de molécule suscite beaucoup d'intérêt dans la chimie supramoléculaire et des matériaux par sa capacité d'agir comme transporteur de charge ou émetteur de lumière. Ceci a mené à l'utilisation de différents types de triarylamines dans des applications comme la xérographie et les diodes organiques électroluminescentes (OLEDs). La synthèse et la cristallisation de plusieurs tectons dérivés de la triphénylamine ont été effectuées, ainsi que la caractérisation de leurs propriétés optiques et électroniques. Les résultats préliminaires indiquent que la présence de groupements fonctionnels qui peuvent former des ponts hydrogène ne changent pas les propriétés électrochimiques des ces tectons. Cependant, la solubilité limitée des ces composées empêche une analyse détaillée de ces propriétés.

La présence du fluor joue un rôle importante dans l'association et assemblage supramoléculaire de molécules. De plus, l'électronégativité importante du fluor peut aider à stabiliser des espèces réactives comme des carbanions et des radicaux libres. L'exploration d'une nouvelle unité centrale, le polyfluorotriphénylméthane a été entreprise. La synthèse et la cristallisation de plusieurs tectons fluorés dérivés ont été effectuées. Les résultats indiquent que la présence de fluor apporte une influence importante sur les structures cristallines de ces tectons.

Mots-clé: Tectonique moléculaire, chimie supramoléculaire, matériaux opto-éléctroniques, synthèse organique

Summary

Supramolecular chemistry and the exploitation of non-covalent interactions have become indispensable tools for the development of modern materials. *Molecular tectonics* is a strategy for the construction of supramolecular architectures based on the directed association of judiciously chosen molecules. These molecules, which have been called *tectons*, serve as building blocks for the creation of elaborate supramolecular structures. Molecular tectonics is particularly effective for the preparation of crystalline materials, but it can also be used to create less ordered substances such as gels, liquid crystals, and glasses.

Previous studies have shown that derivatives of triphenylamine are good candidates for the construction of supramolecular networks by molecular tectonics. Arylamines have elicited a great deal of interest in supramolecular and materials chemistry for their ability to act as charge transporters or as light emitters. This has led to the application of arylamines in xerography and the production of organic light-emitting diodes (OLEDs). A number of tectons derived from triphenylamine have been synthesized and characterized, and a detailed analysis of their optical and electronic properties has been carried out. Preliminary results show that the presence of hydrogen-bonding functional groups does not significantly alter disrupts the electrochemical properties of these compounds. Detailed analyses are hampered by the limited solubility of the compounds in this study.

Recent work has shown that the presence of fluorine atoms plays an important role in the association and assembly of molecules. In addition, the strong electronegativity of fluorine can help stabilize reactive species such as carbanions and free radicals. Several tectons based on polyfluorinated derivatives of triphenylmethane have been synthesized and characterized, and their crystal structures have been analyzed in detail. Results show that the presence of fluorine atoms profoundly influences the crystal structures of these tectons and can lead to the formation of unique modes of association as well.

Key words: Molecular tectonics, supramolecular chemistry, opto-electronic materials, organic synthesis

Table of Contents

Table of Figures

Table of Schemes

List of Abbreviations

Å	: Ångstrom
Ac	: acetyl
aq	: aqueous
atm	: atmosphere
BINAP	: 2,2'-bis(diphenylphosphino)-1,1'-binaphthalene
Bn	: benzyl
Bu	: butyl
°C	: degree Celsius
cat	: catalytic
CCD	: charge-coupled device
cm	: centimeter
conc.	: concentrated
CV	: cyclic voltammetry
Δ	: heating
δ	: chemical shift
DAT	: diaminotriazine
dba	: dibenzylideneacetone
DMF	: *N,N*-dimethylformamide
DMSO	: dimethyl sulfoxide
DNA	: deoxyribonucleic acid
dppf	: 1,2-bis(diphenylphosphino)ferrocene
dppp	: 1,3-Bis(diphenylphosphino)propane
epr	: electron paramagnetic resonance
FAB	: fast atom bombardment
Fc/Fc^+	: ferrocene/ferrocenium
g	: gram
h	: hour
HOMO	: highest occupied molecular orbital

HFB	: hexafluorobenzene
Hz	: hertz
IR	: infrared
ITO	: indium-tin oxide
J	: coupling constant
kcal	: kilocalorie
L	: litre
LUMO	: lowest unoccupied molecular orbital
M	: molar
m	: meter
Me	: methyl
mg	: milligram
MHz	: megahertz
min	: minute
mL	: milliliter
mm	: millimeter
mmol	: millimole
MOF	: metal-organic framework
mol	: mole
MS	: mass spectrometry
N	: normal
NIR	: near infrared
nm	: nanometer
NMR	: nuclear magnetic resonance
ORTEP	: Oak Ridge Thermal Ellipsoid Plot
Ph	: phenyl
ppm	: parts per million
SOMO	: singly occupied molecular orbital
S-Phos	: 2-dicyclohexylphosphino-2′,6′-dimethoxybiphenyl
SWV	: square wave voltammetry
TBA	: tetra-*n*-butylammonium

TBATB	: tetra-*n*-butylammonium tribromide
TCNE	: tetracyanoethylene
THF	: tetrahydrofuran
TOF	: time of flight
TPB	: *N,N,N',N'*- tetraphenylbenzidine
TPA	: triphenylamine
TPD	: *N,N'*-bis(3-methylphenyl)-*N,N'*-diphenylbenzidine
UV	: ultraviolet
X-Phos	: 2-dicyclohexylphosphino-2′,4′,6′-triisopropylbiphenyl
VIS	: visible

Acknowledgements

First and foremost, I would like to thank Professor James D. Wuest for allowing me to work as a member of his group, while giving me the freedom to undertake and pursue this project. His intelligence and passion for chemistry have been inspiring. I would especially like to thank him for his support and guidance when things appeared insurmountable.

I am grateful for the scientific input of the members of the Wuest research group, both past and present, in particular Thierry Maris, Ken Maly, Dominic Laliberté, Olivier Lebel and Eric Demers. I would also like to thank Eric Gagnon, Emilie Voisin and Patrick Eddy Ryan for their camaradery and penchant for foolishness.

Sergio Andres Peres Guarin and Stéphane Dufresne were instrumental in helping me obtain useful cyclic voltammograms of my compounds. Thank you both.

I am indebted to Lyne Laurin, without whom most deadlines would have passed unnoticed. I would also like to acknowledge the work of Phan Viet Minh Tan, Cédric Malveau, Sylvie Bilodeau and Véronique Desjardins at the Laboratoire de RMN, Alexandra Furtos and the members of the Centre Regional de Spectrometrie de Masse, as well as Francine Bélanger-Gariépy and the team at the Laboratoire d'Analyse Elementaire.

My sincere thanks to my parents and sister for their support, and for accepting "It's like Lego, only smaller" as an explanation.

It is rejuvenating and inspiring to watch someone discover the universe for the first time. I would like to thank my children Lucca and Orciana for reminding me that the ordinary can be extraordinary if you look close enough.

I would never come this far in my life without the constant love and encouragement of my wife, Cynthia. Without her I would be lost. She has earned this as much as I have. Thank you.

"Men love to wonder, and that is the seed of science."

Ralph Waldo Emerson

Society & Solitude
1916

CHAPTER 1

Introduction

1 Introduction

1.1 Organic Chemistry and Modern Materials Science

Modern chemistry is directly involved in nearly every industrial domain, from ceramics and coatings to pharmaceuticals and polymers. The importance of synthetic and biological chemistry in the pharmaceutical industry has been well established, and many recent breakthroughs have brought materials science to the forefront of high technology. Electronics, as well as sensors, drug-delivery systems and materials, all are being pushed past their previous limits.[1,2,3] Electronic devices need to be faster and smaller, pharmaceutical agents need to be delivered with greater precision in the body, and materials need to be lighter, more robust and more responsive. Concrete examples of applications of organic chemistry in materials science include organic light-emitting diodes (OLEDs) that can be used for displays or ambient lighting, drug encapsulation in micelles and the development thin-film piezoelectric polymers.[4-6]

The common factor in the advancement of these fields is the realization that in order to fully exploit their potential, a thorough understanding of processes at the molecular level is required. A great deal of effort has been devoted to designing molecules that go into these products and devices, leading to remarkable advances.[7] However, it is now understood that the manner in which these molecules interact with each other and with their environment may play a critical role in exploiting these new technologies to their full potential.[8]

1.2 Supramolecular Chemistry and Crystal Engineering

Technological advances, most notably nuclear magnetic resonance (NMR) spectroscopy,[9-11] launched a revolution in synthetic organic chemistry after World War II. At present, the scope and scale of chemical transformations that can be carried out is vast. The complexity and size of the molecules that can be prepared is staggering. As the problems posed by the synthesis of structurally sophisticated compounds are overcome, many researchers are turning their attention to the way molecules interact with one another. This ever-broadening field of research is called *supramolecular chemistry*. It is defined as *"chemistry of the intermolecular bond, covering the structures and functions of the entities formed by the association of two or more chemical species"*.[12]

In nature, complex biological systems are governed by the interaction and spontaneous association of subunits to create a functional entity that has properties different from those of each of its building blocks. This is termed *self-assembly* and it imparts increased complexity and subtlety to such systems. Protein folding, DNA replication and enzyme-substrate recognition are all instances where molecular recognition and self-assembly play critical roles.[13]

Non-natural systems can also be designed to self-assemble into novel architectures that give rise to unique and powerful characteristics and functionality. Drawing inspiration from biological systems, chemists have developed systems such as catenanes, rotaxanes and capsules, which have

become classic examples of the power of supramolecular chemistry.[14,15,16] **Figure 1.1** is an example of a supramolecular capsule built from the self-association of four pyrogallolarene units (**1**) and enclosing one molecule of tetrabutylammonium iodide and one molecule of 4-methylbiphenyl.[15] In wet organic solvents, such capsules contain large volumes (1375 $Å^3$), and the size, shape and polarity of molecules influences their encapsulation. For example, naphthalene, biphenyl and azulene are simultaneously encapsulated with covalent antimony(V) bromides, while longer molecules such as *trans*-stilbene, azobenzene and *n*-heptylbenzene are not.

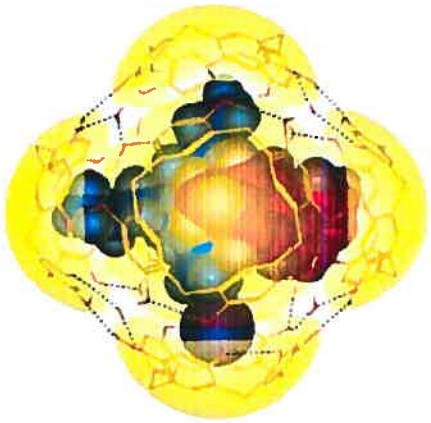

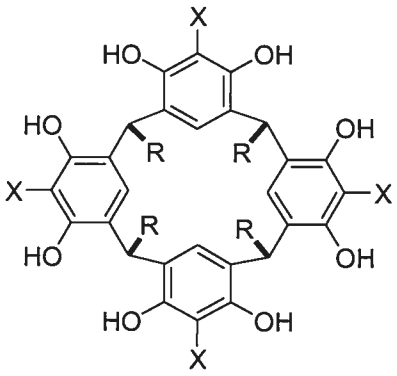

1

Figure 1.1 Supramolecular capsule assembled from four molecules of compound **1** via hydrogen bonding. Hydrogen bonds are shown as faint broken lines. The capsule contains one molecule of tetrabutylammonium iodide (in blue) and one molecule of 4-methylbiphenyl (in red).[15]

Self-assembly occurs in the gas, liquid and solid phases, and it is governed by the spontaneous formation of non-covalent intermolecular bonds. Although covalent bonds are strong and relatively permanent, non-covalent interactions are weak and reversible. This imparts a high-degree of dynamism in structures built via typical self-assembly, allowing them to associate and come

apart spontaneously. The most common intermolecular interactions are hydrophobic interactions, π-stacking, dipole-dipole interactions, van der Waals interactions and hydrogen bonds. Hydrogen bonds are the most commonly employed for the purposeful construction of molecular aggregates because they are directional and relatively strong.[13,17-19] Although non-covalent interactions are much weaker than covalent bonds, their effects are cumulative. Therefore, thermodynamically robust supramolecular structures can be created when multiple interactions are present in a system.[20]

1.2.1 Hydrogen Bonds

Ligand-metal interactions are by far the strongest intermolecular interactions. They can be applied with powerful results in supramolecular chemistry. However, they do present some important drawbacks.[21] Foremost among them is the requirement that a metal atom or ion be present. For example, if the material is to be used as part of an electrical circuit, metal ions will have a tendency to migrate toward the anode, disrupting the supramolecular structure. In contrast, hydrogen bonds require only that one of any number of organic functional groups be present.

The classical hydrogen bond is a primarily electrostatic interaction, and can be represented as D–H···A, where D and A are electronegative atoms (N, O, S, halogen). D is considered the hydrogen-bond donor and A the acceptor. This imparts a partial positive charge on the hydrogen atom.

One broad definition of a hydrogen bond would be *"... a hydrogen bond exists if 1) there is evidence of a bond, and 2) there is evidence that this bond sterically involves a hydrogen atom already bonded to another atom".*[22] While this definition is broad enough to include many modern hydrogen bonds, it can also be considered to include van der Waals interactions, B-H-B bridges and agostic interactions.[23,24]

However, this definition may be somewhat inadequate given recent advances in crystal engineering and structural biology. Many weaker interactions have been observed to have an important impact on supramolecular architecture.[25] Some of these include C-H$\cdots\pi$ and C-H$\cdots$O hydrogen bonds.[26] The traditional range of hydrogen bond energies was considered to be from roughly 1 to 13 kcal/mol.[27] More modern efforts indicate that the true range is from 0.2 to 40 kcal/mol.[27] Among the most studied hydrogen-bonding groups are carboxylic acids, amides, amines and alcohols. These groups are all critical in directing the folding and assembly of biomolecules such as proteins, DNA and RNA.[28] Nitrogen heterocycles built around aminopyridines and pyrimidines are, of course, the basis for all genetic information.

1.2.2 Crystal Engineering

Crystalline substances have long been prized for their beauty. While there are many naturally occurring crystals, science still lacks a profound understanding of the forces that govern the formation and growth of crystals.[29]

For this reason, the design and preparation of crystalline systems, which is called *crystal engineering*, remains an empirical science.[30,31] As the nature of crystals and the mechanism of crystallization are being probed, it becomes clear that crystallization is the result of an exceedingly complex and subtle interplay of forces.

1.3 Molecular Tectonics

Crystal engineering has become a broad field. Its roots are in X-ray crystallography, and many of the pioneers in the field have been crystallographers. This may explain why it is not yet common practice for crystal engineers to fully exploit the potential of chemical synthesis in the pursuit of further understanding of the processes of crystallization. The tendency is to use commercially available products, or molecules that can be prepared with a minimum of synthesis.[27,30,32]

The ability to apply complex synthesis in crystal engineering adds the element of design to the process. Chemists can therefore ask more profound questions of their compounds. By applying the broad power of synthetic chemistry to problems of crystal engineering, *molecular tectonics* can look at the problems of molecular association from many perspectives. Tecton (from the Greek, **tecton**, for builder) is a term that has been coined to describe any molecule *"whose interactions are dominated by particular associative forces that induce the self-assembly of an organized network with specific architectural or*

functional features." [33] Molecular tectonics is a strategy that employs tectons in building supramolecular architectures.[34]

Each tecton is carefully designed so that it will contain all of the information necessary to direct the association of multiple units. **Figure 1.2** shows the directed self-association of a theoretical tecton. The position of the groups that will participate in the non-covalent interactions, as well as the tetrahedral geometry of the molecule, should force the system to adopt a diamondoid architecture.

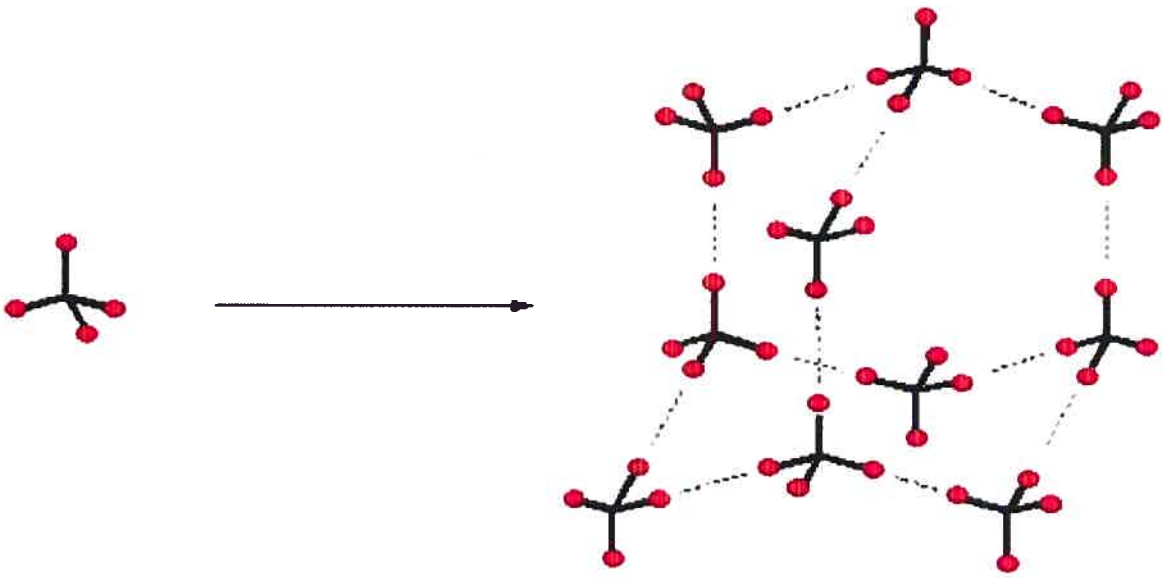

Figure 1.2 Self-association of a theoretical tetrahedral tecton directed by non-covalent interactions, giving rise to a diamondoid network.

The crystallization of most small molecules appears to be governed by van der Waals interactions. The molecules seek to maximize their contact with one another, minimizing any free space in the crystal lattice. By applying the strategy of molecular tectonics, this tendency toward close-packing in the crystalline state can be overcome so that large portions of the volume of a given

crystal can be occupied by guest molecules.[35] This gives rise to open-framework crystalline solids that contain pores or channels that may be accessible from the surface of the object.[36] In many cases, the included guest molecules can be partially removed or completely exchanged without disrupting the integrity of the crystal.

Hydrogen bonds are ideal for the construction of tectonic networks. When present in sufficient number, they are strong enough to maintain a crystalline system while allowing for disassembly (by dissolution) if required. A wide range of organic functional groups participate in the formation of hydrogen bonds. This provides chemists with a plethora of options for incorporating hydrogen-bond forming functional groups into different compounds. Early studies focused on the use of 2-pyridinones as the recognition group, due to the fact that this functional group has a strong tendency to form hydrogen-bonded dimers. More recently, diverse functional groups such as carboxylic and boronic acids as well as the more complex 3,5-diaminotriazine (DAT) group have been employed with much success.[37] Functional groups such as 2-pyridinones that engage in only one recognition motif are valuable because they lend an element of predictability to a supramolecular system. In contrast, DAT groups, which can participate in a wide range of recognition patterns (**Figure 1.3**), sacrifice this predictability for the potential of forming a wider range of supramolecular structures.

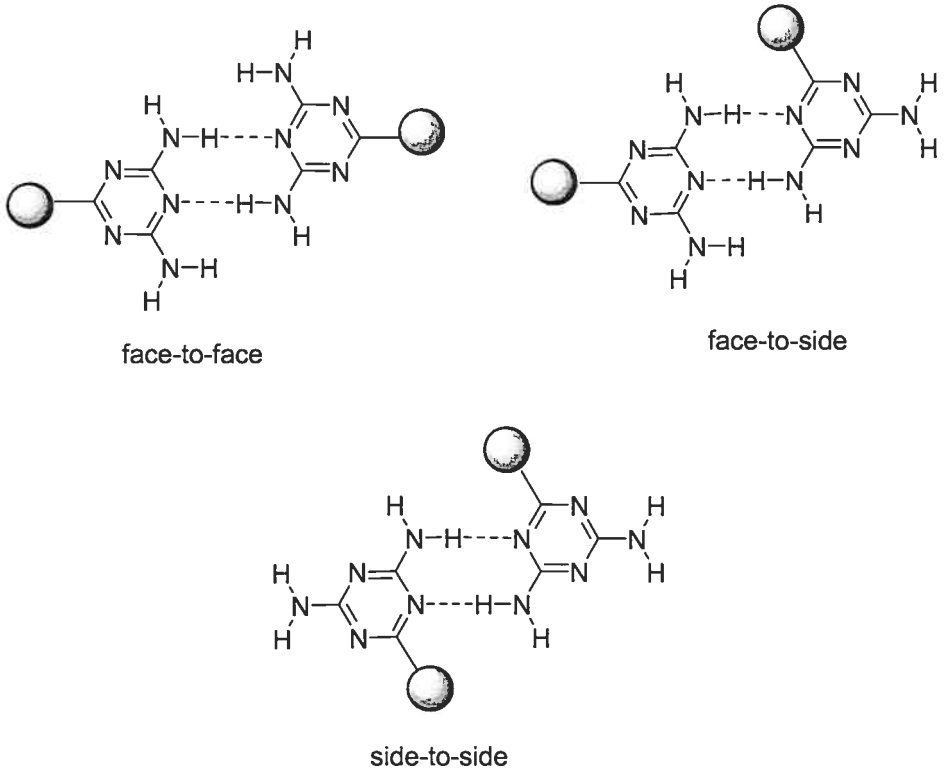

Figure 1.3 Principal hydrogen-bonding motifs of diaminotriazine dimers.

A recent example of using tectons to engineer hydrogen-bonded crystals is provided by the spirobifluorene derivative **2**. Tecton **2** can be separated into two parts: the center (or core) and the recognition groups that control association. In this example, the core of the tecton can be considered to be 9,9'-spirobifluorene. The DAT groups at the periphery of the tecton serve as recognition units. In the case of tecton **2,** four diaminotriazine groups are connected to the core via secondary amines. This compound is crystallized from DMSO-dioxane to give a hydrogen-bonded network in which 75% of the volume is available to guest molecules (**Figure 1.4**).[38] The presence of open channels or cavities in the supramolecular architecture makes the crystal permeable. This

permeability allows for the diffusion of guest molecules in and out of the crystal. Guests can be selected on the basis of size, or can be chosen so that they react with the molecules that comprise the crystal structure.[39,40]

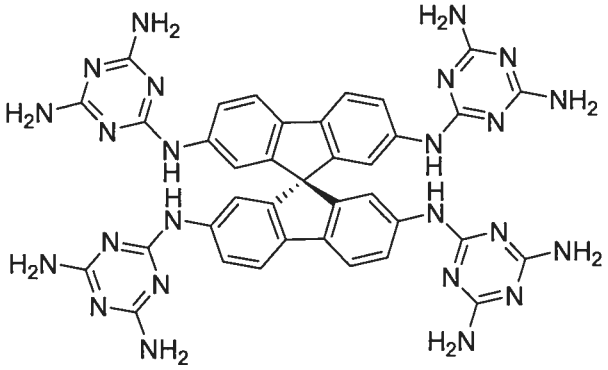

2

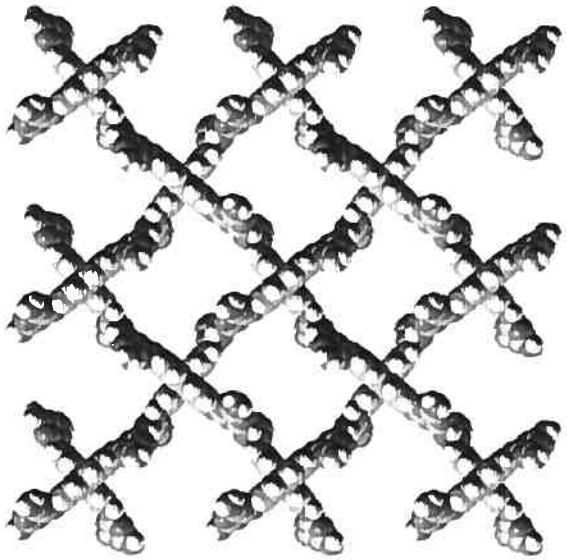

Figure 1.4 View along the c axis of the network constructed from tecton **2** showing a 2 × 2 × 4 array of unit cells. Guests are omitted, and atoms are shown as spheres of van der Waals radii in order to reveal the cross sections of the channels. Atoms of hydrogen appear in white, atoms of carbon in light gray, and atoms of nitrogen in dark gray.

Although many tectons are neutral molecules, it is equally possible to employ either anionic or cationic compounds in the construction of supramolecular structures. Borate **3** can be used to create an open-framework crystalline network that can participate in size-exclusion ion exchange.[41]

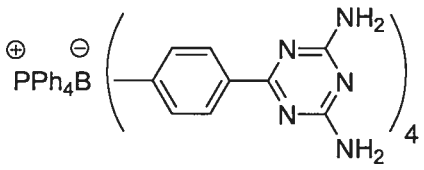

3

A striking example of the power of molecular tectonics involves carrying out reactions on crystals obtained from the self-assembly of tectons. **Scheme 1.1** describes the photochemical addition of various thiols within crystals of tecton **4**, which has accessible functional groups. This addition occurs without destroying the crystal network. When an appropriately selected dithiol is employed in the same manner, reticulation of the crystal occurs, forming a robust supramolecular polymeric crystal that is inaccessible by any other means (**Figure 1.5**).[40] The reticulation is a single-crystal to single-crystal transformation, and the new polymer retains the crystalline architecture of the starting solids.

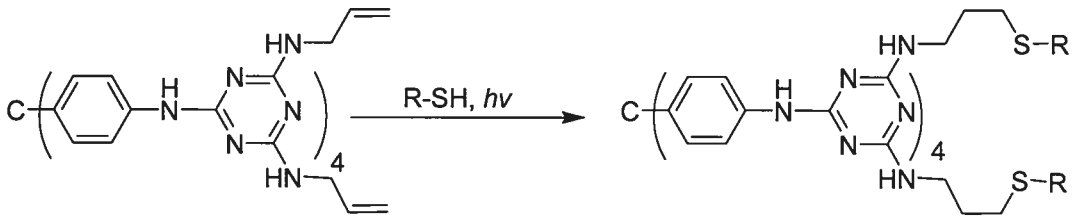

4 **5**

Scheme 1.1 Photochemical addition of thiols to allyl-substituted tecton **4**.

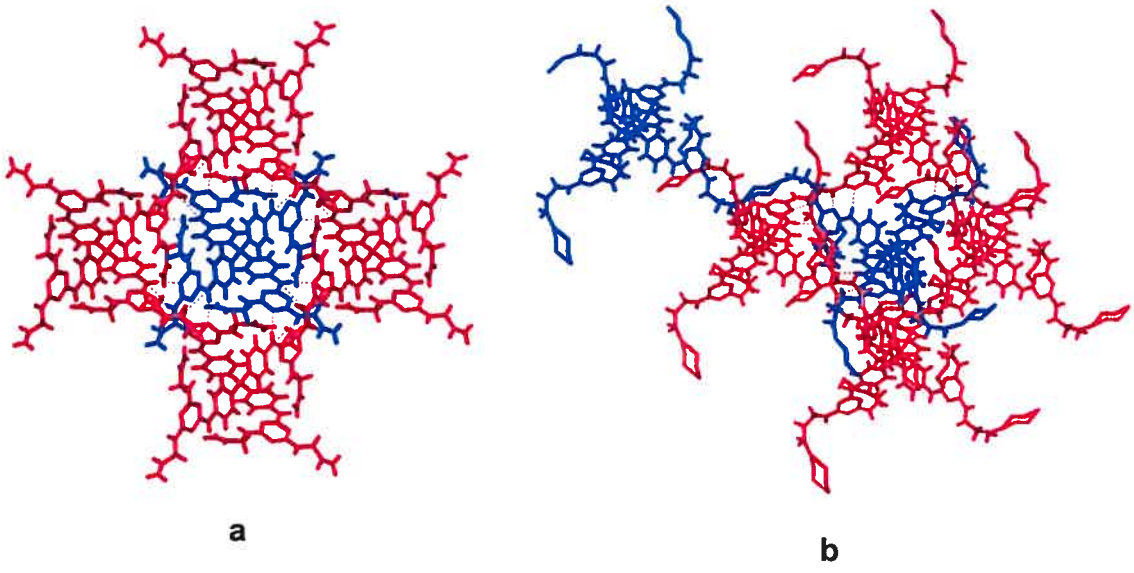

Figure 1.5 **a)** Crystal structure of tecton **4** viewed along the *c* axis showing one tecton in blue and the four neighbours with which it forms hydrogen bonds in red. **b)** Crystal structure of the novel polymer formed by the photochemical solid-state reaction of tecton **4** with 1,2-ethanedithiol, shown approximately along the *c* axis. One tecton shown in blue forms hydrogen bonds with four neighbours shown in red, and it becomes covalently linked to a farther tecton (also shown in blue).

The scope of molecular tectonics is not limited to purely organic small molecule systems. It has been used to describe a wide range of processes from the assembly of viral skeletons to biomineralization.[42]

1.4 Objectives

Many molecular cores used in molecular tectonics are chosen for their well defined geometry and conformation, such as tecton **2**. Of particular interest are cores that exhibit optical or electronic properties, such as luminescence, charge transport or magnetism. For example, anthracene **6** and triarylamine **7** were instrumental in showing how molecular tectonics might be used to prepare functional supramolecular materials.[43,44] Tecton **6** is luminescent, and the crystal

structure of tecton **7** places the central nitrogen atoms in close proximity to one another, which may be ideal for charge transport.

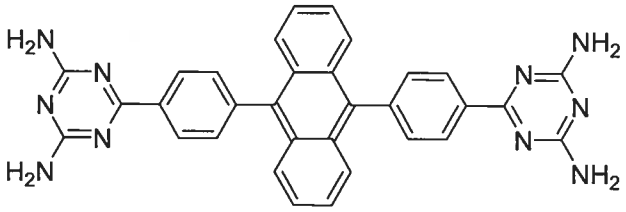

6

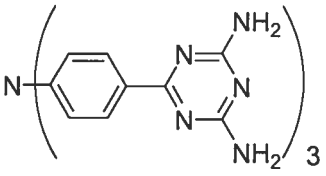

7

The objectives of the present study are two-fold: First, to extend the scope of functional materials made by the strategy of molecular tectonics, and second to begin to examine how the presence of hydrogen-bonding functional groups affects the optical and electronic properties of these materials. The research is divided into three main sections. Chapter 2 presents the synthesis and crystal structures of tectons derived from triarylamines. The optical and electronic characterization of these compounds is described in Chapter 3. Chapter 4 introduces a novel core, tris(polyfluorophenyl)methane, and describes synthetic and crystallographic work leading toward new tectons that may have unique molecular magnetic properties.

CHAPTER 2

Triarylamines

2 Triarylamines

2.1 Introduction to Triarylamines

First observed in anthracene crystals, electroluminescence has been the subject of intense research.[45] Much of this research has been geared toward the development of lightweight, robust and efficient organic light-emitting diodes (OLEDs) and other organic electronics.[46] OLEDs are light-emitting devices where at least one of the components is an organic compound. OLEDs are primarily used as the display element in devices such as digital media players, digital cameras and cellular telephones (**Figure 2.1**).[47] The primary advantage of OLEDs is that they do not require a backlight. A backlight is unnecessary because the emissive layers in the OLED are coloured. This permits wider viewing angles and reduces the amount of power required to run a device.[48]

Figure 2.1 Two commercial products that use OLED displays: **a)** the Sony CE-P digital music player[49] and **b)** the Kodak EasyShare LS633 digital camera.[50]

The structure of a simple OLED, shown in **Figure 2.2a,** consists of the anode, the hole-transport layer, the emitting layer, the electron-transport layer and finally a cathode. Hole-transport materials carry positive charge (holes) from the anode to the emissive layer. The anode is typically glass or plastic coated with indium-tin oxide (ITO). The subsequent layers are then deposited either by vapour deposition, micro-block printing or inkjet printing.[46] The cathode is typically an inert metal such as silver or magnesium, but plastic cathodes can be used as well. When a current is applied across the OLED, an exciton (a bound excited electron and hole pair) is generated inside the emissive layer. The recombination of the hole and the electron can cause a photon to be emitted.

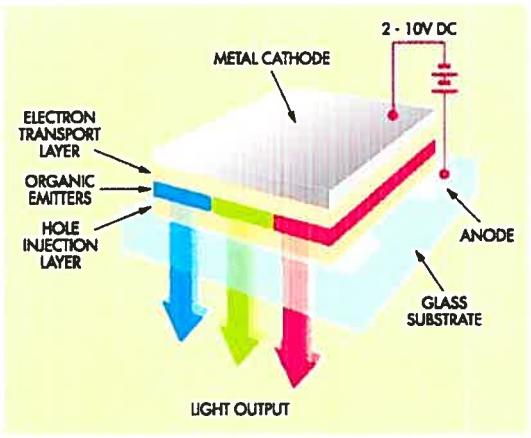

a

b

Figure 2.2 a) Schematic of a simple organic light-emitting diode (OLED) and **b)** a prototype OLED display that is only 2 mm thick.

Current devices do not yet exploit the full potential of organic electronics. The use of conductive polymers and non-glass substrates will allow for ultra-thin displays

and circuits to be fabricated on flexible plastic or even fabric.[51,52] Triarylamines are ubiquitous in organic electronics, where they are employed either as hole-transporters or as light emitters.[53,54,55] In the case of triarylamines, the hole is generated by the removal of one electron from the aryl nitrogen. This leaves behind one electron, resulting in the formation of a radical cation. Contact between adjacent molecules allows the hole to migrate across the layer.

2.1.1 Triarylamine Radical Cations

The existence of triarylamine radical cations was first proposed in 1963, spurred by electron paramagnetic resonance (epr) studies of the reaction of triphenylamine (TPA) with iodine in a wide range of solvents.[56] The first proposed structure involved the formation of an N-N bond resulting in a bimolecular cation (**8**).

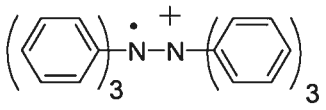

8

Further analysis revealed that the observed species was actually the radical cation of *N,N,N',N'*-tetraphenylbenzidine (TPB). The proposed mechanism proceeded via the dimerization of two TPA radical cations followed by one-electron oxidation, as shown in **Scheme 2.1**.[55] It soon became clear that triarylamine radical cations were stable under a wide range of conditions, including exposure to air and moisture. Furthermore, once the mechanism of dimerization was elucidated, it became evident that *para*-substituted derivatives of triphenylamine would be unable to undergo this type of reaction, which would lead to enhanced stability.

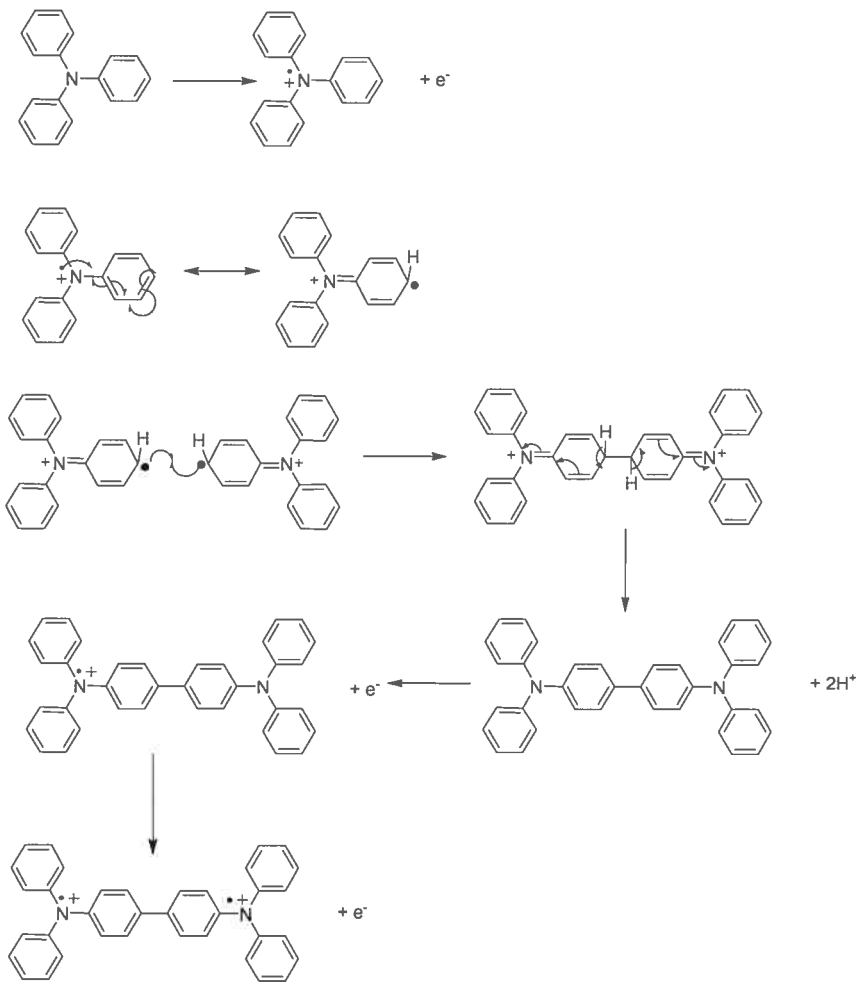

Scheme 2.1 Mechanism for the formation of the triphenylaminium radical cation and its subsequent dimerization.[55]

2.1.2 Triarylamines in Xerography and Organic Electronics

The continued push toward increasingly smaller and faster organic electronics ensures that interest in triarylamines remains intense.[46,57-64] The first industrial application of triarylamines came in xerography.[65,66] Xerographic applications, such as photocopying and laser printing, use triarylamines in their toner material. In

essence, toner is the dry ink of copiers. In a xerographic process, a rotating drum is charged with static electricity. A document is then loaded onto a glass plate. Using an array of lights and mirrors, an image of the document is displayed onto the drum, causing the charge to drain away from the drum except in the image area. Toner with the opposite charge is cascaded over the drum, and the powder sticks to the drum in charged areas, making an image. Paper is then given an electrostatic charge, the same as that on the drum, but strong enough to draw the toner particles from the drum to the paper. The toner is then fused to the paper by heating, resulting in the transfer of the image.[66]

In the case of organic light-emitting diodes, triarylamines are most frequently used in the hole-transport layer, although triarylamine-containing polymers are increasingly being employed as blue and green emitters as well.[67] The efficient functioning of a device requires that the component molecules come into contact with one another in such a way that allows for the movement of charge. Typically, amorphous materials are employed, because the random distribution ensures that at least a certain percentage of the molecules participate in contacts that allow for charge transport. Crystalline systems have traditionally been avoided because they can pose serious problems. Although charge transport through amorphous materials may not always be very efficient, in a crystal it is possible that the molecules are arranged so there are no contacts that allow for charge transport. There may also be problems controlling the shape and morphology of a crystal, as well as ensuring proper alignment with adjacent layers in a device. Lastly, there may be boundaries

between domains of crystallinity within a given layer that hinder the movement of charge.

Recent work has shown that notable improvements in the efficiency of charge-transport materials can be achieved by carefully designing the molecules employed in organic electronics so that their orientation, contacts and interfaces in the device are properly controlled.[68] Molecular tectonics may be an ideal strategy developing for new hole-transport materials that self-assemble into well-defined crystalline solids. Triarylamines could be ideal candidates for this exploration, since there is little or no difference in the conformation of the neutral and radical cation species.[69] This implies that the transfer of charge across a tectonic network would not necessarily lead to a disruption of the crystalline structure.

2.1.3 Preparation of Triarylamines

The classical method for the synthesis of triarylamines is the copper-mediated Ullmann coupling of an aryl iodide and aniline.[70-72] The reaction must be performed in high-boiling solvents such as diphenyl ether and is very sensitive to air and moisture. Reaction times for this coupling are long, often requiring many days to complete, and yields are modest. The reaction is difficult to control, and preparing differentially substituted triarylamines in high yield is nearly impossible. Catalytic versions of this reaction have been developed, using various copper (I) salts and a wide range of ligands.[73-76] Among the more popular ligands used in the modified Ullmann coupling is 1,10-phenanthroline. These conditions allow for somewhat shorter reaction times and the use of solvents with more moderate boiling points such as toluene.[77]

The success and popularity of palladium-catalyzed reactions, such as Suzuki and Sonogashira couplings, used for the formation of carbon-carbon bonds made it inevitable that the formation of aromatic carbon-nitrogen bonds using similar methods was explored.[57,78] Early efforts using binaphthol (BINAP) ligands showed promise, but the reactions lacked broad applicability.[79] After several iterations, highly hindered ligands were shown to have the greatest reactivity and most general applicability.[62] Tri(*tert*-butyl)phosphine (**9**) is a good ligand for a wide range of substrates, but it is a pyrophoric liquid at room temperature and degrades rapidly in the presence of air or moisture. In contrast, 2-dicyclohexylphosphino-2′,4′,6′-triisopropylbiphenyl (X-Phos, **10**) and 2-dicyclohexylphosphino-2′,6′-dimethoxybiphenyl (S-Phos, **11**) are solids at room temperature and do not degrade under ambient conditions.[80-82] These and other ligands are now commercially available, and couplings catalyzed by complexes of such ligands have become important methodologies for organic synthesis.[83-87]

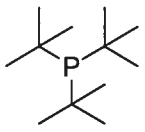

9

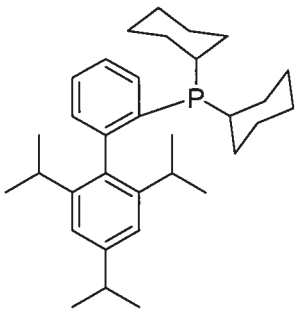

10

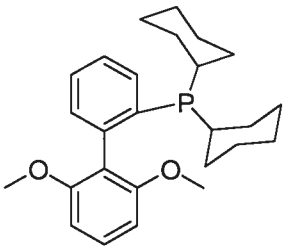

11

2.2 Reactions of Triarylamines

The relative stability of certain triarylamine radical cations makes them ideal reagents or catalysts for various chemical transformations. One of the best known of

these is tris(4-bromophenyl)aminium hexachloroantimonate ($\mathbf{12^{+\cdot}SbCl_6^-}$). The compound is air-stable and participates in a wide range of chemical transformations such as cyclopropanations, polymerizations and Diels-Alder reactions.[88]

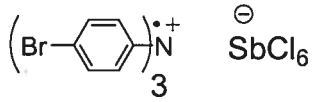

$\mathbf{12^{+\cdot}\ SbCl_6^-}$

Radical cation-mediated polymerizations and Diels-Alder cyclizations often give rise to markedly different products or to pronounced selectivities when compared with other methods. Glycosylation of a wide range of sugar derivatives proceeds smoothly and efficiently when promoted by single electron transfer from a radical cation (**Scheme 2.2**). The reaction is initiated when a tris(4-bromophenyl)aminium ion abstracts an electron from a glycoside. Subsequent cleavage of the C_1–X bond forms an oxocarbenium ion which is susceptible to nucleophilic attack by an alcohol to provide the new glycosidic bond.[89]

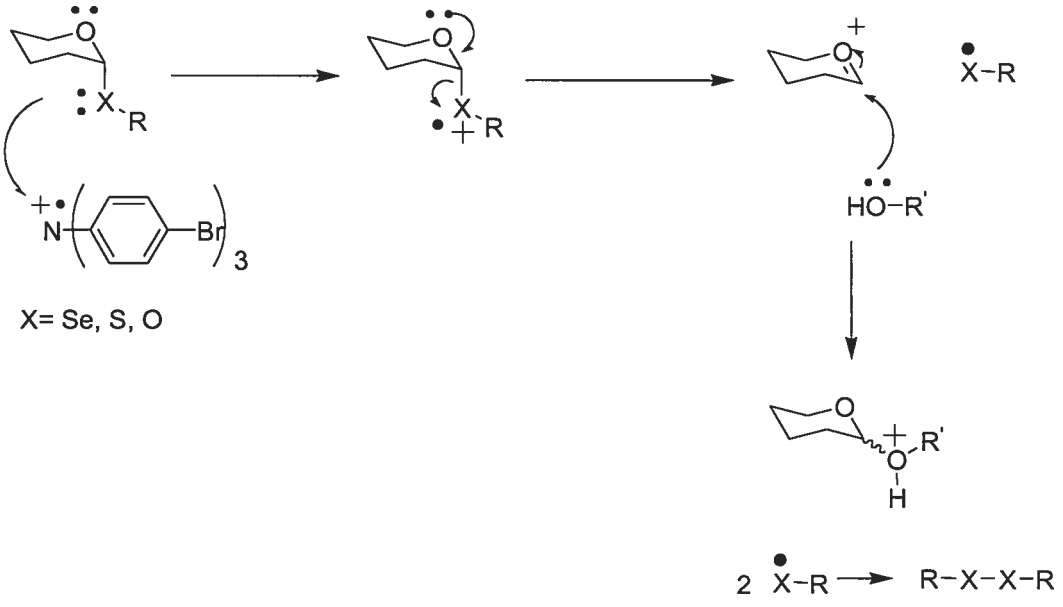

Scheme 2.2 Radical cation-promoted glycosylation.

More recently, tris(4-bromophenyl)aminium hexachloroantimonate has been used in conjunction with a range of copper-phenanthroline complexes to model the activity of the enzyme galactose oxidase (GOase).[90] It has also been found that radical cation-initiated [3 + 2] cycloadditions of chalcone epoxides and aromatic imines offer a convenient method for the preparation of 1,3-oxazolidines, which are commonly used as chiral auxiliaries in organic synthesis (**Scheme 2.3**).

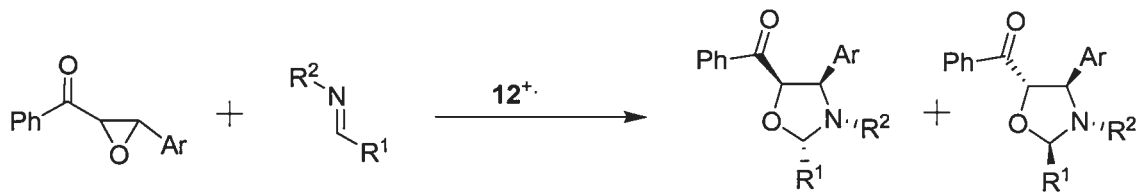

13 **14** **15** **16**

Scheme 2.3 Radical cation-initiated [3+2] cycloaddition of a chalcone epoxide and an aromatic imine. R^1 and R^2 are aromatic groups.[91]

Remarkably, this reaction shows a pronounced preference for the *trans,cis* diastereoisomer, with as much as 55:1 selectivity in some cases.[91] Other methods of synthesizing 1,3-oxazolidines have achieved similar, or even better, selectivities but they often require activation of the substrates and more elaborate protecting groups.[92]

2.3 Geometry of Triarylamines

Crystallographic and computational studies of amines have shown that three-coordinate nitrogen atoms are often sp^3 hybridized and adopt an approximately tetrahedral pyramidal geometry.[93,94] Three corners of the pyramid are occupied by atoms bound to nitrogen, and the fourth corner is occupied by a lone pair of electrons. In the case of quaternary ammonium cations, this fourth position is occupied by a bond to another atom (**Figure 2.3**).

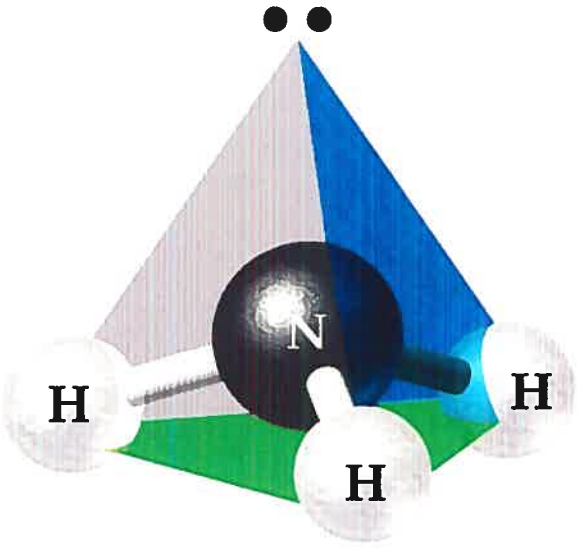

Figure 2.3 Representation of the geometry of ammonia (NH_3). [93-95]

Carbon atoms adopt a tetrahedral geometry when connected to four atoms. When the four atoms are different, this creates a chiral center in a molecule. In contrast, having three different substituents on a nitrogen atom in addition to the lone pair will result in a chiral center that is configurationally labile, because the nitrogen-centered tetrahedron can undergo rapid inversion.[96] However under certain conditions, such as low temperature, the influences of the chiral center can be observed. Nitrogen atoms can also be sp^2 or *sp*-hybridized, as is the case for pyridines and nitriles, respectively. In situations where the lone pair is delocalized by resonance, nitrogen atoms will adopt the trigonal planar geometry that is characteristic of sp^2 hybridization. This is the case for amides and triarylamines. In the case of triarylamines, the lone pair of electrons that resides on the nitrogen atom interacts with the π systems of the aromatic groups. This $p\pi$-conjugation requires that the orbital that contains the lone pair and the aromatic orbitals be aligned, which leads to a planar geometry for the nitrogen atom. The crystal structure of triphenylamine confirms that the nitrogen atom does in fact favour a planar trigonal bonding.[97] The aromatic groups that surround the nitrogen atom take on a propeller conformation, in order to minimize steric hindrance. Other arylamines adopt the same geometry about the nitrogen atom as triphenylamine. For example, **Figure 2.4** shows the crystal structure of *N,N,N',N'*-tetrakis(3-methylphenyl)benzidine (**17**).[98] The main conformational difference between triphenylamine and its various derivatives is found in the angles of torsion between the different substituents about the nitrogen atom.

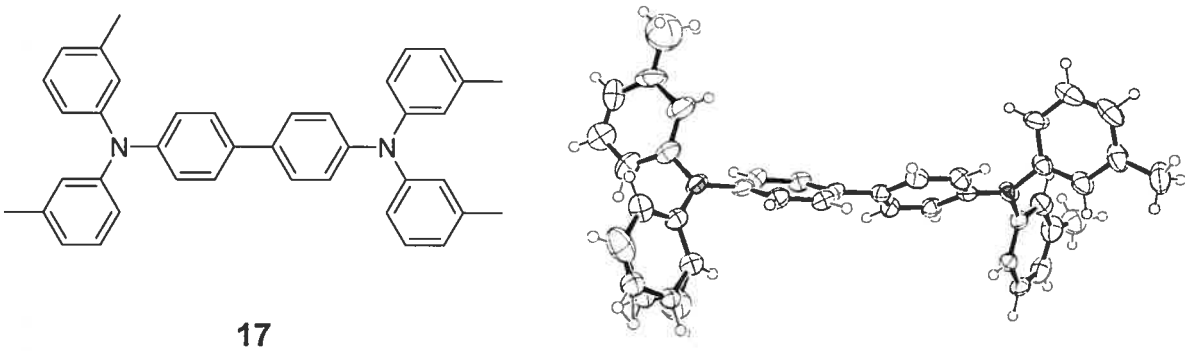

17

Figure 2.4 ORTEP diagram of compound **17**. Note the planar geometry of the nitrogen atoms.[98]

2.4 Triarylamines in Supramolecular Chemistry

The trigonal planar geometry of triphenylamine and its derivatives has made this class of compounds attractive as the starting point for a number of supramolecular building blocks or synthons.[99] Derivatives of triphenylamine have been used to build metal-organic frameworks (MOFs), as well as supramolecular tetrahedra.[100,101] Much of this work has been carried out using carboxylic acid groups as the recognition unit, either for hydrogen bonding or chelation with metals.[100] **Figure 2.5** shows the starburst triphenylamine derivative **H_6TTA** (**18**) and how it complexes with zinc nitrate hexahydrate to form the supramolecular structure **MODF-1**.[100] Each of the four nitrogen atoms in **H_6TTA** is planar, and each of the six carboxylate groups coordinates to two zinc ions. The complex defines an infinite array, referred to as a metal-organic framework (MOF). MOFs are of particular interest to chemists for their very large surface area–to–volume ratio, which may lead to applications in catalysis and gas storage.[21,102] The formation of open-framework crystalline structures characteristic of MOFs is analogous to the type of architecture formed by purely organic compounds with molecular tectonics.

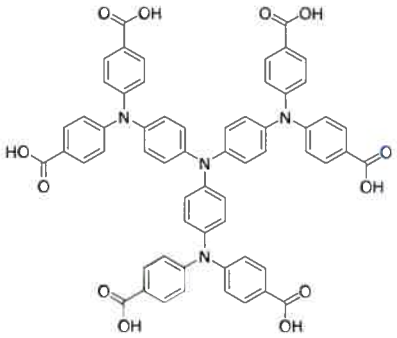

18

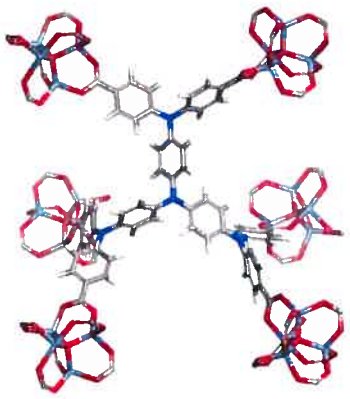

MODF-1

Figure 2.5 Triphenylamine derivative **H_6TTA** (**18**) is a ligand for twelve zinc atoms in the supramolecular structure **MODF-1**. Each zinc atom is in turn bound to three different molecules of **H_6TTA**. [100]

In other instances different carboxylic acid derivatives, such as ortho-substituted triarylamine **19**, can assemble into discrete tetrahedra via hydrogen bonding. **Figure 2.6** describes the self-assembly of aggregator **19**.[101]

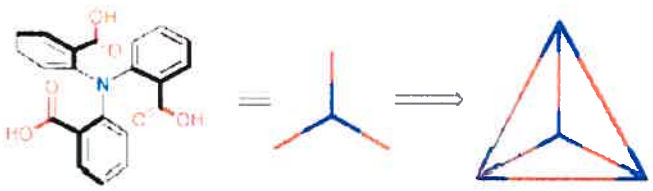

19

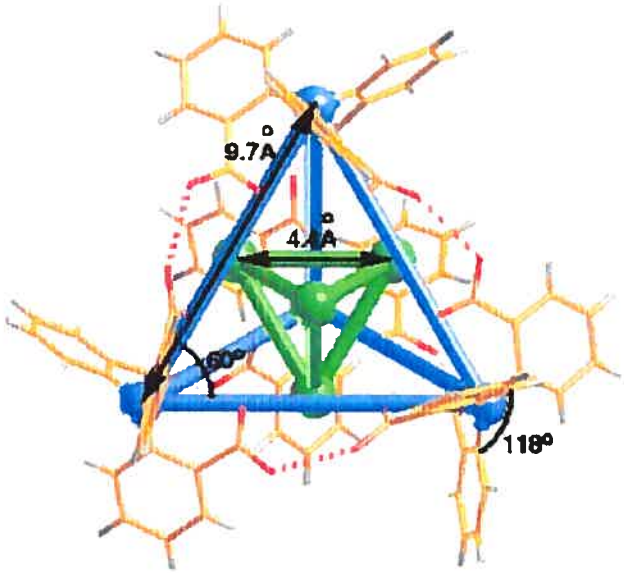

Figure 2.6 Crystal structure of tris(2-carboxyphenyl)amine (**19**) and representation of the polyhedra formed by the four molecules. In the upper portion of the figure, the blue lines represent the branches of the molecule and the orange lines represent the hydrogen-bonding interactions between molecules. The green lines show the center to center distance between phenyl rings on adjacent molecules.[101]

2.5 Other Trigonal Tectons

The nature of the supramolecular architecture that results from the self-association of a tecton is in large part influenced by the geometry and conformation of that molecule. Tetrahedral tectons, such as compound **20**, have been extensively studied, in part because of their tendency to form diamondoid networks (**Figure**

1.2).[103] In order to access a wider range of network architectures, tectons with other geometries and conformations have been explored.[36,104-106]

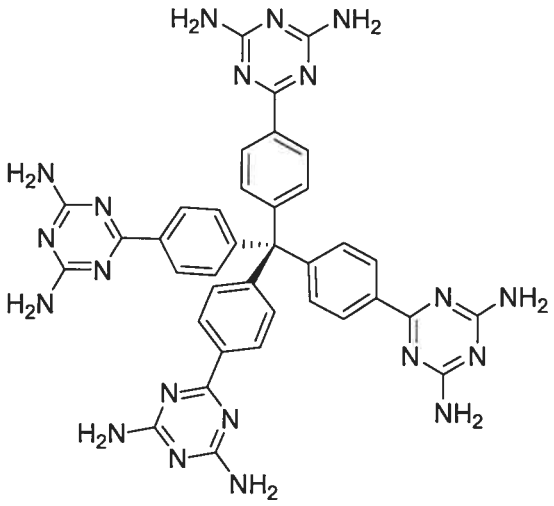

20

Tectons that have a trigonal planar geometry are attractive targets for accessing a broader range of supramolecular architectures. Specifically, trigonal tectons are ideal candidates for exploring layered structures. Derivatives of 1,3,5-triphenylbenzene have been prepared and studied in order to explore layered structures. Triphenylamine, which is trigonal planar belongs to the same family as triphenylphosphine, and triphenylantimony and triphenylbismuth, which are not.[107,108] Derivatives of triphenylphosphine, have been been prepared and studied as well. Although these compounds have three branches, like triphenylamine, they are pyramidal rather than planar. Derivatives of triphenylphosphine are readily oxidized to tetrahedral triphenylphosphine oxide, often simply upon exposure to air. Currently, the only convenient way to prepare a trigonal tecton based on phosphorus is to use derivatives of tris(2,5-xylyl)phosphine such as compound **21**, which is more resistant

to oxidation. Tris[1,3,5-(3,5-diamino-2,4,6-triazinyl)-2,4,6-trimethyl]benzene (**22**) is one of the earliest trigonal tectons prepared,[105] while more recent work has shown that certain planar borane derivatives, like compound **23**, are good candidates for molecular tectonics as well.[109]

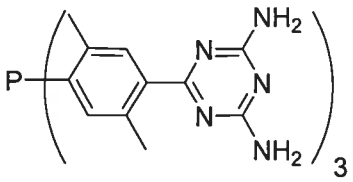

21

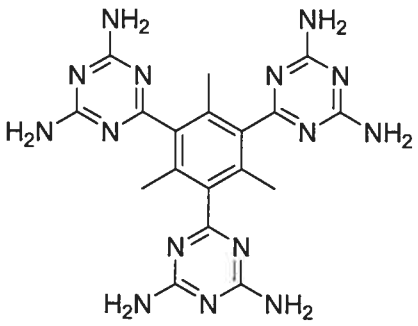

22

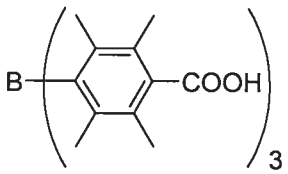

23

Figure 2.7 describes the crystal structure of tecton **22**. One tecton, shown in white, is hydrogen-bonded to four nearest neighbours, shown in grey, via side-to-side interactions of the diaminotriazine groups (**Figure 1.3**). Two of the branches of the compound participate in these hydrogen-bonding interactions, while the third arm does not. The hydrogen bonds extend to form two-dimensional corrugated layers that are stacked one on top of another to create a three-dimensional array. The branch of the tecton that does not participate in any hydrogen bonds points toward the next layer, resulting in a distance of approximately 13.8 Å between adjacent sheets.[105]

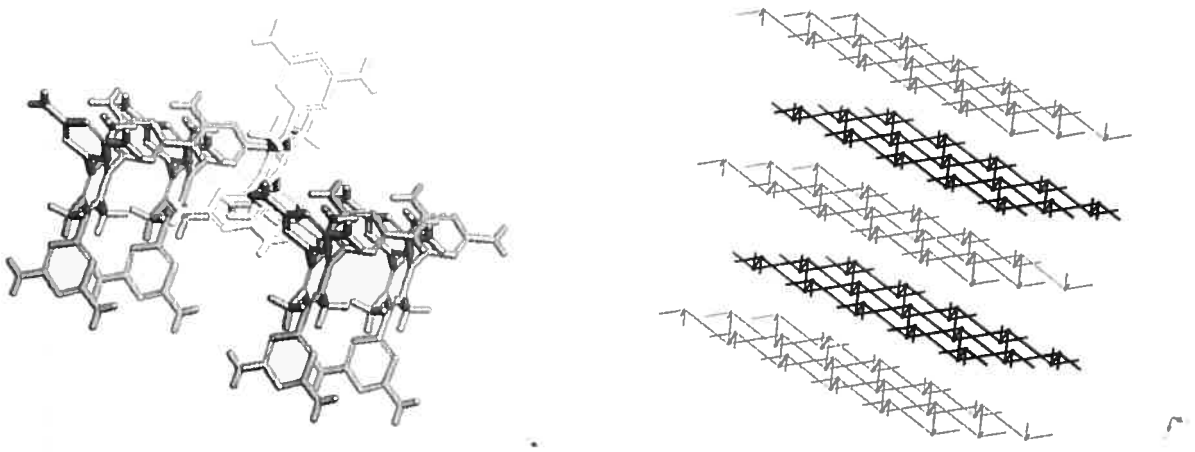

a b

Figure 2.7 Crystal structure of tecton **22**. **a)** One tecton, shown in white, is hydrogen-bonded to four nearest neighbours, shown in grey. **b)** Representation of the hydrogen-bonding network present in the crystal structure of compound **22**. Connecting lines are drawn between the center of the benzene ring of hydrogen-bonded neighbours of compound **22**. The network consists of stacked corrugated sheets.

2.6 Triarylamines in Molecular Tectonics

In light of the increasing interest in the role that supramolecular organization plays in modulating the properties of functional compounds such as triarylamines, we were eager to examine how the inclusion of hydrogen-bonding functional groups would influence the opto-electronic properties of various triphenylamine derivatives. In addition, we expected that comparison of crystal structures obtained in this study with those of analogous compounds lacking certain structural features would prove interesting.

A series of derivatives of triphenylamine substituted with either diaminotriazine groups or pyridinone groups were selected for initial assessment. These recognition

groups were chosen for two reasons: their propensity for associating by forming hydrogen bonds, and their synthetic accessibility.

The first triarylamine to be examined as a candidate for engineering structures by molecular tectonics was a triphenylamine substituted with a diaminotriazine group in the *para*-position of each phenyl ring. In order to simplify the identification of the various compounds being examined, a naming scheme was devised. Accordingly, this most simple derivative of triphenylamine, compound **7**, is referred to as **1_ADAT**. The abbreviation is comprised of three parts: a number, a subscript letter and finally a three letter suffix. The suffix indicates which type of recognition group is present in the molecule. **DAT** represents the 3,5-diamino-2,4,6-triazinyl group; similarly **PYR** indicates the 3-pyridinone unit. The subscript letter refers to the molecular core that the tecton is built around. **A** is used when triphenylamine is the basic unit, while **B** signifies tetraphenylbenzidine.

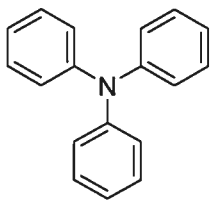

A

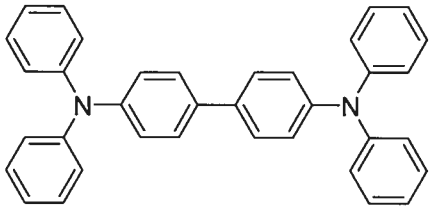

B

Finally, the number represents the generation that the compound belongs to. The term *generation* in this case should be applied in the same sense that it is for dendrimers and starburst molecules. First-generation compounds are those that have the recognition group grafted directly onto the core. Subsequent generations

incorporate spacers such as phenyl or acetyl groups between the core and the recognition group.

2.7 Tecton 1_ADAT

2.7.1 Synthesis of Tecton 1_ADAT

Scheme 2.4 describes the synthesis of tecton **1_ADAT (7)**. Triphenylamine (**24**) was brominated with tetra-*n*-butylammonium tribromide (TBATB) in chloroform. Electron-rich substrates such as **24** are activated toward electrophilic aromatic substitution, making it difficult to control reactions such as bromination when strong reagents such as liquid bromine are used. A mixture of poly-brominated products can sometimes be obtained, reducing yields and making purification time-consuming. When mild brominating reagents such as TBATB are used with activated substrates, reactions proceed rapidly and the extent of bromination is readily controlled by varying the reaction time.[110] The bromination of compound **24** was completed in 20 min at room temperature, affording the known compound tris(4-bromophenyl)amine (**12**) in 85% yield after recrystallization from glacial acetic acid.[111]

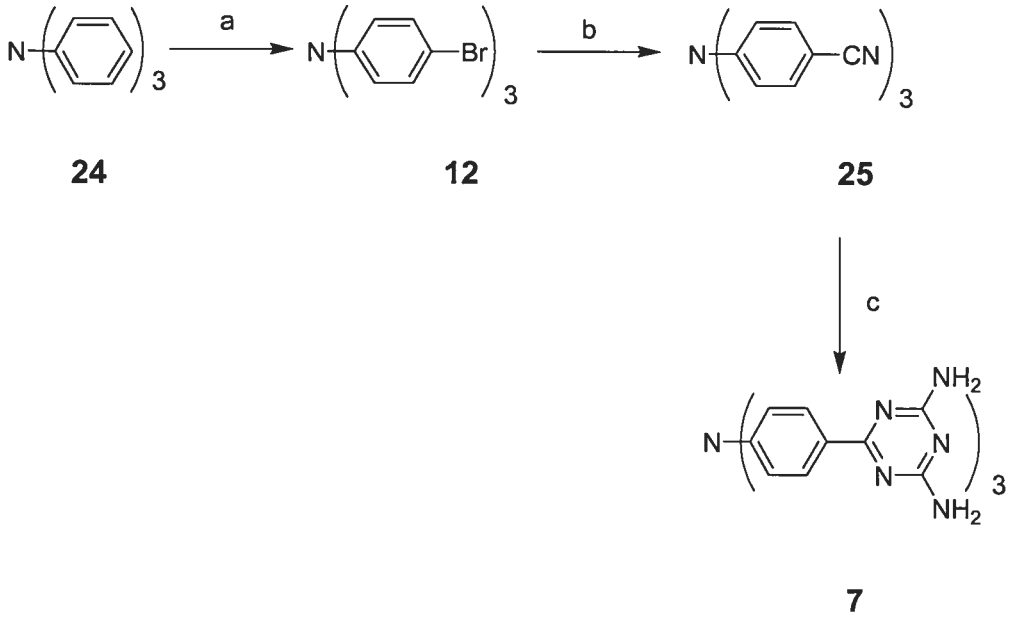

24 **12** **25**

7

Scheme 2.4 a) Tetra-*n*-butylammonium tribromide, $CHCl_3$, RT, 85%; **b)** CuCN, DMF, reflux, 82%; **c)** dicyandiamide, KOH, 2-methoxyethanol, reflux, 84%.[43]

Tris(4-cyanophenyl)amine (**25**) was prepared in 82% yield by reacting bromide **12** with copper(I) cyanide under standard conditions.[112] The diaminotriazine groups were introduced by condensing intermediate **25** with dicyandiamide using known conditions.[113,114] The resulting yellow product was dissolved in DMSO and precipitated with ethanol. The pure tecton **1_ADAT** (**7**) was recovered in 85% yield after suction filtration and drying in a vacuum oven.

2.7.2 X-ray Crystallographic Analysis of Crystals of Tecton 1_ADAT

Tecton **1_ADAT** was crystallized from DMSO solution by diffusion of ethanol vapours, and the structure was determined by X-ray diffraction. Tecton **1_ADAT** forms an open-framework hydrogen-bonded crystalline network. The molecule crystallized in the trigonal R-3 space group with lattice parameters $a = b = 34.185(2)$ Å, $c =$

8.4889(9) Å and a volume of 8591.3(12) $Å^3$ ($\alpha = \beta = 90°$, $\gamma = 120°$). The ORTEP diagram (**Figure 2.8**) shows that the resulting crystal consists of the ordered tecton and two partially disordered molecules of DMSO.[103,115,116] **Figure 2.9** shows that each tecton is hydrogen-bonded to three nearest neighbours via face-to-face interactions (**Figure 1.3**) of the diaminotriazine groups. The phenyl rings connected to the central nitrogen atom are twisted into a propeller-like conformation. The rings are twisted 36.73° out of the plane formed by the bonds to the central nitrogen atom. This torsion makes each molecule chiral, and this chirality can be described using the *M* and *P* notation.[117,118] In **Figure 2.10** the tectons in black are *M* and are hydrogen bonded to three nearest neighbours shown in white, which are *P*. In addition, the molecules directly above and below the black tecton also have the opposite chirality. The overall network is therefore racemic, because there are an equal number of tectons of opposite chirality.

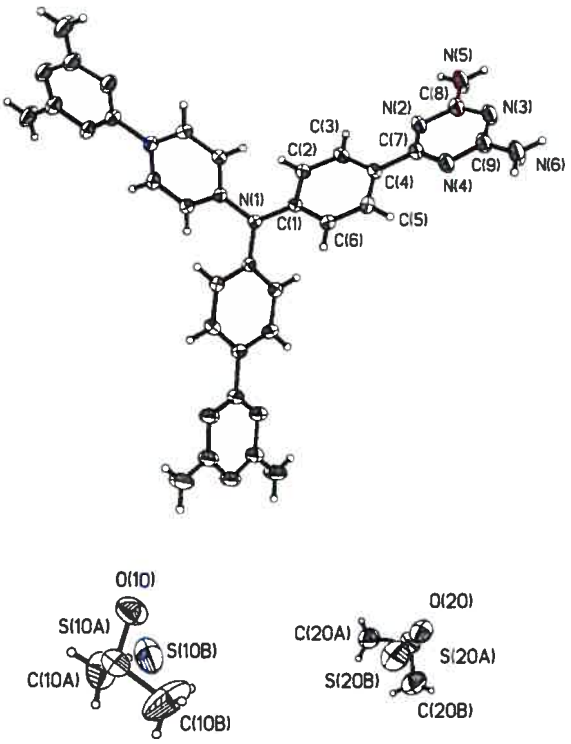

Figure 2.8 ORTEP view of the structure of **1_ADAT** with the numbering scheme adopted. Ellipsoids are drawn at 30% probability level. Hydrogen atoms are represented by a sphere of arbitrary size. Note the presence of two disordered molecules of DMSO.

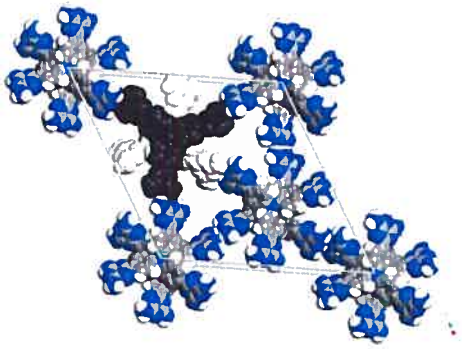

Figure 2.9 Unit cell of tecton **1_ADAT** seen along the *c* axis. Guest molecules (DMSO) are removed for clarity. Carbon atoms are grey, nitrogen atoms are blue and hydrogen atoms are white. One tecton is represented in black and one in white in order to differentiate between adjacent layers. The unit cell is delimited by the solid light grey lines.

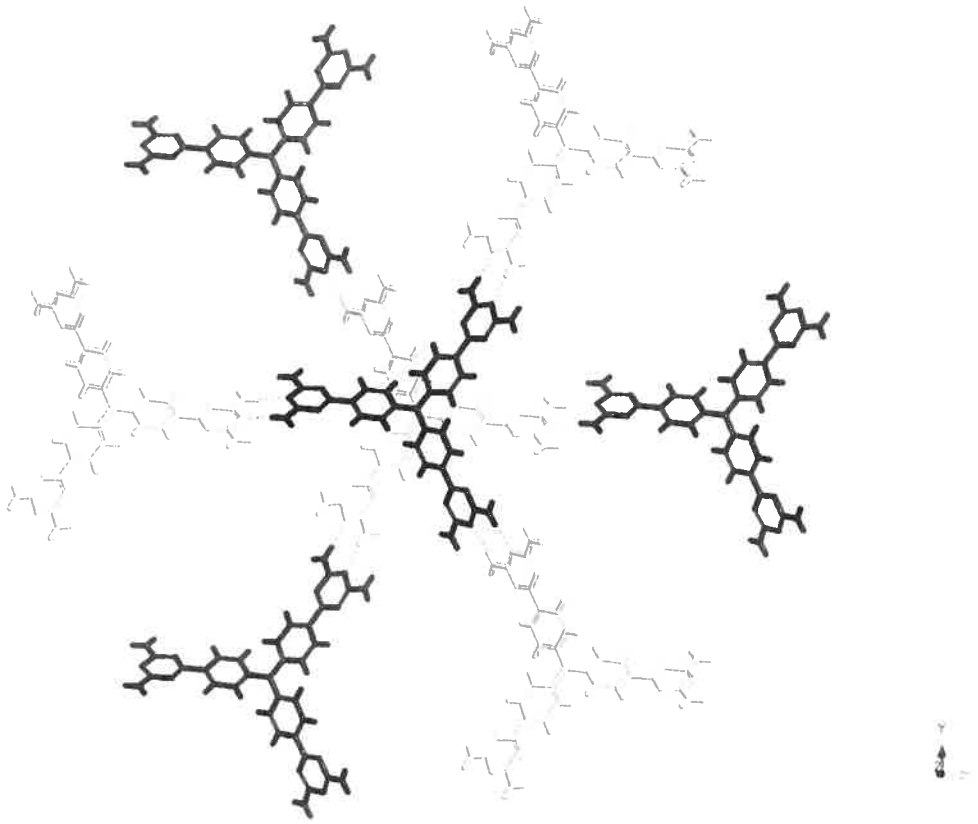

Figure 2.10 Crystal structure of tecton $\mathbf{1_A DAT}$. The chiral tectons shown in black have the *M* configuration and are connected via hydrogen bonding or π-stacking to the tectons shown in white, which are *P*.

The molecules in the crystals are arranged in honeycomb-shaped sheets that are stacked one on top of another (**Figure 2.11**). The structure is elaborated in three dimensions by a series of three repeating sheets, shown in yellow, red and blue. The sheets formed by hydrogen-bonding interactions are connected to one another by π-stacking of adjacent tectons (**Figure 2.12a**). The center-to-center distance of the π-stacked rings in the yellow and blue sheets is 5.077(2) Å and 5.177(2) Å between the blue and red sheets.[119] This layered structure places the central nitrogen atoms in columns with an inter-atomic distance of 4.17(1) Å (yellow-blue) and 4.31(1) Å (blue-red) (**Figure 2.12b**). The proximity of the central nitrogen atoms means that it might

be possible for charge to pass from one atom to the next. Studies have shown that the radical cations of triarylamines have conformations similar to those of the neutral molecules.[120] This means that the integrity of the crystal structure should not be compromised by the transport of charge through the material. In addition, the presence of interconnected channels could permit the flow of a small counter-ion through the structure.

The network defined by the association of tecton **1_ADAT** is porous, having 62% of its volume available for the inclusion or exchange of guest molecules. The porosity is determined by tracing the movement of the center of a sphere along the van der Waals surfaces of the crystal. **Figure 2.13** is a representation of the void spaces in the crystal structure of tecton **1_ADAT**. The image is generated using the "Cavities" option in ATOMS by tracing the movement of the center of a sphere with a radius of 2.5 Å over the van der Waals surfaces of the crystal.[121] Although the structure is porous in all directions, the majority of the space is arranged in channels along the *c* axis. The cavities have a triangular form and have a base that is 13.21 Å across and a height of 11.72 Å.

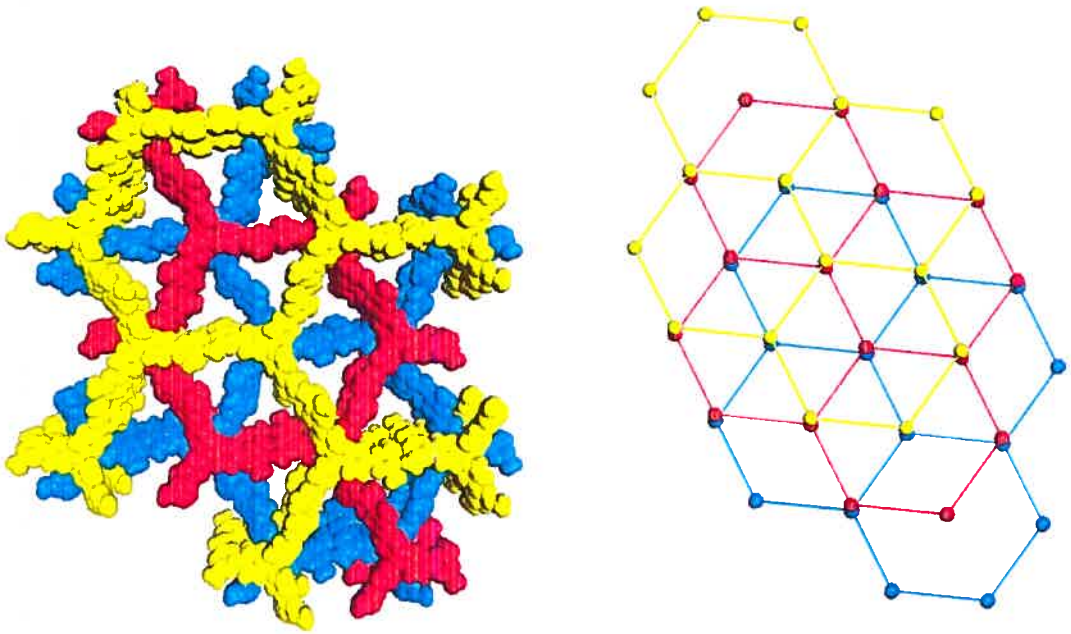

a b

Figure 2.11 Two different views of the layered hydrogen-bonded network present in the crystal of **1_ADAT**. **a)** The network consists of three repeating honeycomb layers, shown in yellow, red and blue. Guest molecules are removed for clarity. The image shows the cross-section of the channels formed by the association of **1_ADAT**. **b)** Representation of the same network. The spheres represent the central nitrogen atoms, which are connected via solid lines that represent the hydrogen-bonding interactions.

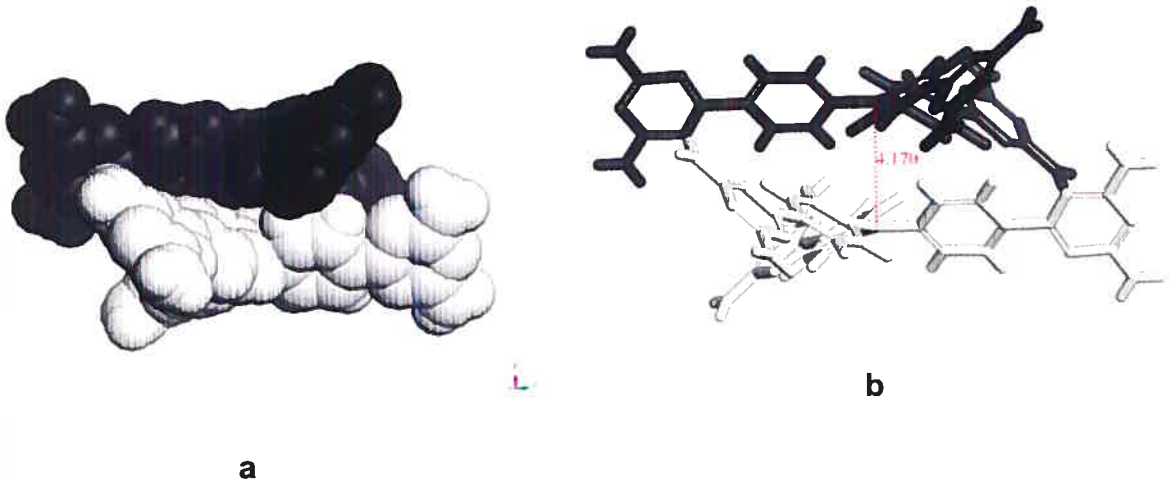

a b

Figure 2.12 **a)** Close packing of two molecules of **1_ADAT**, which results in the formation of columns. **b)** The close packing brings the central nitrogen atoms into proximity.

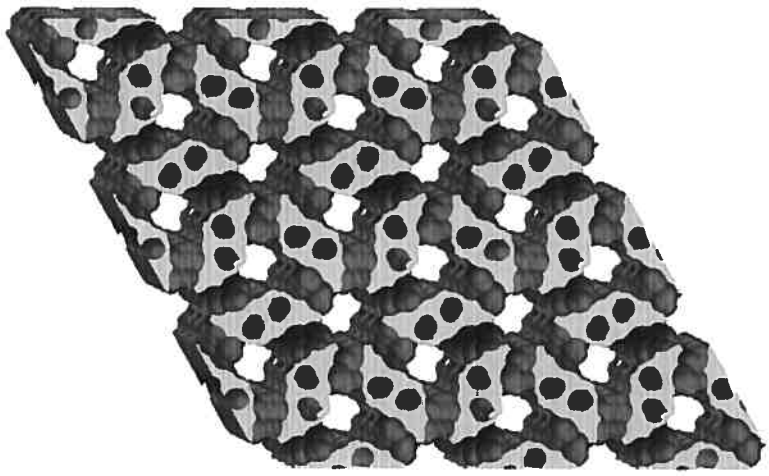

Figure 2.13 Representation of the channels defined by the network formed by tecton $\mathbf{1_A DAT}$. The image shows a 2 x 2 x 2 array of unit cells and is created by tracing the movement of a sphere with a diameter of 2.5 Å over the interior van der Waals surface of the crystal. The channels are shown in grey. Empty portions of the image actually contain molecules of tecton $\mathbf{1_A DAT}$.[121]

In order to expand the study of triarylamines in molecular tectonics, a series of related compounds were prepared. These compounds were carefully selected for their similarity to materials that are important in organic electronics, or for their relationship to other tectons that have been previously examined. The use of "spacer" groups in molecular tectonics is well documented. The strategy generally consists of adding aryl or alkynyl groups between the core of the tecton and their recognition sites in an effort to increase the dimensions of the voids in the open-framework structure. In many cases, however, the crystal structure compensates for increased dimensions of the voids through a phenomenon known as interpenetration.[122,123] Interpenetration occurs when at least two independent hydrogen-bonded networks exist within a crystal. Molecules from one network are not linked to molecules of another network. Interpenetration results in a reduction of the overall space available to included guests within the network. **Figure 2.14** shows the crystal structure of tetrakis(4-

hydroxyphenyl)methane (**26**), which forms a hydrogen-bonded porous architecture when crystallized from ethyl acetate.[124] The tecton (**Figure 2.14a**) forms hydrogen bonds with six nearest neighbours to define a simple cubic network. **Figure 2.14b** is a representation of the two-fold interpenetration that is present in the crystal. Each network occupies part of the void space formed by the other network.

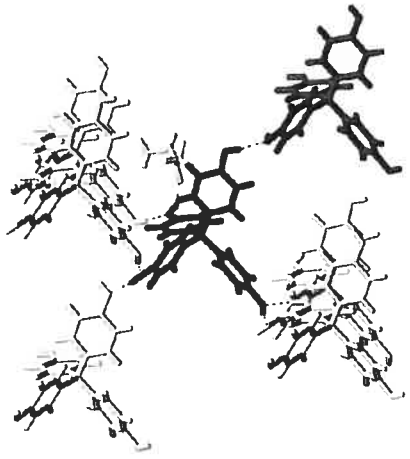

a

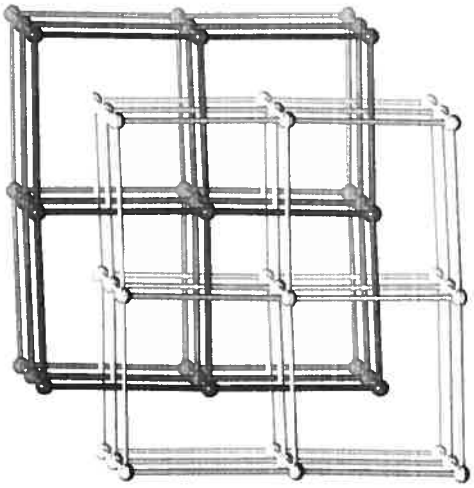

b

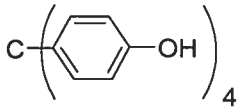

26

Figure 2.14 a) View of the structure of tetrakis(4-hydroxyphenyl)methane (**26**) and included ethyl acetate, showing a central molecule (black) surrounded by its hydrogen-bonded neighbours. **b)** Representation of the two-fold interpenetration present in the cubic network defined by the assembly of tecton **26**. The spheres represent the central carbon atom of each molecule and the solid lines represent the interactions with the six neighbouring tectons.[124]

Tectons **2_ADAT** and **3_ADAT** belong to a logical sequence of expanding tectons starting with **1_ADAT**. The inclusion of aryl and alkynyl groups could result in larger cavities, given the layered architecture and absence of interpenetration in the crystal structure of **1_ADAT** (**Figure 2.11**). Tecton **1_APYR** is similar in size to **1_ADAT** and

presents the opportunity to carry out a detailed comparison of the crystal structures of the two compounds.

In contrast to the other tectons presented here, tecton **1_BDAT** is not limited to a strictly planar geometry. Although the local geometry of each of the nitrogen atoms will be planar trigonal, the overall conformation of the tecton is not so limited. This could lead to the formation of other types of supramolecular architectures.

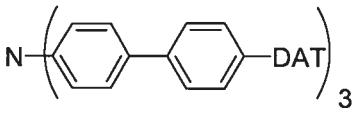

2_ADAT

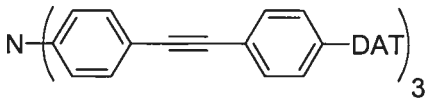

3_ADAT

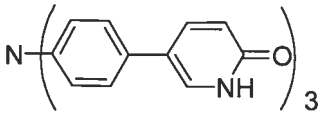

1_APYR

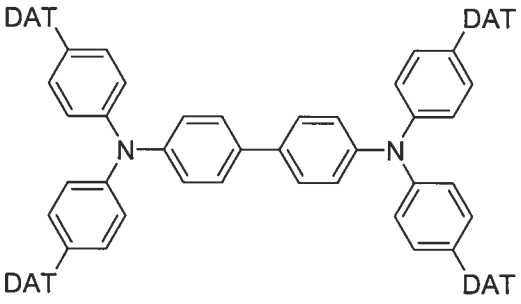

1_BDAT

2.8 Tecton 2_ADAT

2.8.1 Synthesis of Tecton 2_ADAT

The addition of a phenyl group between the triphenylamine core and the diaminotriazine recognition group was selected as a reasonable starting point for expanding the study of triarylamine tectons. In order to keep the number of synthetic

steps to a minimum, the phenyl spacer was introduced already bearing the functional group necessary for the introduction of the recognition group. Tris(4-bromophenyl)amine was subjected to a Suzuki coupling with 4-cyanophenylboronic acid to give tris[4-(4'-cyanophenyl)phenyl]amine (**27**), which was isolated by column chromatography and purified by recrystallization from acetonitrile (**Scheme 2.5**).[125] Such nitriles present interesting intermediates, since it has been shown that in addition to being precursors to other functional groups such as carboxylic acids and amides, they can act as supramolecular building blocks, or synthons, on their own by participating in a variety of weak intermolecular C-H···N interactions.[126] In addition, nitriles are well known for their ability to coordinate metals such as silver and copper.[127]

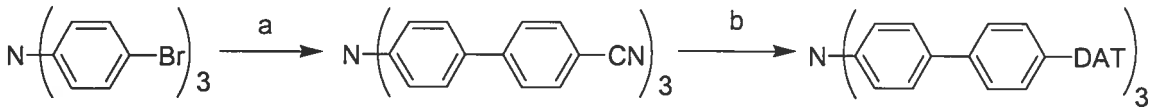

12 **27** **2_ADAT**

Scheme 2.5 a) 4-cyanophenylboronic acid, SPhos, $Pd(OAc)_2$, K_2CO_3, toluene, water, 80 °C, 3 d , 60%; **b)** dicyandiamide, KOH, 2-methoxyethanol, reflux, 85%.

With the nitrile precursor in hand, the introduction of the recognition subunit was achieved via condensation with dicyandiamide under standard conditions to give the diaminotriazine–containing tecton **2_ADAT** as a yellow solid in 85% yield.

2.8.2 Crystallization of Tecton 2_ADAT

As with other compounds containing multiple diaminotriazine groups, tecton **2_ADAT** exhibited poor solubility in most organic solvents. Highly polar solvents such

as DMSO, DMF and various carboxylic acids allowed crystallization attempts to be undertaken. Under such conditions, tecton **2_ADAT** readily crystallized from a wide range of solvent systems, either by vapour or liquid diffusion. However, the bulk of these attempts gave rise to fine, hair-like crystals that were unsuitable for analysis by X-ray diffraction. The only set of conditions that gave crystals large enough to be analyzed involved diffusion of ethanol vapours into a dilute solution of **2_ADAT** in DMSO.

2.8.3 X-Ray Crystallographic Analysis of Tecton 2_ADAT

As expected, tecton **2_ADAT** forms an open-framework hydrogen-bonded crystalline network. The molecule crystallized in the C2/c space group with lattice parameters a = 14.9388(3) Å, b = 22.4945(5) Å and c = 16.0279(3) Å. The unit cell has a volume of 5308.92(19) Å^3 ($\alpha = \gamma = 90^o$, $\beta = 99.707(1)^o$). The ORTEP diagram (**Figure 2.15**) shows that the structure consists of one molecule of tecton **2_ADAT** and one molecule each of ethanol and DMSO. The unit cell is shown in **Figure 2.16**. As in the case of other triarylamines, the central nitrogen atom is planar. The molecule contains a 2-fold axis of symmetry that runs along the molecule from N1 to N3 and follows the b axis of the unit cell. The proximal phenyl rings are tilted at an angle of 44.2^o out of the plane formed by N1, C1', C11 and C11', giving a propeller-like conformation that is similar to the one observed in the crystal structure of tecton **1_ADAT**. This torsion about the central nitrogen makes each molecule chiral. In order to simplify the discussion of the various non-covalent interactions present in the crystal structure, and to differentiate between the different phenyl groups in the tecton, the aromatic rings consisting of C11, C12, C13, C14, C15 and C16, as well as the one

that contains C1', C2, C3, C4, C3' and C2', will be referred to as proximal, since they are close to the nitrogen atom at the center of the tecton. The phenyl rings consisting of C17, C18, C19, C20, C21 and C22, as well as the one containing C5, C6, C7, C8, C7' and C6', will be referred to as distal.

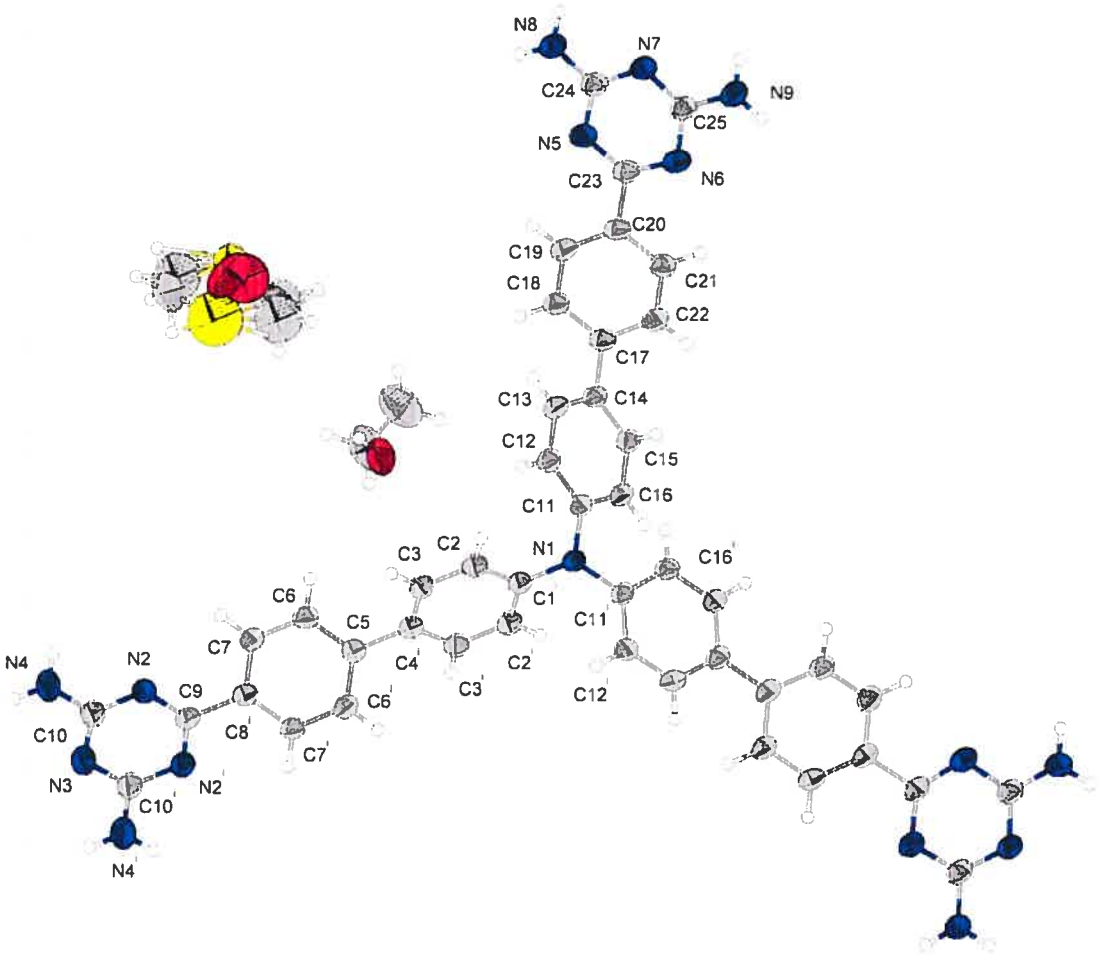

Figure 2.15 ORTEP diagram of **2_ADAT · C_2H_5OH · 1DMSO** drawn at 50% probability. Included molecules of DMSO and ethanol are shown.

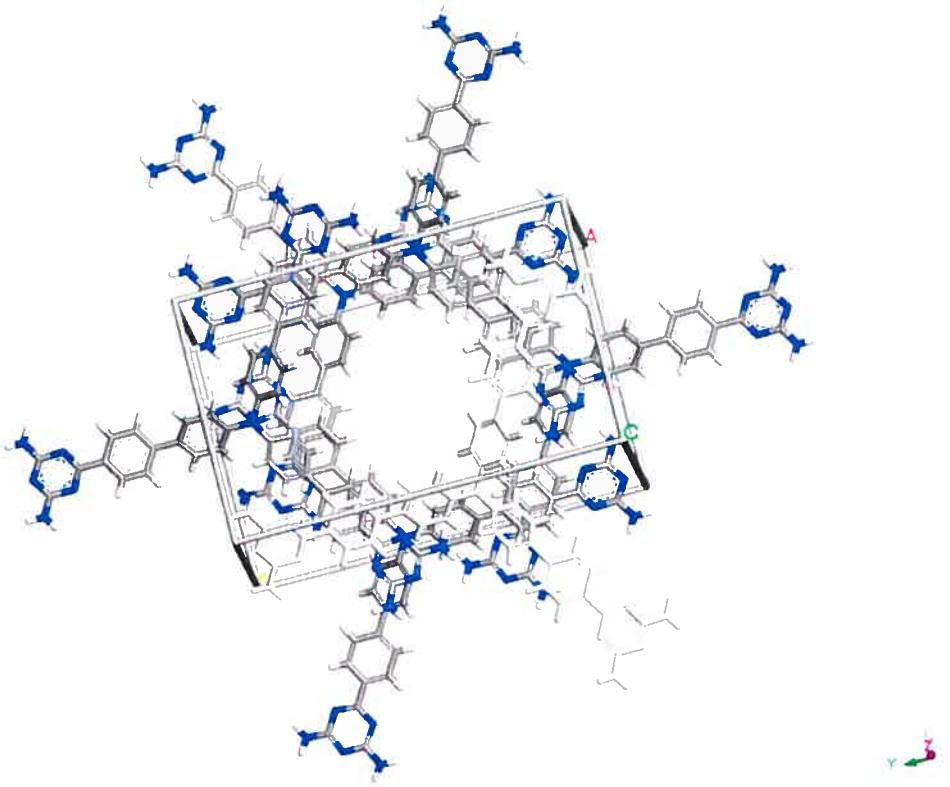

Figure 2.16 Unit cell of tecton **2_ADAT** viewed approximately along the *a* axis. One tecton is shown in white.

Each molecule of tecton **2_ADAT** is hydrogen-bonded to four nearest neighbours as shown in **Figure 2.17**. As in the case of tecton **1_ADAT**, each tecton forms hydrogen bonds only with molecules of opposite chirality. The tecton shown in black is *M* and participates in a side-to-side interaction with each of the molecules shown in grey, which are *P*. In addition, the black tecton participates in a novel recognition motif with each of the two molecules shown in white, which are also *P*. In this interaction, two branches of one molecule form hydrogen bonds with two branches of another molecule. This interaction is referred to hereafter as an *embrace*. The embrace motif consists of two face-to-side hydrogen-bonding interactions (**Figure 1.3**) between

diaminotriazine groups on neighbouring tectons. **Figure 2.18** shows a more detailed view of the hydrogen-bonding pattern of the embrace interaction. Each participant in the embrace has the face of one diaminotriazine group involved in one interaction and the side of one diaminotriazine group involved in the other interaction. As a result of the hydrogen-bonding pattern present in this network, the tectons shown in grey and white in **Figure 2.19** are close-packed. There is a π-stacking interaction between two distal phenyl rings. This interaction has a center-to-center distance of 3.507(13) Å. In addition, there is a C-H$\cdots\pi$ interaction between C15 and one of the distal aromatic rings (**Figure 2.20**). The contact is 3.400(3) Å long (C15 – ring center).

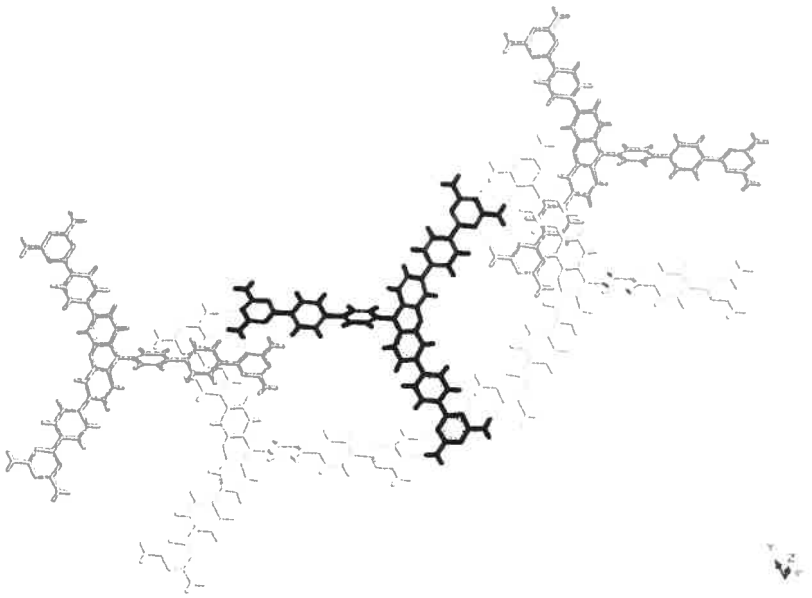

Figure 2.17 View of the crystal structure of tecton **2_ADAT**. The tecton drawn in black has the *M* configuration and is hydrogen-bonded to four nearest neighbours shown in white and grey, which are *P*. Hydrogen bonds are shown as broken lines. Included molecules of DMSO and ethanol are omitted for clarity.

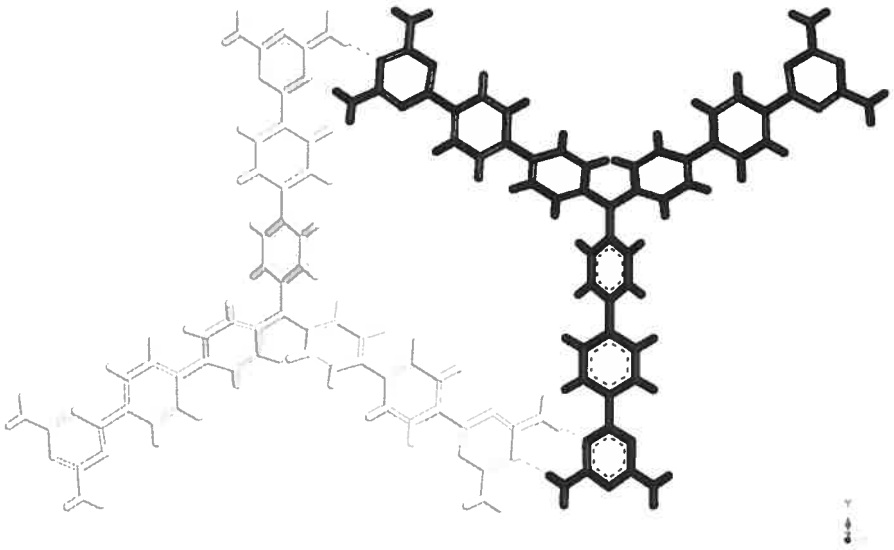

Figure 2.18 View of crystal structure of tecton **2_ADAT**. The tecton in black participates in an embrace interaction with the tecton in white. The embrace consists of two face-to-side interactions.

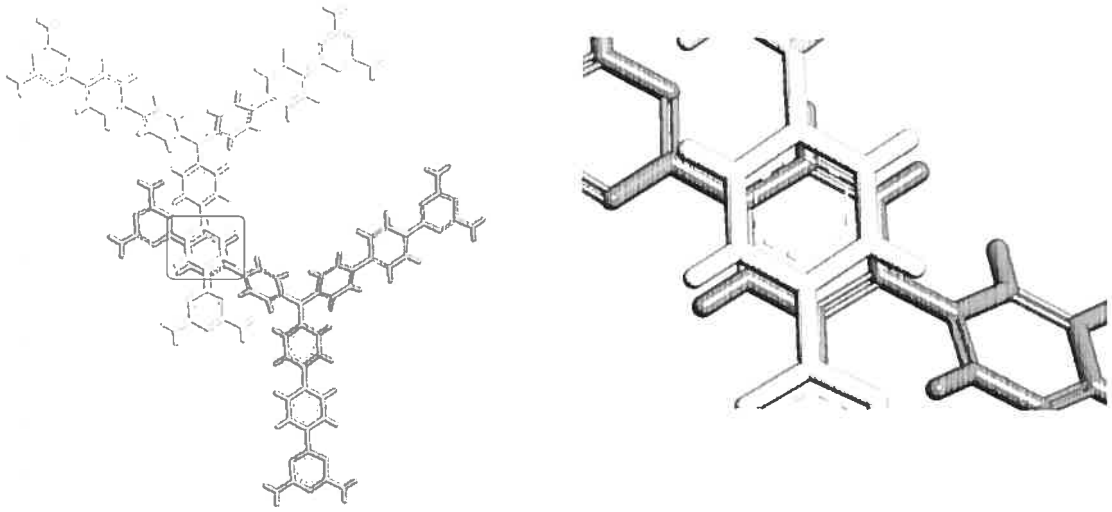

a **b**

Figure 2.19 a) View of the π-π stacking interactions between two distal phenyl rings in the crystal structure of tecton **2_ADAT**. **b)** Magnified view of the same interaction.

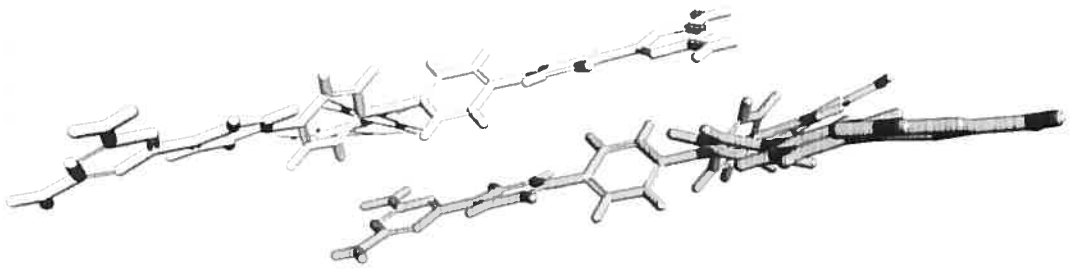

a

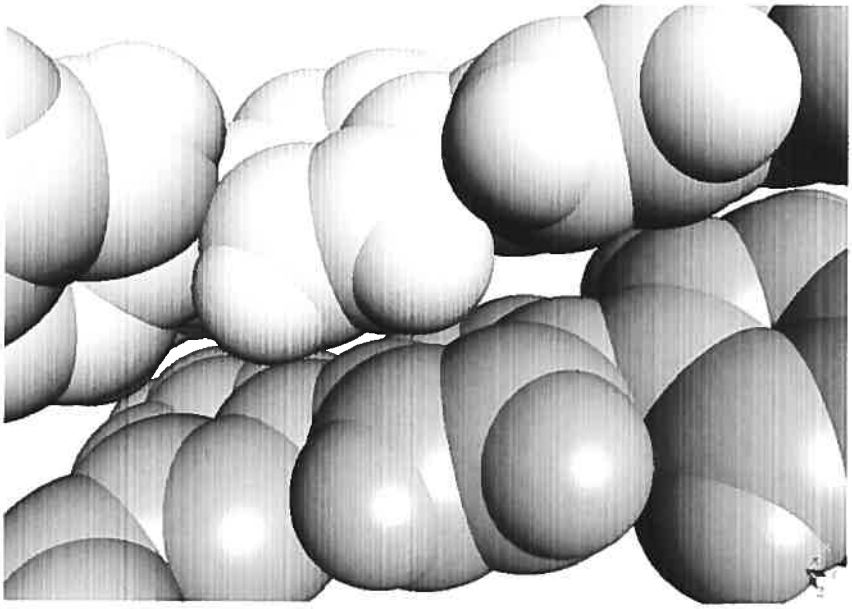

b

Figure 2.20 a) View of the C-H···π interaction present between C15 and one of the distal phenyl rings of tecton **2_ADAT. b)** Magnified space-filling view of the same interaction.

Each tecton participates in twelve hydrogen bonds to other tectons. The infinite hydrogen-bonded network formed by tecton **2_ADAT** defines a distorted diamondoid architecture, represented in **Figure 2.21**. Approximately 36% of the volume of the crystal is available for the inclusion or exchange of guest molecules. **Figure 2.22** is a representation of the channels defined by the network constructed by the self-association of **2_ADAT**. The channels run along the *c* axis and are approximately 7 Å in diameter. A view of the cross section of the channels is shown in **Figure 2.23**. This is in stark contrast to the extensively interconnected void spaces defined by the crystal structure of **1_ADAT**. The extension of the arms of the tecton does not lead to the formation of a network with more space available for the inclusion of guest molecules. The changes to the structure of the molecule cause changes to many different and subtle factors that effect self-association. Examples of these include differences in van der Waals surfaces of the molecules which effect the formation of close contacts. In addition, changes to the angles of torsion in the molecule can influence the manner in which the recognition groups associate. Current understanding of the processes involved in crystallization is inadequate for predicting crystal structures or for thoroughly explaining the differences between the crystal structures of two similar compounds. This highlights the need for the detailed examination and comparison of large numbers of crystal structures.

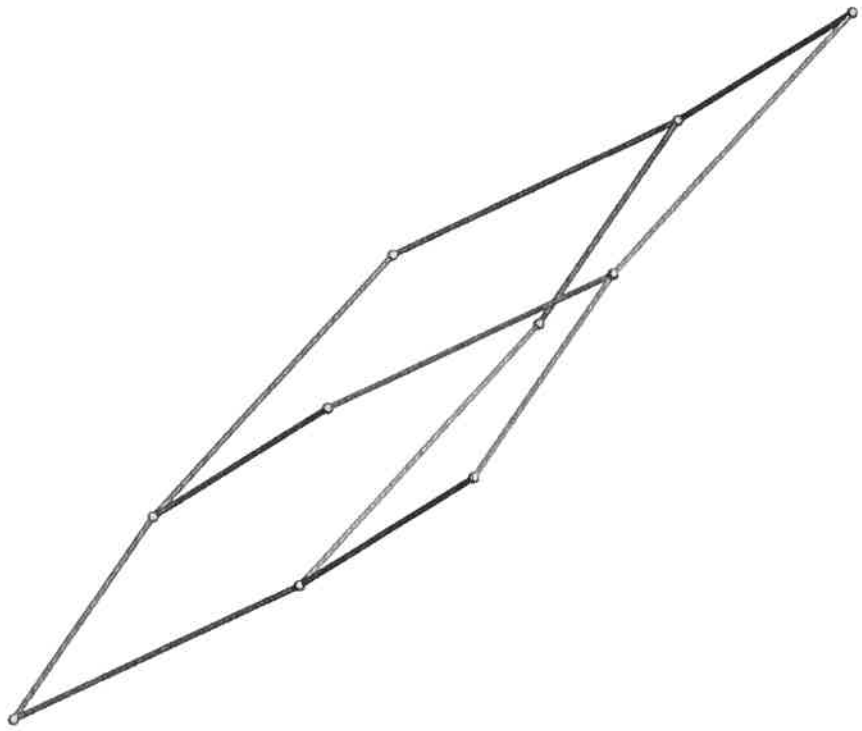

Figure 2.21 Representation of the distorted diamondoid network formed by the association of tecton $\mathbf{2_A DAT}$. In this drawing, the spheres represent the central nitrogen atom of each tecton and the lines represent interactions with neighbouring tectons.

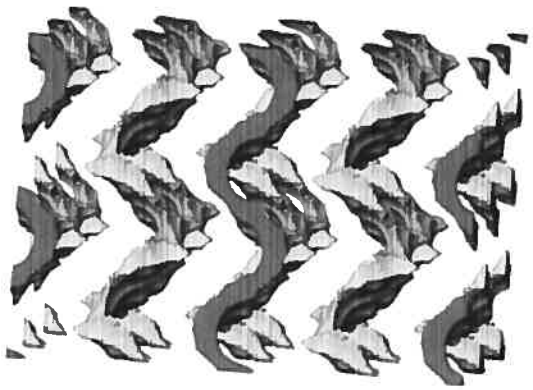

Figure 2.22 Representation of the channels defined by the network constructed from tecton $\mathbf{2_A DAT}$. The image shows a 2 x 3 x 2 array of unit cells viewed roughly along the *a* axis. The outsides of the channels are shown in light grey, and dark grey is used to show where the channels are cut by the end of the array. The channels are defined by the loci of a 2.5 Å diameter sphere as it rolls over the surface of the ordered tectonic network.[121]

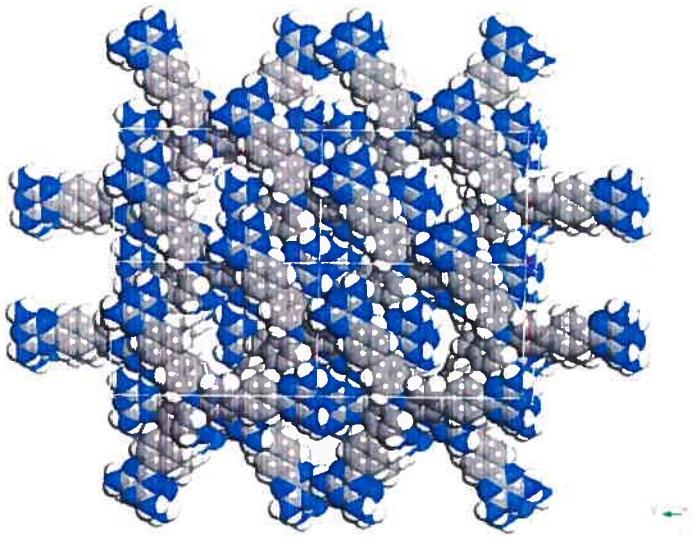

Figure 2.23 Cross section of the channels formed by the association of tecton **2_ADAT** shown along the *c* axis. The figure shows a 2 x 2 x 2 array of unit cells and is shown along the *c* axis. Carbon atoms are shown in grey, hydrogen atoms in white and nitrogen atoms in blue.

2.9 Tecton 3_ADAT

2.9.1 Synthesis of Tecton 3_ADAT

The synthesis of tris[4-([4'-cyanophenyl]ethynyl)phenyl]amine (**32**) has been previously published, and it presents an ideal point from which to access a new tecton.[128] The convergent synthesis of tecton **3_ADAT** is presented in **Scheme 2.6**. The Sonogashira coupling of (trimethylsilyl)acetylene (**28**) and 4-bromobenzonitrile was carried out in a sealed tube. In order to ensure that the product was of sufficient purity to carry out the subsequent steps, the product was purified by column chromatography. 4-[2-(Trimethylsilyl)ethynyl]benzonitrile (**29**) was isolated as a white powder in 67% yield. The protecting group was removed with potassium carbonate

under mild conditions, to afford 4-ethynylbenzonitrile (**30**) in 88% yield.[129] Concurrently, the mercury(II) oxide–promoted iodination of triphenylamine (**24**) was carried out in refluxing ethanol to give tris(4-iodophenyl)amine (**31**).[130] The synthetic routes then converged in the Sonogashira coupling of intermediates **30** and **31**. The reaction proceeded at room temperature in THF to give known tris[4-(4'-cyanophenylethynyl)phenyl]amine (**32**) in 99% yield after column chromatography. Compound **32** was converted into the diaminotriazine- containing tecton **3_ADAT** by condensation with dicyandiamide. Tecton **3_ADAT** was isolated from the reaction mixture as a yellow solid in 84% yield.

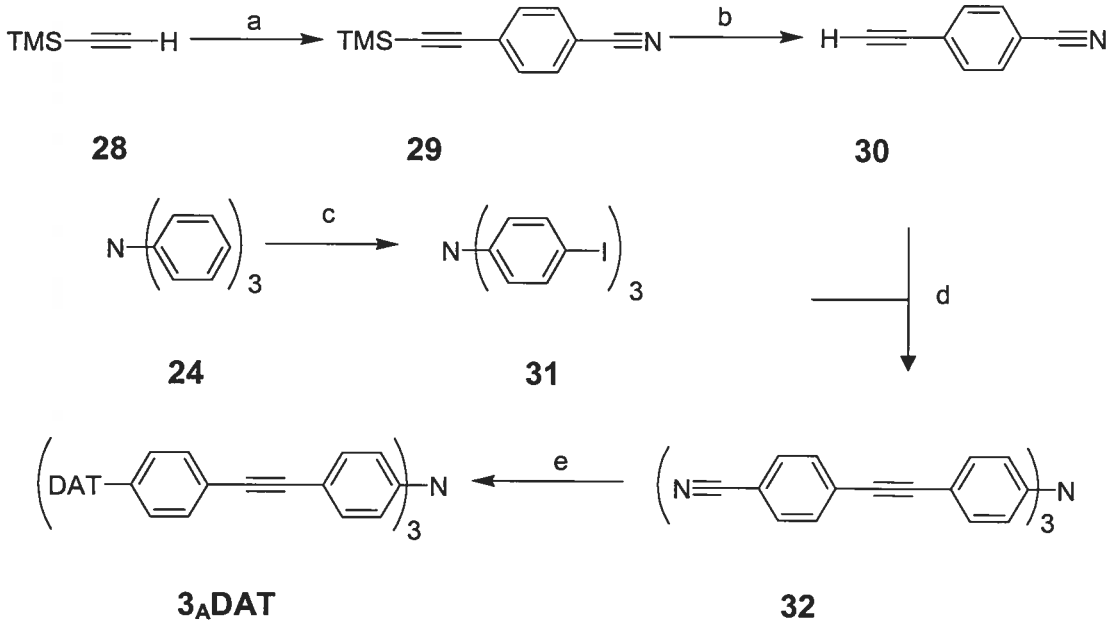

Scheme 2.6 a) 4-bromobenzonitrile, $Pd_2(dba)_3$, CuI, triphenylphosphine, triethylamine, sealed tube, 75 °C, 12 h, 67%; **b)** K_2CO_3, CH_2Cl_2, methanol, 12 h, 88%; **c)** I_2, HgO, ethanol, reflux 18 h, 71%; **d)** $Pd(PPh_3)_2Cl_2$, CuI, THF, triethylamine, 99%; **e)** KOH, dicyandiamide, 2-methoxyethanol, reflux, 84%[128]

2.9.2 Crystallization of Tecton 3_ADAT

With the target molecule in hand, crystallization attempts were undertaken. Methods similar to those used in the crystallization of tectons **1_ADAT** and **2_ADAT** resulted in the formation of crystals but failed to produce any that were suitable for analysis by X-ray diffraction.

2.10 Tecton 1_BDAT

2.10.1 Synthesis of Tecton 1_BDAT

Molecules that contain more than one arylamine moiety, such as the ubiquitous derivatives of tetraphenylbenzidine, are important components of organic electronics. Such compounds are also attractive targets as cores for molecular tectonics, because of their multiple branching points. **Scheme 2.7** depicts the synthesis of a tecton derived from tetraphenylbenzidine (**33**). Freshly recrystallized arylamine **33** was brominated with tetra-*n*-butylammonium tribromide in chloroform. After washing with sodium thiosulfate to remove excess halide and recrystallization from acetic acid, we isolated known target tetrabromide **34** as colourless crystals in 83% yield. Tetrabromide **34** is an important synthetic intermediate, since it opens up the possibility of extending the arms further by adding phenyl or alkynyl groups, or simply introducing carboxylic acids as recognition sites. Reacting **34** with copper(I) cyanide in refluxing DMF gave tetranitrile **35** in 74% yield. The product was sufficiently pure to be employed directly in the following step, but could also be recrystallized from acetonitrile. The conversion of the nitrile groups into diaminotriazines was carried out

by condensation with dicyandiamide under standard conditions and afforded tecton **1_BDAT** in 82% yield after purification.

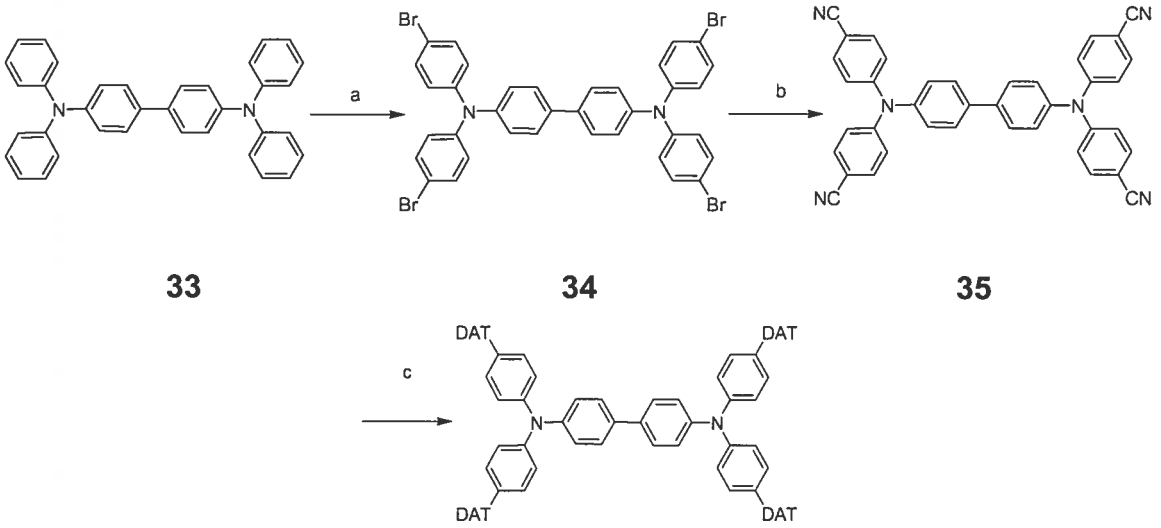

Scheme 2.7 a) tetra-n-butylammonium tribromide, $CHCl_3$, RT, 83%; **b)** CuCN, DMF, reflux, 74%; **c)** dicyandiamide, KOH, 2-methoxyethanol, reflux, 82%.

2.10.2 Crystallization of Tecton 1_BDAT

The common solubility problems encountered in molecular tectonics were exacerbated here by the large, relatively planar geometry of tecton **1_BDAT**. This molecule has only marginal solubility in DMSO, DMF and formic acid. Regardless, crystals suitable for analysis by X-ray diffraction were obtained by the diffusion of ethanol vapours into a solution of **1_BDAT** in DMSO.

2.10.3 X-Ray Crystallographic Analysis of Tecton 1_BDAT

Tecton **1_BDAT** crystallized as an open-framework supramolecular structure maintained by extensive hydrogen bonding. The ORTEP diagram in **Figure 2.24**

shows that the fundamental composition of the crystals consists of one molecule of tecton **1_BDAT**, two molecules of DMSO and one molecule of ethanol. The compound crystallized in the P-1 space group, with a = 10.3770(13) Å, b = 11.3536(12) Å and c = 16.1445(17) Å. The unit cell has a volume of 1759.2(3) Å^3 (α = 105.854(6)°, β = 105.309(6)°, γ = 90.104(16)°), as shown in **Figure 2.25**. The conformation of the tecton is such that it contains a center of inversion in the middle of the bond between C1 and C1'. The biphenyl core of **1_BDAT** is twisted nearly 60° out of the plane formed by the two arms that bear the DAT groups. Unlike tectons **1_ADAT** and **2_ADAT**, tecton **1_BDAT** has a center of inversion and is achiral.

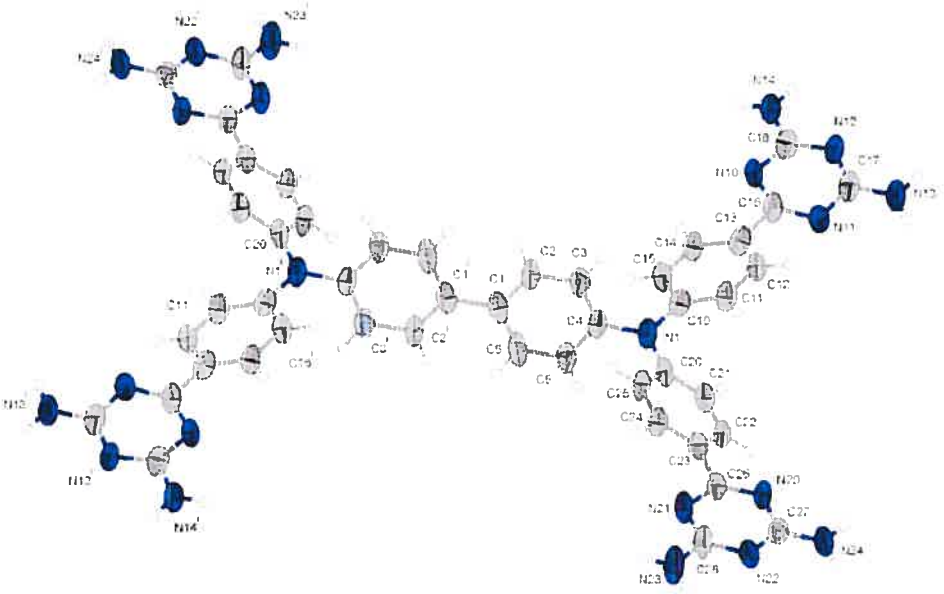

Figure 2.24 ORTEP diagram of tecton **1_BDAT · 2 DMSO · 1 CH_3CH_2OH**, with the numbering scheme. Thermal ellipsoids are drawn at 50% probability.

Each tecton is hydrogen-bonded to four nearest neighbours (**Figure 2.26**). The two molecules shown in grey form face-to-face hydrogen-bonding interactions (**Figure**

1.3) with the central tecton, drawn in white. In addition the two black tectons each participate in an embrace interaction with the white molecule.

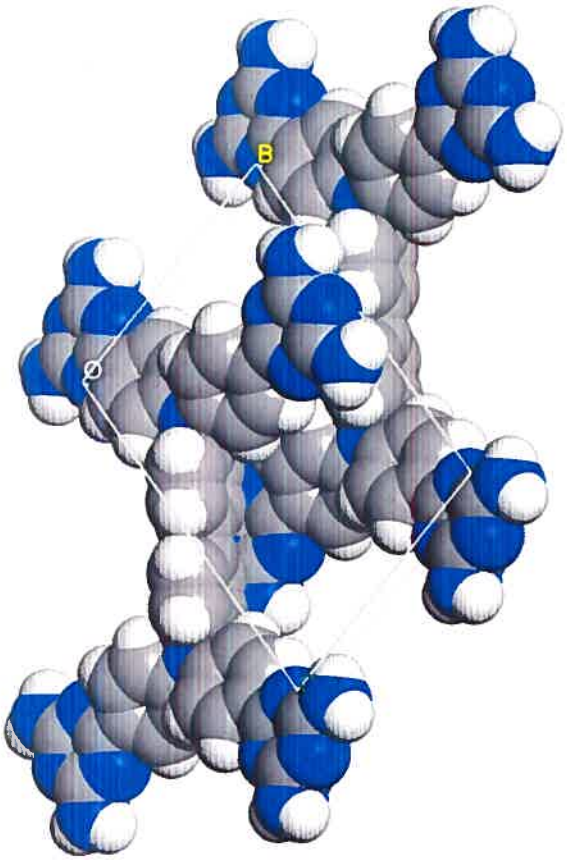

Figure 2.25 Unit cell of tecton **1_BDAT** seen approximately along the *a* axis. Solvent molecules have been removed for clarity.

The hydrogen-bonding pattern creates a two-dimensional sheet that runs diagonal to the *b* axis. These sheets are elaborated into a three-dimensional architecture via aromatic π-stacking. The superstructure is made up of two offset layers, as shown in **Figure 2.27**.

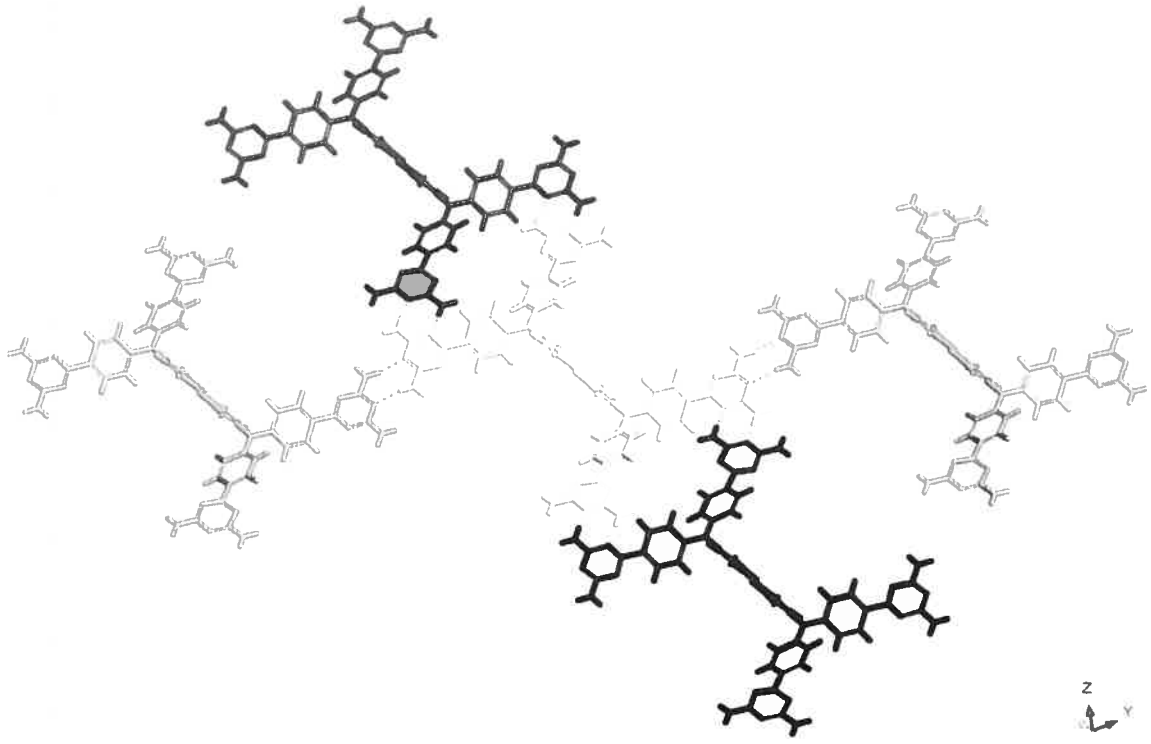

Figure 2.26 Hydrogen bonding in the crystal structure of tecton **1_BDAT**. One tecton, shown in white, forms a face-to-face interaction with each of the tectons shown in grey. In addition, the white molecule participates in an embrace interaction with each of the tectons shown in black. Hydrogen bonds are shown as broken lines.

The repeating layers are held together by π-stacking between the arms of the tectons in adjacent layers. The phenyl group of one molecule interacts with a diaminotriazine ring in the next layer, as shown in **Figure 2.28**. The inter-layer distance is 4.350(3) Å (center-to-center). Adjacent layers are also connected by a C-H···π interaction between C2 and one of the DAT groups. The interaction has a distance of 3.574(5) Å and is shown in **Figure 2.29**. Together, these two weak interactions serve to elaborate the two-dimensional hydrogen-bonded sheets into a three-dimensional structure.

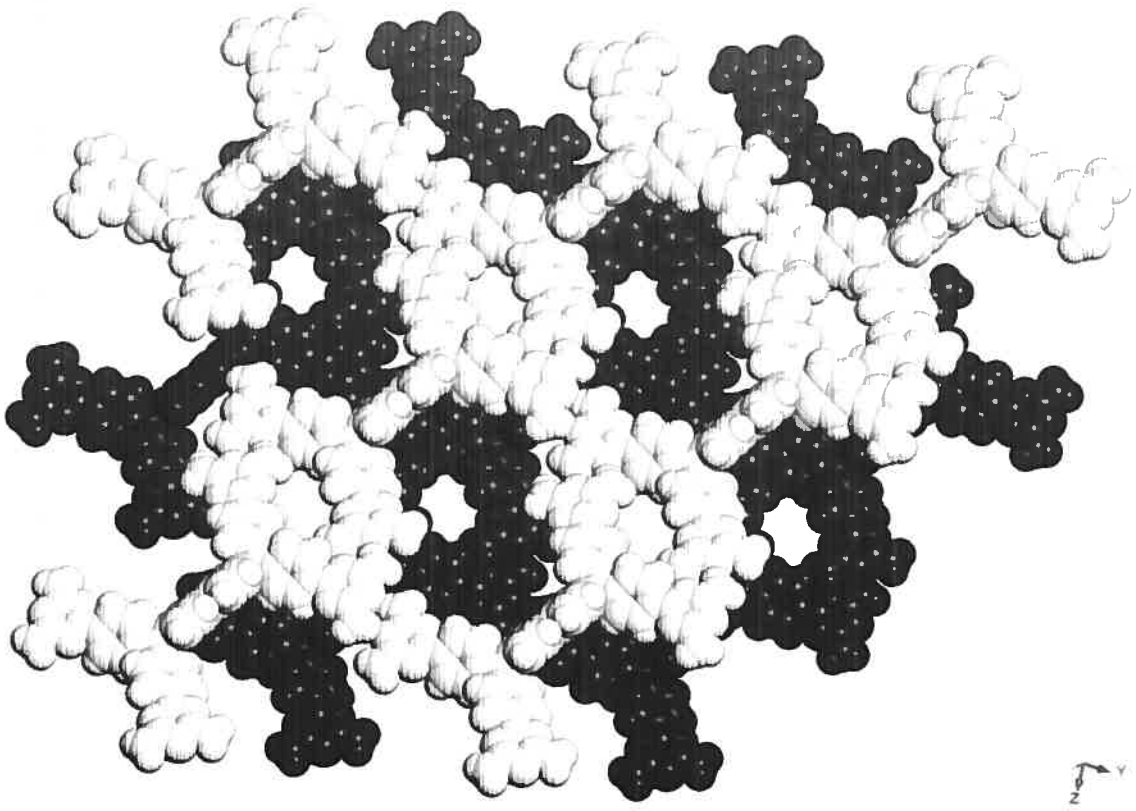

Figure 2.27 Adjacent sheets (black and white) formed by the hydrogen-bonding interactions of tecton **1_BDAT** are stacked via edge-to-face π-interactions to extend the network into three dimensions. The cross sections of the channels formed by the network are also visible.

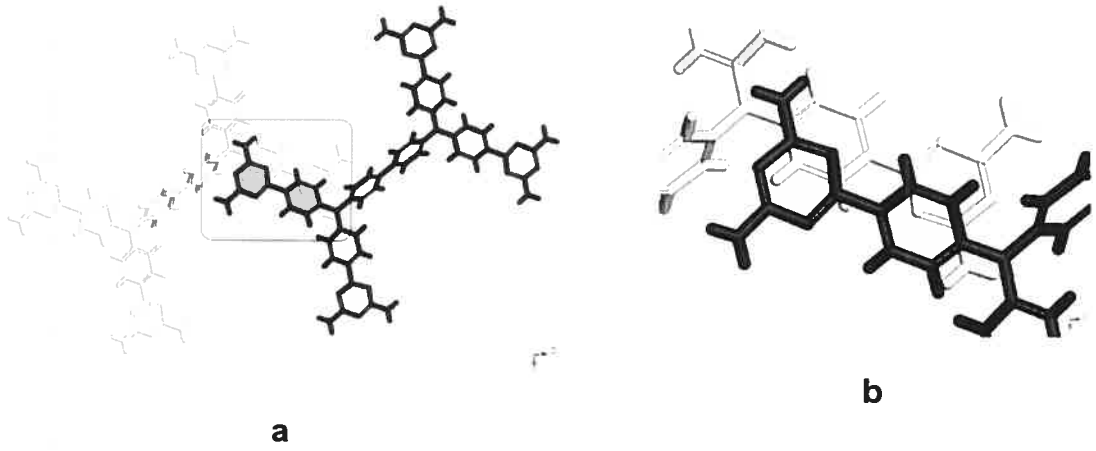

Figure 2.28 a) View of the π-stacking interaction present in the crystal structure of tecton **1_BDAT**. The interaction occurs between tectons in adjacent layers. **b)** Magnified view of the same interaction.

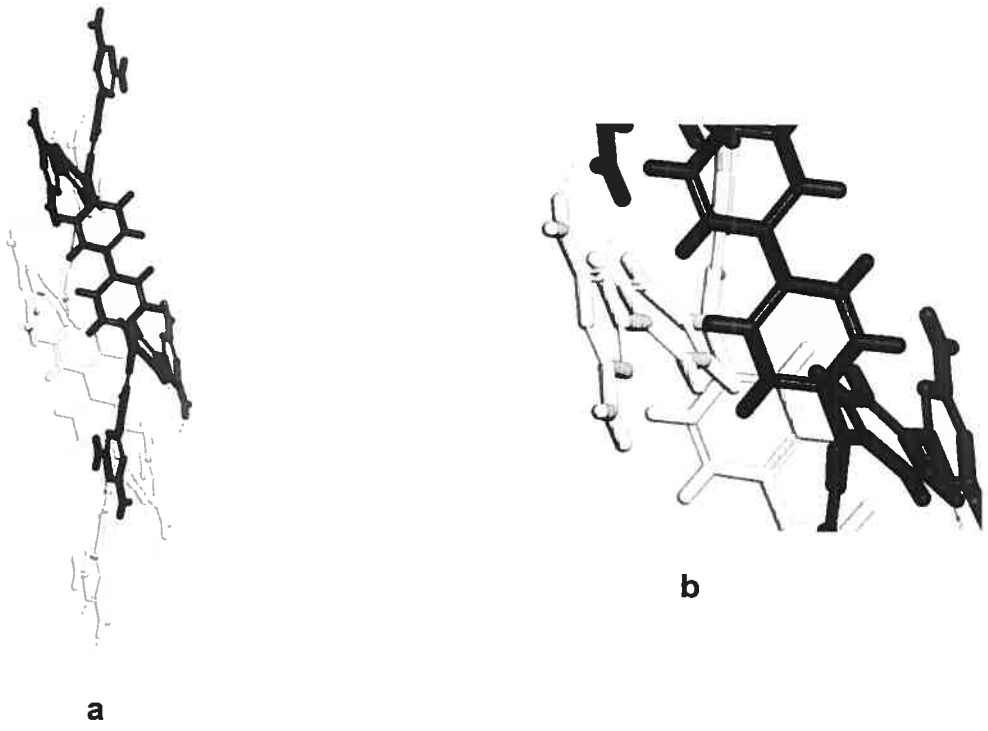

Figure 2.29 a) View of the C-H···π interaction present in the crystal structure of tecton **1_BDAT**. **b)** Magnified view of the same interaction.

The hydrogen-bonding interactions describe a distorted hexagonal network (**Figure 2.30**). Each layer has void spaces inside each hexagon, but the offset positioning of adjacent layers significantly reduces the overall space available for the inclusion of guest molecules. As a result the crystals have a porosity of 46%.[131]

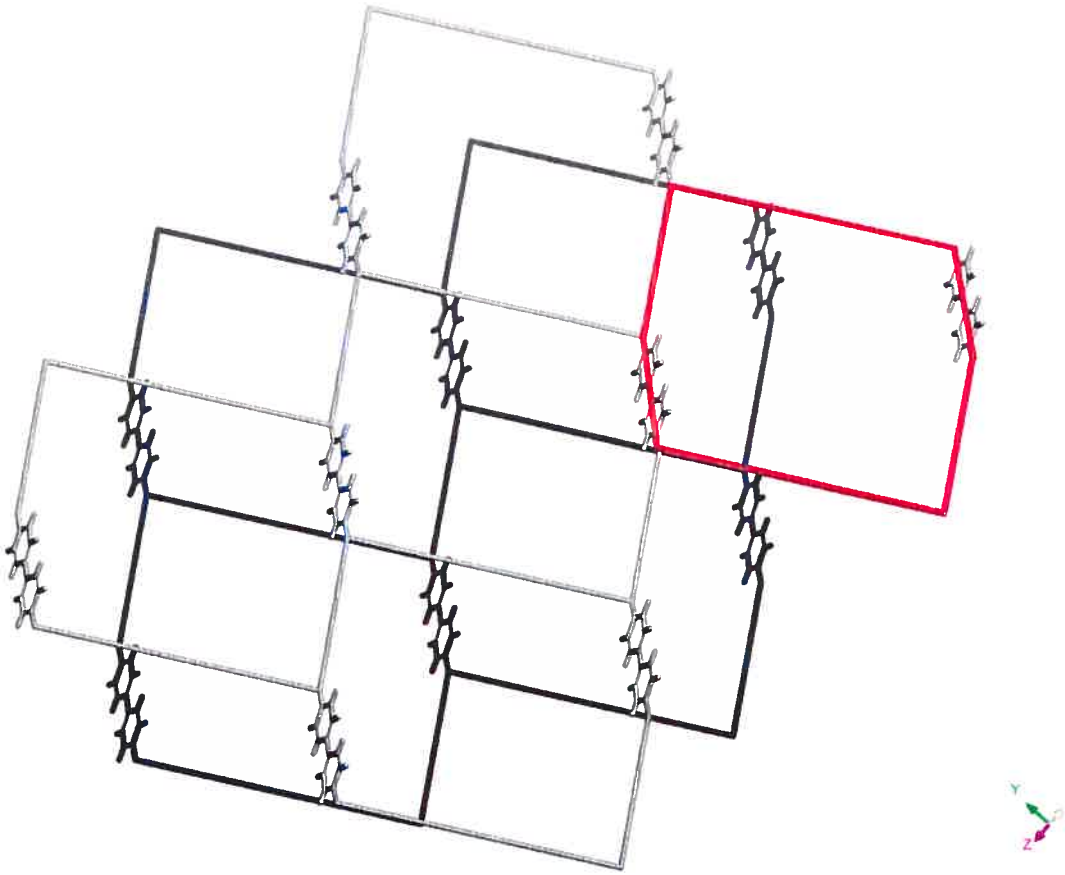

Figure 2.30 Representation of the network formed by the association of tecton **1_BDAT** viewed roughly along the *a* axis. In this drawing, the biphenyl cores that connect the aryl nitrogens are shown. The solid lines represent the association between the tectons. The red overlay shows the distorted hexagon that is repeated to form the network.

Figure 2.31 is a representation of the void spaces in the supramolecular structure formed by the association of tecton **1_BDAT**. The channels are drawn by tracing the movement of the center of a sphere with a diameter of 2.5 Å over the van der Waals surfaces defined by the ordered network of tecton **1_BDAT**. The channels

run roughly parallel to the *c* axis. The channels are comprised of larger pockets with narrow connections, due to the offset position of adjacent layers of molecules. The cross section of the channels can be seen in **Figure 2.27**.

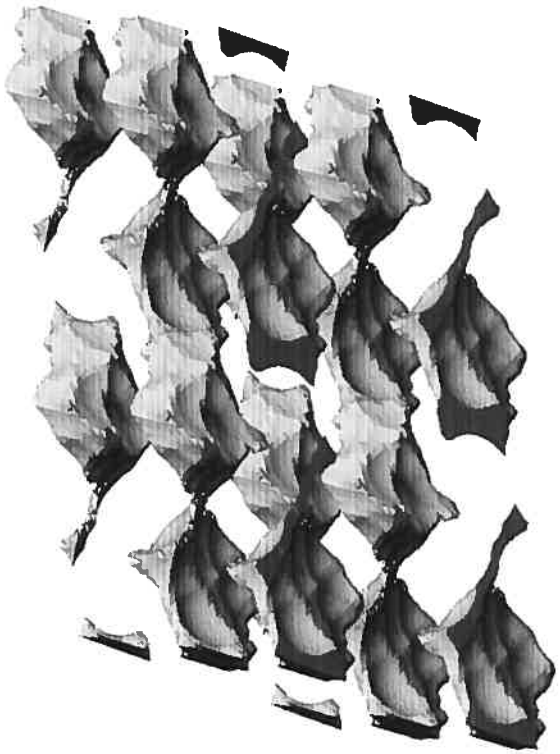

Figure 2.31 Representation of the channels defined by the association of tecton **1_BDAT**. The image shows a 2 x 2 x 2 array of unit cells as seen along the *a* axis. The drawing describes the locus of the center of a sphere with a 2.5 Å diameter rolling along the van der Waals surface inside the crystal.[121]

2.11 Tecton 1_APYR

Although diaminotriazines have become prominent as recognition groups in molecular tectonics, other groups such as carboxylic and boronic acids have also been the object of intense research efforts. One of the first families of recognition subunits studied in the context of molecular tectonics were pyridinones.[132] Pyridinones are of interest in molecular tectonics because they are readily grafted

onto a wide range of molecular cores and have a reasonably predictable recognition pattern. Pyridinones are well known for forming dimers by hydrogen bonding (**Figure 2.32**).[133,134] **Figure 2.33** shows a sample of the wide range of tectons that bear pyridinones as their recognition group. The accessible synthesis and the element of predictability in self-association, which is less strong in the case of diaminotriazines, made tecton **1_APYR** an attractive target.

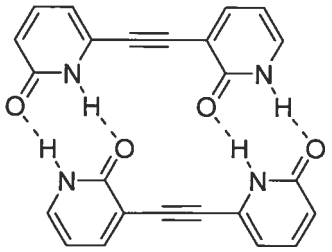

Figure 2.32 Hydrogen-bonded dimer of a bis(pyridinone).

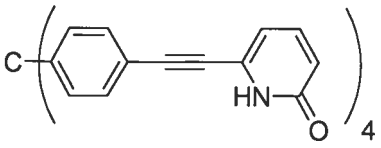

36

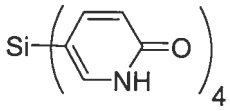

37

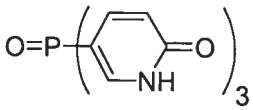

38

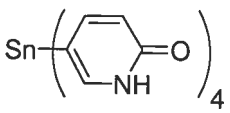

39

Figure 2.33 Previously synthesized tectons bearing pyridinones as the recognition group.[34,133]

2.11.1 Synthesis of Tecton 1_APYR

Scheme 2.8 describes the synthesis of tecton **1_APYR** from tris(4-bromophenyl)amine (**12**). The protected 2-pyridinone recognition site was introduced by the Suzuki coupling of compound **12** and 2-(benzyloxy)-5-(5,5-dimethyl-1,3,2-dioxaborinan-2-yl)pyridine catalyzed with palladium (II) acetate and SPhos (**11**).[135] The product, tris[4-([2'-benzyloxy]pyridinyl)phenyl]amine (**40**) was purified by column chromatography and isolated in 59% yield. The benzyl group was removed by deprotection with trifluoroacetic acid. The pure compound was isolated by evaporation of the acid, followed by quenching with ammonium hydroxide. Tecton **1_APYR** was recovered as a white solid in 99% yield. [34]

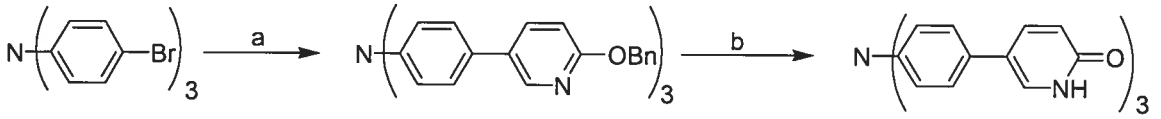

12 **40** **1_APYR**

Scheme 2.8 a) 2-(benzyloxy)-5-(5,5-dimethyl-1,3,2-dioxaborinan-2-yl)pyridine, $Pd(OAc)_2$, SPhos, K_3PO_4, toluene, water, 100 °C, 18 h; **b)** trifluoroacetic acid, RT, 99%

2.11.2 Crystallization of Tecton 1_APYR

The target tecton was crystallized from DMSO-ethanol. Remarkably, the white solid dissolved in DMSO only upon gentle heating, and it formed a purple solution. Upon addition of ethanol, the rapid formation of blue crystals was observed. These crystals proved to be surprisingly robust compared to those of other tectons, and they maintained their birefringence for months while exposed to the atmosphere.

2.11.3 X-Ray Crystallographic Analysis of Tecton 1_APYR

As expected, tecton **1_APYR** associates in the solid state to form an extensively hydrogen-bonded network. The ORTEP diagram (**Figure 2.34**) shows that the crystal consists of the tecton as well as one molecule each of DMSO and ethanol. **Figure 2.35** is a representation of the unit cell of tecton **1_APYR**. The compound crystallizes into the $P2_1/c$ space group with a = 13.8423(5) Å, b = 18.6565(6) Å and c = 12.3250(4) Å^3. The unit cell has a volume of 3002.01(17) Å ($\alpha = \gamma = 90$ °, β = 109.410(2) °). For clarity, the tectons in the unit cell are coloured according to their orientation. Accordingly, two tectons are shown in white and two in black.

As expected, each arm participates in a hydrogen-bonding interaction, via the classic motif of pyridinone dimerization illustrated in **Figure 2.32**. This results in three nearest neighbours as shown in **Figure 2.36**. As in the case of the other tectons derived from triphenylamine, each molecule is chiral in the solid state. In **Figure 2.36**, the tecton in white adopts the *P* configuration while its three neighbours shown in black have the *M* configuration. As a result, the network is achiral.

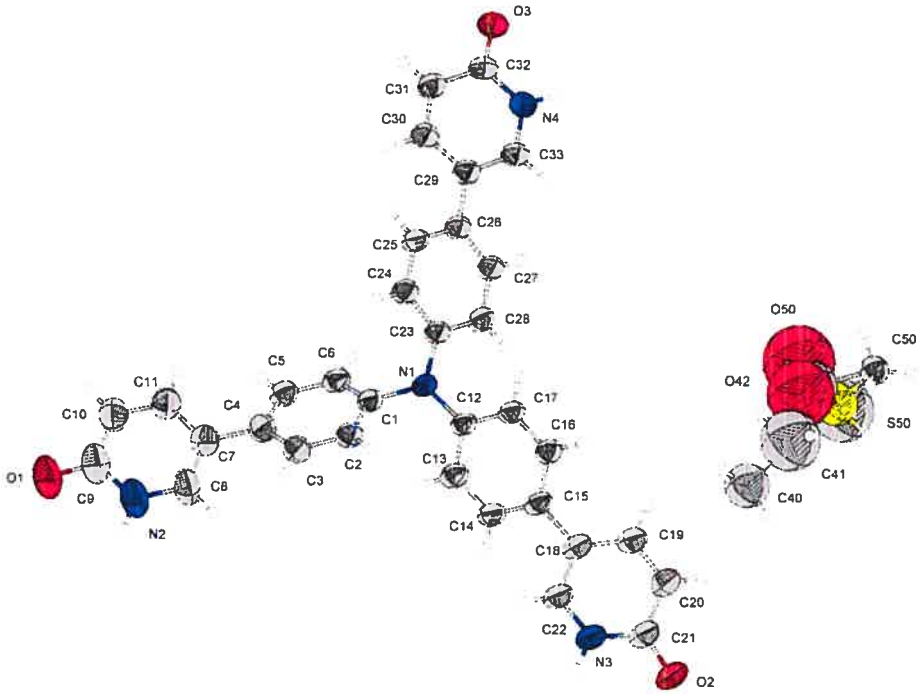

Figure 2.34 ORTEP diagram of tecton **1_APYR** with numbering scheme shown. Thermal ellipsoids are drawn at 50% probability.

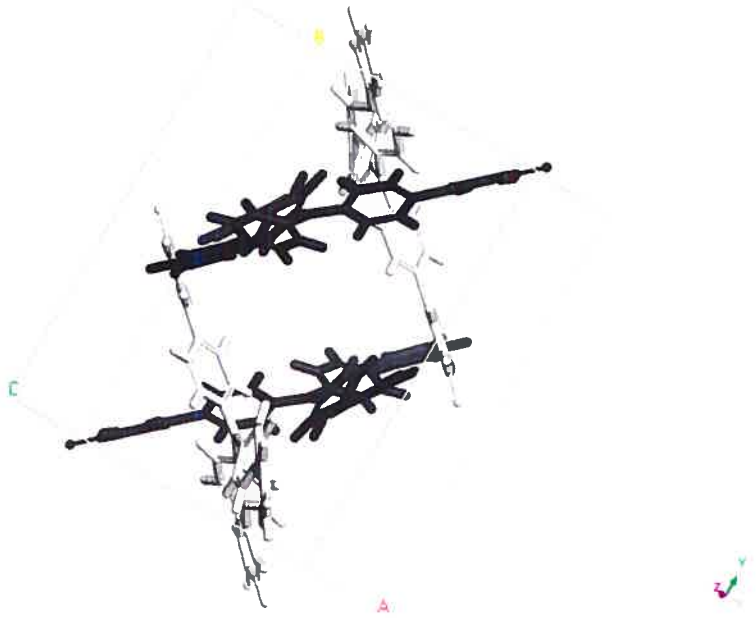

Figure 2.35 Unit cell of tecton **1_APYR** seen roughly along the *c* axis. Parallel tectons are illustrated in the same colour. Solvent molecules are removed for clarity.

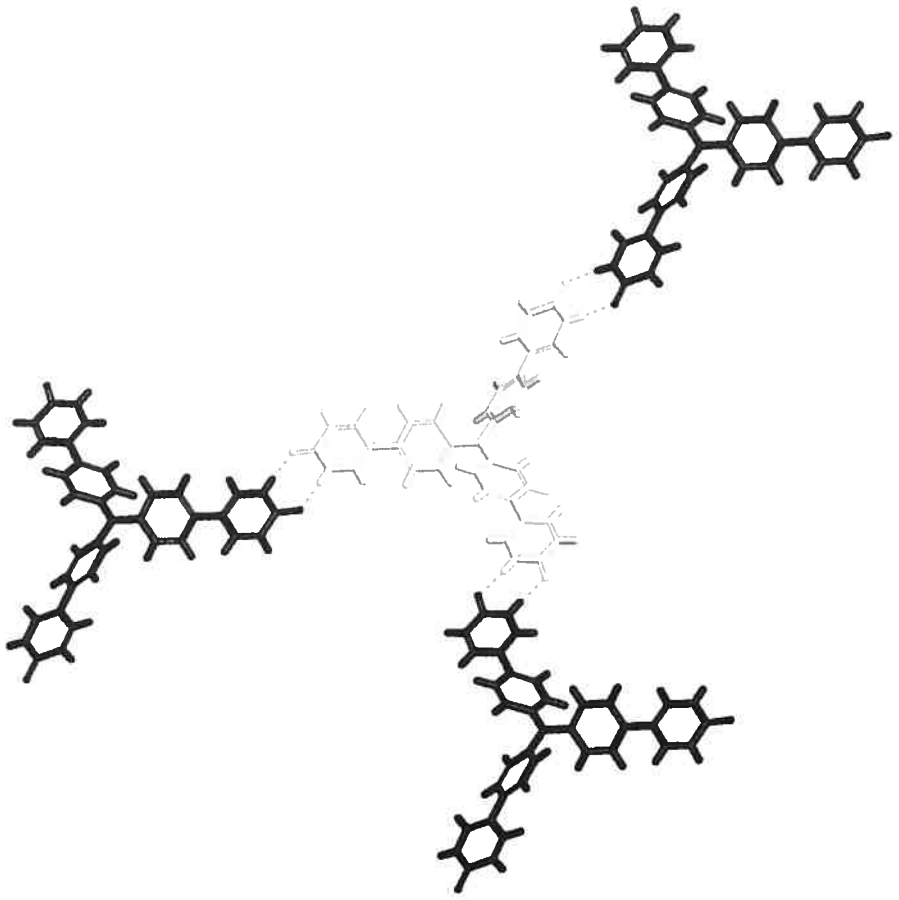

Figure 2.36 One molecule of tecton **1_APYR**, shown in white, forms hydrogen bonds with three neighbours, shown in black. Hydrogen bonds are represented by broken lines.

The hydrogen-bonding interactions describe a two-dimensional hexagonal layer. Adjacent layers are connected by π-stacking interactions. The shortest of these interactions occurs between two pyridinone groups. The two rings are offset and have a center-to-center distance of 3.766(3) Å, as shown in **Figure 2.37**.

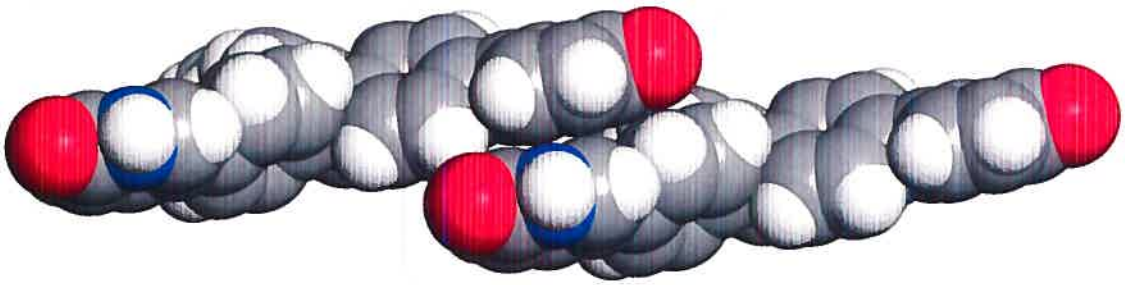

a

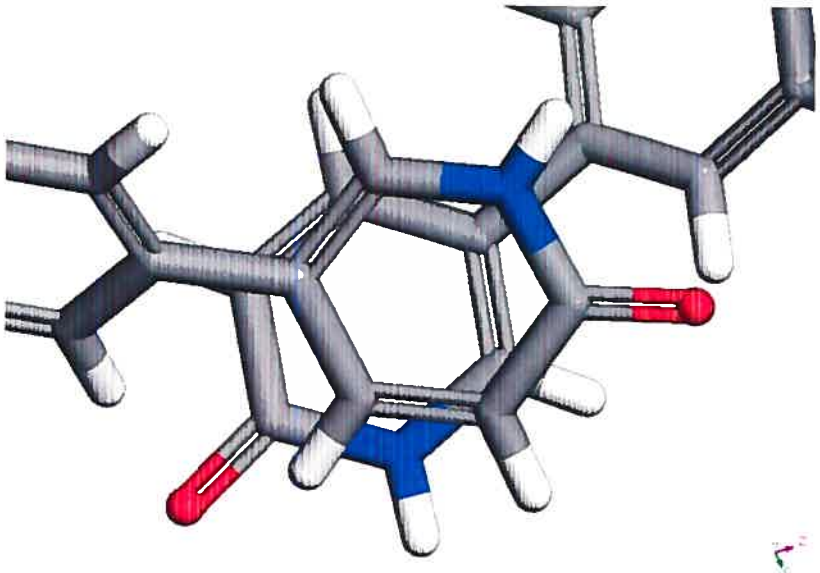

b

Figure 2.37 a) Space-filling model of the π-stacking interaction between molecules in adjacent layers in the crystal structure of tecton $\mathbf{1_A}$**PYR**. **b)** Magnified view of the same interactions, shown perpendicular to the first image.

The hexagons that form each layer are irregular and have dimensions of 45.18 x 33.79 x 34.98 Å. There are two sets of sheets that are orthogonal to one another. The two orthogonal sets of sheets give rise to eight-fold interpenetration, which leads to a significant decrease in the porosity of the system (**Figure 2.38**). The interpenetration can be classified as 2D-inclined.[122] The extensive interpenetration

means that only 21% of the volume of the crystal is available for the exchange or inclusion of guest molecules.[131] Nevertheless, there are channels that run parallel to the *c* axis (**Figure 2.39**). The channels are rectangular, with dimensions of 8.66 Å by 9.45 Å across. The reduced porosity of the system may explain the enhanced stability of crystals of $\mathbf{1_APYR}$ with respect to the other crystals in this study, which are quite fragile.

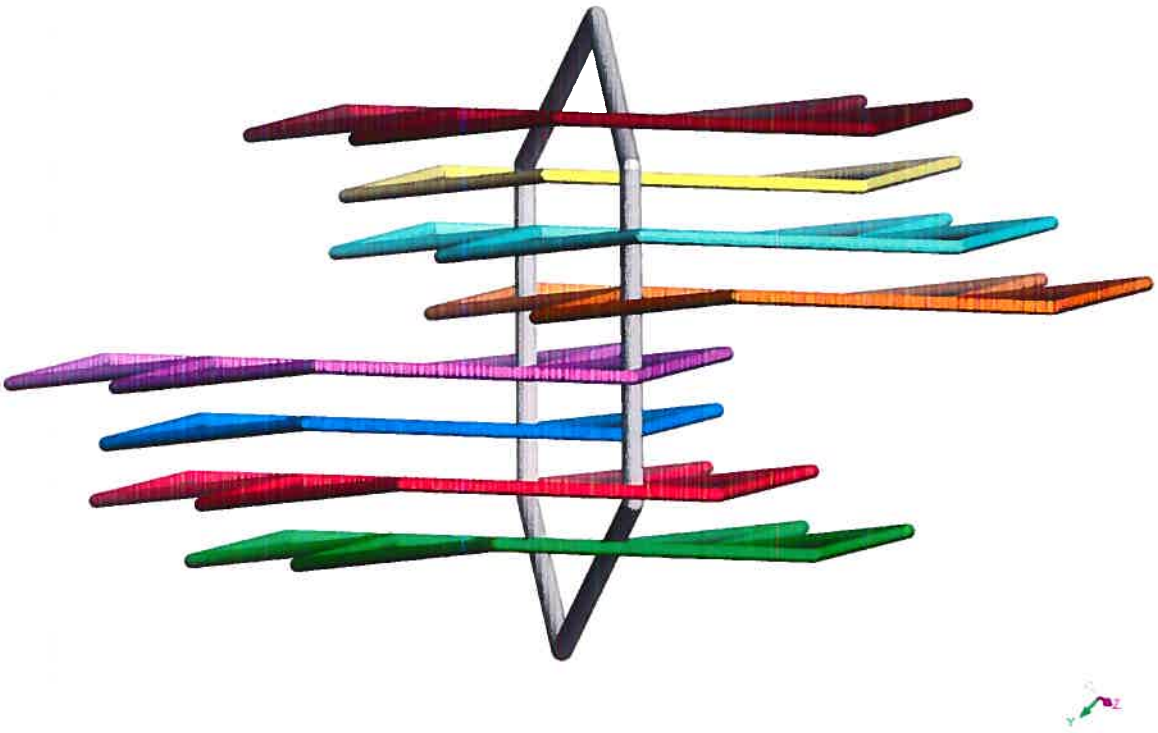

Figure 2.38 Representation of the network formed by the association of tecton $\mathbf{1_APYR}$. The hexagons are drawn by connecting the central nitrogen atoms of hydrogen-bonded neighbours. The 2D inclined network exhibits eight-fold interpenetration.

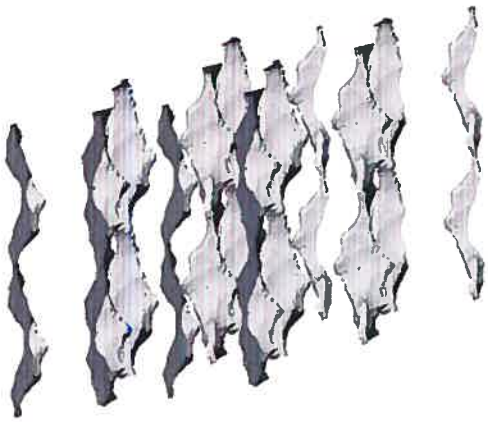

a

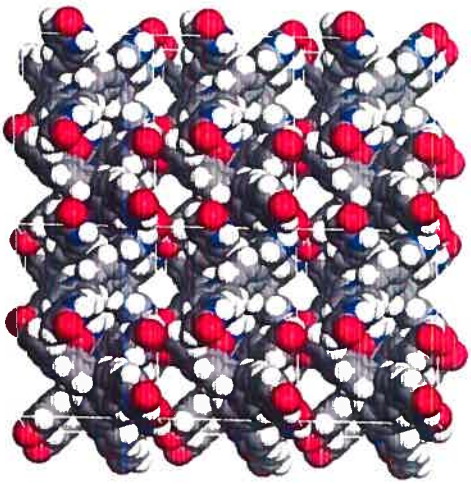

b

Figure 2.39 **a)** Representation of the channels formed by the network resulting from the association of tecton $\mathbf{1_A PYR}$. The drawing shows a 2 x 2 x 2 array of unit cells and is displayed roughly along the *a* axis. The channels are defined by tracing the movement of the center of a sphere of 2.5 Å as it rolls along the van der Waals surfaces of the network.[121] **b)** Cross section of the same channels. The figure shows a 3 x 3 x 3 array of unit cells and is displayed along the *c* axis.

The crystallographic data do not explain the colour of the crystals. No counter-ions were observed, and the possibility of the compound forming a salt with itself was eliminated because the only labile proton is seen clearly by X-ray diffraction.

2.12 Further Explorations

2.12.1 Poly(triaryl)amines

In order to expand the scope of this study even further, the use of other triarylamines as cores has been undertaken. The synthesis and crystallization of tectons that contain two or three central nitrogen atoms is of particular interest, since these tectons would have extended conjugation and should have enhanced opto-electronic properties. Although the synthesis of the unsubstituted arylamine cores is readily achieved by conventional methods, the standard methods of bromination described for other molecules in this series appear to fail with these targets. Some success has been achieved by introducing iodine in place of bromine, but yields remain modest. Compounds **42-45** (X = I) are all ideal starting materials for expanding the family of tectons derived from triarylamines.[136]

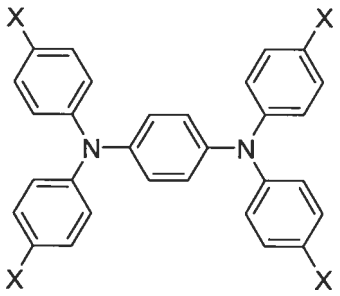

41

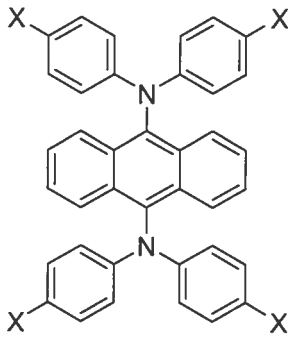

42

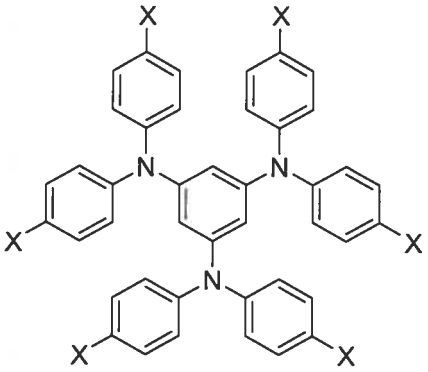

43

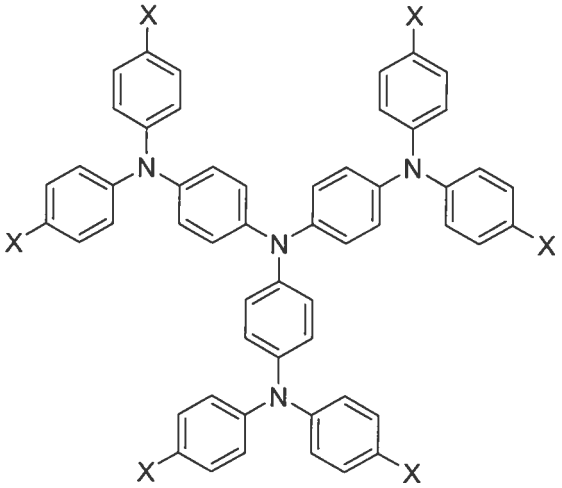

44

2.12.2 Triaminotriazines as Recognition Groups

The use of triaminotriazines as a recognition site has been important in molecular tectonics.[124,137,138] This unit introduces an added degree of rotational freedom to a tecton by placing an amine between the recognition site and the end-most aromatic ring. For example, tecton **1_ATAT** is related to the previously studied diaminotriazine **1_ADAT**. The suffix TAT refers to the triaminotriazine recognition group.

The synthesis of tecton **1_ATAT** was carried out in three steps, starting from commercially available tris(4-nitrophenyl)amine, as described in **Scheme 2.9**.[139,140] Tecton **1_ATAT** was isolated in 55% yield from compound **47**, and crystallization attempts are in progress.

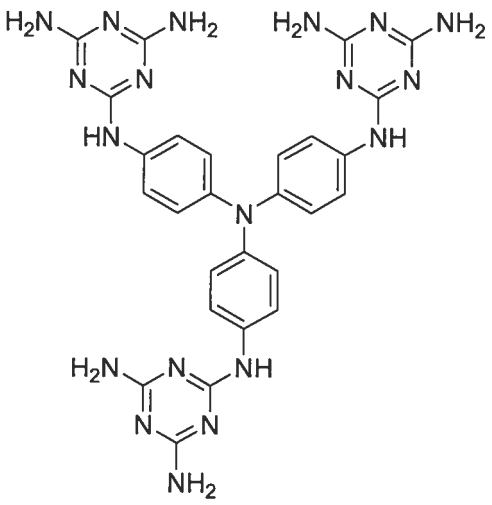

1_ATAT (45)

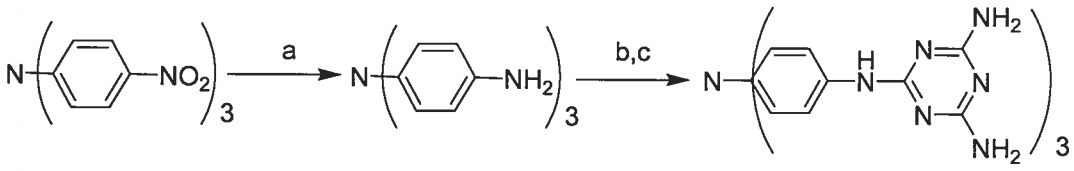

46 **47** **1_ATAT**

Scheme 2.9 a) 10% Pd/C, 200 psi H_2, THF, 24 h, 98%; **b)** Cyanuric chloride, acetone, -10 °C; **c)** NH_4OH, reflux, 18 h, 55% (2 steps)

2.13 Summary

The synthesis and crystal structure of four tectons derived from triarylamines were elaborated. Significantly, a new recognition motif for diaminotriazines was discovered. The embrace motif occurs when two molecules form hydrogen bonds with one another at two recognition groups. In the case of triarylamines, the angles between the groups on a given compound (roughly 120°) make it appear as though two sets of arms are embracing. This motif plays an important role in the crystal structures of tectons **2_ADAT** and **1_BDAT**.

There appears to be no direct correlation between the porosity of the different systems and the size or shape of the molecule. Tecton **1_ADAT** has the most porous crystal structure, in which about 62% of the volume is available for the inclusion of guests, while similarly sized **1_APYR** has only 21% available.

None of the crystalline compounds on their own are suitable for inclusion in opto-electronic devices, since (with the exception of **1_APYR**) the crystals all fracture when the solvent is removed. However, the use of these or similar compounds as dopants in multi-component systems is feasible, depending on their opto-electronic properties. In the next chapter, these properties will be examined and compared with those of other important triarylamines.

CHAPTER 3
Optical and Electronic Properties

3 Optical and Electronic Properties of Triarylamine Tectons

3.1 Introduction

The electrochemical properties of triarylamines have been studied since the early 20th century.[141] Recent studies have focused primarily on preparing compounds that are suitable for inclusion into opto-electronic devices such as OLEDs, either as hole-transporters or light-emitters.[142,143] In the case of hole-transporters the goal is to tune the band gap, which is the energy difference between the HOMO of the neutral compound and the SOMO of the radical cation. The band gap must be tuned so that it overlaps well with the band energy of the materials in the adjacent layers of the device. For molecules used as fluorescent emitters, the goal is to match the band gap (in this case the energy difference between the HOMO and LUMO of the neutral compound) with the desired wavelength for the emission.

It is well understood that the modification of the structure of an organic compound will result in changes to the physical properties of the molecule.[144] For example, in the case of ionic liquids based on quaternary ammonium salts, there is an inverse correlation between the length of the alkyl substituents and the melting point of the compound. As the length of alkyl chain increases, the melting point decreases.[145] This type of correlation between structure and characteristics exists for electronic properties such as the energy of the HOMO and the excited states of a molecule as well. In order to probe these properties in the structurally unique target molecules described in Chapter 2, they were studied by fluorescence and ultraviolet-visible-near infrared spectroscopy (UV-Vis-NIR), as well as by cyclic voltammetry

(CV). There exists a large body of literature on the opto-electronic properties of triarylamines, which has allowed us to carry out a detailed comparative analysis of these tectons with other, more common molecules such as triphenylamine and the ubiquitous TPD.[143] This is an important step in understanding how the presence of hydrogen-bonding functional groups impacts the electronic properties of these compounds.

One of the most important features to be considered in triarylamines is their HOMO ionization energy. This property is critical for building ever more efficient devices. Since most devices are built using an indium-tin oxide (ITO) cathode, it is important that the ionization energy of the hole-transport material be close to the work function of the cathode.[146] A direct correlation between molecular structure and ionization has yet to be determined. However, it has been shown that the ionization energy of hole-transporting triarylamines can be lowered by synthesizing compounds with multiple units connected in *para*, thereby extending conjugation.[147] It is possible that the use of supramolecular strategies such as molecular tectonics will have unique and desirable effects not only on ionization energy but on other physical properties as well.[148] Notably, it has been shown that by including a non-fluorescent dye (**48**) in an amylase host, a fluorescent complex is formed (**Figure 3.1**).[149]

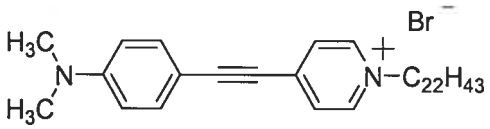

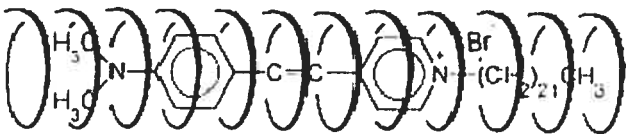

48

Figure 3.1 The non-fluorescent dye $DASPC_{22}$ (**48**) and the fluorescent dye-amylose inclusion complex (right).

3.2 Cyclic Voltammetry

In order to observe and quantify the oxidation processes that occur in tectons **1_ADAT**, **2_ADAT**, **3_ADAT** and **1_BDAT**, cyclic voltammetry (CV) experiments were undertaken. CV measures the current of a system with respect to applied voltage potential. In a CV experiment, the potentials are scanned first in one direction, then in reverse, resulting in a waveform that resembles two isosceles triangles. This allows for the observation of reversible electronic processes, and an accurate determination of oxidation potentials. Due to the linear manner in which the potentials are scanned, CV suffers from decreased sensitivity and poor resolution. This makes it difficult to separate two distinct transitions that lie close to one another. In order to resolve overlapping redox processes, square wave voltammetry (SWV) is often employed as a complement to CV experiments. SWV scans the current of a system versus an applied potential in discrete steps. A comparison of the waveforms of both CV and SWV is shown in **Figure 3.2**. Although SWV is generally carried out only in one direction, the ability to scan potential in discrete steps confers greater sensitivity and higher resolution on this method.

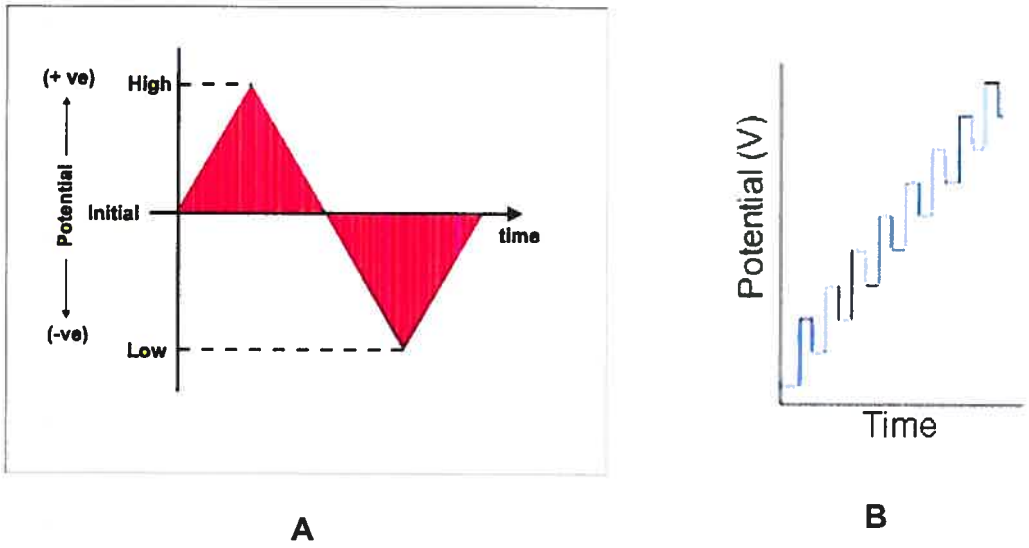

Figure 3.2 a) Waveform of a typical cyclic voltammetry experiment. Potential is scanned in a linear manner in one direction and then in the other. **b)** Waveform of a typical square wave voltammetry experiment. Potential is scanned in small increments in one direction.

3.2.1 Cyclic Voltammetry of Triarylamines

The ability of triarylamines to undergo reversible oxidation is critical to their importance in modern electronic devices. The study of a huge array of triarylamine derivatives has created a large body of literature on this subject, providing reference points for the current project. It has been clearly shown that the energy required to oxidize various triphenylamine derivatives is directly related to the nature and number of substituents present. **Figure 3.3** shows the structure of three chlorinated triphenylamine derivatives with the corresponding oxidation potential. The energy required to remove one electron and form the radical cation increases with the number of electron-withdrawing chlorine atoms present. As a comparison, tris(4-tolyl)amine has a one-electron oxidation potential of 332 mV and that of tris(4-

methoxyphenyl)amine is 109 mV (vs. ferrocene).[120] The presence of strongly electron-withdrawing diaminotriazine groups in the tectons studied in this thesis may therefore play a determining role in their oxidation potentials.

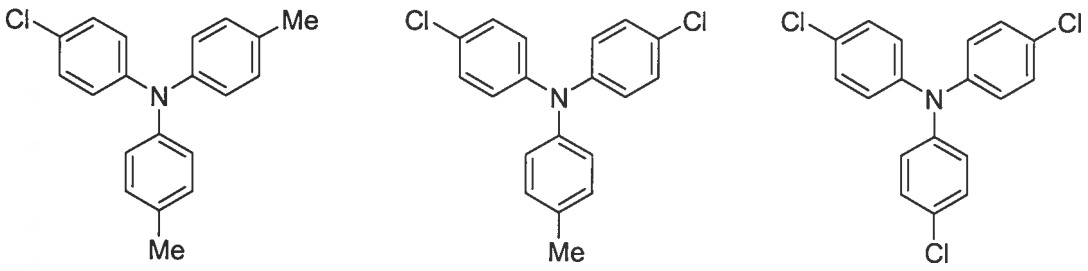

49 E_o = 460 mV

50 E_o = 576 mV

51 E_o = 691 mV

Figure 3.3 Some derivatives of triphenylamine and their corresponding oxidation potentials normalized against ferrocene.[120]

Compounds with only one (or only one type) of redox-active functional group will tend to give the most clear and uncomplicated cyclic voltammograms. Tectons built on triarylamine cores will show redox activity from the aryl nitrogen, but may also have added activity from the recognition groups that are present. Melamine and its derivatives, such as triazines, show a redox couple near -1000 mV.[150-152] This is significantly removed from the area where the oxidation of the arylamine will be expected and should not lead to any overlapping of the different signals. The tectons in this study exhibit poor solubility in most solvents, with the exception of DMSO, DMF and some organic acids. These solvents are not typically employed in CV experiments involving triarylamines and may cause some added complexity.

To examine the feasibility of using CV to study the redox processes of these tectons in such solvents, we measured the cyclic voltammogram of triphenylamine in DMF, using tetra-*n*-butylammonium hexafluorophosphate ($TBAPF_6$) as the electrolyte with ferrocene (Fc/Fc^+) as the internal reference (**Figure 3.4**).[153,154,155] Normalization against ferrocene was done by adding the compound to the electrochemical cell during an experiment. The measured redox potential for ferrocene was then compared to the standard redox potential of ferrocene in the appropriate solvent. In DMF, the standard potential for ferrocene is 406 mV versus an Ag/AgCl reference electrode. Under the experimental conditions of this study, the measured redox potential was 571 mV. All of the measured potentials in this study have been normalized against ferrocene by placing the ferrocene/ferrocenium redox couple at zero. The cyclic voltammogram of triphenylamine in DMF solution is complicated by the breakdown of the system that is observed at either extremity of the spectrum. The peak corresponding to the oxidation of the triarylamine nitrogen atom appears as a shoulder on the larger signal that indicates the breakdown of the system. The corresponding reduction of the triarylaminium radical cation is clearly observed as well as one other redox couple. Although the exact position of the wave corresponding to the oxidation of the central nitrogen atom is difficult to determine, the maximum appears near 0.6 V. The oxidation of triphenylamine leads to dimerization (**Scheme 2.1**) and formation of tetraphenylbenzidine (TPB). **Figure 3.4** shows the cyclic voltammograms of triphenylamine taken at different scan rates. In **Figure 3.4a**, the voltage was scanned at a rate of 50 mV/s and the voltammogram showed one irreversible oxidation wave at near 0.6 V. In this case, the radical cation formed by

the one-electron oxidation triphenylamine had sufficient time to dimerize before the scan direction was reversed. When the scan rate was increased to 10 000 mV/s in **Figure 3.4b**, the reduction wave was observed. At this scan rate, the triarylaminium radical cation was reduced before the dimerization occurred. These results correspond well with the published cyclic voltammograms of triphenylamine taken in acetonitrile, where oxidation is seen near 1000 mV taken versus sce.[156] It is well understood that the solvent can have a strong influence on the redox potential of a system, and therefore only qualitative comparisons can be made with systems that are studied in other solvents.[157] Our results suggest that triphenylamine is oxidized more easily in the polar environment of DMF solution. Although these experiments indicate that the use of DMF as a solvent creates some difficulty in the interpretation of the cyclic voltammograms, we proceeded with the analysis of tectons **1_ADAT**, **2_ADAT**, **3_ADAT** and **1_BDAT**.

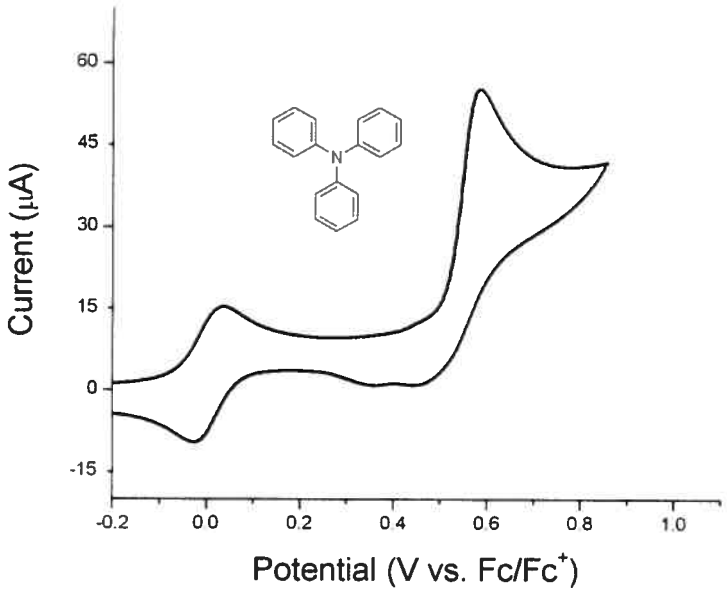

A

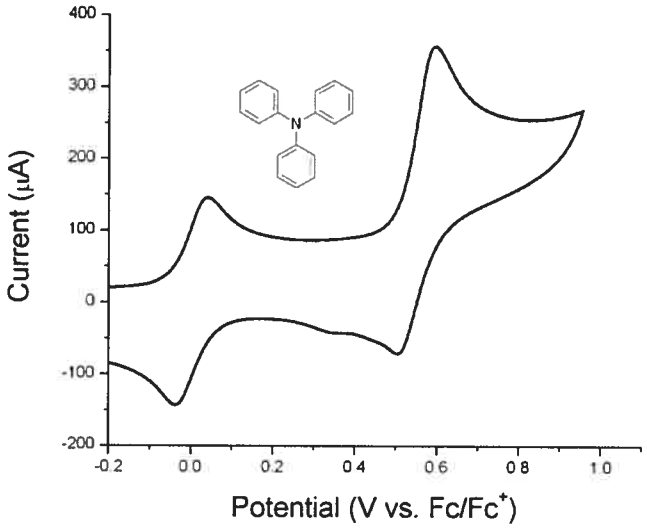

B

Figure 3.4 a) Cyclic voltammogram of triphenylamine in DMF solution, measured against ferrocene. The scan rate is 50 mV/s. **b)** Cyclic voltammogram of triphenylamine in DMF under the same conditions, with a scan rate of 10000 mV/s.

3.2.2 Cyclic Voltammetry of Tecton 1_ADAT

Compared to the straightforward voltammograms obtained for triphenylamine, the CV data obtained for tecton **1_ADAT** show a much greater degree of complexity. The quality of the data makes it difficult to interpret the voltammogram, **Figure 3.5** shows the cyclic voltammogram of tecton **1_ADAT** in DMF with $TBAPF_6$ as the electrolyte, and presents a degree of uncertainty due to the quality of the data. In order to better ascertain where the onset of the oxidation of the central nitrogen atom occurs, square-wave voltammetry was carried out. The square-wave voltammogram for the oxidation of tecton **1_ADAT,** shown in **Figure 3.6**, reveals that the oxidation of the central nitrogen occurs just below 0.5 V. This is only slightly lower than the potential measured for triphenylamine under the same conditions. While factors such as choice of solvent may have an impact on the observed potential, torsion of the phenyl rings around the central nitrogen could disrupt the conjugation of the compound. The crystal structure of tecton **1_ADAT** shows that in the solid state the phenyl rings are rotated 38.5° out of the plane formed by the bonds to the central nitrogen, and the DAT group is twisted an additional 33.8°. These are the same as in triphenylamine. As a result, the DAT groups are nearly perpendicular to the plane formed by the bonds to the central nitrogen (**Figure 3.7**). This conformation could reduce the conjugation between the central nitrogen and the terminal DAT groups, lessening their impact on the oxidation potential of the compound. The concentration of the tecton in the solution may also play an important role in determining the oxidation potential of the central nitrogen atom. The low solubility of tecton **1_ADAT** means that voltammetry experiments were carried out on nearly saturated solutions.

Hydrogen-bonding between tectons in solution could have a delocalizing effect that would reduce the oxidation potential of the central nitrogen atom.

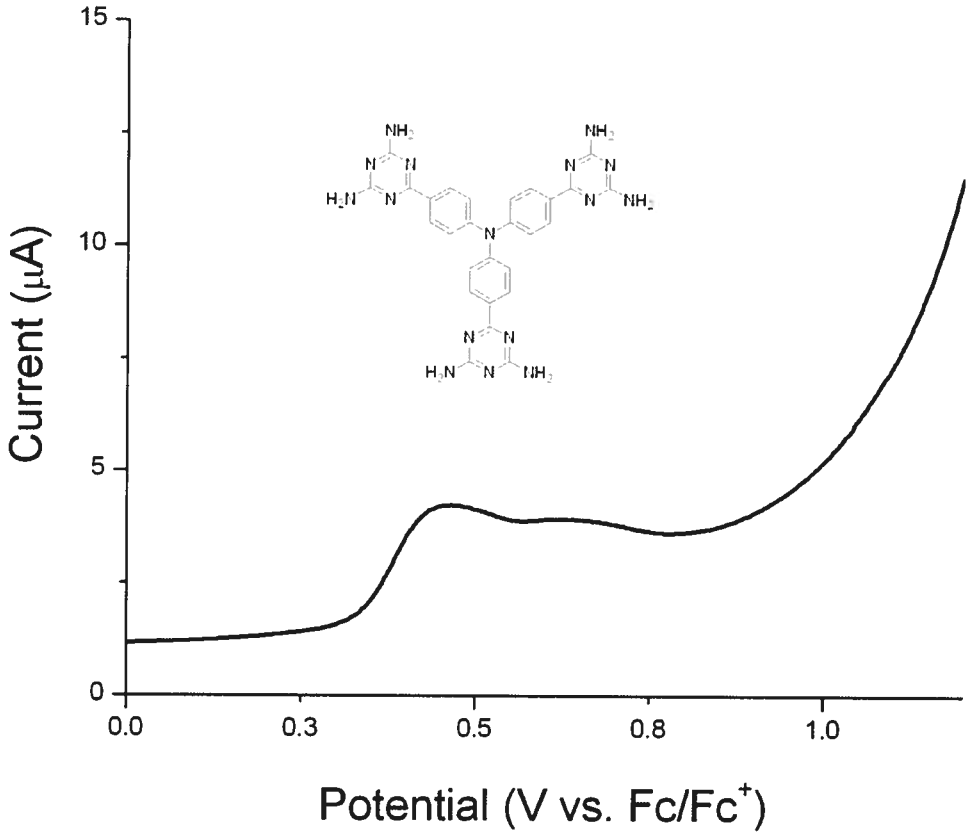

Figure 3.5 Square wave voltammogram of tecton **1_ADAT** in DMF measured against ferrocene, shown over the range 0 – 1.5 V.

In addition to the redox activity of the central nitrogen atom, the diaminotriazine groups can undergo reversible reduction. **Figure 3.6** shows the square-wave voltammogram for the reduction of tecton **1_ADAT**. Two waves are observed, one near -0.8 V and the other near -1.4 V.

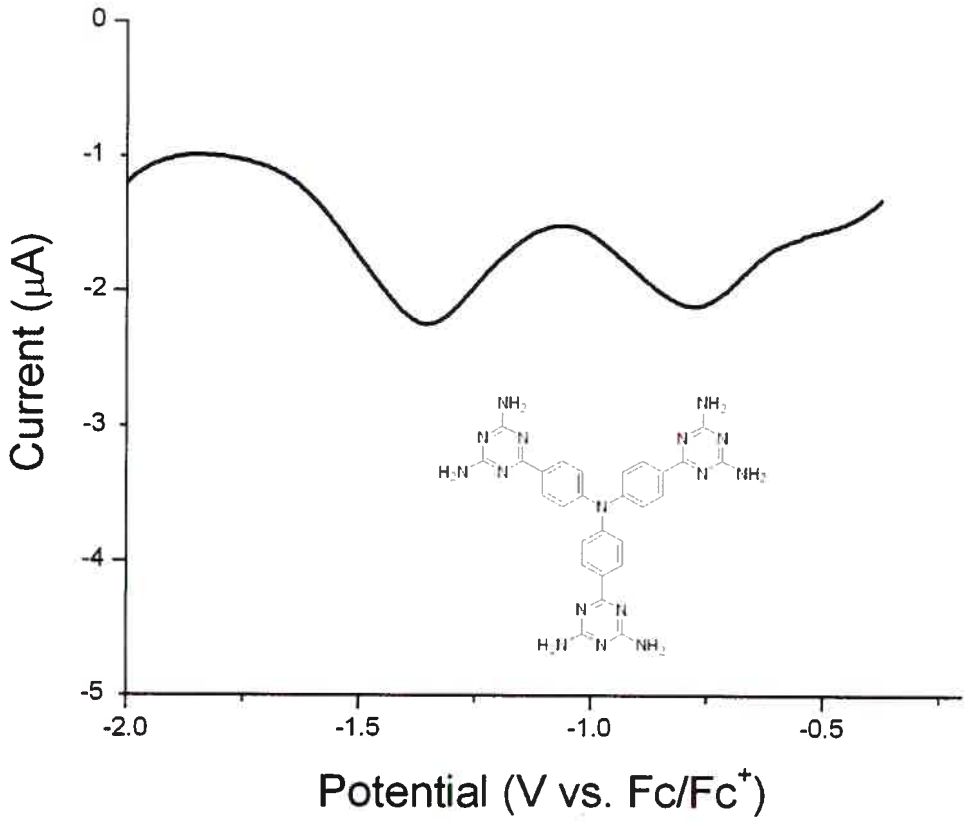

Figure 3.6 Square-wave voltammogram for the reduction of tecton **1_ADAT** in DMF solution.

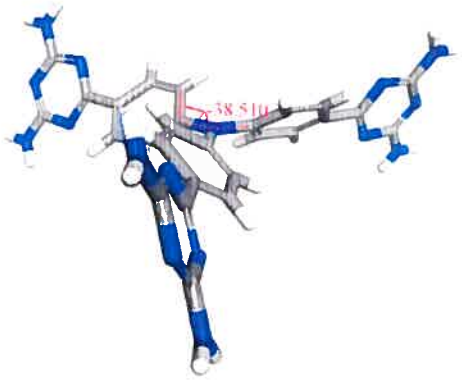

Figure 3.7 Crystal structure of tecton **1_ADAT** showing the torsion angle between the plane formed by the bonds to the central nitrogen atom and the adjacent phenyl groups.

3.2.3 Cyclic Voltammetry of Tecton 2_ADAT

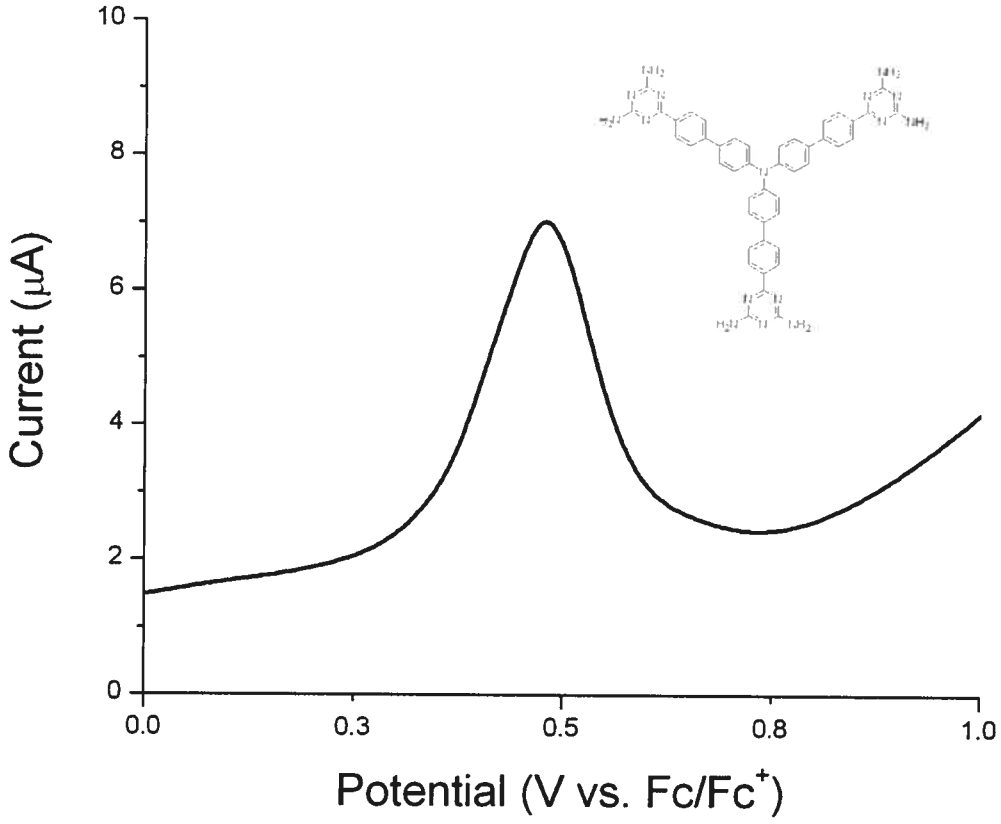

Figure 3.8 Square-wave voltammogram for the oxidation of tecton **2_ADAT** in DMF solution versus ferrocene, measured at 1000 mV/s taken over the range 0 – 1.5 V.

The square-wave voltammogram for the oxidation of tecton **2_ADAT** is shown in **Figure 3.8**. As mentioned previously, SWV is carried out in one direction, and therefore only provides information about the oxidation of the triphenylamine nitrogen, and not the subsequent reduction. The oxidation of the central nitrogen atom is observed just below 0.5 V, as was the case for tecton **1_ADAT**. This is similar to the oxidation potential observed for tecton **1_ADAT**, but is substantially larger than that

recorded for tecton **2_ADAT**'s parent compound, tris(4-biphenyl)amine (**52**).[158] The electrochemistry of compound **52** has not been thoroughly explored. Investigations of the oxidation of *para*-substituted triarylamines by titration with lead(IV) in acetonitrile solution found that compound **52** had an oxidation-reduction potential of 0.5 V versus Ag/AgCl. However, these investigations were hampered by the poor solubility of compound **52** in acetonitrile.[159] Preliminary CV experiments involving compound **52** in DMF revealed that the onset of oxidation is near 0.2 V.[160] Compound **52** has more extensive conjugation than triphenylamine, which results in the lower oxidation potential for the central nitrogen. The increase in oxidation potential observed between compound **52** and tecton **2_ADAT** is striking, since no such trend is observed when tecton **1_ADAT** is compared to its parent, triphenylamine. This difference may correlate to the difference in torsion angles about central nitrogens of the two tectons. In the crystal structure of tecton **2_ADAT**, the two phenyl rings bearing C1 and C1' (**Figure 2.15**) are 44.2° out of the plane formed by the bonds to the central nitrogen. In contrast, the arm bearing C11 is only 29.3° out of this plane. In addition, the torsional angle between the two phenyl spacers (about the C14 – C17 bond) is 35.2°, resulting in a DAT group that is nearly coplanar with the bonds to the central nitrogen. This may be less disruptive to the conjugation in the compound, allowing the DAT group to exert greater influence on the oxidation potential of the central nitrogen. The oxidation potential observed for compound **52** is substantially lower than the value observed for tecton **2_ADAT**, indicating that conjugation between the central nitrogen and the DAT group is extensive and has an impact on the oxidation potential of the tecton.

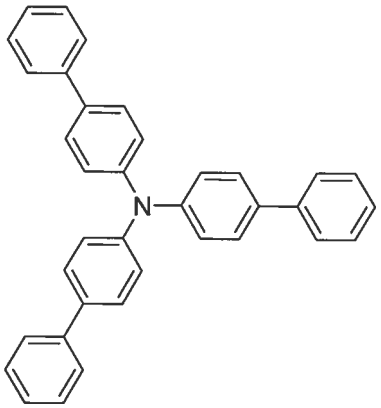

52

Figure 3.9 is a plot of the square wave reduction of tecton **2_ADAT**. Two reduction waves are observed, at -0.8 V and at -1.4 V. These can be attributed to the reduction of the triazine groups and corresponds with the data collected for tecton **1_A-DAT**.

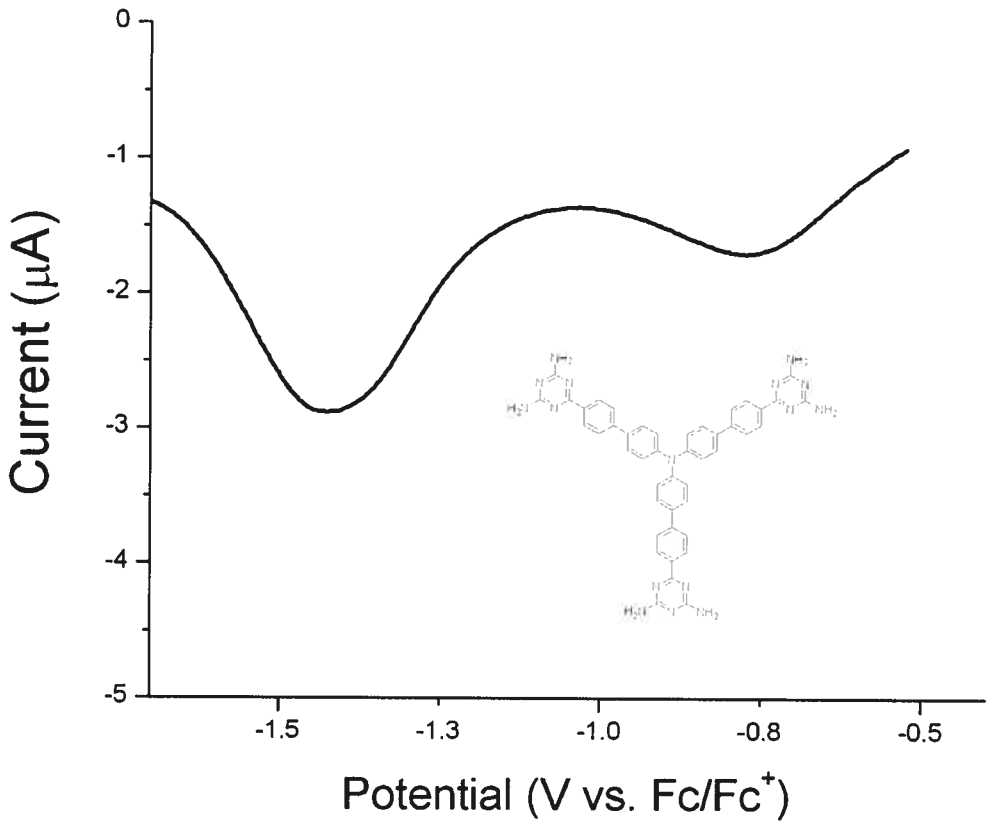

Figure 3.9 Square-wave voltammogram for the reduction of tecton **2_ADAT** taken over the range 0 to -2 V.

3.2.4 Cyclic Voltammetry of Tecton 3_ADAT

The square-wave voltammogram obtained for the oxidation of tecton **3_ADAT** is even less well-defined than those observed for the two previous compounds (**Figure 3.10**). Regardless, the overall features remain similar to those observed for tectons **1_ADAT** and **2_ADAT**. The oxidation of the central nitrogen atom in tecton **3_ADAT** is observed near 0.3 V. No structural data are yet available for tecton **3_ADAT**, and no electrochemical studies of its parent (compound **53**) have been carried out to date. The extensive conjugation present in compound **53** make it likely that the oxidation of

the central nitrogen would occur at an even lower potential than either compound **52** or triphenylamine. The square-wave reduction of tecton **3$_A$DAT**, shown in **Figure 3.11**, is similar to those observed for the previous two tectons, with bands near -0.8 V and -1.4 V However, no conclusions can be drawn without more investigations into the properties of compound **53** and the crystal structure of tecton **3$_A$DAT**.

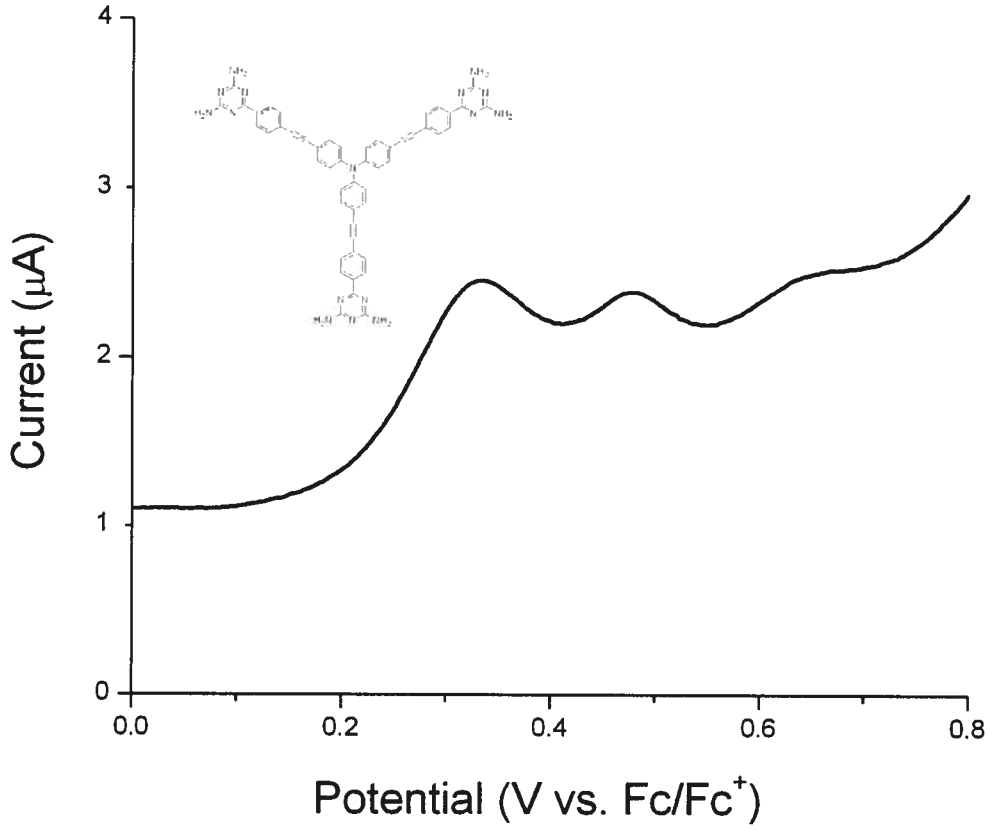

Figure 3.10 Square-wave voltammogram for the oxidation of tecton **3$_A$DAT** in DMF solution versus ferrocene.

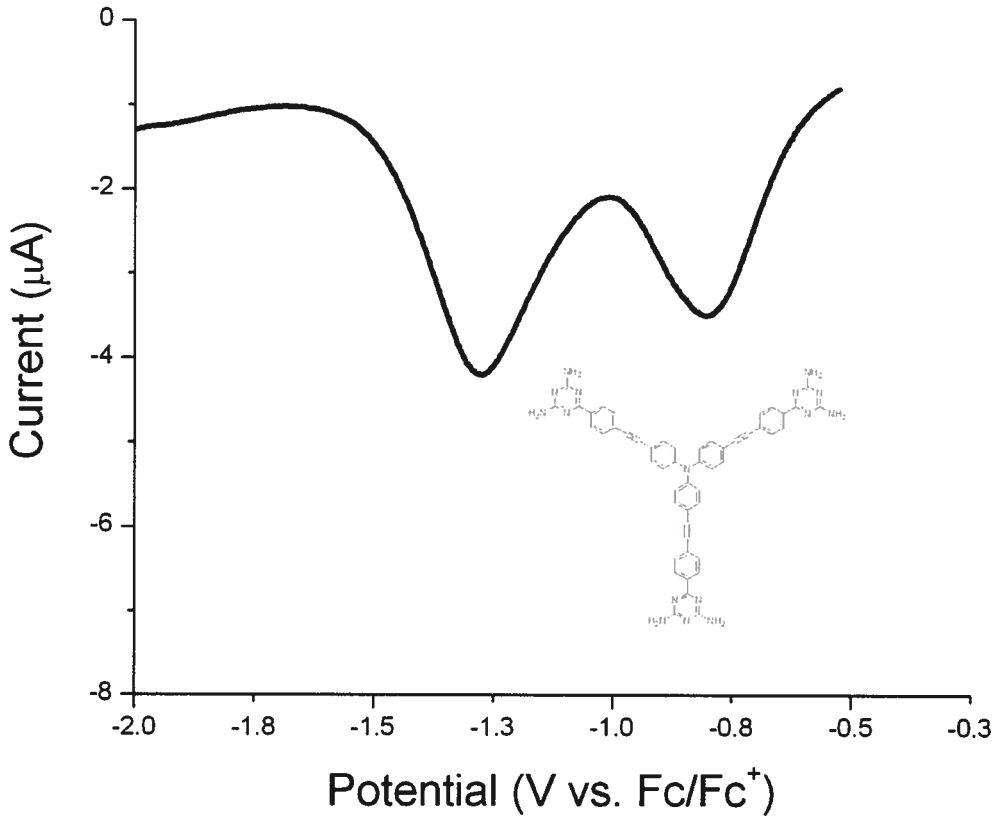

Figure 3.11 Square-wave reduction of tecton **3_ADAT** over the range -0.3 V to 2 V.

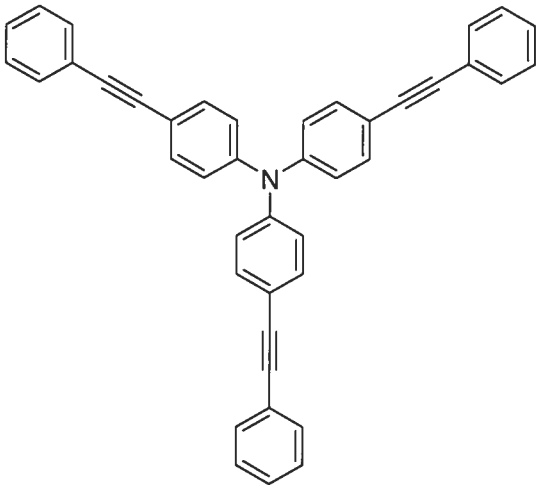

53

3.2.5 Cyclic Voltammetry of Tecton 1_BDAT

The cyclic voltammogram of tecton **1_BDAT**, shown in **Figure 3.12**, clearly displays the reversible oxidation of the triarylamine nitrogen atoms. The oxidation of the two triarylamine nitrogen atoms are observed simultaneously near 0.4 V in the voltammogram. Although the two central nitrogen atoms are ostensibly connected via resonance across the biphenyl spacer, this is not the case. In compounds containing multiple central nitrogens connected by resonance via a phenylene unit or a polyene link, the oxidation of the first central nitrogen makes the subsequent oxidation more difficult. This is readily observed in the cyclic voltammograms of such compounds, where two distinct waves are seen.

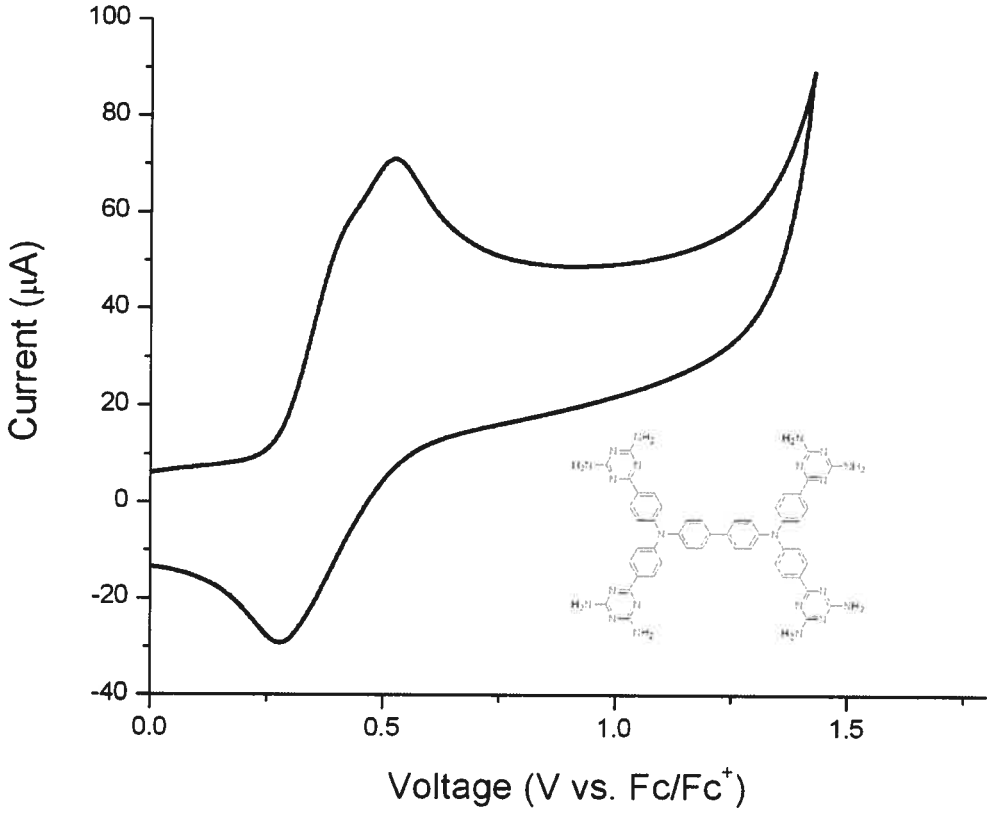

Figure 3.12 Cyclic voltammogram of tecton **1_BDAT** in DMF taken at 1000 mV/s, versus ferrocene.

The cyclic voltammogram of tecton **1_BDAT** shows only one wave in the region corresponding to the oxidation and reduction of the central nitrogen. This indicates that the two atoms are not communicating with one another and are oxidized at approximately the same voltage. This result is entirely consistent with CV data obtained for similar compounds where a biphenyl unit separates two central nitrogen atoms. For example, both TPB and TPD show one oxidation wave in their respective CV spectra.[153] **Figure 3.13** shows the crystal structure of tecton **1_BDAT** and reveals that the biphenyl spacer is twisted 59.7° out of the plane formed by the bonds to the

central nitrogen atoms, effectively cutting off communication between them. Square-wave voltammetry can be used to resolve the two overlapping oxidation processes. The square-wave voltammogram of tecton **1_BDAT** in **Figure 3.14** shows the sequential oxidation of the two triarylamine nitrogen atoms. The first oxidation occurs at 0.35 V and the second at 0.45 V. One marked difference between tecton **1_BDAT** and other analogous compounds is the energy gap between the oxidation potential of the two triarylamine nitrogen atoms. In compounds such as tetraphenylbenzidine the gap is typically close to 0.2 V.[161] In the case of tecton **1_BDAT** however, the gap is reduced to around 0.1 V. This may be related to the use of DMF as a solvent for these compounds or could be caused by the presence of electron-withdrawing substituents. A more complete understanding of this phenomenon requires a thorough investigation of a range of similar molecules under the same conditions.

The square-wave voltammogram for the reduction of tecton **1_BDAT** is shown in **Figure 3.15**. Only one reduction wave is observed near -1.4 V. Unlike the other tectons in this study, there are only two triazine-containing groups on each of the central nitrogen atoms. The absence of conjugation between the central nitrogens may allow two of the groups to be reduced simultaneously.

Figure 3.13 Crystal structure of tecton **1_BDAT**, showing the 59.7° torsion between the biphenyl core and the plane formed by the bonds to the central nitrogen atoms.

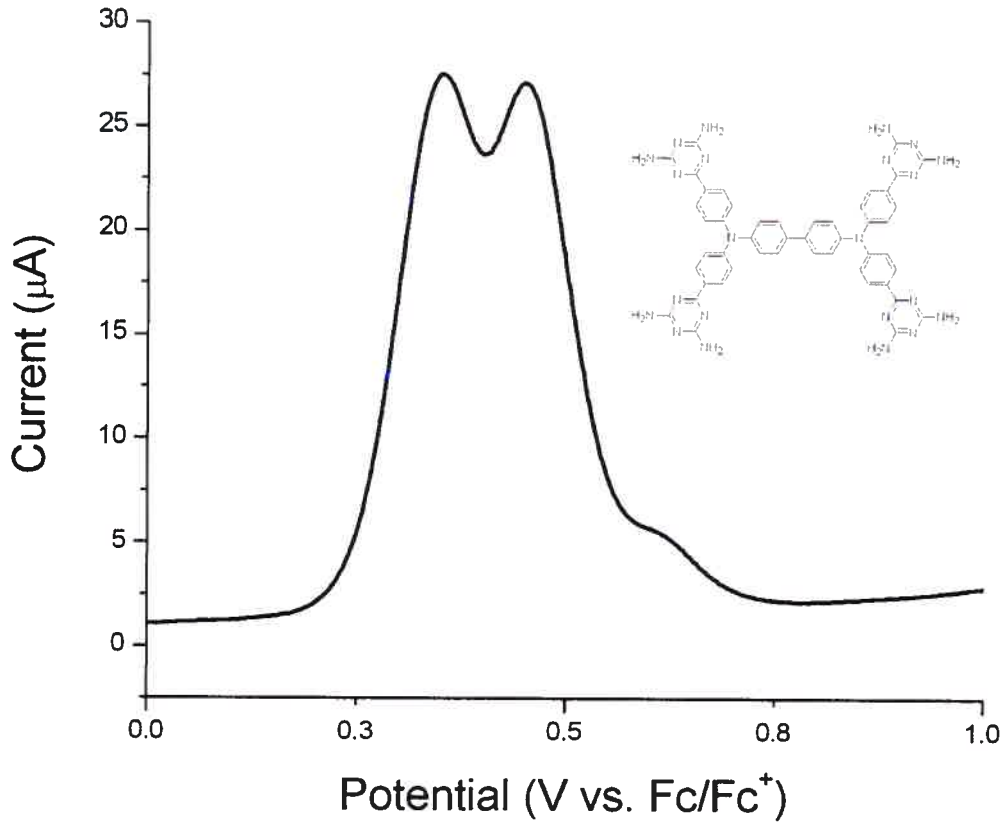

Figure 3.14 Square-wave oxidation of tecton **1_BDAT** in DMF solution over the range 0 mV to 2000 mV. The two peaks that correspond to the oxidation of the central nitrogen atoms are resolved .

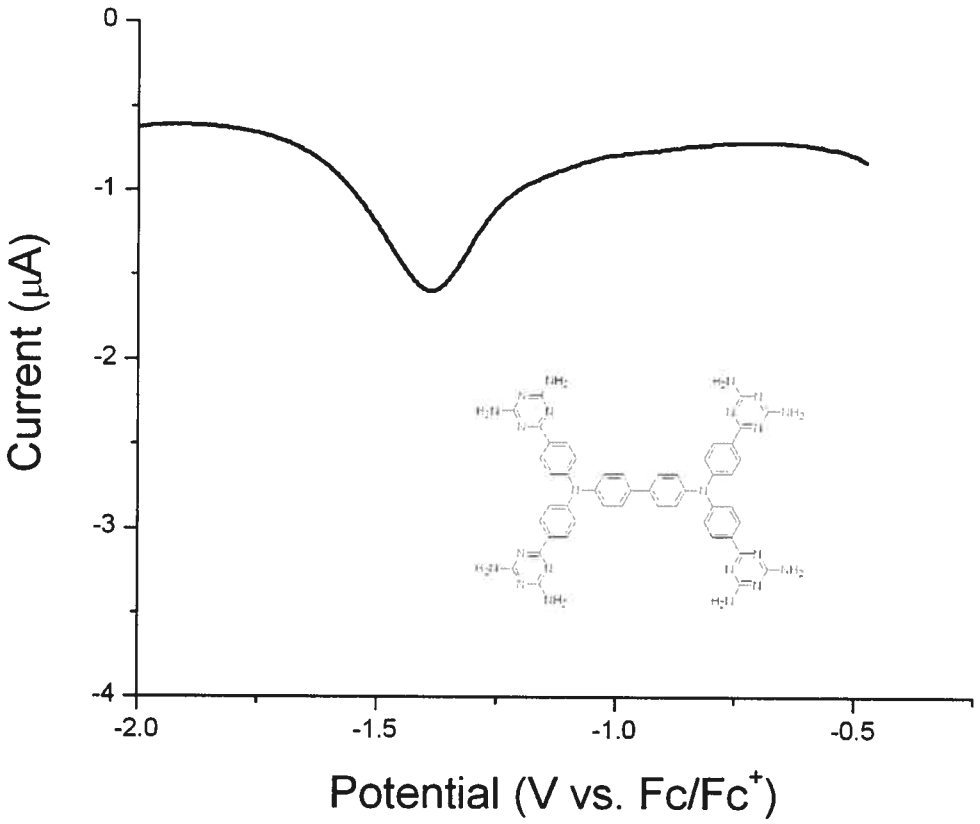

Figure 3.15 Square-wave voltammogram for the reduction of tecton **1_BDAT** in DMF versus ferrocene.

3.2.6 Summary

Cyclic voltammetry and square-wave voltammetry measurements of tectons derived from triarylamines reveal that the central nitrogen atoms undergo reversible redox processes as expected. The requirement that DMF be used as a solvent hampers the analysis to a certain extent. In some cases the oxidation of the triarylamine nitrogen atom is masked by the breakdown of the solvent. In the case of the three compounds derived from triphenylamine - tectons **1_ADAT**, **2_ADAT** and

3_ADAT – the oxidation of the central nitrogen atom occurs between 0.3 and 0.5 V, which is consistent with the structures of these compounds. Interestingly, the reduction of the triarylaminium radical cation in these tectons occurs at a much lower potential than in the parent triphenylamine. In addition, the reduction of two of the triazine groups in these compounds are observed near -0.8 V and -1.4 V respectively. The two central nitrogens of tetraphenylbenzidine derivative tecton **1_BDAT** are oxidized almost simultaneously, which is consistent with the behaviour of other compounds of this type. A comparison of the results obtained for all four tectons shows that more extensive conjugation in a molecule results in a lower oxidation potential for the triarylamine nitrogen atom. In addition, the influence of the electron-withdrawing groups does not cause the oxidation of those nitrogen atoms to occur outside the normal range of potentials usually observed for this type of compound. In order to obtain a deeper and more detailed understanding of the electrochemical behaviour of this type of compound and the influence of hydrogen-bonding, a comparison of oxidation potential versus analyte concentration should be carried out. Solid-state analyses should be undertaken in order to avoid some of the complications encountered in this study.

3.3 Absorption, Luminescence and Spectroscopy

Light and colours have long fascinated scientists, starting from the early observers of fireflies and luminescent algae. When a body emits radiation upon

heating, this is termed incandescence. Emission of light by any other means is termed luminescence. The energy required to initiate luminescence can be derived from a number of phenomena. For instance, electroluminescence occurs when an electric current is used to provide the required energy, while chemiluminescence derives the energy from a chemical reaction. In biological organisms, chemiluminescence is referred to as *bio*luminescence, and is best known in fireflies and a variety of deep-sea organisms (**Figure 3.16**). When the source of energy is ultraviolet, visible or infrared light, the process is termed photoluminescence. Photoluminescence is readily measured by fluorimetry.

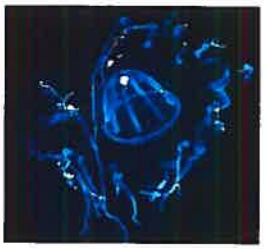

Figure 3.16 Bioluminescence of the deep-water organism *Colobonema* (http://www.mbari.org/itd/retrospective/bioluminescence.html)

3.3.1 Absorption and Emission of Light

As a rule, molecules occupy the lowest vibrational level of the ground electronic state, referred to as S_0. Upon absorption of light, they are raised up to excited states, S_1 or S_2. **Figure 3.17** is a simplified depiction, or Jablonski diagram, of a molecule's absorption of light and subsequent return to the ground state. [162] When a molecule is excited, it reaches any one of the vibrational sub-levels within a given electronic state. Absorption bands are broadened due to the numerous rotational

levels associated with each vibrational sub-level. This makes resolution of individual transitions impossible.

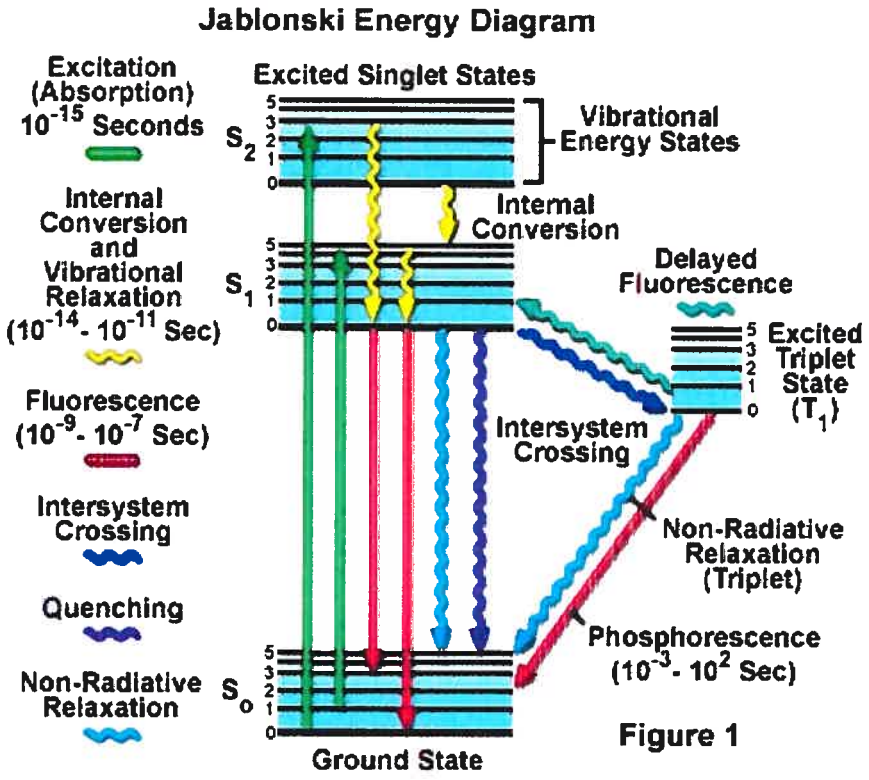

Figure 3.17 Simplified Jablonski diagram of the possible electronic transitions that occur when a molecule absorbs a photon.

The excited molecule rapidly loses any extra vibrational energy by collision and falls to the lowest vibrational level of the excited state. From this level, the molecule can return to one of the vibrational levels of the ground state by releasing its energy by fluorescing (emitting a photon). The absorbed energy may also be dispersed via non-radiative decay or phosphorescence. Some energy is always dissipated by collision and, as a result, less energy will be emitted by fluorescence than was initially absorbed. Correspondingly, absorption always occurs at a shorter wavelength than

emission. The transition between the lowest vibrational level of the ground state to the lowest vibrational level of the excited state, which is the 0 – 0 transition, is observed for both absorption and emission. The energy of the 0–0 transition is found at the overlap of the absorption and emission spectra.

3.4 Ultraviolet and Visible Region Spectroscopy of Triarylamine Tectons

Organic compounds with extended conjugation are well-known for their ability to absorb light in the ultraviolet and visible (UV/Vis) regions of the electromagnetic spectrum. The UV/Vis spectra of tectons **1_ADAT**, **2_ADAT**, **3_ADAT** and **1_BDAT** in DMF solution are shown in **Figure 3.18**. The three tectons derived from triphenylamine all have absorption maxima between 370 and 375 nm. In contrast, tecton **1_BDAT**, which is derived from TPB, has its absorption maximum at 292 nm with a smaller band at 351 nm. The similarities in the absorption spectra are consistent with the similarities observed in the electrochemical analysis of these compounds.

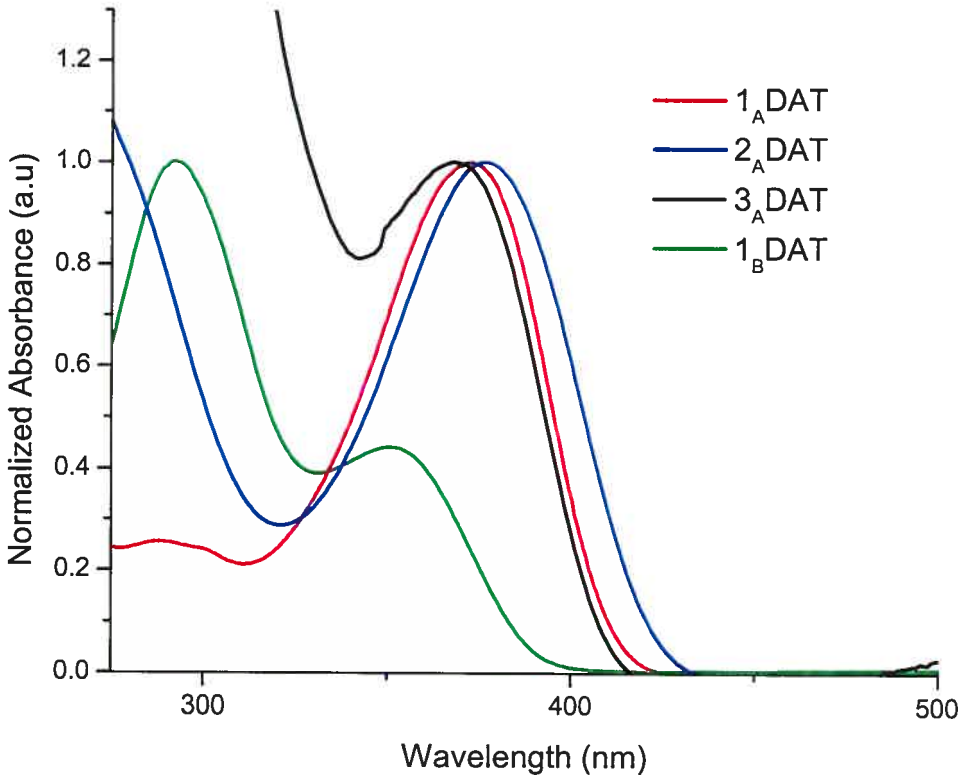

Figure 3.18 UV/Vis absorption spectra of tectons **1_ADAT**, **2_ADAT**, **3_ADAT** and **1_BDAT** in DMF solution.

3.5 Oxidative Titration of Triarylamines

The addition or removal of an electron from a molecule leads to a redistribution of the electron population in molecular orbitals. This redistribution causes a change in the UV/Vis absorption spectrum of a molecule, and is therefore readily followed by spectrometry. The chemical oxidation of triphenylamine and its derivatives is typically carried out using antimony (V) chloride or nitrosonium tetrafluoroborate.[163] These are powerful oxidants which spontaneously remove one electron from the arylamine to give the radical cation. For this study the tectons were dissolved in DMF to give a 1.0

x 10^{-6} M solution. These solutions were then titrated with 1.0 x 10^{-6} M antimony (V) chloride solution in dichloromethane. Following each addition of oxidant, the ultraviolet-visible absorption spectrum was measured.

The study of triarylamines by oxidative titration is generally carried out in solvents such as dichloromethane or chloroform. This is done in order to avoid complications such as interactions between the oxidant and solvent. The limited solubility of the compounds in this study required that DMF be used as the solvent. In order to ensure that these experiments could be carried out in DMF solution, the oxidative titration of triphenylamine was carried out in both DMF and chloroform solution.

The sequential addition of an aliquot containing 1.0 equivalents of antimony (V) chloride to a solution of triphenylamine in chloroform solution gave rise to a marked colour change. The colourless solution rapidly became deep blue. This blue colour is characteristic of triarylamine radical cations. **Figure 3.19** shows the changes seen in the UV spectrum of triphenylamine as the addition occurs. In addition to these changes in the UV region of the spectrum, oxidation of TPA with $SbCl_5$ results in the formation of a broad band with λ_{max} = 673 nm as shown in **Figure 3.20**.

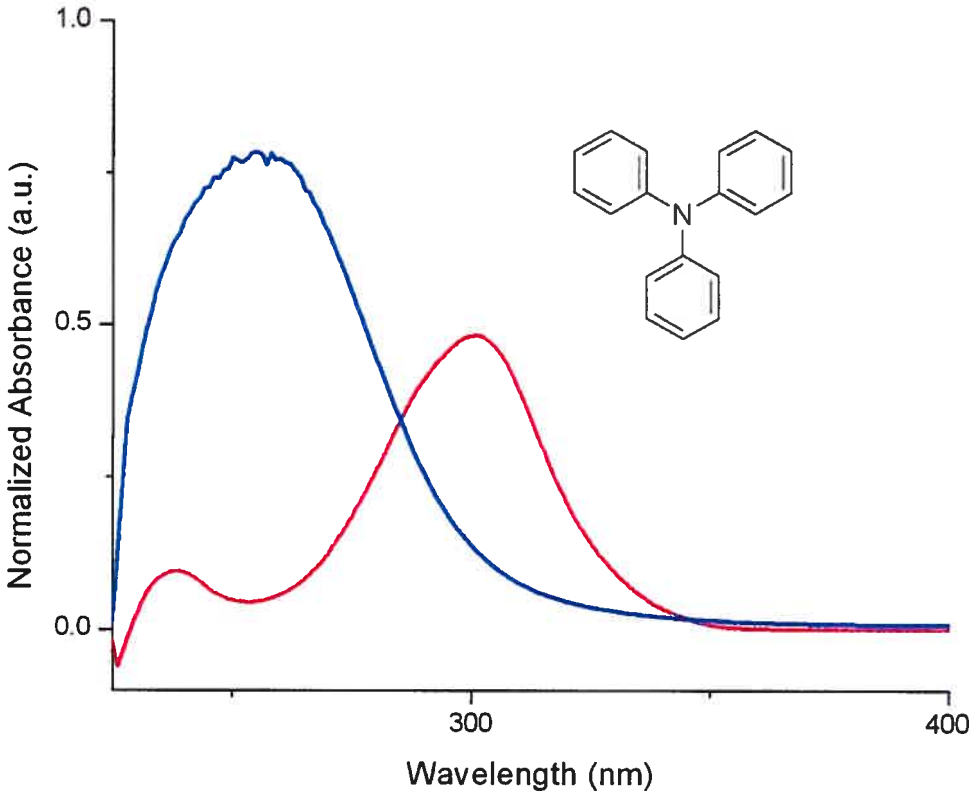

Figure 3.19 UV/Vis spectra of TPA in chloroform solution before (red) and after (blue) oxidation by $SbCl_5$.

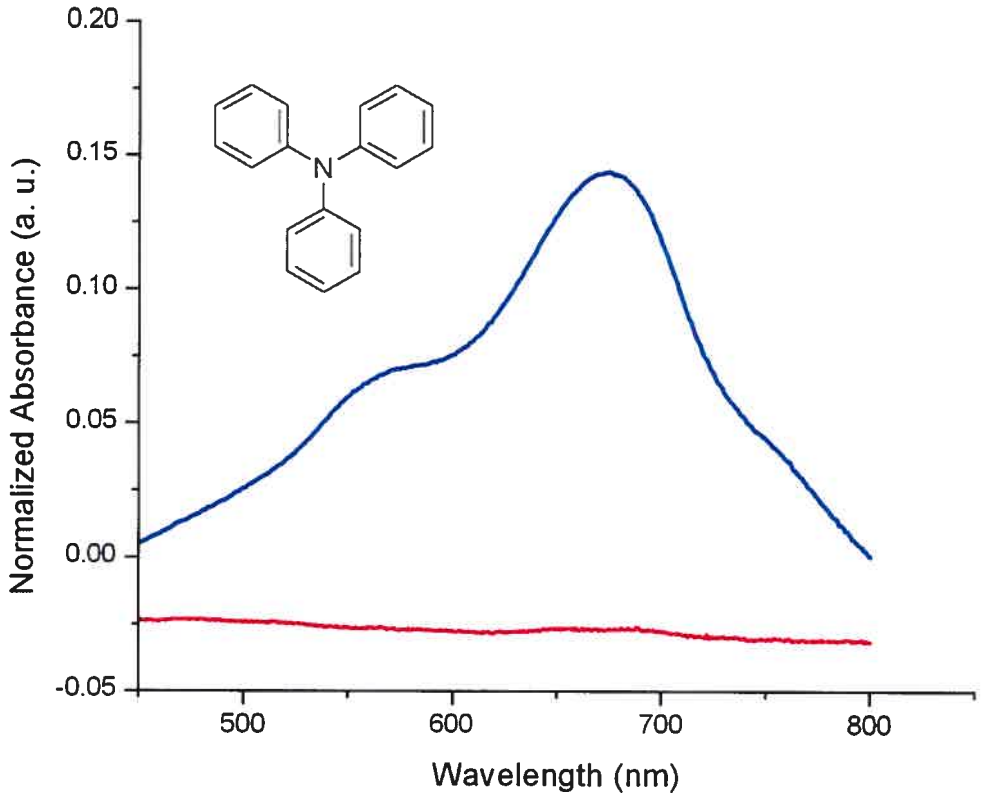

Figure 3.20 Visible spectrum of TPA in chloroform, before (red) and after (blue) the addition of 1.0 equivalent of $SbCl_5$.

In contrast, the same experiment carried out in DMF showed no such drastic colour change. The oxidizing solution, antimony (V) chloride in chloroform, had a deep yellow colour, which did not change or dissipate in any way when this was added to triphenylamine. The UV/Vis spectra recorded during sequential oxidations show the disappearance of the band at 258 nm, as shown in **Figure 3.21**. No new absorbance bands are observed in the visible region of the spectrum, suggesting that the radical cation is not formed during this process. Unfortunately, both DMF and DMSO show strong absorption below 250 nm, which masks this region of the

spectrum. The absence of the dramatic colour change, coupled with the lack of clarity in the recorded spectra, suggest that the solvent has interfered with the normal course of oxidation. The starting triarylamine is destroyed, but no conclusions can be drawn from these data as to the nature of the products formed.

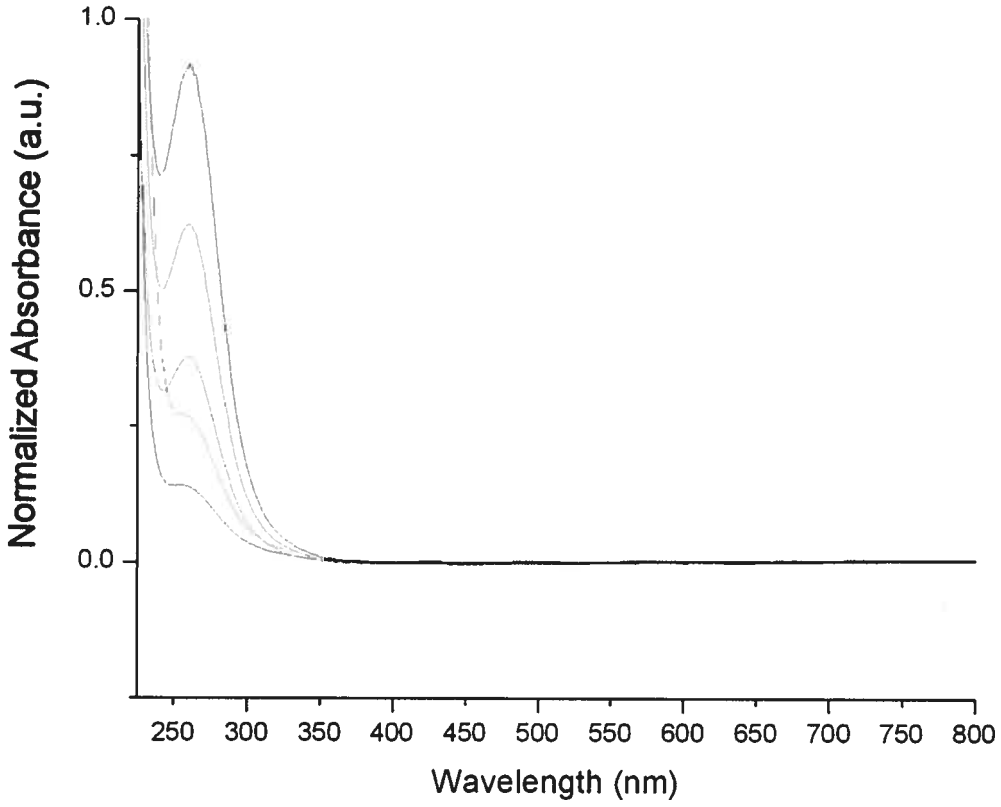

Figure 3.21 UV/Vis spectra of TPA in DMF solution recorded during sequential oxidation with $SbCl_5$. Spectra were recorded after the sequential addition of aliquots containing 0.2 equivalents of oxidant. No changes were recorded in the visible region of the spectra. The black spectrum was that of the neutral compound. After the addition of one equivalent of oxidant, blue spectrum was recorded.

3.5.1 Titration of Tecton 1_ADAT

In DMF solution, **1_ADAT** displayed a λ_{max} for absorption at 373 nm, which corresponds well with literature values for triphenylamines substituted with electron-

withdrawing groups.[163,164] Titration with $SbCl_5$ solution caused the main absorbance band to decrease and broaden, while the band below 250 nm broadened and increased in intensity (**Figure 3.22**). This is consistent with the data obtained for the sequential chemical oxidation of TPA under the same conditions. No conclusions can be drawn about the process occurring in this experiment, or the nature of the products formed.

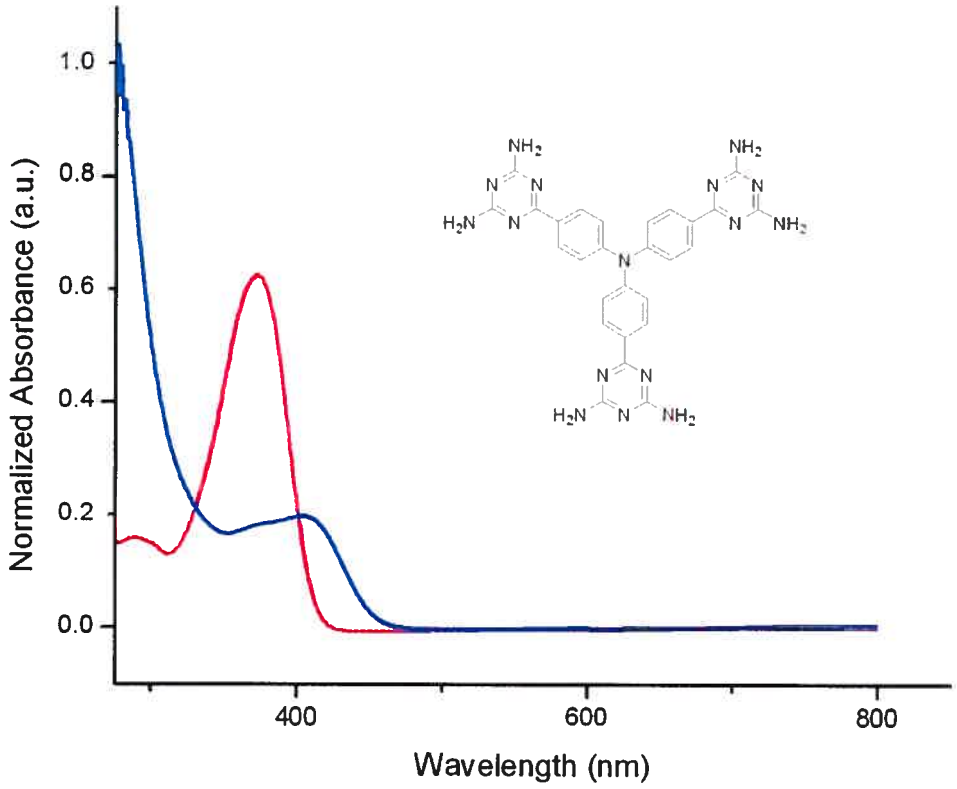

Figure 3.22 UV/Vis spectra of tecton **1_ADAT** in DMF solution before (red) and after (blue) oxidation with $SbCl_5$.

3.5.2 Titration of Tecton 2_ADAT

In DMF solution, tecton **2_ADAT** has λ_{max} = 377 nm. The titration of tecton **2_A-DAT** with $SbCl_5$ proceeded in a similar manner to the titration of **1_ADAT** (**Figure 3.23**). The absorption band of the neutral compound diminished and the band below 300 nm broadened. As in the cases of tecton **1_ADAT** and TPA, the data provide no insight into what may be occurring under these conditions.

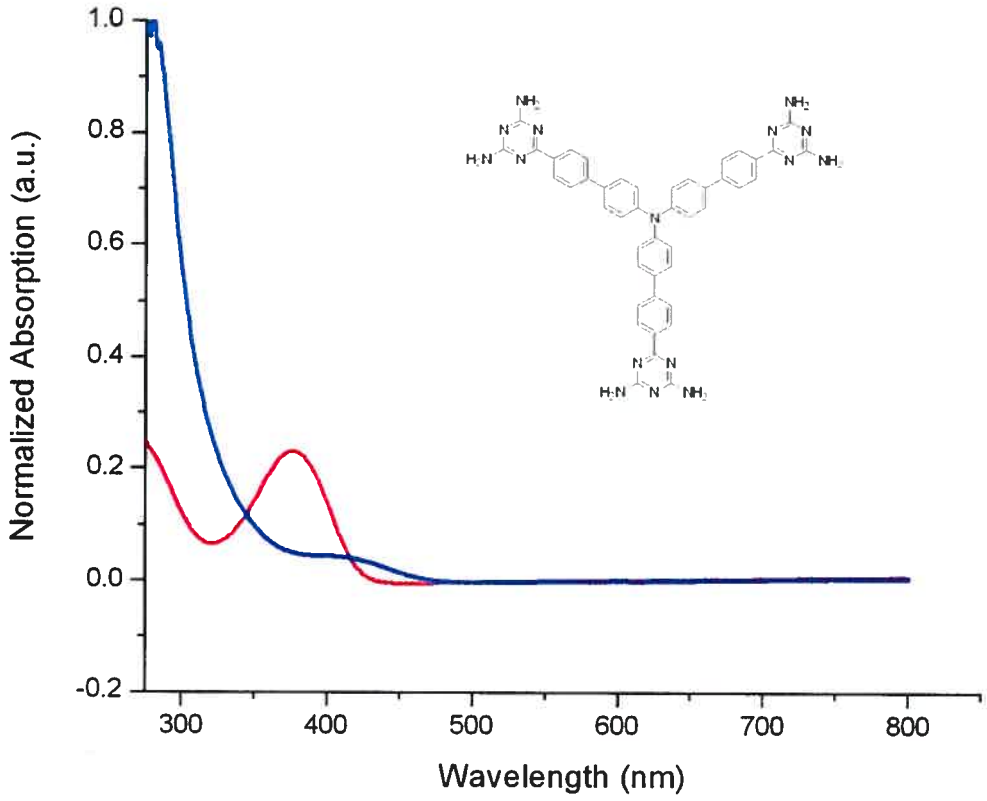

Figure 3.23 UV/Vis spectra of tecton **2_ADAT** in DMF solution before (red) and after (blue) oxidation with $SbCl_5$.

3.5.3 Titration of Tecton 3_ADAT

Figure 3.24 shows UV-Vis spectra recorded during the sequential chemical oxidation of tecton **3_ADAT** with $SbCl_5$. As in the case of the compounds previously examined, the starting material is consumed, but no conclusions can be drawn from the data about what may be occurring.

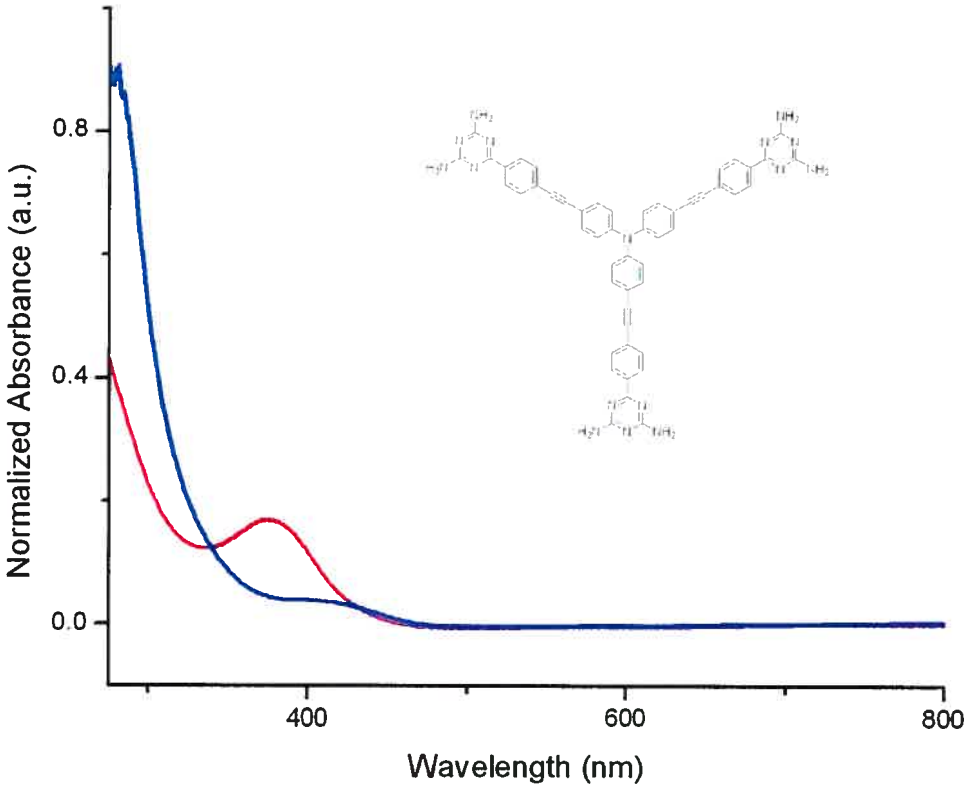

Figure 3.24 UV/Vis spectra of tecton **3_ADAT** before (red) and after (blue) oxidation with $SbCl_5$ in DMF solution.

3.5.4 Titration of Tecton 1_BDAT

The ultraviolet-visible absorption spectrum of tecton **1_BDAT** shows two broad bands at 292 nm and 370 nm. Oxidation of the two triarylamine nitrogen atoms appears to occur in a stepwise manner (**Figure 3.25**). After the addition of the first equivalent of oxidizing agent, the absorption band at 292 nm was broadened until it merged with the absorption from the solvent (~ 250 nm). The addition of the second equivalent of $SbCl_5$ solution caused the lower energy band to decrease. Although the data seem to indicate that two separate processes are occurring, it is still impossible to determine the nature of any products formed or what processes may be occurring.

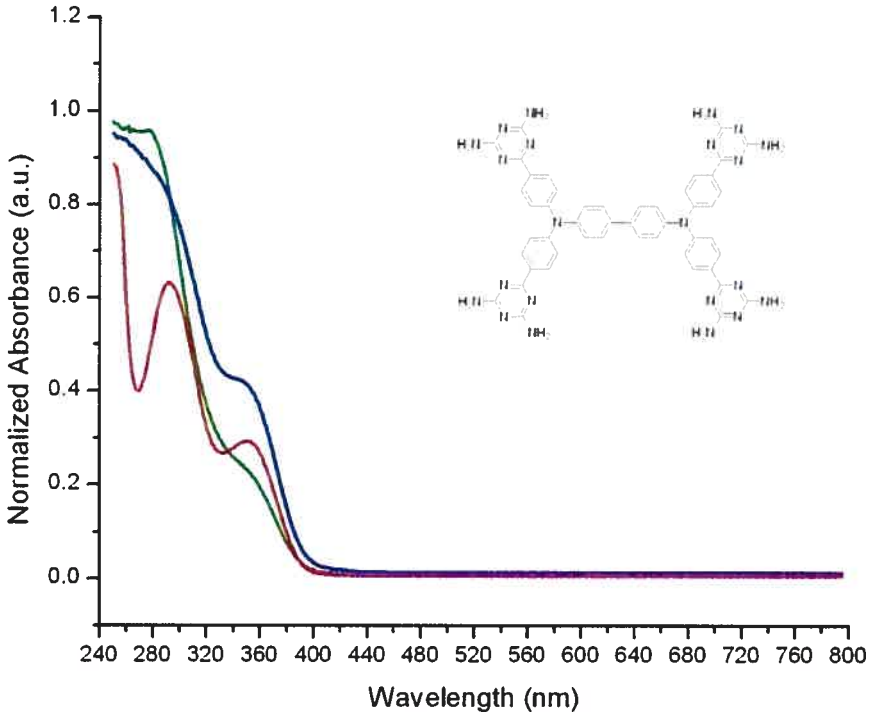

Figure 3.25 UV/Vis spectra of tecton **1_BDAT in** DMF solution before (red), after the addition of one equivalent of $SbCl_5$ solution (blue) and after the addition of two equivalents of $SbCl_5$ solution (green).

3.6 Fluorimetric Analysis

Many triarylamines exhibit fluorescence in solution and in the solid state. This has led to their inclusion in the emissive layers of devices. Some of these compounds can be tuned to fluoresce green and even red, but the vast majority of fluorescent triarylamines fluoresce blue. Tectons **1_ADAT**, **2_ADAT**, **3_ADAT**, and **1_BDAT** are all fluorescent in DMSO solution.

3.6.1 Tecton 1_ADAT

Tecton **1_ADAT** is blue fluorescent in DMSO solution. **Figure 3.26** shows the normalized excitation and emission spectra of tecton **1_ADAT** in DMSO solution. The excitation spectrum, shown in red, exhibits transitions to three excited states with maxima at 300 nm, 343 nm and 393 nm. The emission spectrum, shown in blue, displays one sharp transition with a maximum at 451 nm and a second, broad transition with a maximum at 532 nm. The 0 – 0 transition is found at 414 nm (**Figure 3.26**). The Stokes shift is the difference in wavelength between the λ_{max} for excitation and the λ_{max} for emission and is a measure of how much energy is lost to rotation and vibration. The larger the shift, the greater the amount of energy lost. This has a direct impact on the wavelength of the emitted light. In additions, samples containing compounds with large Stokes shifts may generate more heat. In applications or devices that use photoemission, this is not desirable. The Stokes shift for **1_ADAT** is

58 nm. Triphenylamine (TPA) is not fluorescent in solution, since irradiation leads to the formation of carbazoles.[165] When stabilized in a polystyrene matrix, fluorescence is observed at 365 nm.[166] Polymer **54**, which is comprised of multiple TPA units, has a fluorescence maximum at 412 nm.[167]

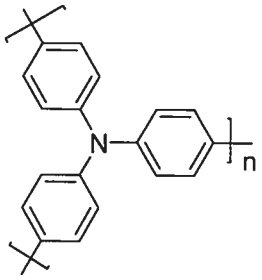

54

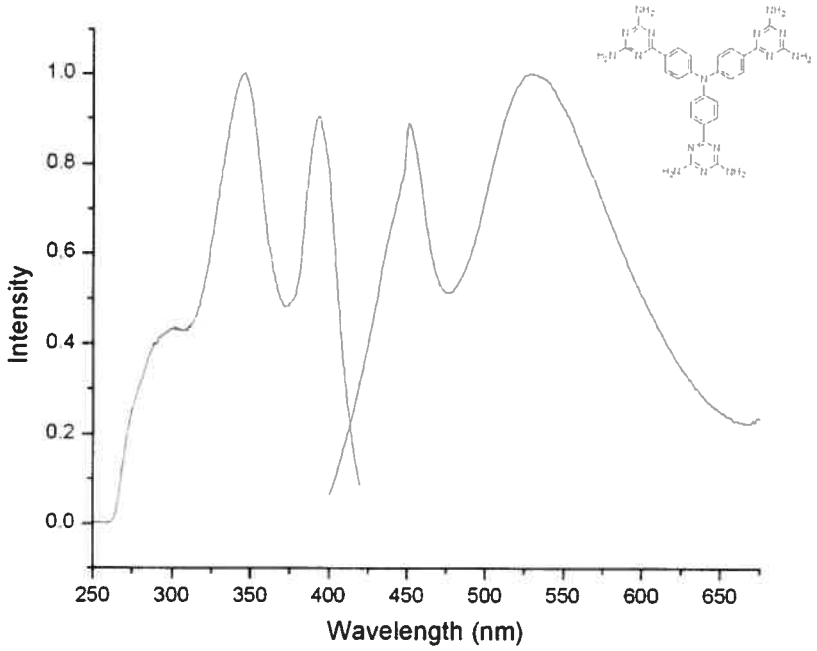

Figure 3.26 Normalized excitation (red) and emission (blue) spectra of tecton $\mathbf{1_A DAT}$ in DMSO.

3.6.2 Tecton 2_ADAT

Tecton **2_ADAT** is blue fluorescent in DMSO solution. **Figure 3.27** shows the normalized fluorescence excitation and emission spectra in DMSO solution. The excitation spectrum, shown in red, exhibits transitions to two excited states, with maxima at 285 nm and 376 nm. The emission spectrum shows one broad band with λ_{max} = 505 nm. The 0 – 0 transition is found at 425 nm. The Stokes shift for **2_ADAT** is 127 nm.

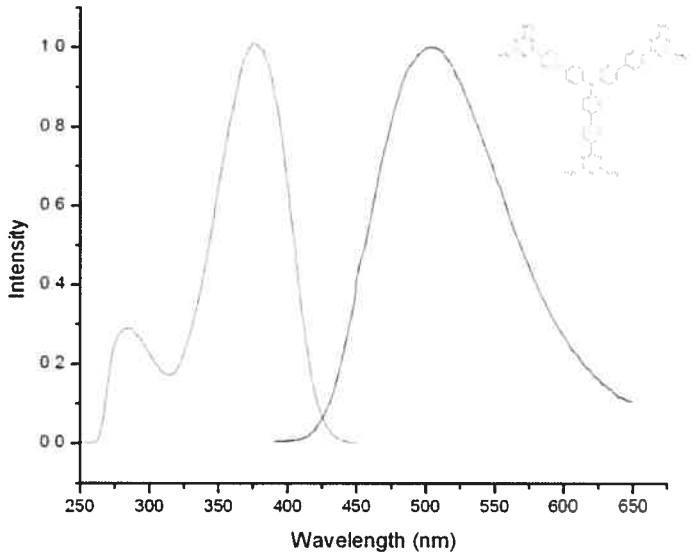

Figure 3.27 Normalized excitation (red) and emission (blue) spectra of tecton **2_ADAT** in DMSO.

The parent compound of tecton **2_ADAT** is tris(4-biphenyl)amine (**52**). In THF solution, compound **52** has absorption maxima at 246 nm and 345 nm and a fluorescence maximum at 408 nm.[168] The red-shift in the absorption and emission spectra of **2_ADAT** with respect to compound **52** is consistent with the one seen in the comparison of the spectra of tecton **1_ADAT** and triphenylamine.

3.6.3 Tecton 3_ADAT

In DMSO, tecton **3_ADAT** is blue fluorescent (**Figure 3.28**). As in the case of tecton **2_ADAT**, compound **3_ADAT** displays two bands in the excitation spectrum, at 300 nm and 389 nm. The λ_{max} for emission is 505 nm and the 0 – 0 transition is at 425 nm. It is important to note the small difference in Stokes shifts for compounds **2_ADAT** and **3_ADAT**. The Stokes shift for **3_ADAT** is 116 nm.

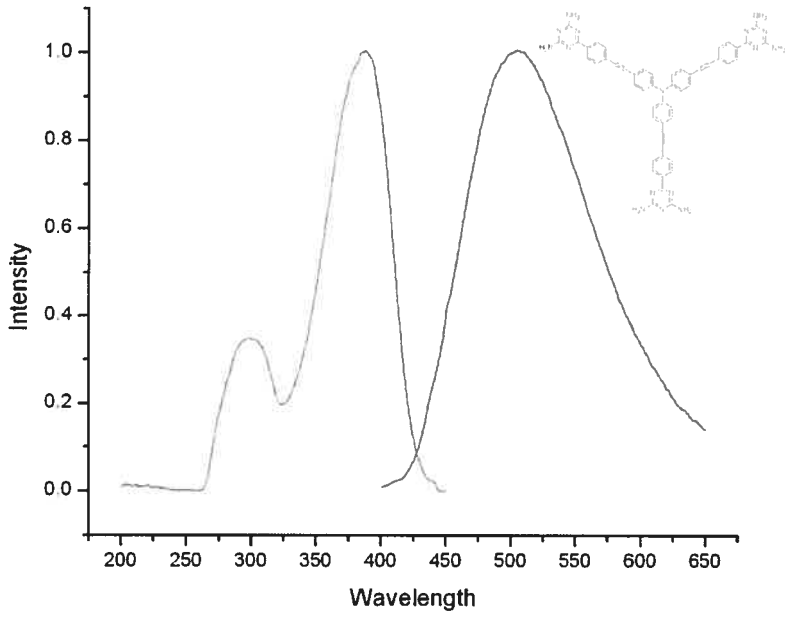

Figure 3.28 Normalized excitation (red) and emission (blue) spectra of tecton **3_ADAT** in DMSO solution.

3.6.4 Tecton 1_BDAT

Like the previous compounds, tecton **1_BDAT** is blue fluorescent in DMSO solution (**Figure 3.29**). The excitation spectrum, shown in red, displays one large band with λ_{max} = 352 nm and a shoulder at 311 nm. In the case of tectons **2_ADAT** and **3_ADAT**, the energy gap between the S_1 and S_2 excited states is large enough to allow

for at least partial resolution of the two bands in the spectra. In the case of **1_BDAT,** however, the energy gap is smaller (Δ = 41 nm), resulting in significant overlap between the two excited states. The λ_{max} for emission is 405 nm and the 0 – 0 transition lies at 382 nm. The Stokes shift for **1_BDAT** is 53 nm.

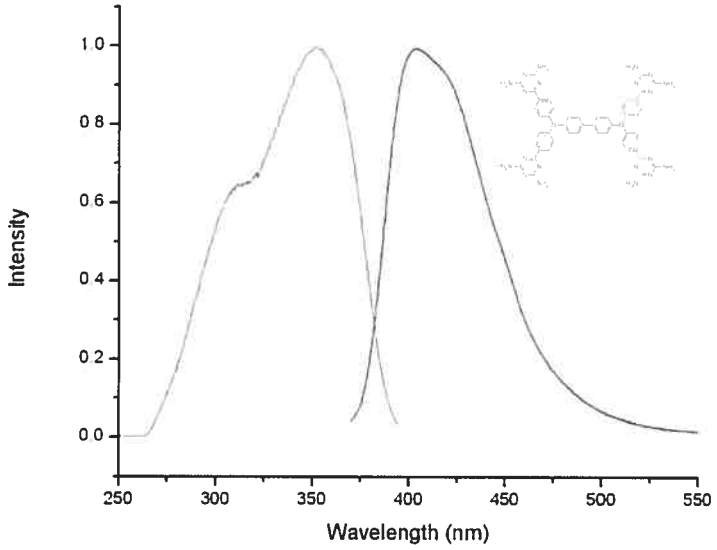

Figure 3.29 Normalized excitation (red) and emission (blue) spectra of tecton **1_BDAT** in DMSO solution.

3.7 Summary

Cyclic voltammograms obtained for the triarylamine tectons show that the strongly electron-withdrawing diaminotriazine does not appear strongly influence the oxidation potential of the compound. In the case of tecton **1_BDAT**, the two triarylamine nitrogen atoms are oxidized at almost the same potential, indicating that the torsion of the biphenyl spacer prevents the two atoms from communicating with one another. The quality of the data obtained is hampered by the limited solubility of

these compounds. Solid-state studies are required in order obtain a more thorough understanding of the electrochemistry of these compounds.

Oxidative titration of the triarylamine tectons leads to a disruption and blue-shifting of the absorbance bands of the neutral compounds, which is consistent with observations made for triarylamines that do not bear recognition groups. However, these experiments must be considered as failures, because of the dramatic difference in absorption spectra and colour change when carried out in DMF as opposed to chloroform. As a result, no concrete information can be inferred about the processes occurring under these conditions, or the nature of the products formed.

Tectons **1_ADAT**, **2_ADAT**, **3_ADAT** and **1_BDAT** are "sky" blue fluorescent (λ_{max} > 390 nm).[67] Sky or pale blue fluorescence is the most common type of blue emission observed in triarylamines and other aromatic organic compounds. The optimal colour for inclusion in OLEDs is "deep" blue (λ_{max} < 390 nm) because it provides better colour purity. Deep blue fluorescence occurs at a higher energy than sky blue emission and, as a consequence, more energy is required for the initial excitation.[169] This poses serious problems for the long-term efficiency of OLEDs, since the increased energy requirements also lead to accelerated deterioration of the device. A comparison of the Stokes shift of the four tectons reveals that **1_ADAT** and **1_BDAT** (53 nm and 58 nm respectively) have significantly smaller shifts than **2_ADAT** and **3_ADAT** (127 nm and 116 nm). This is a significant difference, indicating that the tectons with the shorter arms lose less energy to non-emitting processes. Tecton **1_BDAT** has a fluorescence

maximum that approaches the deep-blue range and tectons constructed of more than one triarylamine unit connected to recognition sites by short arms may yield even better results

The data in this chapter shows that the presence of a hydrogen-bonding functional group, 3,5-diaminotriazine, does not have a significant impact on the electrochemical properties of these triarylamine derivatives. In order to further analyze the processes that occur during the chemical oxidation of this class of compound, molecules such as **55** may be prepared in order to overcome some of the limitations imposed by the marginal solubility of the tectons in this study.

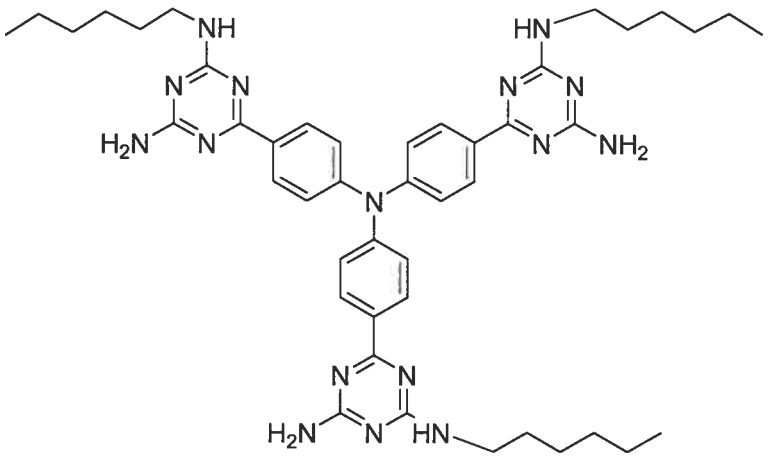

55

CHAPTER 4

Polyfluorinated Tectons

4 Polyfluorinated Tectons

4.1 Introduction: Fluorine in Crystal Engineering

Fluorine is the most electronegative, the most reactive, and the most powerful oxidizing agent of the elements. Consequently, the compounds of fluorine are among the most stable and inert known, chlorofluorocarbons being the most notable.[170] Fluorine was isolated for the first time in 1886 by the French scientist F. F. Hnri Moissan from the mineral fluorspar (CaF_2). This discovery earned him the Nobel Prize in chemistry in 1906. In modern science and industry, elemental fluorine and its compounds have become indispensable.[171] Fluoroalkyl polymers such as Teflon® have become commonplace as oil- and water-repellent coatings on textiles and other surfaces. Inorganic fluorides in drinking water and dental products are critical for good oral hygiene. In addition, the widespread success of modern portable electronics would be impossible without $LiPF_6$ – based high-density batteries.[172]

Fluorine is among the smallest of the elements, being closest in size to hydrogen. It is well understood that the replacement of a hydrogen atom by fluorine can have a dramatic impact on the chemical and physical characteristics of a compound.[173,174] For example, the fluorinated analogues of many enzyme substrates are resistant to metabolism, although they are readily recognized.[175,176] The electron density of perfluoroaromatic rings is the opposite of that of their hydrogen-bearing counterparts. These important differences are due to the electronegativity, bond strength and inherent low polarizability of fluorine atoms, and suggests that their presence mayhave a profound impact on intermolecular association.

4.1.1 F···F Interactions

Recent work in crystal engineering has shown the vast extent to which halide interactions can influence crystal structures.[177] However, the existence of F···F interactions in this category is the subject of intense debate. Although iodine, bromine and even chlorine can be employed reliably to construct supramolecular synthons, fluorine rarely produces this type of interaction (**Figure 4.1**).[178]

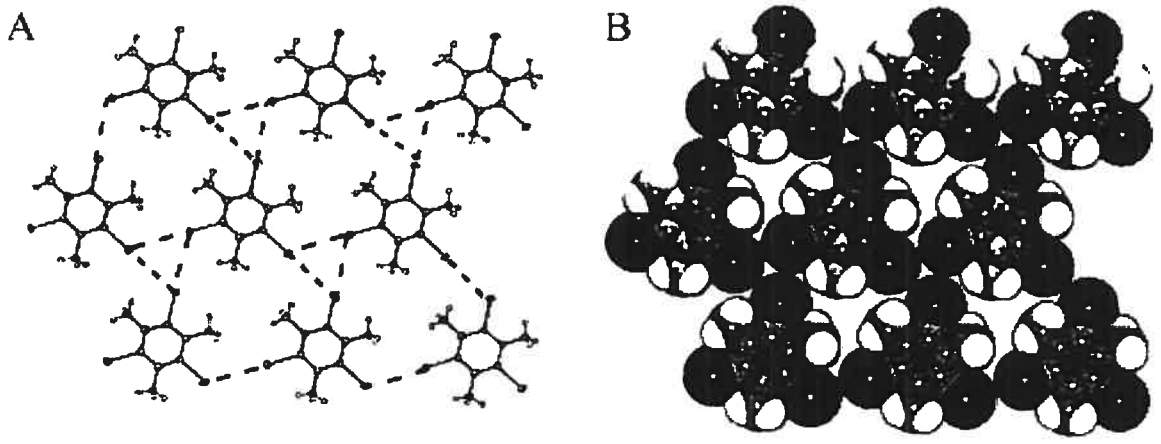

Figure 4.1 A) View of a portion of a sheet of triiodomesitylene molecules with thermal ellipsoids drawn at 50% probability. Iodine-iodine contacts shown with dashed lines. **B)** Space filling representation of the same sheet.[179]

There are two broad types of halogen interactions, which are differentiated by the angles between the halogen atoms, as shown in **Figure 4.2**. Studies have shown that interactions of Type I result only from close contacts and are not actually stabilizing. Type II interactions, on the other hand, result from polarization of the two halogen atoms that participate and give rise to a stabilizing force. Consistent with the low polarizability of fluorine atoms, very few crystal structures of fluorinated compounds display Type II contacts.

Figure 4.2 Classification of halogen interactions.[180]

4.1.2 X-H···F Interactions

The role of H···F interactions is not without controversy either. Although the X-H···F hydrogen bond is generally accepted, it has been argued that it is in fact a charged dipole interaction of the type $(X\text{-}H)^{\delta+}\cdots\cdots F^{\delta-}\text{-}C^{\delta+}$.[181] The most general method for differentiating between the two interactions is by measuring the X – F interatomic distance. When the distance is in the range of 2.20 – 2.55 Å, the interaction is regarded as a hydrogen bond.[182] **Figure 4.3** shows representations of the crystal structures of water and charged amide adducts of tris(pentafluorophenyl)borane and tris(pentafluorophenyl)alane, and it clearly demonstrates the presence of O-H···F and N-H···F hydrogen bonds.[183]

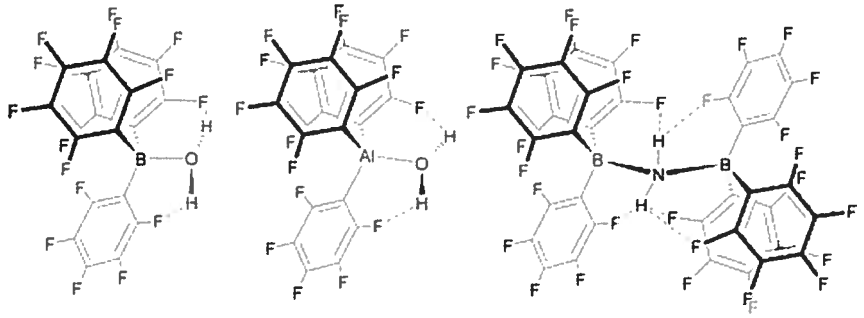

Figure 4.3 Crystal structures of various adducts of tris(pentafluorophenyl)borane and tris(pentafluorophenyl)alane. X-H···F bond distances range from 2.30-2.40 Å.[183]

The strong electronegativity of fluorine has given rise to a number of reliable supramolecular synthons. This is especially evident in the case of fluoroaromatics (**Figure 4.4**). Hydrogen bonds involving fluorine atoms are found to have similar lengths as those that involve other acceptor atoms such as nitrogen or oxygen, with the majority falling into the 2.30 – 2.90 Å range.

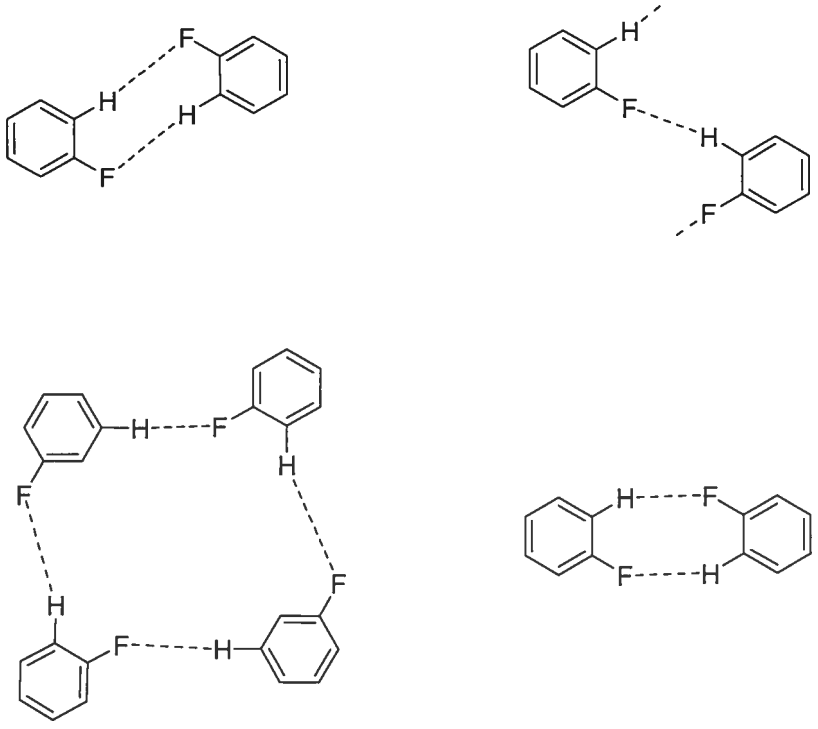

Figure 4.4 Supramolecular synthons observed in fluoroaromatic compounds. [182]

4.1.3 Phenyl – Perfluorophenyl Interactions

Perhaps the most striking intermolecular interaction involving fluorine-containing compounds is the phenyl – perfluorophenyl interaction. Standard aromatic compounds have their highest electron density at the center of the ring, but the strong electronegativity of fluorine moves this electron density to the perimeter of the ring for

perfluoroaromatics. This displacement of the ring current leads to very strong π-π interactions between aromatic systems and their fluorinated analogs.

One of the earliest and still most striking instances of this interaction is the co-crystal of benzene and hexafluorobenzene (HFB).[184] In the crystalline phase, both benzene and HFB exhibit the classical edge-to-face aromatic interaction, often referred to as a C-H···π interaction.[185,186] In this type of π interaction, a ring-bound hydrogen atom of one molecule points toward the center of the ring in another molecule, creating a herringbone pattern.[10] When fluorinated and non-fluorinated compounds are co-crystallized, this type of interaction is not present. Rather "π-stacking" is observed. There is a strong electrostatic interaction between the electron-rich non-fluorinated rings and the electron-poor fluorinated rings.[187,188] The strength of this interaction is powerfully illustrated by the melting point of the 1:1 co-crystal of benzene and hexafluorobenzene (**Figure 4.5**). While both pure compounds are liquids at room temperature, their co-crystal remains solid until 25 °C.

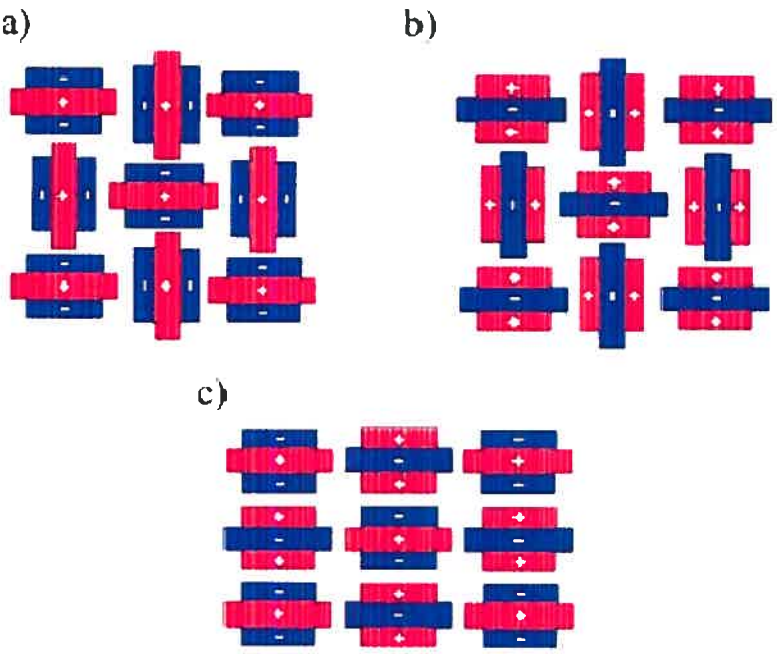

Figure 4.5 Representative crystal structures of **a)** benzene, **b)** hexafluorobenzene and **c)** benzene-hexafluorobenzene co-crystal.[180]

4.1.4 Electronic Effects

The presence of multiple fluorine atoms in a compound results in dramatic changes in polarization and electron delocalization. Not only does this cause an inversion of polarization in fluoroaromatic compounds, but it can also lead to the stabilization of negative charge. This is most readily demonstrated by comparing the pK_a values for two simple organic acids, acetic acid (4.75) and trifluoroacetic acid (-0.25).[189] Trifluoroacetic acid is better able to donate its labile proton because of the strong inductive effect of the three fluorine atoms There is also growing evidence that the presence of multiple fluorine atoms in a molecule can be used to stabilize the presence of a free radical, which may have important implications for the development of materials such as organic magnets.[190]

4.2 Polyhalogenated Carbon-Centered Radicals as Molecular Magnets

4.2.1 The Development of Molecular Magnetism

Magnets have been a source of fascination and study since the behaviour of lodestone, Fe_3O_4, was first observed. The first man-made magnets were prepared by magnetizing iron roughly 400 years ago. Since that time, much has been learned about the relationship between electricity and magnetism, and this knowledge has been applied in many ways. Perhaps most importantly, the use of dynamos has made affordable electricity widely available. An atomic-scale understanding of magnetism was not achieved until the advent of quantum mechanics in the early twentieth century. This showed that the critical element in magnetic behaviour is electron spin. The proximity, number and coupling of electron spins govern the magnetic properties of materials. Magnetic behaviour is quantified by the magnetic susceptibility (χ), which obeys the Curie Law. While the mathematical details of the Curie Law are beyond the scope of this text, suffice it to note that χ is controlled by the spin quantum number of the system and is inversely proportional to temperature.[191] Typically when spins are brought into proximity, they will arrange themselves such that they oppose each other, which leads to a reduction or even elimination of magnetic susceptibility. This is known as antiferromagnetic coupling. Ferromagnetic coupling occurs when the spins of a system align themselves to enhance magnetic susceptibility, resulting in magnetic behaviour.[192]

The first requirement for magnetic behaviour is the presence of an unpaired electron. Understanding this allowed for the development of the first synthetic magnets which had the electron residing in the *d*- and *f*-orbitals of metals. These magnets, such as Co_5Sm, are made by high-temperature metallurgical methods. More recently, there has been a great deal of interest in creating magnets where the unpaired electron resides in a *p*-orbital of a non-metal. This interest was spurred by the revelation that organic materials can behave as conductors of electricity. Research has led to a number of organometallic compounds that exhibit magnetic behaviour. While most of these materials are magnetic at temperatures in the range of 1 – 10 K, a complex with the composition $V[TCNE]_x \cdot yCH_2Cl_2$ is magnetic at room temperature.[193] TCNE is tetracyanoethenide radical anion.

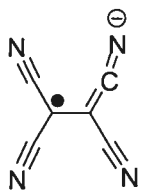

$[TCNE]^{\cdot -}$

This complex is a strong enough magnet that it can be isolated from its reaction mixture with a stirring bar. The composition of this magnetic material remained unknown for some time, until thin-film X-ray photoelectron spectroscopy revealed that it contained a mixture of V(II), V(III), $[TCNE]^{2-}$ and $[TCNE]^{\cdot -}$. While details about the structure of this substance remain elusive, the critical realization is that at least one unpaired electron resides on the organic ligand and not on the metal. This discovery has prompted researchers to push toward the development of a purely organic

magnet. Nitronyl nitroxides and verdazyl radicals are the two classes of compounds that have generated the most interest in this field (**Figure 4.6**), but another class, carbon centered radicals, is gaining popularity, especially with supramolecular chemists.[194]

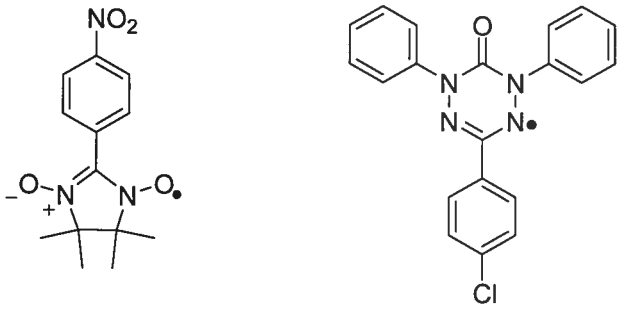

p-NPNN
0.65 K

p-CDpOV
0.21 K

Figure 4.6 Two low-temperature organic magnets and the temperature at which they are magnetic.[194]

4.2.2 Crystal Engineering Toward Organic Magnets

Many compounds contain stable radicals but very few exhibit magnetism. This is because the organization of the spins of the unpaired electrons in a material determines whether or not ferromagnetic coupling will occur. Supramolecular chemists and crystal engineers have become increasingly interested in organic magnets, and they have demonstrated that magnetic coupling can be transmitted across hydrogen bonds.[195]

Carbon-centered radicals have a long and varied history starting with the discovery of the triphenylmethyl (trityl) radical, and they continue to be the subject of intense research efforts.[196-198] While many radicals decay rapidly by reactions with

themselves or other compounds, those radicals that can persist for extended periods of time have received special attention.[199,200] Stable organic radicals are now commonly employed in a wide range of synthetic processes, including polymerizations and enantioselective additions.[201,202]

The trityl radical is not normally considered a stable or persistent radical, but its derivative, perchlorotriphenylmethyl, is.[203] Studies have shown that the stabilization of the radical is primarily due to the conformation of the molecule and also to delocalization by the electronegative chlorine atoms. The steric bulk of the chlorine atoms, in particular at the ortho positions, forces the compound into a propeller shape that shields the radical site from reaction.[204]

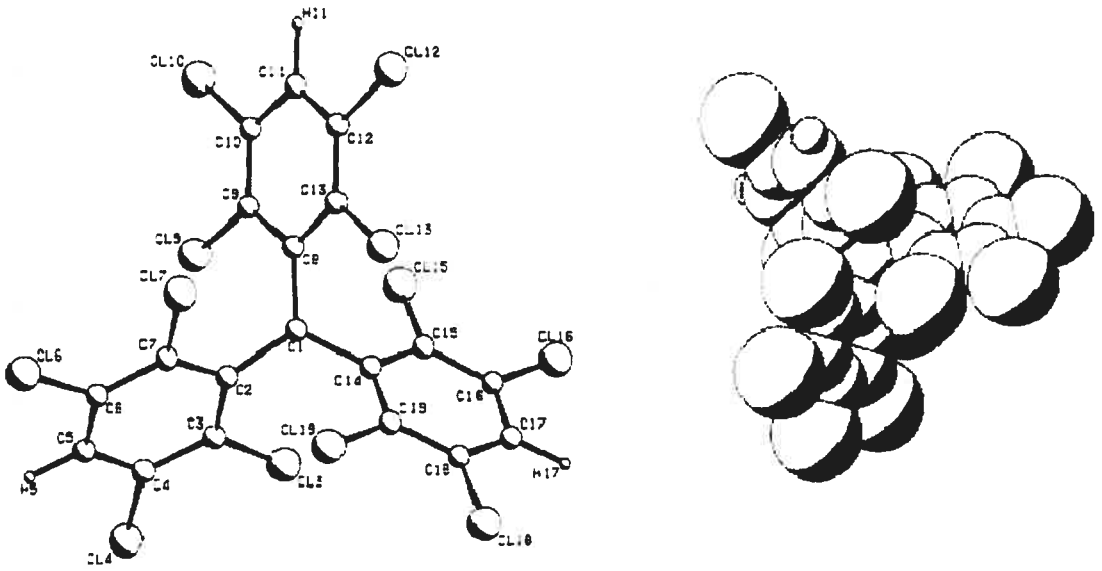

Figure 4.7 a) Perspective view of tris(2,3,5,6-tetrachlorophenyl)methyl with atom numbering and **b)** space-filling model of tris(2,4,6-trichlorophenyl)methyl.

A striking example of the potential role that supramolecular chemistry might play in the development of a purely organic magnet is the synthesis and crystallization of radical **56**.[205] The compound can be crystallized from hexanes and dichloromethane, giving an open framework crystal structure consisting of three repeating two-dimensional hydrogen-bonded sheets (**Figure 4.8**). Each molecule of **56** participates in two distinct hydrogen-bonding interactions. In the first case, one carboxylic acid group participates in hydrogen bonds with two separate molecules. This results in the formation of a cyclic hexamer. The second interaction is a classic carboxylic acid dimer, which links each hexamer to six other hexamers. The sheets are offset and their stacking is maintained by Cl···Cl interactions. The architecture of the system results in an open-channel structure with large, accessible cavities, as shown in **Figure 4.9**. The system is also surprisingly robust, maintaining its crystallinity up to 275 °C.[205]

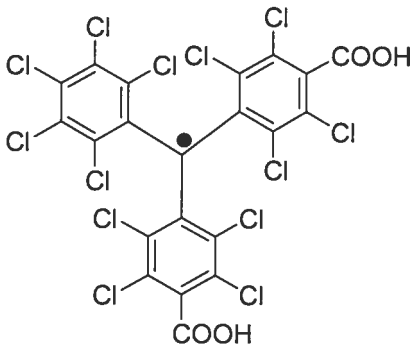

56

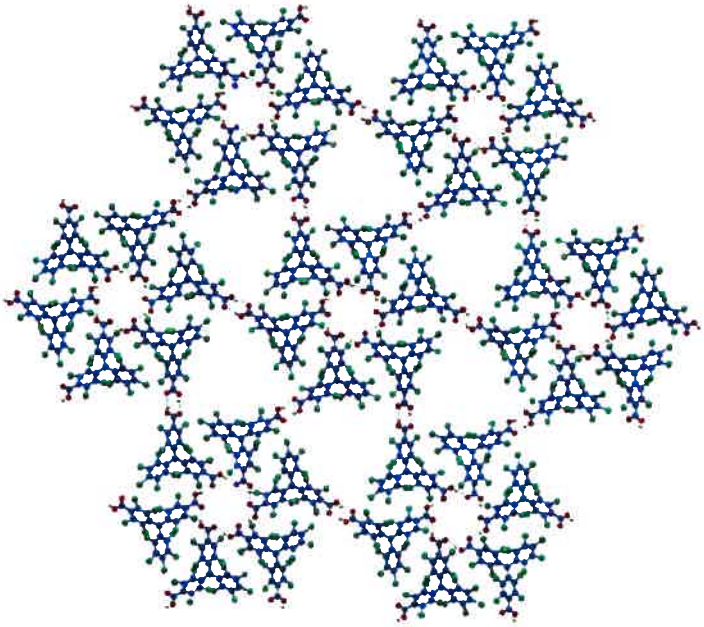

Figure 4.8 One sheet of the crystal structure of **56**. Guest molecules are omitted for clarity. Note the seven interconnected hexamers. The molecules of a given hexamer are connected by a cyclic hydrogen-bonding pattern. The radical centers are found at the center of each hexamer. Each hexamer is connected to six others via a hydrogen-bonded dimer of carboxylic acids. Carbon atoms are shown in blue, oxygen in red and chlorine in green.

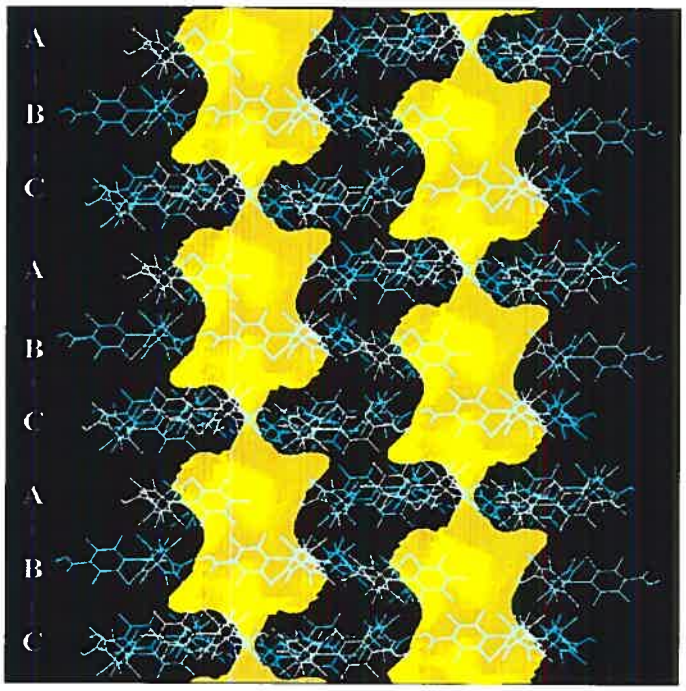

Figure 4.9 Representation of the void spaces in POROF-1 that contain the radical centers.

4.2.3 Fluorine and Molecular Magnetism

Perfluorinated analogues of compound **56** have been studied for some time, due to their ability to form cations, anions and radicals.[206-208] Although lacking the steric stabilization of compounds such as **56**, radicals such as perchloro derivative **58** are long lived in the absence of oxygen. **Scheme 4.1** describes the two-step preparation of radical **58** from hydrogen-bearing **57**. Although radical **58** has not been isolated, it is has been characterized by epr.[190] These results may be the first step toward building organic magnets from highly fluorinated molecules.

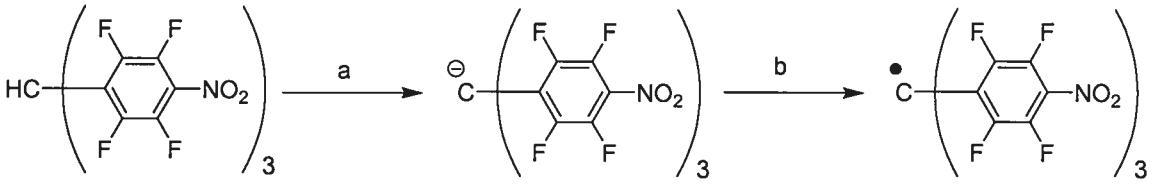

57 **58**

Scheme 4.1 a) 0.1M NaOH, *p*-dioxane, **b)** 0.1 M $KMnO_4$

4.3 Fluorine in Molecular Tectonics

The use of fluorinated compounds in molecular tectonics is not a subject which has received a great deal of attention until now. Recent work has highlighted the failure of compound **59** to participate in F···F interactions.[209] In addition, only one of the four fluorine atoms on the molecule participates in C-H···F interactions. The self-association of compound **59** is directed by C-H···O interactions between the aromatic hydrogen adjacent to the fluorine and the ether oxygens (**Figure 4.10**).[209] More

detailed studies of compounds constructed from polyfluorinated cores are required to further the understanding of the role of fluorine in the self-assembly of tectons.

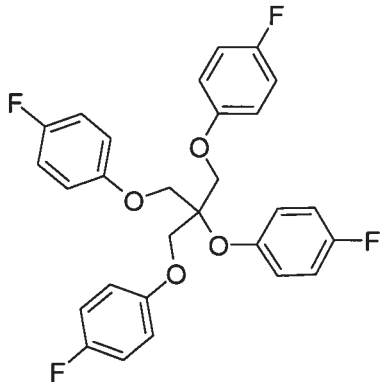

59

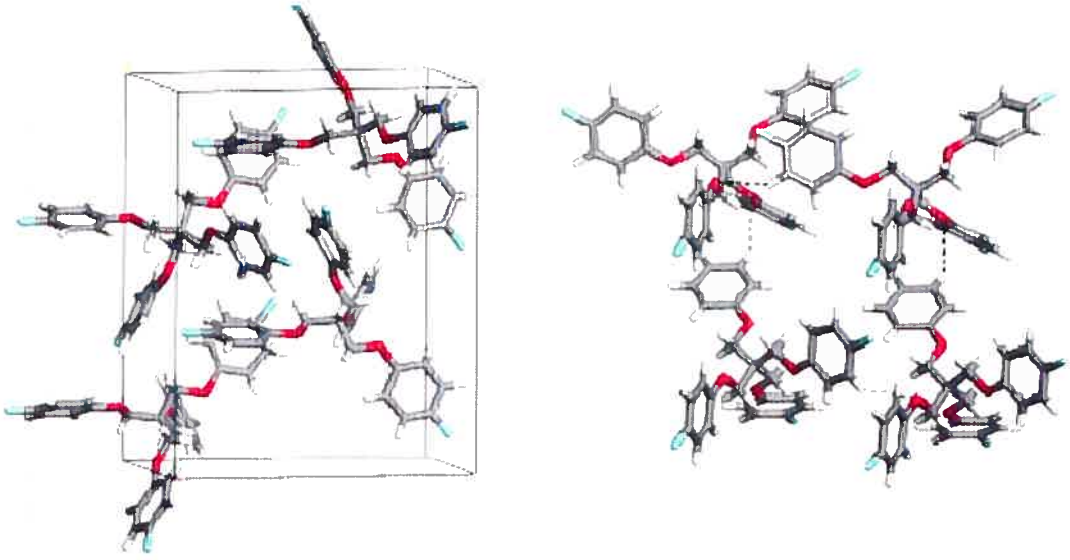

a b

Figure 4.10 a) View of the unit cell of compound **59** and **b)** the C-H···O hydrogen bonding between neighbours.[209]

4.3.1 Synthetic Targets

Derivatives of polychlorotriphenylmethyl are attracting a growing interest from supramolecular chemists and crystal engineers, but their polyfluorinated analogues have yet to achieve this level of popularity, despite their long history and well-developed chemical methodologies. Perfluorotriphenylmethane (**63**) represents an ideal starting point for a foray into the development of fluorinated tectons, since the initial synthetic steps have been well explored, and there is a large body of literature that deals with nucleophilic aromatic substitution.[207,210] The ultimate goal of this project is to prepare tectons with recognition groups such as pyridinones and diaminotriazines grafted on to polyfluorinated cores. Synthesis and crystallization of target molecules such as compounds **60** and **61**, as well as the intermediate compounds along the synthetic routes, could provide deeper insight into the influence of fluorine on the crystal structures of organic molecules.

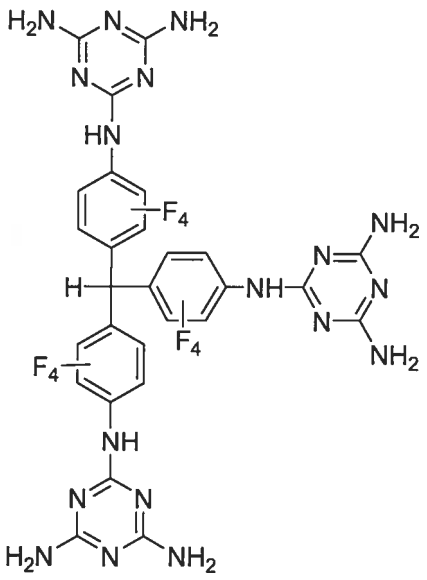

60

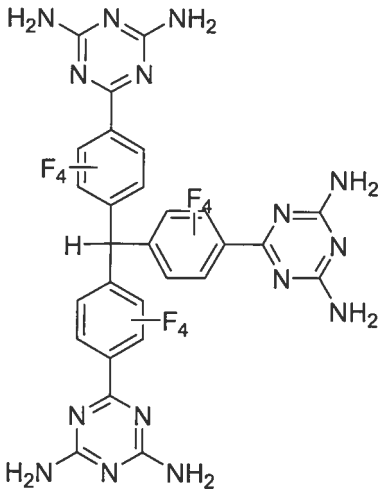

61

4.4 Synthesis of Tecton 60

4.4.1 Tris(2,3,4,5,6-pentafluorophenyl)methane (63)

Both tectons **60** and **61** are built around a tris(2,3,4,5,6-pentafluorophenyl)methane (**63**) core. The earliest, and most direct, route to compound **63** involves the Friedel-Crafts alkylation of pentafluorobenzene with chloroform.[210] Alternatively, the target can be reached in two steps by the reaction of pentafluorophenyllithium with pentafluorophenyl methyl ester, followed by a reduction of the resulting alcohol.[207] Much of the synthetic route toward compound **60** has been elaborated,[190] but certain key challenges – such as the grafting of the recognition unit – remain. It is of no little interest that although compound **63** has been known for nearly forty years, no crystal structure has been published, although the compound is readily crystallized from benzene and ethanol. For the purpose of the present study,

the compound **63** core was synthesized using the original Friedel-Crafts route (**Scheme 4.2**). While the yield of this reaction was moderate, the direct access to the compound is attractive.

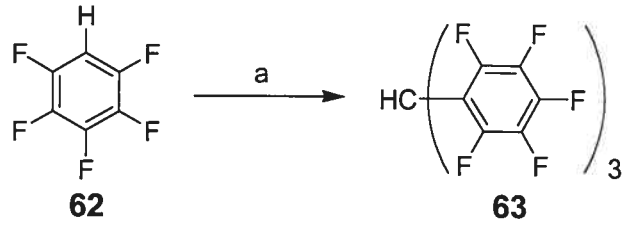

62 **63**

Scheme 4.2 a) $AlCl_3$, $CHCl_3$, neat, 150 °C, 36 h, 65%

Compound **63** was isolated in crystalline form as colourless needles, which were studied by X-ray diffraction. The ORTEP diagram (**Figure 4.11**) shows that the crystals consist of only compound **63** and do not contain any included guests.

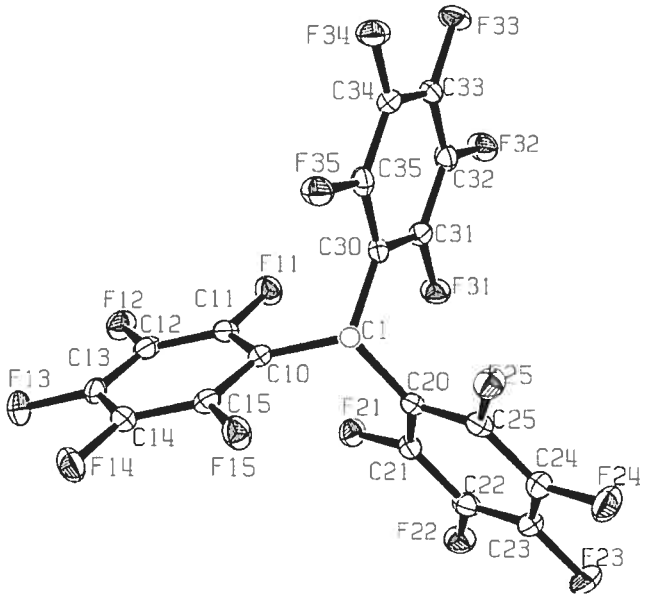

Figure 4.11 ORTEP diagram of tris(2,3,4,5,6-pentafluorophenyl)methane, drawn at 50% probability. There are no included guests, and each arm is symmetry-independent.

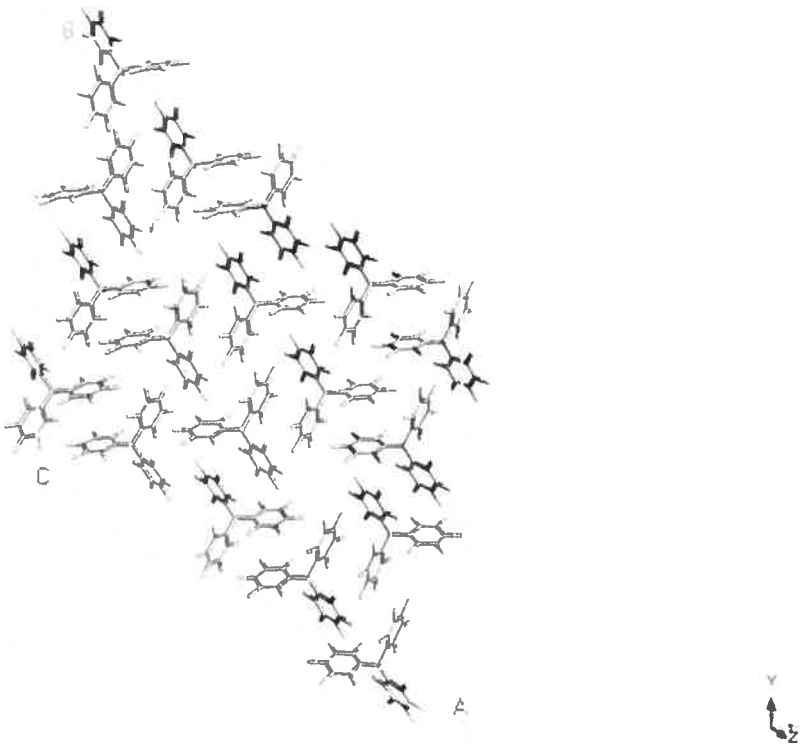

Figure 4.12 View of the unit cell of the crystal structure of compound **63** seen along the *c* axis.

The compound crystallizes in the R-3 space group (**Figure 4.12**) with the unit cell parameters $a = b = 37.8257(5)$ Å, $c = 6.1199(2)$ Å and $\alpha = \beta = 90^{\circ}$, $\gamma = 120^{\circ}$. The volume of the unit cell is 7583.1(3) Å^3. There are no F·····F contacts present. All of the intermolecular contacts are due to close packing. The conformation of the molecule presumably prevents the α – hydrogen atom (on C1) from participating in intermolecular interactions. The molecules are arranged in columns that run along the *c* axis. There are two sets of columns, as shown in **Figure 4.13**. The black and white sets of columns run antiparallel to one another.

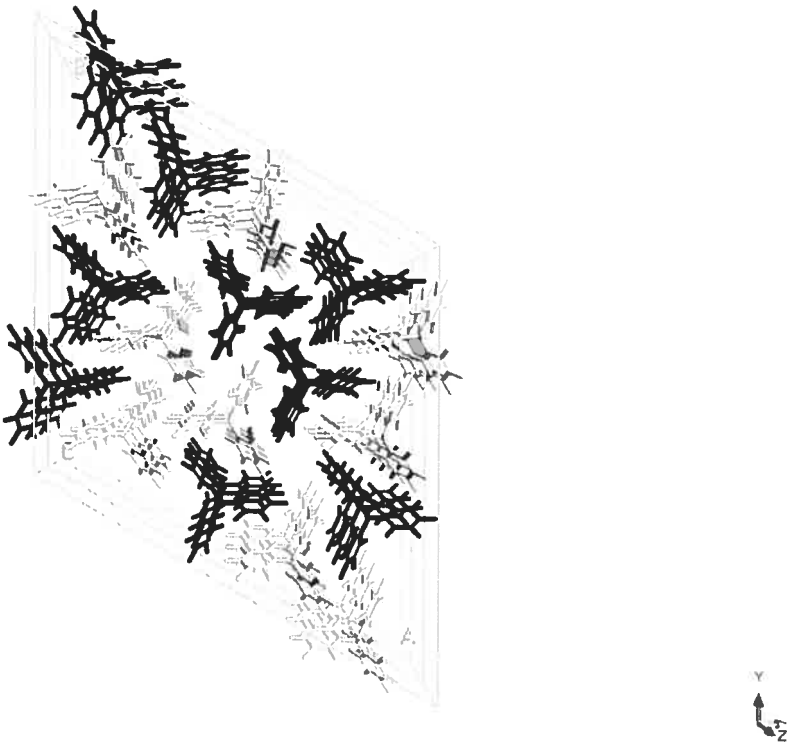

Figure 4.13 Perspective view of a 1 x 1 x 3 array of unit cells of compound **63** as seen along the *c* axis. Antiparallel columns of molecules are depicted in black or white.

4.4.2 Tris(4-hydrazinyl-2,3,5,6-tetrafluorophenyl)methane (64)

The electrophilic substitution of highly electron-deficient aromatic systems is problematic, because it is difficult for such systems to act as nucleophiles. The functionalization of compound **63** must be done by nucleophilic aromatic substitution (S_NAr). In the S_NAr mechanism, the aromatic ring will act as the electrophile and undergo attack from a nucleophile. Although numerous nucleophiles can be employed, hydrazine was selected because of the ability of the hydrazinyl group to participate in the formation of hydrogen bonds, and because the synthesis is already known.[190] Tris(2,3,4,5,6-pentafluorophenyl)methane (**63**) was reacted with hydrazine

monohydrate in refluxing *p*-dioxane (**Scheme 4.3**). Tris-(4-hydrazinyl-2,3,5,6-tetrafluorophenyl)methane (**64**) was isolated in 90% yield after crystallization from toluene, giving off-white crystals which were analyzed by X-ray diffraction.

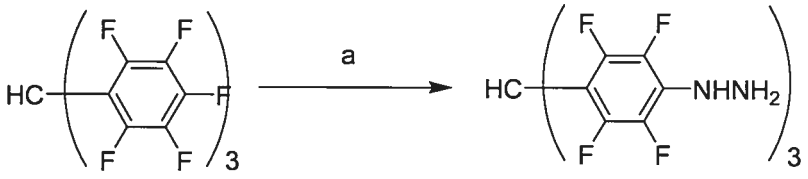

63 **64**

Scheme 4.3 a) Hydrazine monohydrate, p-dioxane, reflux, 90 %

As expected, compound **64** crystallized as an extensively hydrogen-bonded network. The ORTEP diagram (**Figure 4.14**) shows that the crystal is comprised of compound **64** and one disordered molecule of toluene. The molecule crystallizes in the P2/c space group with a = 13.9976(4) Å, b = 6.1918(2) Å and c = 25.6809(7) Å (α = γ = 90°, β = 103.596(2)°) and a unit cell volume of 2163.40(11) Å^3. There are six intramolecular N-H···F hydrogen bonds that direct the orientation of the hydrazinyl groups.[183,211] This directing effect of the aromatic fluorine atoms is critical to the overall supramolecular architecture of the system.

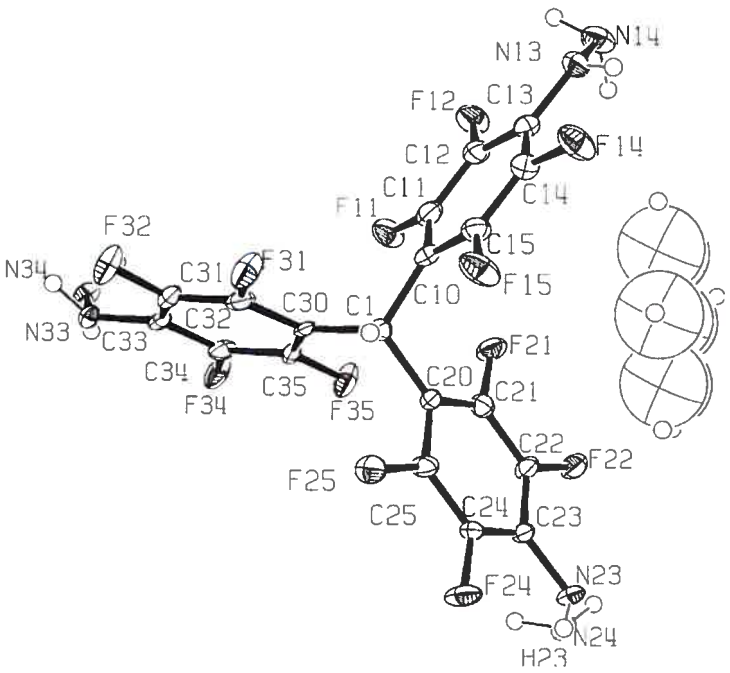

Figure 4.14 ORTEP diagram of compound **64** · **1** C_7H_8, with numbering scheme present. Ellipsoids are drawn with 50 % probability.

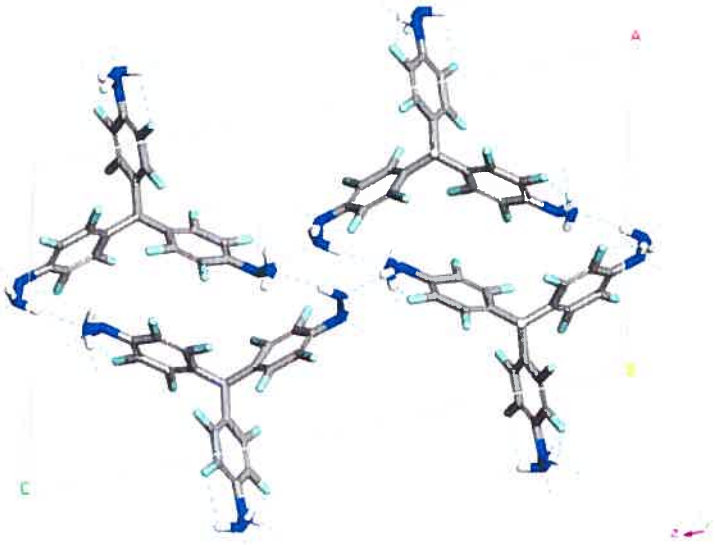

Figure 4.15 View of the unit cell of compound **64**, seen along the *b* axis. Carbon atoms are shown in grey, hydrogen atoms are shown in white, fluorine atoms are shown in teal and nitrogen atoms are shown in blue. Hydrogen bonds are drawn as broken lines. Guest molecules of toluene are removed for clarity.

Compound **64** associates in the solid state to form a two-dimensional layered structure. The association is directed by the formation of a hydrogen-bonded tetramer. The assembly is held together by four intermolecular N-H···N hydrogen bonds (**Figure 4.16**).

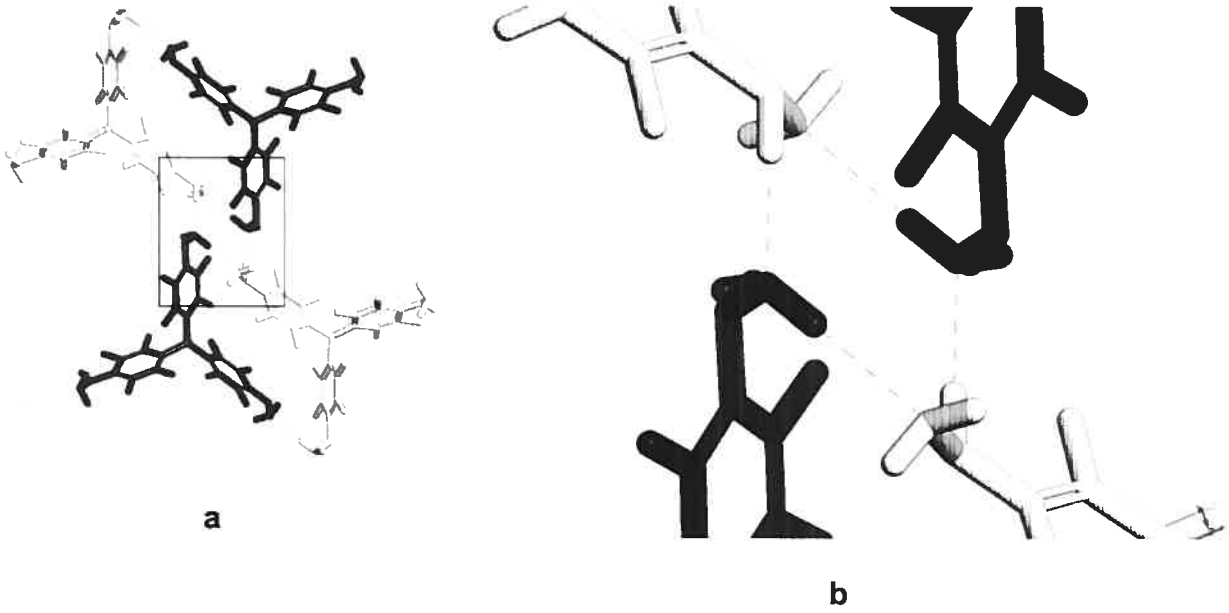

Figure 4.16 a) Hydrogen-bonded tetramer of tecton **64**. Each molecule shown in white has both of the nitrogen atoms from the hydrazine group participating in the recognition, while the black molecules have only one nitrogen atom each in the motif. **b)** Magnified view of the same hydrogen-bonded tetramer.

Both hydrazinyl nitrogen atoms of the two molecules drawn in white (**Figure 4.16a**) participate in the formation of the hexagonal motif. The hydrazine groups are antiparallel. The two molecules drawn in black give only their terminal nitrogen atom to the hexagon, and they are *trans* to one another across the ring formed by the hydrogen bonds. A search of the Cambridge Structural Database for this hydrogen-bonding motif in compounds containing hydrazine functional groups revealed no hits.Search of the Cambridge Structural Database v.5.28[212April 4, 2007,213] The layers

have a honeycomb structure, although the hexagons are divided into three sections (**Figure 4.17**).

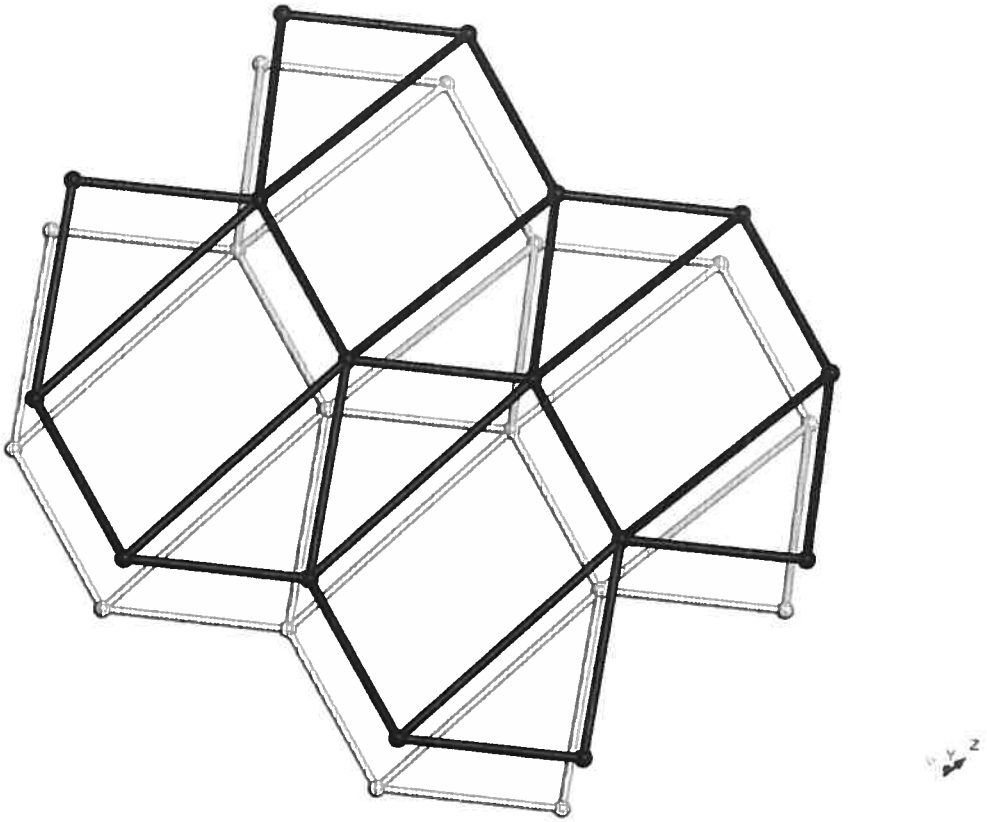

Figure 4.17 Representation of the network formed by the self-assembly of compound **64**. In the drawing, the spheres represent the central carbon atoms of the molecule and the solid lines represent the hydrogen-bonding interactions.

4.4.3 Tris-(4-amino-2,3,5,6-tetrafluorophenyl)methane (65)

In order to proceed toward the target molecule **60**, an attempt to reduce the hydrazinyl group of compound **64** was made by the standard method of treatment with refluxing hydroiodic acid followed by recrystallization from methylcyclohexane.[190] Tris-(4-amino-2,3,5,6-tetrafluorophenyl)methane (**65**) was isolated as yellow crystals in

63% yield (**Scheme 4.4**). Some of the crystals obtained were of sufficient quality to be analyzed by X-ray diffraction.

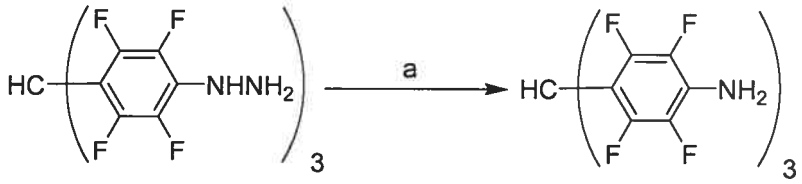

64 **65**

Scheme 4.4 $HI_{(aq)}$, reflux 48 h, 63%.

The ORTEP diagram (**Figure 4.18**) shows that the stoichiometry of the crystals consist of one molecule of methylcyclohexane for every two tectons. The three branches of the tecton are symmetry-independent. Tecton **65** crystallized in the monoclinic P2/n space group, with the unit cell (**Figure 4.19**) having a = 14.3870(15) Å, b = 7.7327(8) Å and c = 19.596(2) Å ($\alpha = \gamma = 90.0^{\circ}$, $\beta = 96.617(4)^{\circ}$). The unit cell has a volume 2165.5(4) $Å^3$. As expected, compound **65** participates in numerous hydrogen-bonding interactions. In particular, each tecton forms N-H···F hydrogen bonds with five nearest neighbours (**Figure 4.20**). One tecton (shown in white) is the hydrogen-bond donor in the interaction with the molecules shown in blue and black. The tecton in white is also the hydrogen-bond acceptor in the interactions with the molecule drawn in red. With each of the molecules indicated in grey, the white tecton forms two hydrogen bonds each.

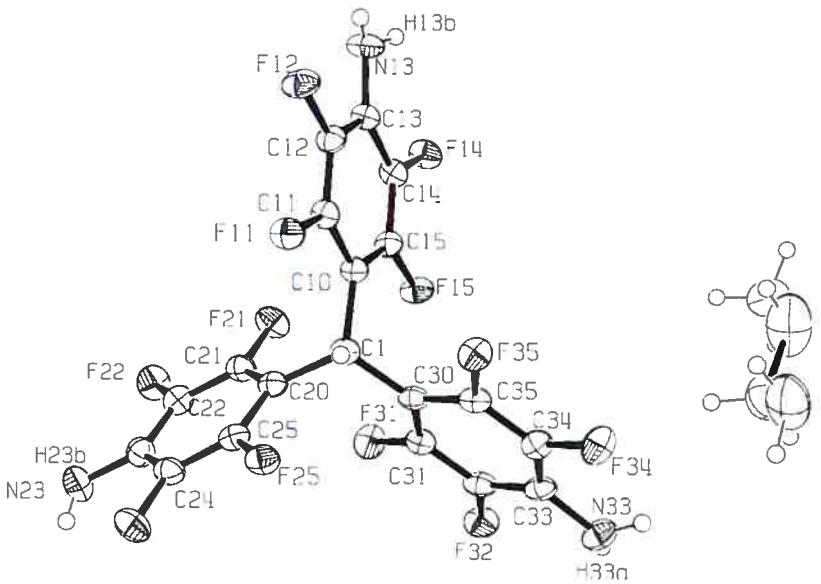

Figure 4.18 ORTEP diagram of tecton **65** with ellipsoids drawn at 50% probability. One-half molecule of methylcyclohexane is included.

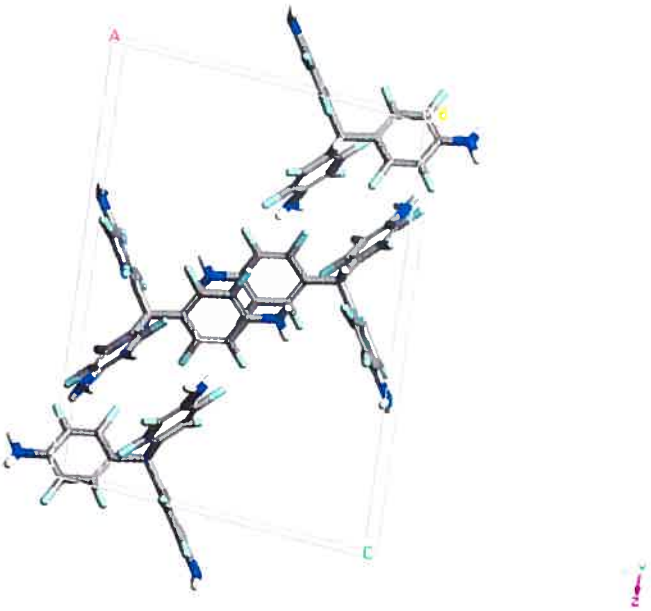

Figure 4.19 Unit cell of tris(4-amino-2,3,5,6-tetrafluorophenyl)amine (**65**) as seen along the *b* axis. Guest molecules are removed for clarity. The two molecules in the center of the unit cell are related by π-stacking. Each of these participates in hydrogen bonds with the two other molecules, found in the corners of the unit cell. Carbon atoms are shown in grey, hydrogen in white, nitrogen in blue and fluorine in teal.

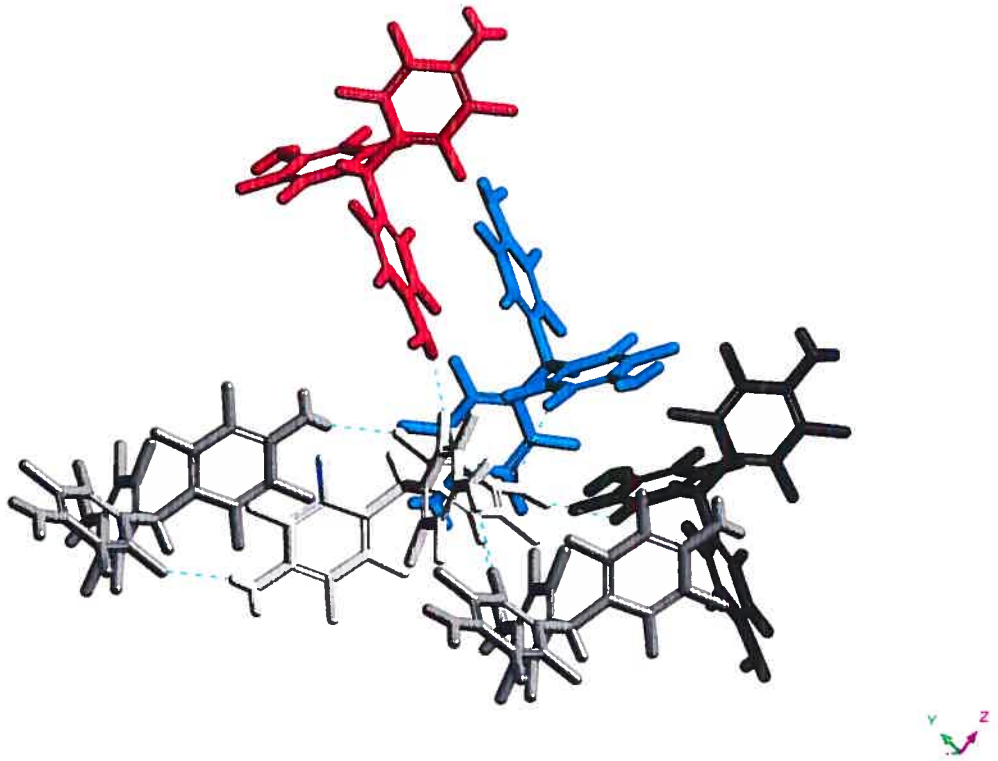

Figure 4.20 Representation of the hydrogen bonding in the crystal structure of tecton **65**. One tecton, shown in white, forms N-H···F hydrogen bonds with five nearest neighbours. The white molecule participates in two hydrogen bonds with each of the tectons drawn in grey and one each with the molecules shown in black, blue and red. Hydrogen bonds are shown as broken lines.

The association of tecton **65** creates a three-dimensional network (**Figure 4.21**). There is only one network present in the structure, without any interpenetration. The network defines a set of channels that run along the *b* axis (**Figure 4.22**).

Figure 4.21 Representation of the three-dimensional network formed by the association of tecton **65**. The spheres represent the central carbon atom of each molecule, and the solid lines represent the hydrogen-bonding interactions between them.

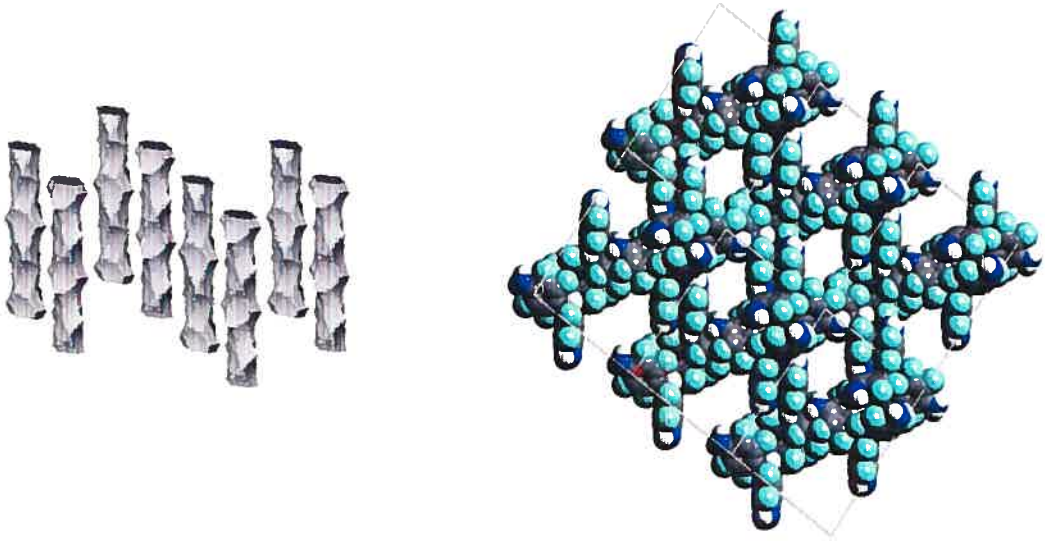

a **b**

Figure 4.22 **a)** Representation of the channels defined by the network formed by the association of tecton **65**. The drawing shows a 2 x 2 x 2 array of unit cells as seen approximately along the *a* axis. The channels are created by tracing the movement of the center of a sphere with a 2.5 Å diameter along the van der Waals surfaces inside the crystal. The channels run along the *b* axis. **b)** Cross section of the same channels seen along the *b* axis.

Conversion of intermediate **65** into target **60** requires conversion of the amino groups into triaminotriazine groups. The introduction of the recognition subunit typically involves reaction of the aminated core with cyanuric chloride, followed by displacement of the chlorine atoms using ammonium hydroxide (**Scheme 4.5**). Initial attempts to synthesize tecton **60** were carried out under standard conditions and were unsuccessful. Variations of this method, which included carrying out the reaction at higher temperatures and increasing the ratio of the reactants, also failed to bear fruit. The reaction should proceed via the nucleophilic attack of the amine on cyanuric chloride, resulting in the liberation of hydrochloric acid. The presence of four fluorine atoms on each phenyl ring of compound **65** delocalizes the lone pair on the amine to such an extent that the the initial nucleophilic attack is impossible.

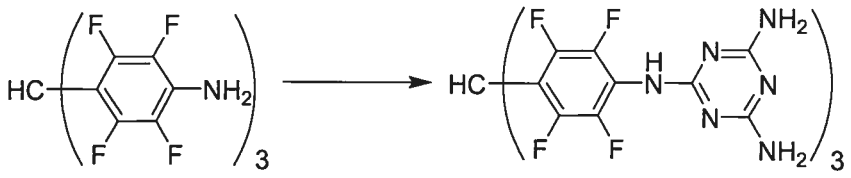

65 **60**

Scheme 4.5 General transformation of amine **65** into tecton **60**.

In order to compensate for the low electron density of its amines, compound **65** was deprotonated with tetra-*n*-propyl ammonium hydroxide prior to being reacted with cyanuric chloride. A solution of compound **65** in *p*-dioxane turns cobalt blue when treated with base. The reaction of anilines with cyanuric chloride produces one equivalent of HCl. For this reason, the reaction was carried out in excess of base.

After reaction and work-up, only compound **65** was isolated. Further attempts using NaH to achieve quantitative deprotonation of the starting material also proved unsuccessful.

As an alternative to the triaminotriazine motif of compound **60**, compound **66** was envisioned, where the triazine is linked to the core via a hydrazine bridge (**Scheme 4.6**). The second nitrogen atom of the hydrazine is not conjugated with the strongly electron-withdrawing core of the compound. The attempted preparation of tecton **66** proceeded via the addition of **64** to a solution of commercially available 2-chloro-4,6-diamino-1,3,5-triazine in acetone at -10 °C, followed by quenching with sodium carbonate (**Scheme 4.6**).[214] Only compound **64** was recovered after the reaction. Repeating the experiment in the presence of a strong base (NaH) was also unsuccessful. Although the terminal amine of the hydrazine is not directly conjugated with the polyfluorinated core of compound **64**, the inductive effect may be important enough to prevent the reaction from occurring. The failure of this experiment is surprising, and a wider range of experimental conditions should be considered.

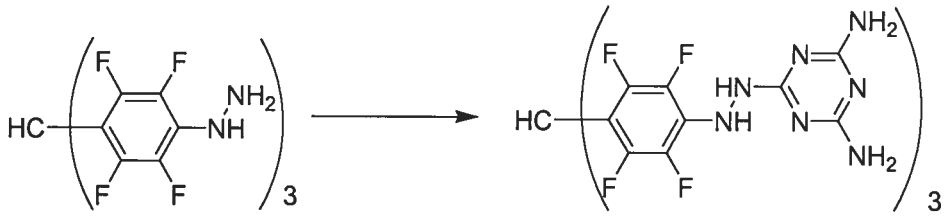

64 **66**

Scheme 4.6 Proposed transformation of hydrazine **64** into tecton **66**.

4.5 Tecton 61

4.5.1 Tris(4-bromo-2,3,5,6-tetrafluorophenyl)methane (68)

As an alternative to tecton **60**, where the recognition group is separated from the core by an amine, tecton **61** would have the diaminotriazine grafted directly. To prepare this compound, tris(4-bromo-2,3,5,6-tetrafluorophenyl)methane (**68**) was synthesized as a possible precursor. The synthesis was carried out in the same manner as for tris(pentafluorophenyl)methane, using 4-bromo-2,3,5,6-tetrafluorobenzene (**67**) instead of pentafluorobenzene, as in **Scheme 4.7**. The reaction proceeded with similar yields, and a beige solid was recovered and recrystallized from toluene. The crystals obtained were of sufficient quality to be examined by X-ray diffraction.

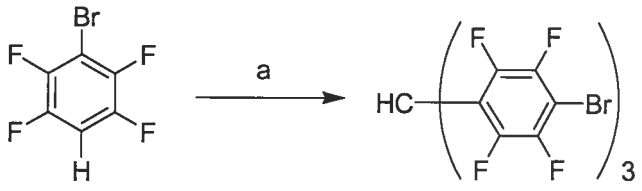

67 **68**

Scheme 4.7 a) $AlCl_3$, $CHCl_3$, sealed tube, 150 °C, 36 h, 65%.

The ORTEP diagram (**Figure 4.23**) shows that compound crystallizes as a close-packed structure with no included guests. The crystals belong to the C2/c

space group with unit cell parameters a = 18.448(9) Å, b = 16.573(8) Å, c = 13.733(6) Å and $\alpha = \gamma = 90.0°$, β = 100.02(3)°.

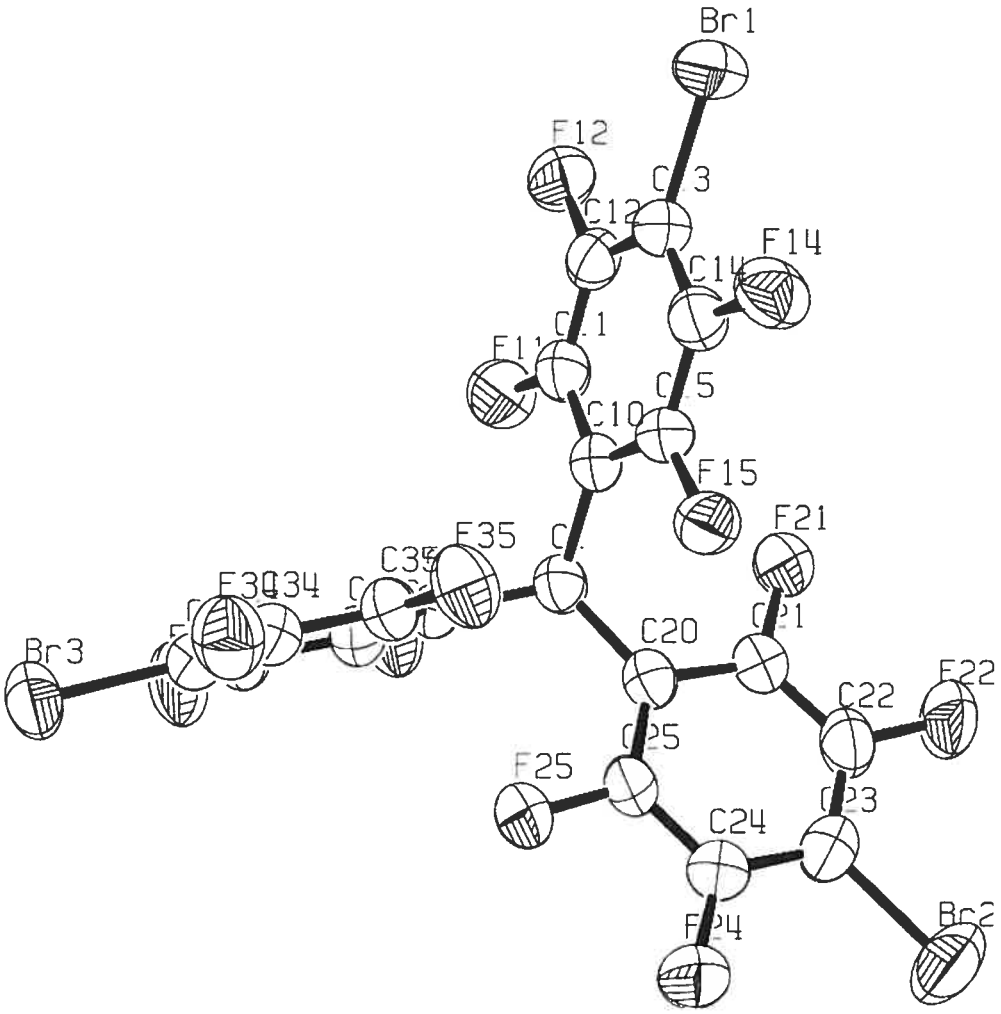

Figure 4.23 ORTEP diagram of tris(4-bromo-2,3,5,6-tetrafluorophenyl)methane (**68**), with the numbering scheme in place. Thermal ellipsoids are drawn at 50% probability.

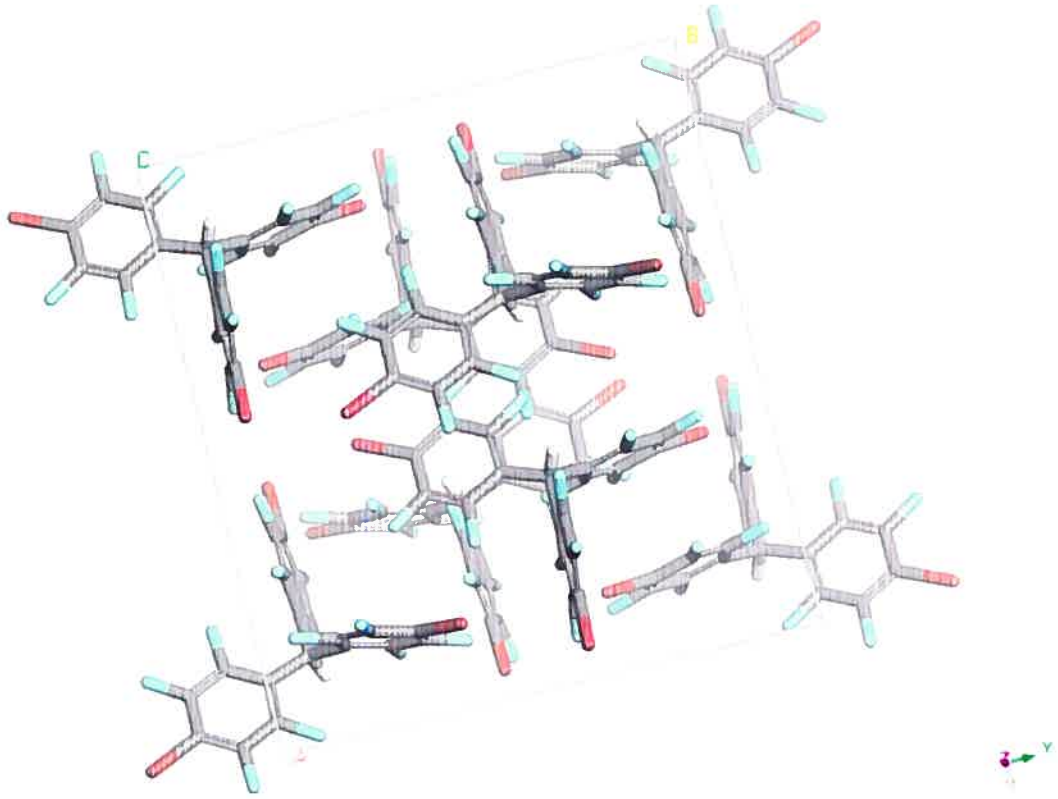

Figure 4.24 Unit cell of compound **68** seen along the *c* axis. Carbon atoms are shown in grey, hydrogen atoms in white, fluorine atoms in green and bromine atoms in red.

This crystal structure demonstrates a number of interesting features. The principal recognition motif is a dimer formed by two bromine – bromine interactions between Br1 and Br2. The two bromines form a type II halogen contact (**Figure 4.2**). The third bromine atom does not participate in any close contacts. The bromine atoms are separated by a distance of 3.693 Å. There are also π-interactions, and what at first appears to be an F···F contact. The distance between the two fluorine atoms is 2.972 Å, which is too large for this to be considered an actual F···F contact.

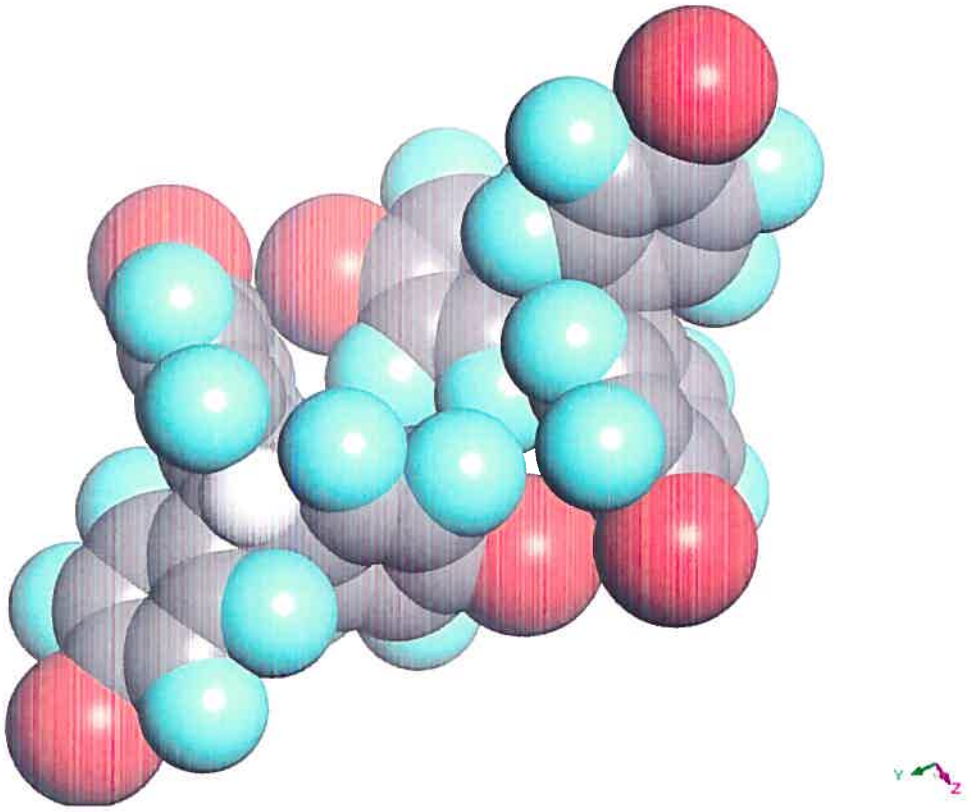

Figure 4.25 Weak interactions in the crystal structure of compound **68**. Bromine – bromine contacts and π – stacking direct the association of the two molecules shown.

4.5.2 Synthesis of Tecton 61

With intermediate **68** in hand, the conversion of the bromide to the known nitrile was carried out via the standard route affording the blood-red compound **69** in 15% yield.[190] This then sets the stage for the condensation to the DAT-bearing target (**Scheme 4.8**).[190] Unfortunately, the standard conditions for the condensation of a nitrile with dicyandiamide failed to afford tecton **61**.

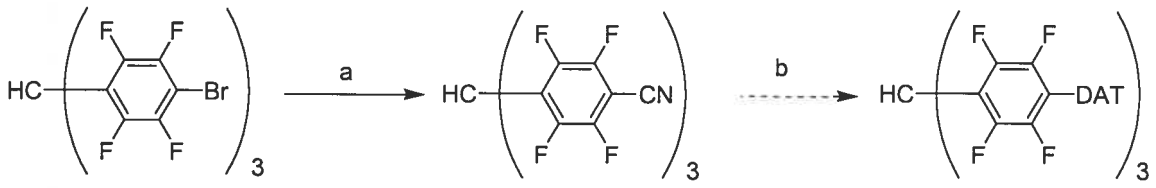

68 **69** **61**

Scheme 4.8 **a)** CuCN, DMF, reflux, 12% **b)** KOH, dicyandiamide, 2-methoxyethanol, no reaction.

4.6 Tetrakis(2,3,4,5,6-pentafluorophenyl)methane (70)

The synthesis of tetrakis(pentafluorophenyl)methane (**70**) would be a landmark in fluoroaromatic chemistry, and it presents a unique opportunity to compare the crystal structure of analogous fluorinated and non-fluorinated compounds such as tetraphenylmethane. The initial approach taken in an attempt to synthesize compound **70** was to elaborate on the Friedel-Crafts methodology employed in the synthesis of tris(pentafluoropheny)methane.

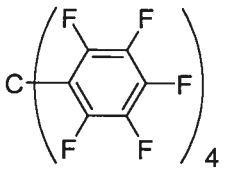

70

In this approach, shown in **Scheme 4.9**, carbon tetrachloride was used instead of chloroform as the alkylating agent. Repeated attempts failed to yield any product that could be isolated. Compound **62** is electron deficient and is simply not reactive enough to carry out the number of substitutions required by this route.

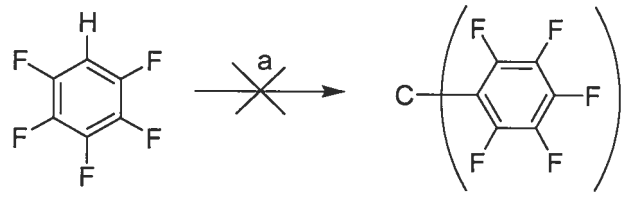

62 **70**

Scheme 4.9 a) $AlCl_3$, CCl_4, sealed tube, 150 °C, 72 h. No reaction.

An alternative approach involves using the tris(pentafluorophenyl)methyl anion as a nucleophile and substituting a fluorine atom on hexafluorobenzene. Nucleophilic aromatic substitution, S_NAR, is readily carried out on highly electron- deficient rings such as hexafluorobenzene and halogenated pyridines. Tris(pentafluorophenyl)methane is readily deprotonated by hydroxide and forms bright blue and purple solutions in polar organic solvents. Methylation of the anion was seen as a critical step in the pursuit of this project. Isolation of resulting compound **71** would provide insight into the use of the tris(pentafluorophenyl)methyl anion as a nucleophile as well as being an important synthetic target. Replacing the central hydrogen atom with a methyl group could overcome some of the difficulties encountered in the synthesis of tecton **61.** In order to ensure quantitative deprotonation, tris(pentafluorophenyl)methane was reacted with sodium hydride in dry dioxane under an inert atmosphere. The reaction proceeds smoothly, and the purple anion is isolated in quantitative yield. Complete deprotonation is confirmed by the disappearance of the signal corresponding to the labile proton in the NMR spectrum of the product. Methylation of the anion was attempted under a wide range of conditions, including reaction in neat methyl iodide and reaction in neat

dimethylsulfate at 100 °C in a sealed tube. In each case, either the anion itself, or the reprotonated tris(pentafluorophenyl)methane, was recovered.

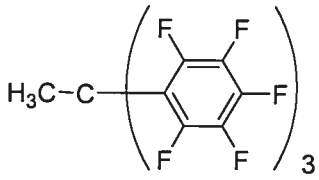

71

The stability of the tris(pentafluorophenyl)methyl anion was further tested by bubbling oxygen through a solution of deprotonated **63** in DMSO. No deterioration in the colour of the solution was noted, and no changes were noted in the NMR spectrum of the compound.

The strong delocalizing effect of the multiple fluorine atoms in the tris(pentafluorophenyl) anion make it unreactive towards most electrophiles, with the exception of protonation. The central hydrogen can be replaced by a deuterium atom by reacting a solution of deprotonated **63** in dioxane with trifluoroacetic acid – *d*. The solution rapidly turns from purple to colourless and deuterated **72** was isolated after neutralization of the resulting solution, followed by evaporation of the solvent, as in **Scheme 4.10**. Preliminary investigations of compound **72** confirmed the presence of the deuterium atom by IR spectroscopy (C-D stretch: 2120.36 cm^{-1}).

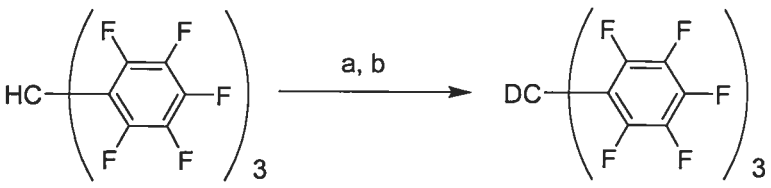

63 **72**

Scheme 4.10 a) NaH, dioxane, 99%. **b)** TFA-*d*, dioxane, 99%.

In order to better explore the reactivity of the tris(pentafluorophenyl)methyl anion, mechanisms other than S_N2 must be explored. The use of carbocationic substrates as well as benzyl and allyl targets should be considered, but are beyond the scope of this study.

In light of the challenges encountered in the study of this class of compounds, simple derivates such as **73** should be considered as well.

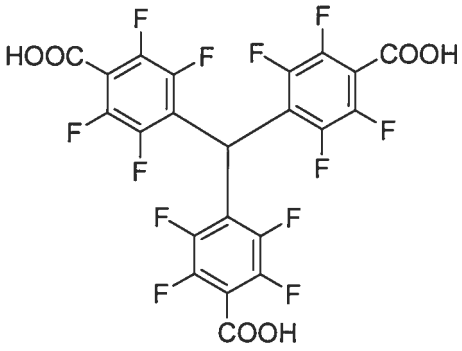

73

4.7 Summary

The presence of one or many fluorine plays an important role in determining the steric and electronic properties of a molecule. The polyfluorinated analogues of triphenylmethane and tetraphenylmethane are an interesting class of compounds that have yet to be explored by crystal engineers. Analysis of the crystal structures of several representatives of this class of compounds reveals that hydrogen-bonding functional groups can have a profound impact on the assembly of these compounds in the solid state, giving rise to rarely-observed recognition motifs. A number of key hurdles have yet to be overcome in making more complex derivatives of this class of compound. Preliminary results indicate that these of compounds could provide important insights into using molecular tectonics to build open-framework crystalline networks containing reactive species.

CHAPTER 5

Conclusions and Future Research

5 Conclusions and Future Research

5.1 Triarylamine Tectons

5.1.1 Conclusions

The design, synthesis and characterization of supramolecular networks that serve as functional materials are important goals in molecular tectonics. Triarylamines have attracted a great deal of interest for modern opto-electronic applications and are particularly well-suited to explorations in molecular tectonics due to their rigid trigonal geometry and synthetic accessibility.

Chapter 2 describes the synthesis of tectons based on triarylamine cores. These compounds crystallize as open-framework supramolecular networks maintained by hydrogen bonds. X-ray diffraction analysis shows that modifications to the molecular structure may lead to drastic changes in the resulting crystal architecture. A novel "embrace" recognition motif was observed in the crystal structures of tectons **2_ADAT** and **1_BDAT**. The presence of this motif may be predicated on the length of the arms of a tecton, and it results in less porous structures than hexagonal networks like the one formed by tecton **1_ADAT**.

The optical and electronic characterization of the triarylamine tectons is outlined in Chapter 3. These compounds readily undergo one-electron oxidation of the central nitrogen in the presence of a strong oxidant, such as antimony (V) chloride. Cyclic

voltammetry reveals that the tectons undergo reversible oxidation processes. The presence of multiple diaminotriazinyl groups is experienced differently by the different compounds. There is a correlation between the angles of torsion of the substituents about the triarylamine nitrogen atom and the oxidation potential of the compound. When large torsional angles are observed in the crystal structure, as is the case for tecton **1_ADAT**, the oxidation potential is virtually unchanged from the unsubstituted parent compound. Correspondingly, when smaller torsional angles are observed in the crystal structure, as is the case for tectons **2_ADAT** the oxidation of the central nitrogen occurs at a higher potential than in the undecorated core.

5.1.2 Future Research

In order to fully explore the potential of molecular tectonics in the development of functional materials based on triarylamines, a greater number of tectons in this family need to be prepared and crystallized. In addition, the solid-state electrochemistry of these compounds needs to be examined, both in the crystalline and amorphous phases.

The use of crystalline materials in organic opto-electronic devices presents many serious drawbacks and may prove to be impractical. The current trends in device design and fabrication are geared toward the use of amorphous polymers and small molecules. Nevertheless, the use of compounds that can associate by hydrogen bonding as additives or dopants may lead to enhanced function or improved mechanical properties. Recent work has shown that appropriately designed small molecules that can form multiple hydrogen bonds can also be used to prepare

molecular glasses.[215] Triarylamine tectons containing differentially substituted recognition groups are important targets in this exploration. Triaminotriazines similar to compound **74** are accessible via well-understood synthetic routes.[216] The presence of N-alkyl groups on the recognition sites should lead to greater solubility and better miscibility in host polymers such as polycarbonate. Compound **47**, mentioned in Chapter 2, is an obvious precursor for making target **74**.

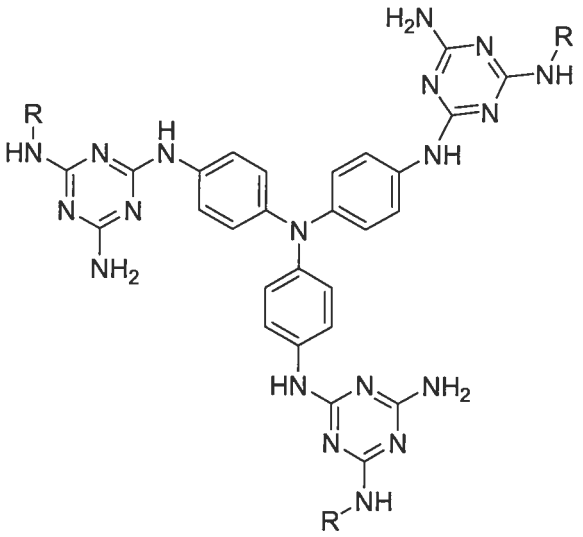

74

(R = alkyl)

In addition, asymmetrically substituted triarylamines could be used to prepare supramolecular discotic liquid crystals. The strategies of molecular tectonics have only recently been applied to materials other than crystals, and liquid crystals present an interesting avenue for exploration. Compounds such as triarylamine **75** are able to form hexagons by hydrogen bonding (**Scheme 5.1**). These hexagons could, under the appropriate conditions, assemble into columnar liquid crystal phases.

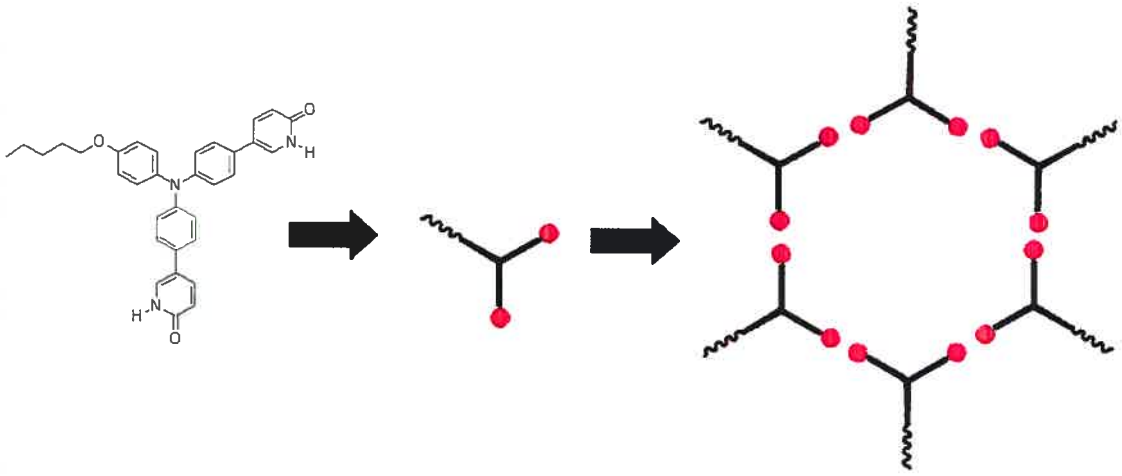

75

Scheme 5.1 Hypothetical self-assembly of tecton **75** into discrete hexagons.

5.2 Polyfluorinated Tectons

5.2.1 Conclusions

The quest for a purely organic room temperature magnetic material has inspired supramolecular chemists to seek to control spin alignment using various non-covalent interactions. Derivatives of perfluorotriphenylmethane are of interest for the development of organic magnets and for crystal engineering in general. The crystal structure of a number of polyfluorotetraphenylmethane derivatives has revealed that the presence of multiple fluorine atoms has a profound impact on the resulting crystal structure, sometimes leading to new recognition motifs.

5.2.2 Future Research

The synthesis of tectons derived from polyfluorinated molecular cores remains a critical goal in molecular tectonics. Once compounds such as **60** and **61** have been prepared and characterized, they could be used to prepare stable carbon-centered radicals. Careful control of the conditions of crystallization could lead to new materials with ferromagnetic properties. Future research will be focused on the use of combinatorial methods for preparing and evaluating large numbers of crystals.

CHAPTER 6
Experimental Details

6 Experimental Details

6.1 General Considerations

All melting points were measured with a Thomas-Hoover melting point apparatus and are uncorrected. Infrared (IR) spectra were recorded on a Perkin-Elmer Spectrum One FT-IR spectrometer using potassium bromide discs (KBr) or as neat liquid samples.

Proton (^{1}H) and carbon (^{13}C) NMR spectra were measured on either a Bruker AV-300 spectrometer (300 MHz for ^{1}H, 75 MHz for ^{13}C) or a Bruker AV-400 instrument (400 MHz for ^{1}H, 100.6 MHz for ^{13}C). Chemical shifts (δ) were measured in parts per million (ppm) in reference to an internal standard that was either dimethyl sulfoxide (DMSO, δH 2.49, δC 39.5) or chloroform ($CHCl_3$, δH 7.27, δC 76.9). Coupling constants are expressed in Hz, and the abbreviations used are: s = singlet, d = doublet, t = triplet, q = quartet, m = multiplet and bs = broad signal.

High-resolution and low-resolution mass spectra (Fast Atom Bombardment and Time-of-Flight) were recorded at the Centre Régional de Spectrométrie de masse du Département de Chimie de l'Université de Montréal.

All solvents were purified in the following manner prior to use. Toluene, ether, tetrahydrofuran (THF), dichloromethane, chloroform and N,N-dimethylformamide were passed through drying and filtration columns under anhydrous argon. All other solvents and reagents were commercially available and did not require further purification, unless otherwise indicated.

Reactions requiring anhydrous conditions were carried out under prepurified nitrogen, which was further dried by passing through a $CaSO_4$ column. Glassware for these reactions was oven-dried or flame-dried and allowed to cool under a current of nitrogen. Where indicated, apparatus was assembled in a glove box.

Fluorimetric and ultraviolet-visible absorption measurements were made in a 10 mm cuvette using deaerated and anhydrous dimethyl sulfoxide or *N,N*-dimethylformamide. Cyclic voltammetry measurements were done in deaereated anhydrous *N,N*-dimethylformamide with 0.1 M Bu_4NPF_6 using a saturated Ag/AgCl reference electrode, platinum working and platinum auxiliary electrodes. Typical sweep rates were either 500 mV/sec or 1000 mV/sec. All the oxidation potentials are referenced and normalized against ferrocene (406 mV vs. Ag/AgCl) under the same experimental conditions.

6.2 Synthetic Details

Tris(4-bromophenyl)amine (12)[111]

Triphenylamine (**24**, 5.00 g, 20.4 mmol) was dissolved in chloroform (20 mL). A solution of tetra-*n*-butylammonium tribromide (33.0 g, 67.3 mmol) in chloroform (20 mL) was added dropwise at room temperature. Once the addition was complete, the mixture was allowed to stir for an additional 20 min at room temperature. Saturated aqueous sodium thiosulfate (50 mL) was added to quench the reaction. After 5 min of stirring, the mixture was transferred to a separatory funnel. The aqueous layer was removed, and the organic phase washed repeatedly with brine and then water. The organic layer was dried over sodium sulfate and the solvent was evaporated. The resulting glassy solid was recrystallized from hot acetic acid to give colourless crystals of tris(4-bromophenyl)amine (**12,** 8.85 g 18.4 mmol, 90%). Melting point: 140-142 °C (lit. 141-143 °C); ^{1}H NMR (DMSO-d_6, 400 MHz): δ 7.35 (d, 6H, ^3J = 9 Hz), 6.69 (d, 6H, ^3J = 9 Hz); ^{13}C NMR (DMSO-d_6, 100 MHz): δ 144.4, 137.5, 131.7, 118.8; MS (FAB): m/z 482.5.

Tris(4-cyanophenyl)amine (25)[112]

Tris(4-bromophenyl)amine (**12**, 1.50 g, 3.11 mmol) and CuCN (0.918 g, 10.2 mmol) were placed in a 25 mL oven-dried round bottom flask fitted with a condenser and magnetic stirring bar. The flask was evacuated and refilled with nitrogen. Dry *N,N*-dimethylformamide (10 mL) was added via cannula. The solution was heated to reflux for 18 h. The hot reaction mixture was poured into a solution of ethylenediamine (40 mL) in H_2O (100 mL) and stirred for 5 min. The organic phase was then extracted with benzene and washed with 5% $NaCN_{aq.}$ (2 x 100 mL) in order to remove any water-soluble impurities. The organic layer was dried and the solvent removed by rotary evaporation. The resulting solid was triturated with methanol and recrystallized by slow evaporation of benzene. Tris(4-cyanophenyl)amine (**25**, 0.790 g, 2.40 mmol, 82%) was recovered as a yellow solid. Melting point: > 300°C (lit. 346-348°C); ^{1}H NMR (DMSO-d_6, 400 MHz): δ 7.60 (d, 6H, ^3J = 9 Hz), 7.16 (d, 6H, ^3J = 9Hz); ^{13}C NMR (DMSO-d_6, 100 MHz): δ 145.9, 132.9, 122.5, 116.9, 106.3; MS (FAB): m/z 321.1; High-Resolution MS (FAB/NBA): m/z 320.1016, calc. 320.1062 (for $C_{21}H_{12}N_4$).

Tecton 1_ADAT

Tris(4-cyanophenyl)amine (**25**, 0.250 g, 0.781 mmol) and dicyandiamide (0.673 g, 8.00 mmol) were placed in an oven-dried round-bottom flask equipped with a stirring bar and condenser. The flask was evacuated and refilled with nitrogen three times. A solution of 15 mol% KOH in 2-methoxyethanol (10 mL) was then added via syringe. The mixture was heated to reflux overnight and then cooled to room temperature. A yellow solid was precipitated with water. The solid was filtered and washed repeatedly with water and methanol. Tris[4-(3,5-diamino-2,4,5,6-triazinyl)phenyl]amine (**1_ADAT**, 0.375 g, 0.656 mmol, 84%) was recrystallized from DMSO/ethanol. Melting point: > 300 °C; ^{1}H NMR (DMSO-d_6, 400 MHz): δ 8.13 (d, 6H, ^3J = 8 Hz), 7.08 (d, 6H, ^3J = 8 Hz), 6.65 (s, 12H); ^{13}C NMR (DMSO-d_6, 75 MHz): δ

170.3, 168.2, 149.8, 132.8, 130.1, 124.2; MS (FAB): m/z 460.1, 307.1; High Resolution MS (TOF): m/z 572.2411, calc. 572.2370 (for $C_{27}H_{24}N_{16}$).

Tris[4-(4'-cyanophenyl)phenyl]amine (27)

In a dry three-neck round-bottom flask fitted with a condenser, tris-(4-bromophenyl)amine (**12**, 0.440 g, 0.803 mmol) was dissolved in toluene (30 mL) and water (5 mL) then purged vigorously with nitrogen for 30 min. Palladium(II) acetate (0.010 g, 0.0460 mmol) and 2-dicyclohexylphosphino-2',6'-dimethoxybiphenyl (Sphos, 0.045 g, 0.110 mmol) were added to the flask and the mixture was heated gently for 15 min. 4-Cyanophenylboronic acid (0.485 g, 3.30 mmol) and potassium carbonate (0.878 g, 4.14 mmol) were added and the mixture was heated to 80 °C. The progress of the reaction was followed by thin-layer chromatography. After three days, the reaction was judged to be complete. The mixture was cooled to room temperature and the solvent removed by evaporation. The crude residue was purified by flash chromatography with ethyl acetate/hexanes (5:95). After evaporation of the solvent, the resulting white solid was recrystallized from acetonitrile giving tris[4-(4'-cyanophenyl)phenyl]amine (**27**, 0.310 g, 60%). Melting point: > 300 °C; IR (cm^{-1}): 1592.45, 1490.18 (-CN); ^{1}H NMR ($CHCl_3$, 400 MHz): δ 7.75 (d, 6H, ^3J = 9 Hz), 7.71 (d, 6H, ^3J = 9 Hz), 7.57 (d, 6H, ^3J = 9 Hz), 7.29 (d, 6H, ^3J = 9 Hz); ^{13}C NMR ($CHCl_3$, 100 MHz): δ 140.6, 139.7, 132.4, 130.7, 128.2, 127.9, 122.8, 118.5, 111.9; MS (FAB): m/z 548.64; High-Resolution MS (FAB/NBA): m/z 549.2009, calc. 549.2079 (for $C_{39}H_{25}N_4$ = $[M+1]^+$).

Tecton 2_ADAT

Dicyandiamide (0.205 g, 0.244 mmol), KOH (0.0410 g, 0.732 mmol), and tris(4'-cyanobiphenyl)amine (**27**, 0.148 g, 0.270 mmol) were dissolved in 2-methoxyethanol (25 mL) and heated to reflux for 18 h. Water (25 mL) was poured into the hot reaction mixture. The resulting yellow precipitate was recovered by filtration and suspended in dichloromethane (50 mL) and stirred vigorously for 20 min

in order to remove all unreacted starting material. The solid was recovered by filtration, dissolved in DMSO and precipitated with ethanol. Tecton **2_ADAT** was recovered (0.184 g, 0.230 mmol, 85%) as a yellow solid. Melting point: > 300 °C; IR (cm^{-1}): 3469, 3331, 3187, 1597, 1542, 1398; ^{1}H NMR (DMSO-d_6, 400 MHz): δ 8.33 (d, 6H, ^3J = 9 Hz), 7.79 (d, 6H, ^3J = 9 Hz), 7.77 (d, 6H, ^3J = 9 Hz), 7.22 (d, 6H, ^3J = 9 Hz), 6.72 (s, 12H); ^{13}C NMR (DMSO-d_6, 100 MHz): δ 170.4, 169.0, 141.1, 139.6, 133.2, 130.4, 129.0, 128.6, 123.5, 111.7; High-Resolution MS (FAB/NBA): m/z 800.3203, calc. 800.3309 (for $C_{45}H_{36}N_{16}$).

4-[(Trimethylsilyl)ethynyl]benzonitrile (29)[217]

In a heavy-walled screw-top tube, 4-bromobenzonitrile (2.00 g, 10.9 mmol), $Pd_2(dba)_3$ (0.0660 g, 0.0721 mmol), copper(I) iodide (0.0200 g, 0.106 mmol) and triphenylphosphine (0.144 g, 0.547 mmol) were dissolved in triethylamine (40 mL). The tube was evacuated and backfilled with nitrogen three times. (Trimethylsilyl)acetylene (1.20 mL, 0.851 g, 8.66 mmol) was added via syringe. The mixture was stirred at 75 °C for 18 h, then cooled to room temperature. The solution was diluted with diethyl ether (40 mL), filtered and the solvents removed by rotary evaporation. The resulting solid was purified by column chromatography (18:1 hexanes : ethyl acetate) giving 4-[(trimethylsilyl)ethynyl]benzonitrile (**29**, 1.33 g, 6.68 mmol, 67%) as a white solid. ^{1}H NMR (400 MHz, $CDCl_3$): δ 7.57 (m, 2H), 7.50 (m, 2H), 0.29 (s, 9H); ^{13}C NMR (100 MHz, $CDCl_3$): δ 132.3, 131.5, 127.9, 118.7, 111.3, 102.8, 99.4, -0.3.

4-Ethynylbenzonitrile (30)[217]

4-[(Trimethylsilyl)ethynyl]benzonitrile (**29**, 1.00 g, 5.03 mmol) was dissolved in dichloromethane (10 mL) and methanol (15 mL) , treated with a catalytic quantity of potassium carbonate and stirred at room temperature for 2 h. The solution was then filtered and the solvent removed by rotary evaporation. The crude product was purified by column chromatography (dichloromethane) to give 4-ethynylbenzonitrile (**30**, 0.282 g, 2.22 mmol, 44%) as a white solid. ^{1}H NMR (400 MHz, $CDCl_3$): δ 7.62

(m, 2H), 7.56 (m, 2H), 3.30 (s, 1H); ^{13}C NMR (100 MHz, $CDCl_3$): δ 132.6, 132.0, 126.9, 118.2, 112.2, 81.8, 81.5.

Tris(4-iodophenyl)amine (31) [218]

Triphenylamine (**24**, 2.45 g, 10.0 mmol), red mercury(II) oxide (5.00 g, 23.0 mmol) and iodine (12.7 g, 50.1 mmol) were suspended in anhydrous ethanol (100 mL) and stirred at reflux for 18 h. The solution was then cooled to room temperature. A dark solid was recovered by suction filtration, washed repeatedly with ethanol and then suspended in hot toluene (100 mL), stirred for 1 h and then filtered. The filtrate was passed through a short plug of Al_2O_3 and then the solvent was removed by rotary evaporation. The resulting solid was recrystallized from acetonitrile to give tris(4-iodophenyl)amine (**31**, 4.47 g, 7.11 mmol, 71%) as grey needles. ^1H NMR (400 MHz, $CDCl_3$): δ 7.53 (d, 6H, J = 8 Hz), 6.80 (d, 6H, J = 8 Hz).

Tris-4,4',4' '-(4-cyanophenylethynyl)triphenylamine (32)[219]

An oven-dried heavy-walled screw-top tube was charged with 4-ethynylbenzonitrile (**32**, 0.230 g, 1.81 mmol), tris(4-iodophenyl)amine (**31**, 0.298 g, 0.468 mmol), $Pd(PPh_3)_2Cl_2$ (0.0500 g, 0.0700 mmol), and CuI (26.0 mg, 0.140 mmol). The tube was evacuated and backfilled with nitrogen three times. THF (12 mL) and triethylamine (3 mL) were introduced via syringe. The mixture was stirred at room temperature for 18 h and then concentrated in vacuo. The crude product was taken up in dichloromethane (25 mL), washed with aqueous NH_4Cl and then with aqueous $NaHCO_3$, dried over sodium sulfate, filtered, and concentrated. Column chromatography (dichloromethane) and subsequent evaporation gave tris-4,4',4' '-(4-cyanophenylethynyl)triphenylamine (**32**, 0.285 g, 0.460 mmol, 95%). Melting point: 233-235 °C (lit. 234-236 °C); ^1H NMR ($CDCl_3$, 400 MHz) δ 7.65 d, (6H, ^3J = 8 Hz), 7.61 (d, 6H, ^3J = 8 Hz), 7.46 (d, 6H, ^3J = 9 Hz), 7.11 (d, 6H, ^3J = 9 Hz); ^{13}C NMR ($CDCl_3$, 100 MHz) δ 147.7, 133.1, 132.0, 121.9, 128.3, 124.1, 118.9, 117.8, 110.9, 93.7, 87.4; High-Resolution MS (TOF): m/z 620.2079 calc. 620.2001(for $C_{45}H_{24}N_4$).

Tecton 3_ADAT

Dicyandiamide (0.096 g, 1.15 mmol), a catalytic amount of KOH and tris-4,4',4''-(4-cyanophenylethynyl)triphenylamine (**32,** 0.071 g, 0.110 mmol) were placed in a 50 mL round-bottom flask and dissolved in 2-methoxyethanol (20 mL). The mixture was heated to reflux for 18 h. Water (25 mL) was poured into the hot reaction mixture, affording an orange precipitate which was recovered by suction filtration of the hot mixture. The precipitate was then suspended in dichloromethane and stirred vigorously for 20 min in order to remove all unreacted starting material. The solid was recovered by filtration, dissolved in DMSO and precipitated with ethanol. Tecton **3_ADAT** (0.0539 g, 6.18×10^{-2} mmol, 79%) was recovered as an off-white solid. Melting point: > 300 °C; IR (cm^{-1}): 2952, 2682, 1630, 1403; ^{1}H NMR (DMSO-d_6, 400 MHz): δ 8.27 (d, 6H, ^3J = 9 Hz), 7.63 (d, 6H, ^3J = 9 Hz), 7.56 (d, 6H, ^3J = 9 Hz), 7.12 (d, 6H, ^3J = 9 Hz), 6.81 (s, 12H); ^{13}C NMR (DMSO-d_6, 100 MHz): δ 170.2, 168.1, 147.3, 133.2, 131.9, 131.7, 128.4, 124.0, 117.8, 111.2, 93.6, 87.0; MS (FAB): m/z 872.33; High-Resolution MS (FAB/NBA): m/z 872.3182 calc. 872.3309 (for $C_{51}H_{36}N_{16}$).

***N,N,N',N'*-Tetraphenylbenzidine (33)**[220,221]

An oven-dried 250 mL three-neck round bottom flask was fitted with a water condenser and equipped with septa and a magnetic stir bar. Toluene (125 mL) was added to the flask followed by 4,4'-dibromobiphenyl (5.00 g, 16.0 mmol). The flask was then vigorously degassed with nitrogen for 30 min. Palladium(II) acetate (71.0 mg, 0.300 mmol) and 2-(di-*tert*-butylphosphino)biphenyl (JohnPhos, 179.0 mg, 0.600 mmol) were added and the mixture was heated to 55 °C until the red solution became pale yellow. Diphenylamine (5.95 g, 35.3 mmol), followed by sodium *t*-butoxide (3.80 g, 40.1 mmol) were added and the solution was heated to a reflux. Reaction progress was followed by thin-layer chromatography (80% hexanes/20% ethyl acetate). Completion of the reaction was signalled by the disappearance of the starting material after 90 min (R_f = 0.91). The mixture was cooled to room temperature and diluted with toluene (75 mL) and then extracted with brine (2 x 75 mL) and water (2 x 75 mL). The organic phase was dried with sodium sulfate, filtered and then approximately one half of the volume of the solvent was removed by evaporation. A mixture of equal parts

of the volume of the solvent was removed by evaporation. A mixture of equal parts SiO_2, Al_2O_3 and KCN (~5 g total) was added to the reaction flask, which was heated to reflux for 1 h. The mixture was filtered hot and the product *N,N,N',N'*-tetraphenylbenzidine (**33**, 6.85 g, 14.0 mmol, 87%) was obtained as a white crystalline solid from the cooling filtrate. Melting point: 231-233 °C; ^{1}H NMR (DMSO-d_6, 400 MHz): δ 7.25 (d, 4H, ^3J = 9 Hz), 7.05 (t, 8H, ^3J = 9 Hz), 6.63 (t, 4H, ^3J = 9Hz), 6.52 (d, 4H, ^3J = 9 Hz), 6.42 (d, 8H, ^3J = 9 Hz); ^{13}C NMR (DMSO-d_6, 100 MHz): 141.11, 140.22, 130.98, 129.35, 128.55, 123.65, 123.24, 122.78; MS (FAB): m/z 488.24.

***N,N,N',N'*-Tetrakis(4-bromophenyl)benzidine (34)[222]**

In a 500 mL Erlenmeyer flask, *N,N,N',N'*-tetraphenylbenzidine (**33**, 0.375 g, 0.967 mmol) was dissolved in chloroform (50 mL). A solution of tetra-*n*-butylammonium tribromide (TBATB, 2.08 g, 4.25 mmol) in chloroform (50 mL) was added dropwise. Upon completion of the addition, the mixture was allowed to stir for an additional 20 min. A saturated aqueous solution of sodium thiosulfate (100 mL) was poured into the reaction mixture and stirred for 5 min. The mixture was separated and the organic phase was washed with water (3 x 50 mL) and dried over sodium sulfate. Following evaporation of the solvent, the resulting crude product was recrystallized from glacial acetic acid. The product, *N,N,N',N'*-tetrakis-(4-bromophenyl)benzidine (**34**, 0.698 g, 0.872 mmol, 91%) was obtained as colourless crystals. Melting point: 254-257 °C ; ^{1}H NMR ($CDCl_3$, 400 MHz): δ 7.45 (d, 8H, ^3J = 9 Hz), 7.36 (d, 4H, ^3J = 9Hz), 6.98 (d, 8H, ^3J = 9 Hz), 6.10 (d, 4H, ^3J = 9 Hz); ^{13}C NMR ($CDCl_3$, 100 MHz): δ 146.8, 144.3, 132.8, 130.5, 128.1, 126.0, 124.9, 116.1; MS (FAB): m/z 802.2, 460.5, 307.1; High Resolution MS (FAB/NBA): m/z 804.8719, calc. 804.2053 (for $C_{36}H_{25}N_2Br_4$ = $[M+1]^+$).

***N,N,N',N'*-Tetrakis(4-cyanophenyl)benzidine (35)**

In an oven-dried 100 mL round bottom flask fitted with a condenser and a stir bar, copper(I) cyanide (0.558 g, 6.23 mmol) and *N,N,N',N'*-tetrakis-(4-

under nitrogen for 18 h. The reaction mixture was cooled to room temperature, poured into a 1:1 mixture of water and ethylenediamine (100 mL) then stirred for five minutes. The blue mixture was extracted with toluene (3 x 75 mL). The combined organic phases were washed with brine (75 mL) and water (2 x 75 mL) then dried with sodium sulfate, filtered and the solvent was removed in vacuo. The crude off-white solid was recrystallized from acetonitrile to give *N,N,N',N'*-tetrakis(4-cyanophenyl)benzidine (**35**, 0.544 g, 0.925 mmol, 74%). Melting point: > 300 °C ; ^{1}H NMR (DMSO-d_6, 400 MHz): δ 7.47 (d, 4H, ^{3}J = 9 Hz), 7.38 (d, 8H, ^{3}J = 9 Hz), 7.12 (d, 4H, ^{3}J = 9Hz), 7.00 (d, 8H, ^{3}J = 9Hz) ; ^{13}C NMR ($CDCl_3$, 100 MHz): δ 146.8, 140.2, 135.9, 132.8, 128.1, 126.0, 124.9, 116.1, 108.1; MS (FAB): m/z 588.66; High Resolution MS (FAB/NBA): m/z 589.2064, calc. 588.2062 (for $C_{40}H_{25}N_6$ = $[M+1]^+$).

Tecton 1_BDAT

Dicyandiamide (0.779 g, 9.26 mmol), KOH (cat.), 2-methoxyethanol (20 mL) and *N,N,N',N'*-tetrakis(4-cyanophenyl)benzidine (**35**, 0.454 g, 0.772 mmol) were placed in a 50 mL round-bottom flask, fitted with a condenser and a stir-bar. The mixture was heated to reflux for 18 h. Water (25 mL) was poured into the hot reaction mixture. The resulting beige precipitate was recovered by filtration of the hot mixture and then suspended in dichloromethane. The suspension was stirred vigorously for 20 min in order to remove all unreacted starting material. The solid was recovered by suction filtration, dissolved in DMSO and precipitated with ethanol. Tecton **1_BDAT** (0.586 g, 0.633 mmol, 82%) was recovered as an off-white solid. Melting point: > 300 °C; IR (cm^{-1}): 3028, 1586, 1487, 1275; ^{1}H NMR (DMSO-d_6, 400 MHz): δ 8.10 (d, 8H, ^{3}J = 9 Hz), 7.33 (d, 8H, ^{3}J = 9 Hz), 7.11 (d, 4H, ^{3}J = 9 Hz), 6.62 (s, 16H), 6.43 (d, 4H, ^{3}J = 9 Hz); ^{13}C NMR (DMSO-d_6, 100 MHz): δ 170.2, 168.2, 149.9, 139.2, 130.9, 129.7, 129.0, 128.4, 125.1, 122.9; MS (FAB): m/z 924.98; High-Resolution MS (FAB/NBA): m/z 925.3818, calc. 925.9865 (for $C_{48}H_{41}N_{22}$ = $[M+1]^+$).

Tris[4-(4-(benzyloxy)pyridin-3-yl)phenyl]amine (40)

In an oven-dried round bottom flask, which was thoroughly purged with nitrogen, tris(4-bromophenyl)amine (**12**, 0.380 g, 0.793 mmol), 2-(benzyloxy)-5-(5,5-dimethyl-1,3,2-dioxaborinan-2-yl)pyridine[223] (0.775 g, 2.60 mmol), palladium(II) acetate (10.0 mg, 0.0396 mmol), 2-dicyclohexylphosphino-2',6'-dimethoxybiphenyl (SPhos, 39.0 mg, 0.0950 mmol), K_3PO_4 (0.841 g, 3.96 mmol), toluene (12 mL) and water (1 mL) were heated for 24 h at 100 °C. The mixture was cooled to room temperature and washed repeatedly with water. The organic layer was passed through a short silica plug and the solvent removed by evaporation. Tris[4-(6-benzyloxy)pyridin-3-yl)phenyl]amine (**40**, 0.491 g, 62%) was recovered as a white solid and was of sufficient purity to use in the subsequent step. Melting point: > 300 °C; ^{1}H NMR (400 MHz, DMSO-d_6): δ 8.41 (d, 3H, ^4J = 2 Hz), 7.81 (dd, 3H, ^4J = 2 Hz, ^3J = 9 Hz), 7.43 (m, 21H), 7.25 (d, 6H, ^3J = 9 Hz), 6.90 (d, 3H, ^3J = 9 Hz), 5.45 (s, 6H); ^{13}C NMR (100 MHz, DMSO-d_6): δ 163.2, 147.2, 144.9, 137.7, 132.9, 130.2, 128.9, 128.4, 128.3, 127.9, 127.3, 125.0, 111.6, 68.25; MS (FAB): m/z 795.92; High-Resolution MS (FAB/NBA): 796.3221, calc. 796.3257 (for $C_{53}H_{42}N_5O_3$ = $[M+1]^+$).

Tecton 1_APYR

Tris[4-(6-benzyloxy)pyridine-3-yl)phenyl]amine (**40,** 0.196 g, 0.245 mmol) was dissolved in trifluoroacetic acid (20 mL) and heated to 70 °C for 48 h. The mixture was then cooled to room temperature and the acid removed by evaporation. The resulting solid was triturated with 5 % aqueous ammonium hydroxide, and washed repeatedly with water, ethyl acetate and hexanes. An off-white solid, **1_APYR** (0.119 g, 0.228 mmol, 93%) was recovered and purified by recrystallization from DMSO – ethanol. Melting point: > 300 °C; ^{1}H NMR (DMSO-d_6, 400 MHz): δ 13.65 (s, 3H), 7.49 (t, 3H, ^4J = 2 Hz, ^3J = 9 Hz), 7.43 (d, 3H, ^4J = 2 Hz), 7.34 (d, 6H, ^3J = 9 Hz), 7.23 (d, 6H, ^3J = 9 Hz), 6.60 (d, 3H, ^2J = 9 Hz); ^{13}C NMR (DMSO-d_6, 100 MHz): δ 163.2, 137.8, 129.0, 128.1, 125.3, 119.2, 116.4, 113.5, 110.7; MS (TOF): 525.194 (MH^+); High Resolution MS (TOF): 525.19211, calc. 524.18484 g/mol (for $C_{33}H_{24}N_4O_3$).

Tris(4-aminophenyl)amine (47)[224]

In a Parr reactor, tris-(4-nitrophenyl)amine (**46**, 2.00 g, 5.26 mmol) and 10% palladium on charcoal (0.200 g) were suspended in THF (50 mL). The mixture was stirred for 24 h under 200 psi of hydrogen gas. The mixture was filtered to remove the catalyst, and the solvent was removed by evaporation, affording tris(4-aminophenyl)amine (**47**, 1.48 g, 5.10 mmol, 98%) as grey crystals. The compound was highly sensitive to air and was stored under inert atmosphere. ^{1}H NMR (THF–d_8, 400 MHz): δ 4.85 (d, 6H, ^{3}J = 9 Hz), 4.59 (d, 6H, ^{3}J = 9 Hz), 2.27 (s, 6H); ^{13}C NMR (THF-d_8, 100 MHz): δ 141.9, 141.4, 122.9, 113.2.

Tecton 1_ATAT

Cyanuric chloride (4.18 g, 22.7 mmol) was dissolved in acetone (40 mL) in a 50 mL round bottom flask and cooled to -10 °C. A solution of tris(4-aminophenyl)amine (**47**, 2.00 g, 6.88 mmol) in acetone (10 mL) was added dropwise, maintaining the temperature. After the addition was completed, the reaction was stirred cold for 1 h, and then allowed to come to room temperature. Potassium carbonate (3.13 g, 22.7 mmol) was added, and the mixture was stirred for an additional 20 min at room temperature. The mixture was poured into cold water (100 mL), and the resulting precipitate was recovered by filtration. The yellow solid was washed repeatedly with water and then suspended in concentrated ammonium hydroxide (30 mL) in a screw-top tube and heated to 100 °C overnight. The reaction mixture was cooled to room temperature and filtered. The resulting solid was extremely sensitive to oxidation, rapidly turning purple when exposed to air. As a result, the compound was dried under nitrogen gas, affording tecton **1_ATAT** (2.36 g, 3.79 mmol, 55%) as an off-white solid. Melting point: > 300 °C; ^{1}H NMR (DMSO-d_6, 400 MHz): δ 6.62 (d, 6H, ^{3}J = 9 Hz), 5.98 (d, 6H, ^{3}J = 9 Hz), 6.27 (s, 12H), 3.37 (s, 3H).

Tris(4-biphenyl)amine (52)[158,168]

In an oven-dried round bottom flask, tris(4-iodophenyl)amine (**31**, 0.210 g, 0.334 mmol), phenylmagnesium bromide (3.0 M in ether, 3.30 mL, 9.90 mmol) and Ni(dppp)Cl_2 (0.00179 g, 3.30 x 10^{-2} mmol) were dissolved in anhydrous THF (25 mL) under an inert atmosphere. The mixture was heated to reflux for 24 h and then cooled

to room temperature. The solution was acidified with 1N HCl then extracted with toluene. The combined organic phases were washed with aqueous sodium hydrogen carbonate then water and dried over sodium sulfate. The solvent was removed in vacuo and the resulting yellow solid was purified by sublimation to give tris(4-biphenyl)amine (**52**, 0.0427 g, 0.0902 mmol, 27%) as colourless crystals. ^{1}H NMR (400 MHz, $CDCl_3$): δ 7.61 (d, 6H, ^3J = 9 Hz), 7.50 (d, 6H, ^3J = 9 Hz), 7.43 (t, 6H, ^3J = 9 Hz), 7.33 (t, 3H, ^3J = 9 Hz), 7.21 (d, 6H, ^3J = 9 Hz).

Tris(2,3,4,5,6-pentafluorophenyl)methane (63) [190,210]

In a heavy-walled screw-top tube, pentafluorobenzene (10.0 g, 59.3 mmol), $AlCl_3$ (14.3 g, 107 mmol) and chloroform (2.12 g, 17.9 mmol) were combined under nitrogen atmosphere. The mixture was heated to 150 °C for 36 h. After cooling to room temperature, the tube was opened carefully, and the reaction quenched with 1N aqueous HCl. The acid layer was extracted with toluene. The combined organic fractions were washed with brine, then water and then dried over Na_2SO_4. The solvent was removed in vacuo and the crude product was purified by sublimation to give tris(2,3,4,5,6-pentafluorophenyl)methane (**63**, 5.96 g, 11.6 mmol, 65%) as colourless crystals. Melting point: 159-161 °C (lit. 158-159.5 °C)[190]; ^{1}H NMR (400 MHz, $CDCl_3$): δ 6.21 (s, 1H); ^{19}F NMR (100 MHz, $CDCl_3$): δ -142.7, -153.6, -162.1.

Tris(4-hydrazino-2,3,5,6-tetrafluorophenyl)methane (64) [190]

Tris(2,3,4,5,6-pentafluorophenyl)methane (**63**, 2.51 g, 4.89 mmol) and hydrazine monohydrate (1.45 mL, 29.3 mmol) were dissolved in *p*-dioxane (30 mL) and heated to reflux for 40 h. The mixture was cooled to room temperature and poured in to water (100 mL). The aqueous solution was extracted repeatedly with ether. The combined organic layers were washed with 1N aqueous HCl. The acidic layers were combined and washed with ether to remove any residual neutral material. The aqueous solution was then carefully made basic with 1N KOH, followed by

extraction with ether. The solvent was removed in vacuo and the crude product was recrystallized from toluene to give tris(4-hydrazino-2,3,5,6-tetrafluorophenyl)methane (**64**, 2.67 g, 4.40 mmol, 90%) as yellow needles. ^{1}H NMR (400 MHz, $CDCl_3$): δ 6.14 (s, 1H), 5.79 (bs, 6H), 3.94 (bs, 3H); ^{19}F NMR (100 MHz, $CDCl_3$): δ -142.1, -161.6.

Tris(4-amino-2,3,5,6- tetrafluorophenyl)methane (65)[190]

Tris(4-hydrazino-2,3,5,6-tetrafluorophenyl)methane (**64**, 2.00 g, 3.29 mmol) was dissolved in aqueous hydroiodic acid (48%, 50 mL) and stirred at reflux for 48 h. The mixture was then cooled to room temperature and poured into water (150 mL), resulting in an oil which rapidly solidified. The solid was recovered by suction filtration and recrystallized from methylcyclohexane to provide tris(4-amino-2,3,5,6-tetrafluorophenyl)methane (**65,** 1.16 g, 2.07 mmol, 63%) as pale yellow crystals. Melting point: 170-171 °C (lit. 170-173 °C)[190]; ^{1}H NMR (400 MHz, $CDCl_3$): δ 6.19 (s, 1H), 4.01 (s, 6H). ^{19}F NMR (100 MHz, $CDCl_3$): δ -141.9, -161.5.

Tris(4-bromo-2,3,5,6-tetrafluorophenyl)methane (68) [190,225]

An oven-dried heavy-walled screw-top tube was charged with 4-bromo-2,3,5,6-tetrafluorobenzene (**67**, 5.00 g, 21.9 mmol), $AlCl_3$ (8.75 g, 65.5 mmol) and chloroform (0.870 g, 7.30 mmol) and heated to 150 °C for 72 h. The mixture was cooled to room temperature and the tube opened carefully. The resulting purple solid was dissolved in 1N HCl. The combined acid fractions were extracted with toluene. The combined organic layers were washed repeatedly with brine, then water and then dried over sodium sulfate. The solution was passed through a short plug of activated charcoal and the solvent removed in vacuo. The resulting solid was recrystallized from hexanes to give tris(4-bromo-2,3,5,6-tetrafluorophenyl)methane (**68**, 3.29 g, 4.75 mmol, 65%) as colourless crystals. Melting point: 139-140 °C (lit: 139-139.5 °C)[190]; ^{1}H NMR (400 MHz, $CDCl_3$): δ 6.22 (s, 1H); ^{19}F NMR (100 MHz, $CDCl_3$): δ -140.8, -163.2.

Tris(4-cyano-2,3,5,6-tetrafluorophenyl)methane (69)[190]

An oven-dried round-bottom flask was charged with tris(4-bromo-2,3,5,6-tetrafluorophenyl)methane (**68**, 1.00 g, 1.44 mmol), copper(I) cyanide (0.774 g, 8.64 mmol) and anhydrous DMF (40 mL). The mixture was heated at reflux under an inert atmosphere for 24 h, and then poured into a solution of ethylenediamine (50 mL) in water (50 mL). The resulting blue solution was extracted repeatedly with toluene. The combined organic phases were washed with water and then dried over sodium sulfate and passed through a short plug of activated charcoal. The solvent was removed in vacuo and the resulting solid recrystallized from toluene-hexanes to give tris(4-cyano-2,3,5,6-tetrafluorophenyl)methane (**69**, 92.4 mg, 0.173 mmol, 12%) as colourless crystals. Melting point: 197-199 °C (lit. 197-202 °C)[190]; ^{1}H NMR (400 MHz, $CDCl_3$): δ 6.33 (s, 1H); ^{19}F NMR (100 MHz, $CDCl_3$): δ -143.3, -165.7.

Tris(2,3,4,5,6-pentafluorophenyl)methane-*d* (72)

Tris(2,3,4,5,6-pentafluorophenyl)methane (**63**, 0.500 g, 0.972 mmol) was dissolved in dry dioxane under a nitrogen atmosphere. NaH (0.026g, 1.07 mmol) was added slowly, and the solution passed from colourless to intense purple. The reaction mixture was stirred for 1 h at room temperature and then trifluoroacetic acid-*d* (3 mL) was added dropwise. The solution rapidly became colourless again. The solvent was removed by rotary evaporation and the resulting yellow solid was purified by sublimation. Tris(2,3,4,5,6-pentafluorophenyl)methane-*d* (**72**, 0.495 g, 0.962 mmol, 99%) was isolated as a white microcrystalline solid. IR (cm^{-1}): 2120 (C-D); ^{19}F NMR ($CDCl_3$, 100 MHz): δ -142.73, -153.53, -161.98; MS (FAB): m/z 515.19.

7 References

(1) Brigger, I.; Chaminade, P.; Marsaud, V.; Appel, M.; Besnard, M.; Gurny, R.; Renoir, M.; Couvreur, P. *Int. J. Pharm.* **2001**, *214*, 37.

(2) Litvinchuk, S.; Sord, N.; Matile, S. *J. Am. Chem. Soc.* **2005**, *127*, 9316.

(3) Esch, J. H. v.; Feringa, B. L. *Angew. Chem. Int. Ed.* **2000**, *39*, 2263.

(4) D'Andrade, B. W.; Forrest, S. R. *Adv. Mater.* **2004**, *16*, 1585.

(5) Rainer, H. *Angew. Chem. Int. Ed.* **2004**, *43*, 278.

(6) Russel, T. P. *Science* **2002**, *297*, 964.

(7) Chen, C.-T.; Marder, S. R.; Cheng, L.-T. *Chem. Mater.* **2004**, *16*, 4389.

(8) Chen, H.; Josowicz, M.; Janata, J. *Chem. Mater.* **2004**, *16*, 4728.

(9) Reilly, C. A. *Anal. Chem.* **1958**, *30*, 839.

(10) Parker, D. *Chem. Rev.* **1991**, *91*, 1441.

(11) Seco, J. M.; Quinoa, E.; Riguera, R. *Chem. Rev.* **2004**, *104*, 17.

(12) Lehn, J.-M. *Angew. Chem. Int. Ed.* **1988**, *27*, 89.

(13) Whitesides, G. M.; Grzybowski, B. *Science* **2002**, *295*, 2418.

(14) Sauvage, J.-P.; Dietrich-Buchecker, C. *Molecular Catenanes, Rotaxanes and Knots: A Journey Through the World of Molecular Topology*; Wiley-VCH: Weinheim, 1999.

(15) Rebek Jr., J. *Angew. Chem. Int. Ed.* **2005**, *44*, 2068.

(16) Harada, A.; Li, J.; Kamachi, M. *Nature* **1992**, *356*, 325.

(17) Rodebush, W. H. *Chem. Rev.* **1936**, *19*, 59.

(18) Steiner, T. *Angew. Chem. Int. Ed.* **2002**, *41*, 48.

(19) Lehn, J.-M. *Science* **2002**, *295*, 2400.

(20) Sherrington, D. C.; Taskinen, K. A. *Chem. Soc. Rev.* **2001**, *30*, 83.

(21) Rowsell, J. L. C.; Yaghi, O. M. *Angew. Chem. Int. Ed.* **2005**, *44*, 4670.

(22) Pimentel, G. C.; McClellan, A. L. *The Hydrogen Bond*; Freeman: San Francisco, 1960.

(23) Steiner, T.; Desiraju, G. R. *J. Chem. Soc. Chem. Comm.* **1998**, 891.

(24) Sanford, M. S.; Henling, L. M.; Day, M. W.; Grubbs, R. H. *Angew. Chem. Int. Ed.* **2000**, *39*, 3451.

(25) Umezawa, Y.; Tsuboyama, S.; Honda, K.; Uzawa, J.; Nishio, M. *Bull. Chem. Soc. Jpn.* **1998**, *71*, 1207.

(26) Gu, Y.; Kar, T.; Scheiner, S. *J. Am. Chem. Soc.* **1999**, *121*, 9411.

(27) Desiraju, G. R. *Acc. Chem. Res.* **2002**, *35*, 565.

(28) Boland, T.; Ratner, B. D. *Proc. Nat. Acad. Sci.* **1995**, *92*, 5297.

(29) Dunitz, J. D. *Chem. Commun.* **2003**, 545.

(30) Desiraju, G. R. *Crystal Engineering: The Design of Organic Solids*; Elsevier: Amsterdam, 1989.

(31) Hollingsworth, M. D. *Science* **2002**, *295*, 2410.

(32) Braga, D.; Grepioni, F.; Desiraju, G. R. *Chem. Rev.* **1998**, *98*, 1375.

(33) Simard, M.; Su, D.; Wuest, J. D. *J. Am. Chem. Soc.* **1991**, *113*, 4696.

(34) Persico, F.; Wuest, J. D. *J. Org. Chem.* **1993**, *58*, 95.

(35) Fournier, J.-H.; Maris, T.; Wuest, J. D. *J. Org. Chem.* **2004**, *69*, 1762.

(36) Wang, X.; Simard, M.; Wuest, J. D. *J. Am. Chem. Soc.* **1994**, *116*, 112119.

(37) Fournier, J.-H.; Maris, T.; Wuest, J. D.; Guo, W.; Galoppini, E. *J. Am. Chem. Soc.* **2003**, *125*, 1002.
(38) Spek, A. *J. Appl. Crystallogr.* **2003**, *36*, 7.
(39) LeFur, E.; Demers, E.; Maris, T.; Wuest, J. D. *J. Chem. Soc. Chem. Commun.* **2003**, 2966.
(40) Brunet, P.; Demers, E.; Maris, T.; Enright, G. D.; Wuest, J. D. *Angew. Chem. Int. Ed.* **2003**, *42*, 5303.
(41) Malek, N.; Maris, T.; Simard, M.; Wuest, J. D. *J. Am. Chem. Soc.* **2005**, *127*, 5910.
(42) Mann, S. *Nature* **1993**, *365*, 499.
(43) Lautman, M. M.Sc., Universite de Montreal, 2002.
(44) Mailloux, J. S. M.Sc., Universite de Montreal, 2002.
(45) Visco, R. E.; Chandross, E. A. *J. Am. Chem. Soc.* **1964**, *86*, 5350.
(46) Kelley, T. W.; Baude, P. F.; Gerlach, C.; Ender, D. E.; Muyers, D.; Haase, M. A.; Vogel, D. E.; Theiss, S. D. *Chem. Mater.* **2004**, *16*, 4413.
(47) See Annex 2, Entry 1
(48) Sempel, A.; Buchel, M. *Org. Electron.* **2002**, *3*, 89.
(49) See Annex 2 Entry 2.
(50) See Annex 2, Entry 3
(51) Pardo, D. A.; Jabbour, G. E.; Peyghambarian, N. *Adv. Mater.* **2000**, *12*, 1249.
(52) Forrest, S. R. *Nature* **2004**, *428*, 911-918.
(53) Law, K.-Y. *Chem. Rev.* **1993**, *93*, 449.
(54) Nelson, R. F.; Adams, R. N. *J. Am. Chem. Soc.* **1967**, *90*, 3925.
(55) Bruning, W. H.; Nelson, R. F.; Marcoux, L. S.; Adams, R. N. *J. Phys. Chem.* **1967**, *71*, 3055.
(56) Stamires, D. N.; Turkevich, J. *J. Am. Chem. Soc.* **1963**, *85*, 2557.
(57) Driver, M. S.; Hartwig, J. F. *J. Am. Chem. Soc.* **1996**, *118*, 7217.
(58) Hartwig, J. F.; Kawatsura, M.; Hauck, S. I.; Shaughnessy, K. H.; Alcazar-Roman, L. M. *J. Org. Chem.* **1999**, *64*, 5575.
(59) Huang, J.; Grasa, G.; Nolan, S. P. *Org. Lett.* **1999**, *1*, 1307.
(60) Kuwano, R.; Utsunomiya, M.; Hartwig, J. F. *J. Org. Chem.* **2002**, *67*, 6479.
(61) Thayumanavan, S.; Barlow, S.; Marder, S. R. *Chem. Mater.* **1997**, *9*, 3231.
(62) Wolfe, J. P.; Tomori, H.; Sadighi, J. P.; Yin, J.; Buchwald, S. L. *J. Org. Chem.* **2000**, *65*, 1158.
(63) Zim, D.; Buchwald, S. L. *Org. Lett.* **2003**, *5*, 2413.
(64) Ali, M. H.; Buchwald, S. L. *J. Org. Chem.* **2001**, *66*, 2560.
(65) Dessauer, J. H.; Clark, H. E. *Xerography and Related Processes*; Focal Press: New York, 1965.
(66) Borsenberger, P. M.; Weiss, D. S. *Organic Photoreceptors for Xerography*; Marcel Dekker: New York, 1998; Vol. 59.
(67) Shih-Wen, W.; Meng-Ting, L.; Chen, C. H. *J. Displ. Tech.* **2005**, *1*, 90.
(68) Eremtchenko, M.; Schaefer, J. A.; Tautz, F. S. *Nature* **2003**, *425*, 602.

(69) Low, P. J.; Paterson, M. A. J.; Yufit, D. S.; Howard, J. A. K.; Cherryman, J. C.; Tackley, D. R.; Brook, R.; Brown, B. *J. Mater. Chem.* **2005**, *15*, 2304.
(70) Fanta, P. E. *Chem. Rev.* **1946**, *38*, 139.
(71) Fanta, P. E. *Chem. Rev.* **1964**, *64*, 613.
(72) Hassan, J.; Sevignon, M.; Gozzi, C.; Schulz, E.; Lemaire, M. *Chem. Rev.* **2002**, *102*, 1359.
(73) Ma, D.; Cai, Q. *Org. Lett.* **2003**, *5*, 3799.
(74) Ma, D.; Cai, Q.; Zhang, H. *Org. Lett.* **2003**, *5*, 2453.
(75) Marcoux, J.-F.; Doye, S.; Buchwald, S. L. *J. Am. Chem. Soc.* **1997**, *119*, 10539.
(76) Antilla, J. C.; Buchwald, S. L. *Org. Lett.* **2001**, *3*, 2077.
(77) Goodbrand, H. B.; Hu, N.-X. *J. Org. Chem.* **1999**, *64*, 670.
(78) Wolfe, J. P.; Buchwald, S. L. *J. Org. Chem.* **1996**, *61*, 1133.
(79) Wolfe, J. P.; Buchwald, S. L. *J. Org. Chem.* **2000**, *65*, 1144.
(80) Kaye, S.; Fox, J. M.; Hicks, F. A.; Buchwald, S. L. *Adv. Synth. Catal.* **2001**, *343*, 789.
(81) Tomori, H.; Fox, J. M.; Buchwald, S. L. *J. Org. Chem.* **2000**, *65*, 5334.
(82) Walker, S. D.; Barder, T. E.; Martinelli, J. R.; Buchwald, S. L. *Angew. Chem. Int. Ed.* **2004**, *43*, 1871.
(83) Corbet, J. P.; Mignani, G. *Chem. Rev.* **2006**, *106*, 2651.
(84) Marion, N.; Ecarnot, E. C.; Navarro, O.; Amoroso, D.; Bell, A.; Nolan, S. P. *J. Org. Chem.* **2006**, *71*, 3816.
(85) Xie, X.; Zhang, T. Y.; Zhang, Z. *J. Org. Chem.* **2006**, *71*, 6522.
(86) Hartwig, J. F. *Acc. Chem. Res.* **1998**, *31*, 852.
(87) Wolfe, J. P.; Wagaw, S.; Marcoux, J.-F.; Buchwald, S. L. *Acc. Chem. Res.* **1998**, *31*, 805.
(88) Stufflebeme, G.; Lorenz, K. T.; Bauld, N. L. *J. Am. Chem. Soc.* **1986**, *108*, 4234.
(89) Mehta, S.; Pinto, B. M. *Carbohydr. Res.* **1998**, *310*, 43.
(90) Wang, Y.; Dubois, J. L.; Herdman, B.; Hodgson, K. O.; Stack, T. D. P. *Science* **1998**, *279*, 537.
(91) Huo, C.; Wei, R.; Zhang, W.; Yang, L.; Liu, Z.-L. *Synlett.* **2005**, 161.
(92) Wills, A. J.; Krishnan-Ghosh, Y.; Balasubramanian, S. *J. Org. Chem.* **2002**, *67*, 6646.
(93) Ghosh, D. C.; Jana, J.; Biswas, R. *Int. J. Quantum Chem.* **2000**, *80*, 1.
(94) Olovsson, I.; Templeton, D. H. *Acta Crystallogr.* **1959**, *12*, 827.
(95) Tro, N. J. *Introductory Chemistry*; Prentice Hall: New York, 2006.
(96) Morgan, W. R.; Leyden, D. E. *J. Am. Chem. Soc.* **1970**, *92*, 4527.
(97) Sobolev, A. N.; Belsky, V. K.; Romm, I. P.; Chernikova, N. Y.; Guryanova, E. N. *Acta. Cryst.* **1985**, *C41*, 967.
(98) Kennedy, A. R.; Smith, W. E.; Tackley, D. R.; David, W. I. F.; Shankland, K.; Brown, B.; Teat, S. J. *J. Mater. Chem.* **2002**, *12*, 168.
(99) Sarma, J. A. R. P.; Desiraju, G. R. *Cryst. Growth Des.* **2002**, *2*, 93.
(100) Chae, H. K.; Eddaoudi, M.; Kim, J.; Hauck, S. I.; Hartwig, J. F.; O'Keeffe, M.; Yaghi, O. M. *J. Am. Chem. Soc.* **2001**, *123*, 11482.

(101) Field, J. E.; Combariza, M. Y.; Vacheta, R. W.; Venkataraman, D. *Chem. Commun.* **2002**, 2260.
(102) Ockwig, N. W.; Delgado-Friedrichs, O.; O'Keefe, M.; Yaghi, O. M. *Acc. Chem. Res.* **2005**, *38*, 176.
(103) Brunet, P.; Simard, M.; Wuest, J. D. *J. Am. Chem. Soc.* **1997**, *119*, 2737.
(104) Dumas, L. M.Sc., Universite de Montreal, 2002.
(105) Helzy, F.; Maris, T.; Wuest, J. D. *Unpublished results.*
(106) Laliberte, D.; Maris, T.; Sirois, A.; Wuest, J. D. *Org. Lett.* **2003**, *5*, 4787.
(107) Cardaci, G. *Int. J. Chem. Kinet.* **1973**, *5*, 805.
(108) Goel, R. G.; Prasa, H. S. *Can. J. Chem.* **1971**, *49*, 2529.
(109) Dang, H.; Wuest, J. D. *Unpublished results.*
(110) Dunn, G. E.; Blackburn, B. J. *Can. J. Chem.* **1974**, *52*, 2552.
(111) Baker, T. N. I.; Doherty, W. P. J.; Kelley, W. S.; Newmeyer, W.; Rogers, J. E.; Spalding, R. E.; Walter, R. I. *J. Org. Chem.* **1965**, *30*, 3714.
(112) Schweikart, K. H.; Hanaek, M.; Luer, L.; Oelkrug, D. *Eur. J. Org. Chem.* **2001**, *2*, 293.
(113) Quirke, J. M. E. *Comprehensive Heterocyclic Chemistry* Pergammon: Oxford, 1984; Vol. 3.
(114) Smolin, E. M.; Rapoport, L. *The Chemistry of Heterocyclic Compounds*; Interscience: New York, 1959; Vol. 13.
(115) Beijer, F. H.; Sijbesma, R. P.; Vekemans, J. A. J. M.; Meijer, E. W.; Kooijman, H.; Spek, A. L. *J. Org. Chem.* **1996**, *61*, 6371.
(116) Farrugia, L. J. *J. Appl. Crystallogr.* **1997**, *30*, 565.
(117) Cahn, R. S.; Ingold, C. K.; Prelog, V. *Angew. Chem. Int. Ed. Eng.* **1966**, *5*.
(118) McNaught, A. D.; Wilkinson, A. *IUPAC Compendium of Chemical Terminology*; 2 ed.; Blackwell Science: Boston, 1997.
(119) Spek, A. L. *J. Appl. Crystallogr.* **2003**, *36*, 7.
(120) Amthor, S.; Noller, B.; Lambert, C. *Chem. Phys.* **2005**, *316*, 141.
(121) *ATOMS*; 6.1 ed.; Shape Software: Kingsport, TN.
(122) Batten, S. R. *CrystEngComm* **2001**, *3*, 67.
(123) Batten, S. R.; Robson, R. *Angew. Chem. Int. Ed.* **1998**, *37*, 1460.
(124) Fournier, J.-H.; Maris, T.; Simard, M.; Wuest, J. D. *Cryst. Growth Des.* **2003**, *3*, 535.
(125) Hird, M.; Toyne, K. J.; Gray, G. W.; Day, S. E.; McDonnell, D. G. *Liq. Cryst.* **1993**, *15*, 123.
(126) Shashanka, S. M. *J. Chem. Phys,* **1962**, *36*, 3286.
(127) Shoeib, T.; El Aribi, H.; Siu, K. W. M.; Hopkinson, A. C. *J. Phys. Chem. A* **2001**, *105*, 710.
(128) McIlroy, S. P.; Clo, E.; Nikolajsen, L.; Frederiksen, P. K.; Nielsen, C. B.; Mikkelsen, K. V.; Gothelf, K. V.; Ogilby, P. R. *J. Org. Chem.* **2005**, *70*, 1134.
(129) Takahashi, S.; Kuroyama, Y.; Sonogashira, K.; Hagihara, N. *Synthesis* **1980**, 627.
(130) Shirota, Y.; Kobata, T.; Noma, N. *Chem. Lett.* **1989**, 1145.

(131) Spek, A. L.; *PLATON, A Multipurpose Crystallographic Tool*; Utrecht University: Utrecht, 2007.
(132) Ducharme, Y.; Wuest, J. D. *J. Org. Chem.* **1988**, *53*, 5787.
(133) Vaillancourt, L.; Simard, M.; Wuest, J. D. *J. Org. Chem.* **1998**, *63*, 9746.
(134) Gallant, M.; Phan Viet, M. T.; Wuest, J. D. *J. Am. Chem. Soc.* **1991**, *113*, 721.
(135) Vidal Juan, B.; Esteve Trias, C.; Soca Pueyo, L.; Eastwood, P. R. In *PCT Int. Appl.* 2007, p 198.
(136) Sonntag, M.; Kreger, K.; Hanft, D.; Strohriegl, P.; Setayesh, S.; deLeeuw, D. *Chem. Mater.* **2005**, *17*, 3031.
(137) Brunet, P.; Demers, E.; Maris, T.; Enright, G. D.; Wuest, J. D. *Angew. Chem. Int. Ed.* **2003**, *42*, 5303.
(138) Breton, M. P.; Boils-Boissier, D. C.; Thomas Jr., J. W.; Titterington, D. R.; Goodbrand, H. B.; Banning, J. H.; Wuest, J. D.; Laliberté, D.; Perron, M. E.; Xerox Corporation (Stamford, CT) U.S. Patent, 2005; Vol. 6,860,928.
(139) Ritschl, F. *Spectrochim. Acta A* **1967**, *23*, 655.
(140) Chiu, K. Y.; Su, T. X.; Li, J. H.; Lin, T.-H.; Liou, G. S.; Chen, S.-H. *J. Electroanal. Chem.* **2005**, *575*, 95.
(141) Piccard, J.; Brewster, R. Q. *J. Am. Chem. Soc.* **1921**, *43*, 2630.
(142) Borsenberger, P. M.; Mey, W.; Chowdry, A. *J. Appl. Phys.* **1978**, *49*, 273.
(143) Shirota, Y. *J. Mater. Chem.* **2000**, *10*, 1.
(144) Katritzky, A. R.; Lobanov, V. S. *Chem. Soc. Rev.* **1995**, *24*, 279.
(145) Earle, M. J.; Seddon, K. R. *Pure Appl. Chem.* **2000**, *72*, 1391.
(146) Friend, R. H.; Gymer, R. W.; Holmes, A. B.; Burroughes, J. H.; Marks, R. N.; Taliani, C.; Bradley, D. D. C.; Santos, D. A. D.; Bredas, J. L.; Logdlund, M.; Salaneck, W. R. *Nature* **1999**, *397*, 121.
(147) Casalbore-Miceli, G.; Degli Esposito, A.; Fattory, V.; Marconi, G.; Sabatini, C. *Phys. Chem. Chem. Phys.* **2004**, 3092.
(148) Benjamin, J. C. *Chem. Eur. J.* **1999**, *5*, 2464.
(149) Clays, K.; Olbrechts, G.; Munters, T.; Persoons, A.; Kim, O.-K.; Choi, L.-S. *Chem. Phys. Lett.* **1998**, *293*, 337.
(150) Thelakkat, M.; Schmidt, H.-W. *Poly. Adv. Technol.* **1998**, *9*, 429.
(151) Fink, R.; Heischkel, Y.; Thelakkat, M.; Schmidt, H. W.; Jonda, C.; Huppauff, M. *Chem. Mater.* **1998**, *10*, 3620.
(152) Comba, P.; Lampeka, Yaroslaw D.; Lötzbeyer, L.; Prikhod'ko, Alexander I. *Eur. J. Inorg. Chem.* **2003**, 34.
(153) Koene, B. E.; Loy, D. E.; Thompson, M. E. *Chem. Mater.* **1998**, *10*, 2235.
(154) Gagne, R. R.; Koval, C. A.; Lisensky, G. C. *Inorg. Chem.* **1980**, *19*, 2854.
(155) Zara, A. J.; Machado, S. S.; Bulhões, L. O. S.; Benedetti, A. V.; Rabockai, T. *J. Electroanal. Chem.* **1987**, *221*, 165.
(156) Seo, E. T.; Nelson, R. F.; Fritsch, J. M.; Marcoux, L. S.; Leedy, D. W.; Adams, R. N. *J. Am. Chem. Soc.* **1966**, *88*, 3498.
(157) Gritzner, G. *J. Phys. Chem.* **1986**, *90*, 5478.

(158) Higuchi, A.; Ohnishi, K.; Nomura, S.; Inada, H.; Shirota, Y. *J. Mater. Chem.* **1992**, *2*, 1109.
(159) Hagopian, L.; Kohler, G.; Walter, R. I. *J. Phys. Chem.* **1967**, *71*, 2290.
(160) Lautman, M.; Dufresne, S.; Wuest, J. D.; Skene, W. *Unpublished results.*
(161) Low, P. J.; Paterson, M. A. J.; Puschmann, H.; Goeta, A. E.; Howard, J. A. K.; Lambert, C.; Cherryman, J. C.; Leeming, D. R. T. S.; Brown, B. *Chemistry - A European Journal* **2004**, *10*, 83-91.
(162) Jablonski, A. *Phys. Rev.* **1945**, *68*, 78.
(163) Ito, A.; Urabe, M.; Tanaka, K. *Angew. Chem. Int. Ed.* **2004**, *42*, 921.
(164) Schroeder, W. A.; Wilcox, P. E.; Trueblood, K. N.; Dekker, A. O. *Anal. Chem.* **1951**, *23*, 1740.
(165) Malkin, Y. N.; Kuz'min, V. A. *Usp. Khim.* **1985**, *54*, 1761.
(166) Skryshevskii, Y. A. *J. Appl. Spectr.* **2002**, *69*, 726.
(167) Zhan, C.; Cheng, Z.; Zheng, J.; Zhang, W.; Xi, Y.; Qin, J. *J. Appl. Polym. Sci.* **2002**, *85*, 2718.
(168) Inada, H.; Ohnishi, K.; Nomura, S.; Higuchi, A.; Nakano, H.; Shirota, Y. *J. Mater. Chem.* **1994**, *4*, 171.
(169) Lee, M.-T.; Liao, C. H.; Tsai, C. H.; Chen, C. H. *Adv. Mater.* **2005**, *17*, 2493-2497.
(170) McFarland, M. *Environ. Sci. Technol.* **1989**, *23*, 1203.
(171) Maienfisch, P. *Chimia* **2004**, *58*, 92.
(172) Dicciani, N. K. *Chem. Eng. News* **2003**, *81*, 48.
(173) Macey, W. A. T. *J. Phys. Chem.* **1960**, *64*, 254.
(174) Philis, J.; Bolovinos, A.; Andritsopolous, G.; Pantos, E.; Tsekeris, P. *J. Phys. B: At. Mol. Phys.* **1981**, *14*, 3621.
(175) Ratko, T. A.; Detrisac, C. J.; Mehta, R. G.; Kelloff, G. J.; Moon, R. C. *Cancer Res.* **1991**, *51*, 481.
(176) Tang, W.; Borel, A. G.; Fujimiya, T.; Abbott, F. S. *Chem. Res. Toxicol.* **1995**, *8*, 671.
(177) Metrangolo, P.; Neukirch, H.; Pilatis, T.; Resnati, G. *Acc. Chem. Res.* **2005**, *38*, 386.
(178) Choudhury, A. R.; Row, T. N. G. *Cryst. Growth Des.* **2004**, *4*, 47.
(179) Bosch, E.; Barnes, C. L. *Cryst. Growth Des.* **2002**, *2*, 299.
(180) Reichenbächer, K.; Süss, H. I.; Hulliger, J. *Chem. Soc. Rev.* **2005**, *34*, 22.
(181) Snyder, J. P.; Chandrakumar, N. S.; Sato, H.; Lankin, D. C. *J. Am. Chem. Soc.* **2000**, *122*, 544.
(182) Dunitz, J. D.; Taylor, R. *Chem. Eur. J.* **1997**, *3*, 89.
(183) Mountford, A. J.; Lancaster, S. J.; Coles, S. J.; Horton, P. N.; Hughes, D. L.; Hursthouse, M. B.; Light, M. E. *Inorg. Chem.* **2005**, *44*, 5921.
(184) Patrick, C. R.; Prosser, G. S. *Nature* **1960**, *187*, 1021.
(185) Cox, E. G.; Cruickshank, D. W. J.; Smith, J. A. S. *Proc. R. Soc. London, Ser. A* **1958**, *247*, 1.
(186) Lindeman, S. V.; Kosynkin, D.; Kochi, J. K. *J. Am. Chem. Soc.* **1998**, *120*, 13268.
(187) Reddy, L. S.; Nangia, A.; Lynch, V. M. *Cryst. Growth Des.* **2004**, *4*, 89.

(188) Collings, J. C.; Smith, P. S.; Yufit, D. S.; Batsanov, A. S.; Howard, J. A. K.; Marder, T. B. *CrystEngComm* **2004**, *6*, 25.
(189) Perrin, D. D. *Dissociation Constants of Organic Bases in Aqueous Solution*; Buttersworth: London, 1965.
(190) Filler, R.; Feibig Jr., A. E.; Mandal, B. K. *J. Fluorine Chem.* **2000**, *102*, 185.
(191) Miller, J. S. *Adv. Mater.* **2002**, *14*, 1105.
(192) Lieb, E.; Mattis, D. *Phys. Rev.* **1962**, *125*, 164.
(193) Miller, J. S.; Epstein, A. J. *J. Chem. Soc. Chem. Comm.* **1998**, 1319.
(194) Blundell, S. J.; Pratt, F. L. *J. Phys.: Cond. Mat.* **2004**, *16*, R771.
(195) Maspoch, D.; Catala, L.; Gerbier, P.; Ruiz-Molina, D.; Vidal-Gancedo, J.; Wurst, K.; Rovira, C.; Veciana, J. *Chem. Eur. J.* **2002**, *8*, 3635.
(196) Tomboulian, P. *J. Org. Chem.* **1959**, *24*, 229.
(197) Reddy, T. J.; Iwama, T.; Halpern, H. J.; Rawal, V. H. *J. Org. Chem.* **2002**, *64*, 4635.
(198) Rathore, R.; Burns, C. L.; Guzei, I. A. *J. Org. Chem.* **2004**, *69*, 1524.
(199) Ballester, M.; Veciana, J.; Riera, J.; Castaiier, J.; Rovira, C.; Armet, O. *J. Org. Chem* **1986**, *51*, 5472.
(200) Ratera, I.; Marcen, S.; Montant, S.; Ruiz–Molina, D.; Rovira, C.; Veciana, J.; Letard, J.-F.; Freysz, E. *Chem. Phys. Lett.* **2002**, *363*, 245.
(201) Fischer, H. *Chem. Rev.* **2001**, *101*, 3581.
(202) Sibi, M. P.; Porter, N. A. *Acc. Chem. Res.* **1999**, *32*, 163.
(203) Armet, O.; Veciana, J.; Rovira, C.; Riera, J.; Castaner, J.; Molins, E.; Rius, J.; Miravitlles, C.; Olivella, S.; Brichfeus, J. *J. Phys. Chem.* **1987**, *91*, 5608.
(204) Ballester, M.; Riera, J.; Castaner, J.; Badia, C.; Monso, J. *J. Am. Chem. Soc.* **1971**, *93*, 2215.
(205) Maspoch, D.; Domingo, N.; Ruiz-Molina, D.; Wurst, K.; Tajeda, J.; Rovira, C.; Veciana, J. *J. Am. Chem. Soc.* **2004**, *126*, 730.
(206) Kulkarni, S. V.; Schure, R.; Filler, R. *J. Am. Chem. Soc.* **1973**, *95*, 1859.
(207) Filler, R.; Wang, C.-S.; McKinney, M. A.; Miller, F. N. *J. Am. Chem. Soc.* **1967**, *89*, 1026.
(208) Filler, R.; Ayyangar, N.; Gustowski, W.; Kang, H. H. *J. Org. Chem.* **1969**, *34*, 534.
(209) Laliberté, D. Ph.D., Université de Montréal, 2003.
(210) Beckert, W. F.; Lowe, J. U. *J. Org. Chem.* **1967**, *32*, 582.
(211) Barbarich, T. J.; Rithner, C. D.; Miller, S. M.; Anderson, O. P.; Strauss, S. H. *J. Am. Chem. Soc.* **1999**, *121*, 4280.
(212) Search of the Cambridge Structural Database v. 5.28 accessed on April 4; CCDC: 2007.
(213) Allen, F. H. *Acta Crystallogr.* **2002**, *B58*, 380.
(214) Zerkowski, J. A.; Mathias, J. P.; Whitesides, G. M. *J. Am. Chem. Soc.* **1994**, *116*, 4305.
(215) Lebel, O.; Maris, T.; Perron, M. E.; Demers, E.; Wuest, J. D. *J. Am. Chem. Soc.* **2006**, *128*, 10372.

(216) Boils-Boissier, D. C.; Breton, M. P.; Thomas Jr., J. W.; Titterington, D. R.; Banning, J. H.; Goodbrand, H. B.; Wuest, J. D.; Perron, M. E.; Monchamp, F.; Duval, H.; Xerox Corporation (Stamford, CT): U.S. Patent, 2004; Vol. 6761758.

(217) Hirsch, K. A.; Wilson, S. R.; Moore, J. S. *J. Am. Chem. Soc.* **1997**, *119*, 10401.

(218) Varnavski, O. P.; Ostrowski, J. C.; Sukhomlinova, L.; Twieg, R. J.; Bazan, G. C.; Goodson, T. *J. Am. Chem. Soc.* **2002**, *124*, 1736.

(219) Liu, X.-J.; Feng, J.-K.; Ren, A.-M.; Cheng, H.; Zhou, X. *J. Chem. Phys,* **2004**, *121*, 8253.

(220) Rapson, W. S.; Saunder, D. H.; Stewart, E. T. *J. Chem. Soc., Chem. Comm.* **1946**, 1110.

(221) Lee, S.; Hartwig, J. F. *J. Org. Chem.* **2001**, *66*, 3402.

(222) Eberson, L.; Larsson, B. *Acta Chem. Scand.* **1987**, *B41*, 367.

(223) Maly, K.; Voisin, E.; Wuest, J. D. *Unpublished results.*

(224) Temme, O.; Dickner, T.; Laschat, S.; Fröhlich, R.; Kotila, S.; Bergander, K. *Eur. J. Org. Chem.* **1998**, 651.

(225) Gerasimova, T. N.; Barkhash, V. A.; Vorozhtsov, N. N. *J. Gen. Chem. USSR* **1968**, *383*, 510.

Annex 1
Crystallographic Analysis Reports

Université de Montréal

CRYSTAL AND MOLECULAR STRUCTURE OF

C39 H60 N16 O6 S6 COMPOUND (JIW492)

Equipe WUEST

Département de chimie, Université de Montréal,

C.P. 6128, Succ. Centre-Ville, Montréal, Québec, H3C 3J7 (Canada)

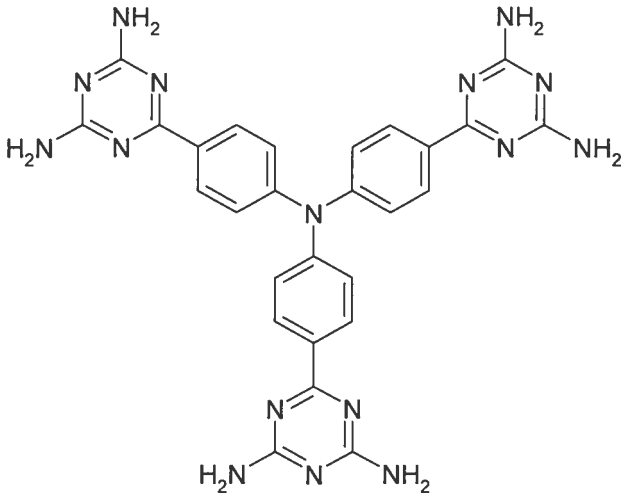

Solvant : DMSO / Ethanol

Structure solved and refined in the laboratory of X-ray diffraction, Université de Montréal by Dr. Thierry Maris.

Table 1. Crystal data and structure refinement for C39 H60 N16 O6 S6.

Identification code	JIW492
Empirical formula	C39 H60 N16 O6 S6
Formula weight	1041.39
Temperature	223(2)K
Wavelength	1.54178 Å
Crystal system	Trigonal (Hexagonal)
Space group	R-3
Unit cell dimensions	a = 34.185(2) Å α = 90° b = 34.185(2) Å β = 90° c = 8.4889(9) Å γ = 120°
Volume	8591.3(12)Å^3
Z	6
Density (calculated)	1.208 Mg/m^3
Absorption coefficient	2.651 mm^{-1}
F(000)	3300
Crystal size	0.5 x 0.45 x 0.23 mm
Theta range for data collection	2.58 to 72.96°
Index ranges	$-42 \leq h \leq 41$, $-42 \leq k \leq 38$, $-9 \leq \ell \leq 10$
Reflections collected	17183
Independent reflections	3720 [R_{int} = 0.0954]
Absorption correction	Semi-empirical from equivalents
Max. and min. transmission	1 and 0.0873
Refinement method	Full-matrix least-squares on F^2
Data / restraints / parameters	3720 / 0 / 223
Goodness-of-fit on F^2	0.960

Final R indices [I>2sigma(I)]	R_1 = 0.0983, wR_2 = 0.2800
R indices (all data)	R_1 = 0.1301, wR_2 = 0.3088
Largest diff. peak and hole	0.584 and -0.421 e/Å^3

Table 2. Atomic coordinates (x 10^4) and equivalent isotropic displacement parameters (Å^2 x 10^3) for C39 H60 N16 O6 S6.

U_{eq} is defined as one third of the trace of the orthogonalized Uij tensor.

	Occ.	x	y	z	U_{eq}
N(1)	1	10000	0	2544(5)	47(1)
C(1)	1	9814(1)	290(1)	2530(3)	42(1)
C(2)	1	9429(1)	176(1)	1665(4)	50(1)
N(2)	1	8895(1)	1035(1)	1477(3)	57(1)
C(3)	1	9248(1)	460(1)	1628(4)	54(1)
N(3)	1	8815(1)	1633(1)	2592(3)	64(1)
C(4)	1	9437(1)	855(1)	2500(3)	46(1)
N(4)	1	9372(1)	1470(1)	3589(3)	55(1)
C(5)	1	9826(1)	966(1)	3386(4)	51(1)
N(5)	1	8376(1)	1218(1)	549(4)	80(1)
C(6)	1	10011(1)	692(1)	3376(4)	48(1)
N(6)	1	9277(1)	2036(1)	4621(4)	85(1)
C(7)	1	9225(1)	1144(1)	2539(4)	50(1)
C(8)	1	8705(1)	1303(1)	1579(4)	59(1)
C(9)	1	9152(1)	1709(1)	3581(4)	62(1)
S(10A)	0.765(4)	596(1)	2809(1)	3809(2)	92(1)
O(10)	1	747(1)	2912(1)	2164(4)	117(1)

	C(10A)	1	604(2)	2307(2)	4309(8)
136(2)					
	C(10B)	1	1013(4)	3166(3)	5020(12)
216(5)					
	S(10B)	0.235(4)	962(2)	2812(3)	3731(11)
142(4)					
	S(20A)	0.471(8)	9943(1)	1918(1)	7979(4)
104(2)					
	S(20B)	0.529(8)	9620(3)	1901(2)	8500(10)
238(4)					
	O(20)	1	9860(2)	2259(2)	7273(5)
138(2)					
	C(20A)	1	9469(2)	1412(2)	7826(7)
134(2)					
	C(20B)	1	9962(3)	1995(3)	9923(10)
186(3)					

Table 3. Hydrogen coordinates (x 10^4) and isotropic displacement parameters ($Å^2$ x 10^3) for C39 H60 N16 O6 S6.

	x	y	z	U_{eq}
H(2)	9289	-96	1096	60
H(3)	8992	383	1002	65
H(5)	9960	1231	3993	61
H(5A)	8243	1378	565	96
H(5B)	8295	1002	-137	96
H(6)	10276	778	3952	58
H(6A)	9143	2195	4650	102
H(6B)	9495	2093	5279	102
H(10A)	368	2054	3733	205
H(10B)	553	2252	5432	205
H(10C)	895	2343	4035	205
H(10D)	1062	3469	4886	325
H(10E)	1289	3163	4768	325
H(10F)	929	3070	6104	325
H(20A)	9300	1410	6906	202
H(20B)	9286	1357	8762	202
H(20C)	9548	1177	7722	202
H(20D)	10057	2309	10145	279
H(20E)	10175	1920	10386	279
H(20F)	9665	1803	10368	279

Table 4. Anisotropic parameters ($Å^2$ x 10^3) for C39 H60 N16 O6 S6.

The anisotropic displacement factor exponent takes the form:

$$-2\pi^2 [h^2 a^{*2} U_{11} + ... + 2 h k a^* b^* U_{12}]$$

	U11	U22	U33	U23	U13	U12
N(1)	29(1)	29(1)	81(3)	0	0	15(1)
C(1)	34(1)	33(1)	61(2)	4(1)	5(1)	18(1)
C(2)	39(1)	42(1)	71(2)	-4(1)	-2(1)	22(1)
N(2)	56(2)	54(1)	76(2)	-3(1)	-5(1)	40(1)
C(3)	43(2)	56(2)	72(2)	-6(1)	-4(1)	31(1)
N(3)	69(2)	63(2)	81(2)	-7(1)	-4(1)	49(1)
C(4)	42(1)	39(1)	59(2)	3(1)	4(1)	23(1)
N(4)	61(2)	56(1)	64(2)	-2(1)	-4(1)	41(1)
C(5)	51(2)	38(1)	66(2)	1(1)	1(1)	23(1)
N(5)	91(2)	88(2)	98(2)	-27(2)	-32(2)	72(2)
C(6)	37(1)	37(1)	67(2)	-1(1)	-2(1)	16(1)
N(6)	101(2)	88(2)	103(2)	-37(2)	-31(2)	75(2)
C(7)	50(2)	42(1)	64(2)	2(1)	4(1)	28(1)
C(8)	60(2)	56(2)	76(2)	0(2)	-3(2)	40(2)
C(9)	64(2)	61(2)	75(2)	-5(2)	-4(2)	43(2)
S(10A)	95(1)	98(1)	90(1)	16(1)	17(1)	55(1)
O(10)	145(3)	81(2)	99(3)	11(2)	36(2)	39(2)
C(10A)	136(5)	88(3)	174(6)	25(4)	-10(4)	47(3)
C(10B)	339(13)	128(5)	182(8)	-54(5)	-127(8)	116(7)
S(10B)	96(5)	148(6)	163(7)	32(5)	20(4)	47(4)

S(20A)	76(2)	134(3)	115(3)	29(2)	2(2)
61(2)					
S(20B)	234(9)	222(6)	258(7)	-39(6)	-29(6)
114(6)					
O(20)	159(4)	126(3)	135(3)	4(3)	-46(3)
75(3)					
C(20A)	156(6)	117(5)	114(4)	1(4)	-10(4)
56(4)					
C(20B)	188(7)	191(8)	140(6)	-19(5)	-46(6)
65(6)					

Table 5. Bond lengths [Å] and angles [°] for C39 H60 N16 O6 S6

N(1)-C(1)#1	1.421(2)	C(2)-C(1)-N(1)	120.2(2)
N(1)-C(1)#2	1.421(2)	C(6)-C(1)-N(1)	121.5(2)
N(1)-C(1)	1.421(2)	C(1)-C(2)-C(3)	120.6(3)
C(1)-C(2)	1.382(4)	C(7)-N(2)-C(8)	112.8(3)
C(1)-C(6)	1.390(4)	C(4)-C(3)-C(2)	121.0(3)
C(2)-C(3)	1.390(4)	C(8)-N(3)-C(9)	115.2(3)
N(2)-C(7)	1.343(4)	C(3)-C(4)-C(5)	117.8(2)
N(2)-C(8)	1.366(3)	C(3)-C(4)-C(7)	120.9(2)
C(3)-C(4)	1.385(4)	C(5)-C(4)-C(7)	121.3(2)
N(3)-C(8)	1.314(4)	C(7)-N(4)-C(9)	114.3(3)
N(3)-C(9)	1.341(4)	C(6)-C(5)-C(4)	120.8(3)
C(4)-C(5)	1.404(4)	C(5)-C(6)-C(1)	121.4(2)
C(4)-C(7)	1.489(3)	N(4)-C(7)-N(2)	127.1(2)
N(4)-C(7)	1.316(4)	N(4)-C(7)-C(4)	118.0(3)
N(4)-C(9)	1.359(4)	N(2)-C(7)-C(4)	114.9(2)
C(5)-C(6)	1.366(4)	N(3)-C(8)-N(5)	117.7(3)
N(5)-C(8)	1.335(4)	N(3)-C(8)-N(2)	126.0(3)
N(6)-C(9)	1.318(4)	N(5)-C(8)-N(2)	116.2(3)
S(10A)-O(10)	1.469(4)	N(6)-C(9)-N(3)	117.8(3)
S(10A)-C(10B)	1.686(8)	N(6)-C(9)-N(4)	117.6(3)
S(10A)-C(10A)	1.780(5)	N(3)-C(9)-N(4)	124.6(3)
S(20A)-O(20)	1.460(5)	O(10)-S(10A)-C(10B)	109.7(5)
S(20A)-C(20B)	1.668(9)	O(10)-S(10A)-C(10A)	106.6(3)
S(20A)-C(20A)	1.682(7)	C(10B)-S(10A)-C(10A)	97.8(3)
		O(20)-S(20A)-C(20B)	106.7(4)
C(1)#1-N(1)-C(1)#2	119.993(7)	O(20)-S(20A)-C(20A)	108.5(3)
C(1)#1-N(1)-C(1)	119.993(7)	C(20B)-S(20A)-C(20A)	100.4(4)
C(1)#2-N(1)-C(1)	119.993(7)		
C(2)-C(1)-C(6)	118.3(2)		

Symmetry transformations used to generate equivalent atoms:

#1 -x+y+2,-x+1,z #2 -y+1,x-y-1,z

Table 6. Torsion angles [°] for C39 H60 N16 O6 S6.

C(1)#1-N(1)-C(1)-C(2)	141.6(3)	(8)-N(2)-C(7)-N(4)	-0.7(4)
C(1)#2-N(1)-C(1)-C(2)	-36.7(6)	(8)-N(2)-C(7)-C(4)	178.8(2)
C(1)#1-N(1)-C(1)-C(6)	-38.5(6)	(3)-C(4)-C(7)-N(4)	168.5(3)
C(1)#2-N(1)-C(1)-C(6)	143.2(3)	(5)-C(4)-C(7)-N(4)	-9.3(4)
C(6)-C(1)-C(2)-C(3)	0.8(4)	(3)-C(4)-C(7)-N(2)	-11.0(4)
N(1)-C(1)-C(2)-C(3)	-179.3(3)	(5)-C(4)-C(7)-N(2)	171.1(3)
C(1)-C(2)-C(3)-C(4)	-2.4(5)	(9)-N(3)-C(8)-N(5)	-179.0(3)
C(2)-C(3)-C(4)-C(5)	1.8(4)	(9)-N(3)-C(8)-N(2)	1.2(5)
C(2)-C(3)-C(4)-C(7)	-176.1(3)	(7)-N(2)-C(8)-N(3)	-0.8(5)
C(3)-C(4)-C(5)-C(6)	0.3(4)	(7)-N(2)-C(8)-N(5)	179.4(3)
C(7)-C(4)-C(5)-C(6)	178.2(3)	(8)-N(3)-C(9)-N(6)	179.8(3)
C(4)-C(5)-C(6)-C(1)	-1.9(5)	(8)-N(3)-C(9)-N(4)	-0.3(5)
C(2)-C(1)-C(6)-C(5)	1.3(4)	(7)-N(4)-C(9)-N(6)	178.9(3)
N(1)-C(1)-C(6)-C(5)	-178.6(3)	(7)-N(4)-C(9)-N(3)	-0.9(5)
C(9)-N(4)-C(7)-N(2)	1.5(4)		
C(9)-N(4)-C(7)-C(4)	-178.0(3)		

Symmetry transformations used to generate equivalent atoms:

#1 -x+y+2,-x+1,z #2 -y+1,x-y-1,z

Table 7. Bond lengths [Å] and angles [°] related to the hydrogen bonding for C39 H60 N16 O6 S6.

D-H	..A	d(D-H)	d(H..A)	d(D..A)	<DHA
N(5)-H(5A)	N(3)#3	0.87	2.12	2.987(3)	173.0
N(5)-H(5B)	O(10)#4	0.87	2.20	2.889(4)	136.2
N(6)-H(6A)	O(10)#5	0.87	2.20	3.045(4)	162.5
N(6)-H(6B)	O(20)	0.87	2.01	2.846(5)	160.9

Symmetry transformations used to generate equivalent atoms:

#1 -x+y+2,-x+1,z #2 -y+1,x-y-1,z #3 -x+5/3,-y+1/3,-z+1/3
#4 x-y+1,x,-z #5 -x+y+2/3,-x+1/3,z+1/3

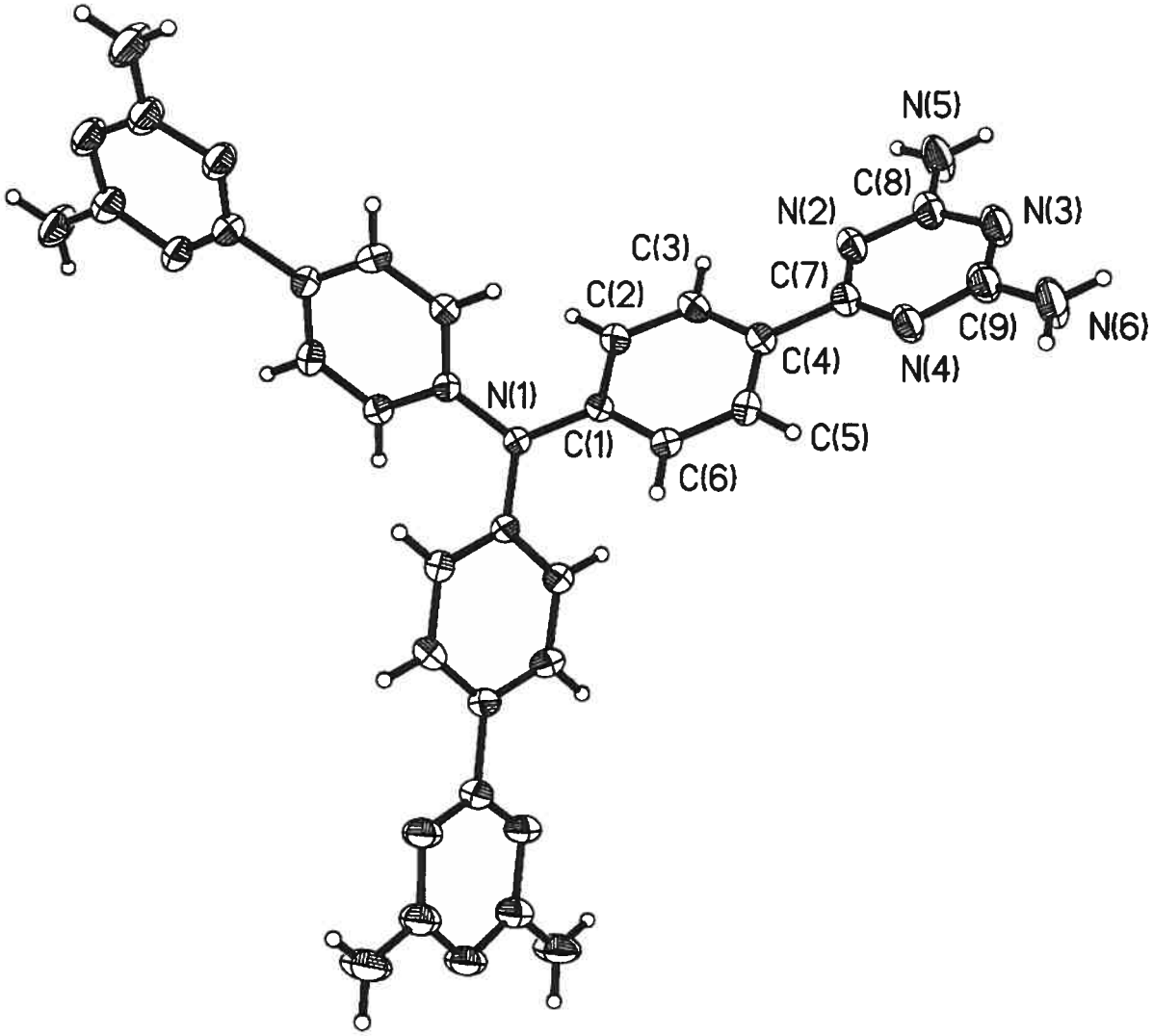
N(5)
C(8)
N(2)
N(3)
C(3)
C(7)
C(2)
C(9)
N(6)
C(4)
N(4)
N(1)
C(1)
C(5)
C(6)

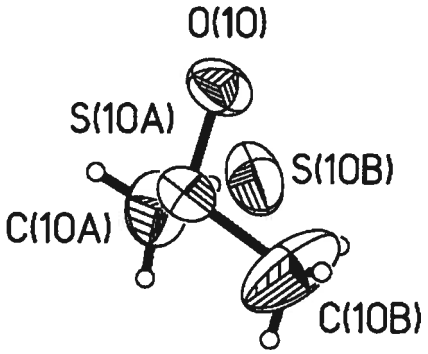
O(10)
S(10A)
S(10B)
C(10A)
C(10B)

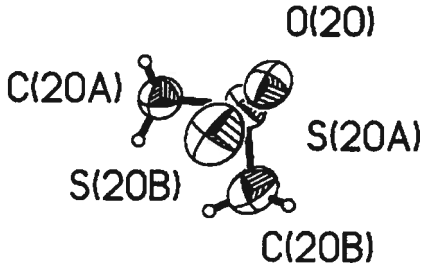
O(20)
C(20A)
S(20A)
S(20B)
C(20B)

ORTEP view of the C39 H60 N16 O6 S6 compound with the numbering scheme adopted. Ellipsoids drawn at 30% probability level. Hydrogens represented by sphere of arbitrary size.

REFERENCES

International Tables for Crystallography (1992). Vol. C. Tables 4.2.6.8 and 6.1.1.4, Dordrecht: Kluwer Academic Publishers.

SAINT (1999) Release 6.06; Integration Software for Single Crystal Data. Bruker AXS Inc., Madison, WI 53719-1173.

Sheldrick, G.M. (1996). SADABS, Bruker Area Detector Absorption Corrections. Bruker AXS Inc., Madison, WI 53719-1173.

Sheldrick, G.M. (1997). SHELXS97, Program for the Solution of Crystal Structures. Univ. of Gottingen, Germany.

Sheldrick, G.M. (1997). SHELXL97, Program for the Refinement of Crystal Structures. Univ. of Gottingen, Germany.

SHELXTL (1997) Release 5.10; The Complete Software Package for Single Crystal Structure Determination. Bruker AXS Inc., Madison, WI 53719-1173.

SMART (1999) Release 5.059; Bruker Molecular Analysis Research Tool. Bruker AXS Inc., Madison, WI 53719-1173.

Spek, A.L. (2000). PLATON, Molecular Geometry Program, 2000 version. University of Utrecht, Utrecht, Holland.

XPREP (1997) Release 5.10; X-ray data Preparation and Reciprocal space Exploration Program. Bruker AXS Inc., Madison, WI 53719-1173.

Université de Montréal

CRYSTAL AND MOLECULAR STRUCTURE OF

C53 H60 N16 O4 S2 COMPOUND (jw1019)

Equipe WUEST

Département de chimie, Université de Montréal,

C.P. 6128, Succ. Centre-Ville, Montréal, Québec, H3C 3J7 (Canada)

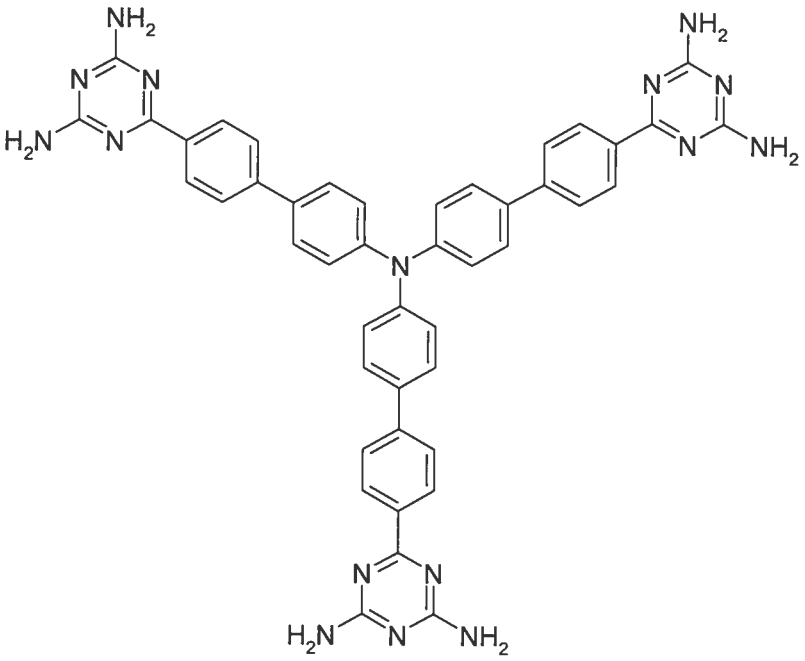

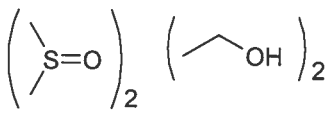

Solvant : DMSO / Ethanol

Structure solved and refined in the laboratory of X-ray diffraction Université de Montréal by Dr. Thierry Maris.

Table 1. Crystal data and structure refinement for C53 H60 N16 O4 S2.

Identification code	JW1019
Empirical formula	C53 H60 N16 O4 S2
Formula weight	1049.29
Temperature	150(2)K
Wavelength	1.54178 Å
Crystal system	Monoclinic
Space group	C2/c
Unit cell dimensions	a = 14.9388(3) Å α = 90° b = 22.4945(5) Å β = 99.707(1)° c = 16.0279(3) Å γ = 90°
Volume	5308.92(19)Å^3
Z	4
Density (calculated)	1.313 g/cm^3
Absorption coefficient	1.411 mm^{-1}
F(000)	2216
Crystal size	0.12 x 0.12 x 0.10 mm
Theta range for data collection	3.59 to 69.06°
Index ranges	$-17 \leq h \leq 17$, $-27 \leq k \leq 27$, $-19 \leq \ell \leq 19$
Reflections collected	36798
Independent reflections	4918 [R_{int} = 0.028]
Absorption correction	Semi-empirical from equivalents
Max. and min. transmission	1.0000 and 0.9200
Refinement method	Full-matrix least-squares on F^2
Data / restraints / parameters	4918 / 6 / 355
Goodness-of-fit on F^2	1.050
Final R indices [I>2sigma(I)]	R_1 = 0.0726, wR_2 = 0.2171
R indices (all data)	R_1 = 0.0862, wR_2 = 0.2355

Largest diff. peak and hole 0.401 and -0.604 e/Å^3

Table 2. Atomic coordinates (x 10^4) and equivalent isotropic displacement parameters (Å^2 x 10^3) for C53 H60 N16 O4 S2.

U_{eq} is defined as one third of the trace of the orthogonalized Uij tensor.

	Occ.	x	y	z	U_{eq}
C(1)	1	5000	445(2)	2500	35(1)
C(2)	1	4438(2)	128(1)	1873(2)	38(1)
C(3)	1	4432(2)	-486(1)	1882(2)	38(1)
C(4)	1	5000	-810(2)	2500	36(1)
C(5)	1	5000	-1468(2)	2500	36(1)
C(6)	1	4202(2)	-1790(1)	2242(2)	39(1)
C(7)	1	4198(2)	-2403(1)	2241(2)	37(1)
C(8)	1	5000	-2720(2)	2500	36(1)
C(9)	1	5000	-3381(2)	2500	39(1)
C(10)	1	4330(2)	-4261(1)	2062(2)	58(1)
C(11)	1	4204(2)	1394(1)	2153(2)	34(1)
C(12)	1	3355(2)	1229(1)	2324(2)	37(1)
C(13)	1	2588(2)	1539(1)	1962(2)	37(1)
C(14)	1	2637(2)	2026(1)	1430(2)	35(1)
C(15)	1	3497(2)	2196(1)	1282(2)	36(1)
C(16)	1	4271(2)	1883(1)	1635(2)	36(1)
C(17)	1	1812(2)	2358(1)	1043(2)	37(1)
C(18)	1	985(2)	2067(1)	782(2)	38(1)
C(19)	1	210(2)	2384(1)	458(2)	40(1)
C(20)	1	235(2)	3000(1)	387(2)	38(1)
C(21)	1	1062(2)	3289(1)	633(2)	42(1)
C(22)	1	1831(2)	2972(1)	957(2)	41(1)
C(23)	1	-593(2)	3350(1)	43(2)	38(1)
C(24)	1	-2110(2)	3412(1)	-398(2)	41(1)
C(25)	1	-1223(2)	4221(1)	-462(2)	41(1)
N(1)	1	5000	1073(1)	2500	36(1)
N(2)	1	4312(2)	-3658(1)	2007(2)	45(1)
N(3)	1	5000	-4578(2)	2500	68(1)
N(4)	1	3630(2)	-4554(1)	1633(3)	84(1)
N(5)	1	-1402(1)	3073(1)	-55(1)	42(1)
N(6)	1	-459(2)	3913(1)	-155(2)	43(1)
N(7)	1	-2062(1)	3988(1)	-603(2)	42(1)
N(8)	1	-2939(2)	3163(1)	-540(2)	50(1)
N(9)	1	-1137(2)	4792(1)	-646(2)	52(1)
S(30)	0.670(3)	6571(1)	3785(1)	1975(1)	70(1)
O(30)	0.670(3)	6364(5)	3793(4)	2892(4)	103(2)
C(30)	0.670(3)	6431(5)	3016(3)	1734(4)	70(2)
C(31)	0.670(3)	5646(5)	4068(4)	1275(8)	109(3)
S(31)	0.330(3)	5762(6)	3410(4)	2138(6)	183
O(31)	0.330(3)	6225(18)	3921(11)	2776(13)	147
C(32)	0.330(3)	5341(17)	3969(11)	1377(16)	134
C(33)	0.330(3)	6601(17)	3147(11)	1613(18)	131

O(40)	1	7361(2)	4396(1)	4133(2)	69(1)
C(40)	1	7168(4)	4210(2)	4924(3)	89(1)
C(41)	1	6791(4)	4663(2)	5385(3)	107(2)

Table 3. Hydrogen coordinates (x 10^4) and isotropic displacement parameters ($Å^2$ x 10^3) for C53 H60 N16 O4 S2.

	Occ.	x	y	z	U_{eq}
H(2)	1	4056	336	1435	46
H(3)	1	4032	-693	1457	46
H(6)	1	3649	-1582	2064	46
H(7)	1	3646	-2611	2062	45
H(12)	1	3303	903	2689	44
H(13)	1	2012	1418	2079	45
H(15)	1	3553	2531	934	43
H(16)	1	4848	2004	1523	43
H(18)	1	954	1647	827	46
H(19)	1	-346	2179	281	48
H(21)	1	1095	3709	577	50
H(22)	1	2388	3178	1124	49
H(4A)	1	3621	-4945	1646	101
H(4B)	1	3175	-4358	1337	101
H(8A)	1	-3416	3377	-756	60
H(8B)	1	-3007	2787	-416	60
H(9A)	1	-1620	5003	-852	62
H(9B)	1	-596	4959	-563	62
H(30A)	0.670(3)	6878	2786	2121	105
H(30B)	0.670(3)	6520	2946	1150	105
H(30C)	0.670(3)	5817	2891	1797	105
H(31A)	0.670(3)	5106	3826	1306	163
H(31B)	0.670(3)	5779	4056	697	163
H(31C)	0.670(3)	5534	4479	1429	163
H(32A)	0.330(3)	4843	3804	965	202
H(32B)	0.330(3)	5830	4100	1083	202
H(32C)	0.330(3)	5118	4308	1666	202
H(33A)	0.330(3)	6704	3435	1179	197
H(33B)	0.330(3)	6410	2766	1343	197
H(33C)	0.330(3)	7164	3092	2017	197
H(40)	1	6939	4289	3748	104
H(40A)	1	7736	4063	5272	107
H(40B)	1	6737	3872	4831	107
H(41A)	1	7226	4990	5508	160
H(41B)	1	6660	4497	5917	160
H(41C)	1	6227	4811	5047	160

Table 4. Anisotropic parameters ($Å^2$ x 10^3) for C53 H60 N16 O4 S2.

The anisotropic displacement factor exponent takes the form:

$$-2\pi^2 [h^2 a^{*2} U_{11} + ... + 2 h k a^* b^* U_{12}]$$

	U11	U22	U33	U23	U13	U12
C(1)	30(2)	33(2)	41(2)	0	2(1)	0
C(2)	32(1)	40(1)	39(1)	1(1)	-5(1)	1(1)
C(3)	34(1)	39(1)	39(1)	-3(1)	-2(1)	-1(1)
C(4)	30(2)	39(2)	40(2)	0	5(1)	0
C(5)	35(2)	36(2)	36(2)	0	6(1)	0
C(6)	31(1)	42(1)	41(1)	-2(1)	2(1)	4(1)
C(7)	30(1)	38(1)	43(1)	-4(1)	2(1)	-1(1)
C(8)	31(2)	39(2)	37(2)	0	3(1)	0
C(9)	29(2)	41(2)	45(2)	0	3(2)	0
C(10)	40(2)	38(2)	86(2)	-5(2)	-16(2)	1(1)
C(11)	28(1)	34(1)	36(1)	-4(1)	-4(1)	1(1)
C(12)	32(1)	37(1)	39(1)	4(1)	0(1)	-2(1)
C(13)	28(1)	43(1)	40(1)	-1(1)	3(1)	-2(1)
C(14)	28(1)	40(1)	35(1)	-4(1)	-2(1)	3(1)
C(15)	31(1)	38(1)	36(1)	3(1)	-1(1)	1(1)
C(16)	26(1)	42(1)	37(1)	0(1)	-1(1)	-3(1)
C(17)	30(1)	44(1)	34(1)	-1(1)	0(1)	5(1)
C(18)	30(1)	44(1)	40(1)	0(1)	1(1)	3(1)
C(19)	28(1)	49(2)	41(1)	0(1)	-1(1)	0(1)
C(20)	29(1)	48(2)	36(1)	-2(1)	0(1)	6(1)
C(21)	37(1)	42(1)	44(1)	-2(1)	-1(1)	5(1)
C(22)	30(1)	46(2)	43(1)	-2(1)	-3(1)	2(1)
C(23)	32(1)	46(1)	34(1)	-2(1)	0(1)	5(1)
C(24)	33(1)	47(2)	41(1)	-2(1)	-2(1)	4(1)
C(25)	33(1)	45(1)	41(1)	-1(1)	-1(1)	3(1)
N(1)	26(1)	34(2)	44(2)	0	-6(1)	0
N(2)	35(1)	37(1)	61(2)	-4(1)	-5(1)	2(1)
N(3)	48(2)	37(2)	104(3)	0	-28(2)	0
N(4)	55(2)	38(1)	139(3)	-9(2)	-42(2)	0(1)
N(5)	32(1)	46(1)	43(1)	0(1)	-3(1)	5(1)
N(6)	31(1)	51(1)	45(1)	1(1)	-1(1)	3(1)
N(7)	30(1)	44(1)	48(1)	-1(1)	-2(1)	3(1)
N(8)	33(1)	46(1)	65(2)	11(1)	-9(1)	1(1)
N(9)	34(1)	47(1)	69(2)	7(1)	-4(1)	-3(1)
S(30)	50(1)	70(1)	86(1)	-7(1)	-4(1)	-3(1)
O(30)	77(3)	137(6)	80(3)	-50(4)	-33(2)	29(3)
C(30)	98(5)	60(3)	51(3)	6(3)	12(3)	3(3)
C(31)	64(4)	92(5)	165(8)	47(5)	5(5)	0(4)
O(40)	82(2)	48(1)	76(2)	6(1)	5(1)	-6(1)
C(40)	129(4)	62(2)	80(3)	11(2)	28(3)	-4(2)
C(41)	137(5)	87(3)	102(4)	18(3)	39(3)	26(3)

Table 5. Bond lengths [Å] and angles [°] for C53 H60 N16 O4 S2

C(1)-C(2)	1.392(3)	O(40)-C(40)	1.410(5)
C(1)-C(2)#1	1.392(3)	C(40)-C(41)	1.430(7)
C(1)-N(1)	1.414(4)		
C(2)-C(3)	1.381(4)	C(2)-C(1)-C(2)#1	118.5(3)
C(3)-C(4)	1.396(3)	C(2)-C(1)-N(1)	120.77(16)
C(4)-C(3)#1	1.396(3)	C(2)#1-C(1)-N(1)	120.77(16)
C(4)-C(5)	1.480(5)	C(3)-C(2)-C(1)	120.5(2)
C(5)-C(6)#1	1.397(3)	C(2)-C(3)-C(4)	121.7(2)
C(5)-C(6)	1.397(3)	C(3)#1-C(4)-C(3)	117.1(3)
C(6)-C(7)	1.378(4)	C(3)#1-C(4)-C(5)	121.47(16)
C(7)-C(8)	1.396(3)	C(3)-C(4)-C(5)	121.46(16)
C(8)-C(7)#1	1.396(3)	C(6)#1-C(5)-C(6)	117.5(3)
C(8)-C(9)	1.487(5)	C(6)#1-C(5)-C(4)	121.25(16)
C(9)-N(2)	1.340(3)	C(6)-C(5)-C(4)	121.25(16)
C(9)-N(2)#1	1.341(3)	C(7)-C(6)-C(5)	121.5(2)
C(10)-N(4)	1.326(4)	C(6)-C(7)-C(8)	120.5(2)
C(10)-N(3)	1.330(3)	C(7)-C(8)-C(7)#1	118.5(3)
C(10)-N(2)	1.359(4)	C(7)-C(8)-C(9)	120.74(16)
C(11)-C(16)	1.391(4)	C(7)#1-C(8)-C(9)	120.74(16)
C(11)-C(12)	1.393(4)	N(2)-C(9)-N(2)#1	124.5(3)
C(11)-N(1)	1.422(3)	N(2)-C(9)-C(8)	117.74(17)
C(12)-C(13)	1.383(3)	N(2)#1-C(9)-C(8)	117.74(17)
C(13)-C(14)	1.397(4)	N(4)-C(10)-N(3)	117.6(3)
C(14)-C(15)	1.399(4)	N(4)-C(10)-N(2)	117.3(3)
C(14)-C(17)	1.485(3)	N(3)-C(10)-N(2)	125.1(3)
C(15)-C(16)	1.390(3)	C(16)-C(11)-C(12)	119.2(2)
C(17)-C(22)	1.390(4)	C(16)-C(11)-N(1)	119.7(2)
C(17)-C(18)	1.398(3)	C(12)-C(11)-N(1)	121.1(2)
C(18)-C(19)	1.384(3)	C(13)-C(12)-C(11)	120.1(2)
C(19)-C(20)	1.391(4)	C(12)-C(13)-C(14)	121.7(2)
C(20)-C(21)	1.394(4)	C(13)-C(14)-C(15)	117.6(2)
C(20)-C(23)	1.492(3)	C(13)-C(14)-C(17)	121.6(2)
C(21)-C(22)	1.378(4)	C(15)-C(14)-C(17)	120.9(2)
C(23)-N(6)	1.329(4)	C(16)-C(15)-C(14)	121.1(2)
C(23)-N(5)	1.343(3)	C(15)-C(16)-C(11)	120.3(2)
C(24)-N(7)	1.341(4)	C(22)-C(17)-C(18)	117.9(2)
C(24)-N(8)	1.343(3)	C(22)-C(17)-C(14)	120.8(2)
C(24)-N(5)	1.345(3)	C(18)-C(17)-C(14)	121.3(2)
C(25)-N(9)	1.329(4)	C(19)-C(18)-C(17)	120.8(2)
C(25)-N(7)	1.343(3)	C(18)-C(19)-C(20)	120.7(2)
C(25)-N(6)	1.355(3)	C(19)-C(20)-C(21)	118.5(2)
N(1)-C(11)#1	1.422(3)	C(19)-C(20)-C(23)	121.6(2)
N(3)-C(10)#1	1.330(3)	C(21)-C(20)-C(23)	119.9(2)
S(30)-O(30)	1.552(8)	C(22)-C(21)-C(20)	120.5(3)
S(30)-C(31)	1.747(8)	C(21)-C(22)-C(17)	121.5(2)
S(30)-C(30)	1.777(6)	N(6)-C(23)-N(5)	125.6(2)
S(31)-O(31)	1.614(17)	N(6)-C(23)-C(20)	116.2(2)
S(31)-C(33)	1.727(17)	N(5)-C(23)-C(20)	118.2(2)
S(31)-C(32)	1.789(17)	N(7)-C(24)-N(8)	116.5(2)

N(7)-C(24)-N(5)	125.2(2)	C(11)-N(1)-C(11)#1	119.0(3)
N(8)-C(24)-N(5)	118.2(2)	C(9)-N(2)-C(10)	114.9(2)
N(9)-C(25)-N(7)	117.6(2)	C(10)-N(3)-C(10)#1	115.1(4)
N(9)-C(25)-N(6)	117.9(2)	C(23)-N(5)-C(24)	114.6(2)
N(7)-C(25)-N(6)	124.6(3)	C(23)-N(6)-C(25)	114.9(2)
C(1)-N(1)-C(11)	120.51(14)	C(24)-N(7)-C(25)	115.0(2)
C(1)-N(1)-C(11)#1	120.52(14)		

Symmetry transformations used to generate equivalent atoms:

#1 -x+1,y,-z+1/2

Table 6. Torsion angles [°] for C53 H60 N16 O4 S2.

C(2)#1-C(1)-C(2)-C(3)	0.84(18)	C(18)-C(19)-C(20)-C(23)	-179.7(2)
N(1)-C(1)-C(2)-C(3)	-179.15(18)	C(19)-C(20)-C(21)-C(22)	-1.5(4)
C(1)-C(2)-C(3)-C(4)	-1.7(4)	C(23)-C(20)-C(21)-C(22)	179.6(2)
C(2)-C(3)-C(4)-C(3)#1	0.86(18)	C(20)-C(21)-C(22)-C(17)	0.4(4)
C(2)-C(3)-C(4)-C(5)	-179.14(18)	C(18)-C(17)-C(22)-C(21)	0.7(4)
C(3)#1-C(4)-C(5)-C(6)#1	-35.18(18)	C(14)-C(17)-C(22)-C(21)	-177.1(2)
C(3)-C(4)-C(5)-C(6)#1	144.82(18)	C(19)-C(20)-C(23)-N(6)	-166.8(2)
C(3)#1-C(4)-C(5)-C(6)	144.82(18)	C(21)-C(20)-C(23)-N(6)	12.1(4)
C(3)-C(4)-C(5)-C(6)	-35.18(18)	C(19)-C(20)-C(23)-N(5)	11.9(4)
C(6)#1-C(5)-C(6)-C(7)	-0.03(17)	C(21)-C(20)-C(23)-N(5)	-169.1(2)
C(4)-C(5)-C(6)-C(7)	179.98(17)	C(2)-C(1)-N(1)-C(11)	29.33(17)
C(5)-C(6)-C(7)-C(8)	0.0(3)	C(2)#1-C(1)-N(1)-C(11)	-150.67(17)
C(6)-C(7)-C(8)-C(7)#1	-0.02(17)	C(2)-C(1)-N(1)-C(11)#1	-150.67(17)
C(6)-C(7)-C(8)-C(9)	179.98(17)	C(2)#1-C(1)-N(1)-C(11)#1	29.33(17)
C(7)-C(8)-C(9)-N(2)	21.09(18)	C(16)-C(11)-N(1)-C(1)	-136.08(18)
C(7)#1-C(8)-C(9)-N(2)	-158.91(18)	C(12)-C(11)-N(1)-C(1)	44.2(3)
C(7)-C(8)-C(9)-N(2)#1	-158.91(18)	C(16)-C(11)-N(1)-C(11)#1	43.92(18)
C(7)#1-C(8)-C(9)-N(2)#1	21.09(18)	C(12)-C(11)-N(1)-C(11)#1	-135.8(3)
C(16)-C(11)-C(12)-C(13)	1.8(4)	N(2)#1-C(9)-N(2)-C(10)	2.7(2)
N(1)-C(11)-C(12)-C(13)	-178.5(2)	C(8)-C(9)-N(2)-C(10)	-177.3(2)
C(11)-C(12)-C(13)-C(14)	-0.8(4)	N(4)-C(10)-N(2)-C(9)	175.2(3)
C(12)-C(13)-C(14)-C(15)	-0.9(4)	N(3)-C(10)-N(2)-C(9)	-5.8(5)
C(12)-C(13)-C(14)-C(17)	-180.0(2)	N(4)-C(10)-N(3)-C(10)#1	-178.0(4)
C(13)-C(14)-C(15)-C(16)	1.5(4)	N(2)-C(10)-N(3)-C(10)#1	3.1(3)
C(17)-C(14)-C(15)-C(16)	-179.3(2)	N(6)-C(23)-N(5)-C(24)	1.1(4)
C(14)-C(15)-C(16)-C(11)	-0.5(4)	C(20)-C(23)-N(5)-C(24)	-177.5(2)
C(12)-C(11)-C(16)-C(15)	-1.1(4)	N(7)-C(24)-N(5)-C(23)	-3.0(4)
N(1)-C(11)-C(16)-C(15)	179.1(2)	N(8)-C(24)-N(5)-C(23)	178.1(2)
C(13)-C(14)-C(17)-C(22)	141.9(3)	N(5)-C(23)-N(6)-C(25)	1.6(4)
C(15)-C(14)-C(17)-C(22)	-37.2(4)	C(20)-C(23)-N(6)-C(25)	-179.8(2)
C(13)-C(14)-C(17)-C(18)	-35.9(4)	N(9)-C(25)-N(6)-C(23)	177.8(2)
C(15)-C(14)-C(17)-C(18)	145.0(3)	N(7)-C(25)-N(6)-C(23)	-2.9(4)
C(22)-C(17)-C(18)-C(19)	-0.9(4)	N(8)-C(24)-N(7)-C(25)	-179.2(2)
C(14)-C(17)-C(18)-C(19)	177.0(2)	N(5)-C(24)-N(7)-C(25)	1.9(4)
C(17)-C(18)-C(19)-C(20)	-0.2(4)	N(9)-C(25)-N(7)-C(24)	-179.4(3)
C(18)-C(19)-C(20)-C(21)	1.3(4)	N(6)-C(25)-N(7)-C(24)	1.3(4)

Symmetry transformations used to generate equivalent atoms:

#1 -x+1,y,-z+1/2

Table 7. Bond lengths [Å] and angles [°] related to the hydrogen bonding for C53 H60 N16 O4 S2.

D-H	..A	d(D-H)	d(H..A)	d(D..A)	<DHA
N(4)-H(4A)	O(40)#2	0.88	2.3	2.942(4)	130
N(4)-H(4B)	N(7)#3	0.88	2.04	2.922(4)	173.9
N(8)-H(8A)	N(2)#3	0.88	2.3	3.057(3)	143.7
N(8)-H(8B)	N(5)#4	0.88	2.31	3.152(3)	161.1
N(9)-H(9A)	O(40)#5	0.88	2.03	2.869(4)	158.1
O(40)-H(40)	O(30)	0.84	1.86	2.649(6)	155.4
O(40)-H(40)	O(31)	0.84	1.92	2.740(18)	164.8

Symmetry transformations used to generate equivalent atoms:

#1 -x+1,y,-z+1/2 #2 -x+1,y-1,-z+1/2
#3 -x,-y,-z #4 -x-1/2,-y+1/2,-z
#5 x-1,-y+1,z-1/2

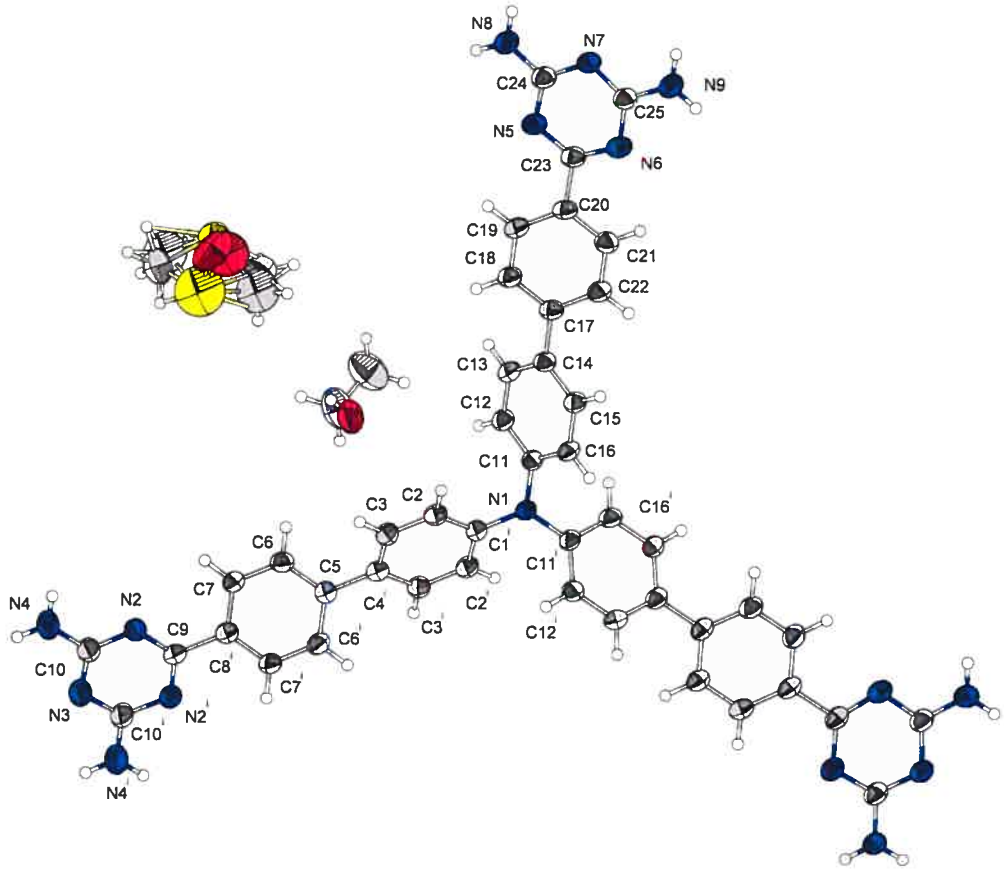

ORTEP view of the C53 H60 N16 O4 S2 compound with the numbering scheme adopted. Ellipsoids drawn at 30% probability level. Hydrogen atoms are represented by sphere of arbitrary size. Symmetry operation i: -x+1,y,-z+1/2

REFERENCES

SAINT (1999) Release 6.06; Integration Software for Single Crystal Data. Bruker AXS Inc., Madison, WI 53719-1173.

Sheldrick, G.M. (1996). SADABS, Bruker Area Detector Absorption Corrections. Bruker AXS Inc., Madison, WI 53719-1173.

Sheldrick, G.M. (1997). SHELXS97, Program for the Solution of Crystal Structures. Univ. of Gottingen, Germany.

Sheldrick, G.M. (1997). SHELXL97, Program for the Refinement of Crystal Structures. Univ. of Gottingen, Germany.

SHELXTL (1997) Release 5.10; The Complete Software Package for Single Crystal Structure Determination. Bruker AXS Inc., Madison, WI 53719-1173.

SMART (1999) Release 5.059; Bruker Molecular Analysis Research Tool. Bruker AXS Inc., Madison, WI 53719-1173.

Spek, A.L. (2000). PLATON, Molecular Geometry Program, 2000 version. University of Utrecht, Utrecht, Holland.

XPREP (1997) Release 5.10; X-ray data Preparation and Reciprocal space Exploration Program. Bruker AXS Inc., Madison, WI 53719-11

Université de Montréal

CRYSTAL AND MOLECULAR STRUCTURE OF

C60 H80 N22 O8 S6 COMPOUND (JIW901)

Equipe WUEST

Département de chimie, Université de Montréal,

C.P. 6128, Succ. Centre-Ville, Montréal, Québec, H3C 3J7 (Canada)

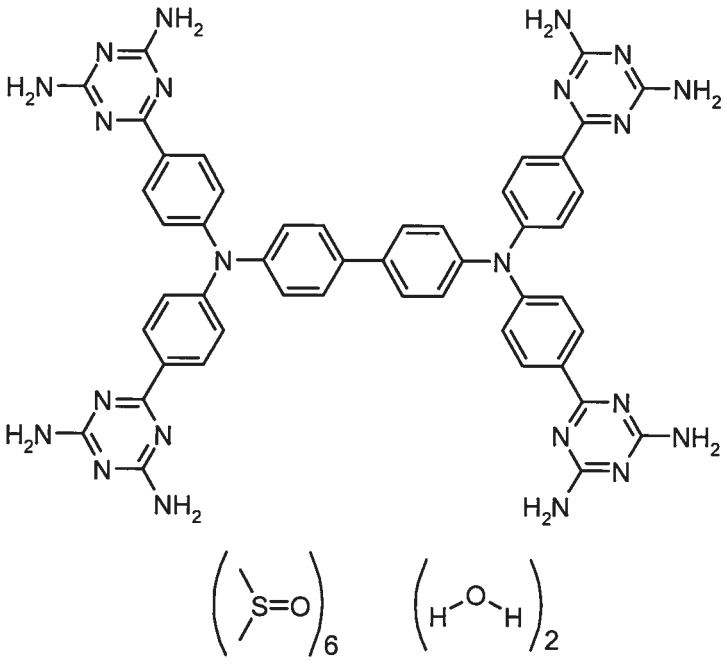

Structure solved and refined in the laboratory of X-ray diffraction Université de Montréal by Dr. Thierry Maris.

Table 1. Crystal data and structure refinement for C60 H80 N22 O8 S6.

Identification code	JIW901
Empirical formula	C60 H80 N22 O8 S6
Formula weight	1429.82
Temperature	100(2)K
Wavelength	1.54178 Å
Crystal system	Triclinic
Space group	P-1
Unit cell dimensions	a = 10.3770(13) Å α = 105.854(6)° b = 11.3536(12) Å β = 105.309(6)° c = 16.1445(17) Å γ = 90.104(6)°
Volume	1759.2(3)Å^3
Z	1
Density (calculated)	1.350 g/cm^3
Absorption coefficient	2.359 mm^{-1}
F(000)	754
Crystal size	0.10 x 0.07 x 0.05 mm
Theta range for data collection	2.96 to 67.72°
Index ranges	$-12 \leq h \leq 11$, $-13 \leq k \leq 13$, $-19 \leq \ell \leq 19$
Reflections collected	12090
Independent reflections	5705 [R_{int} = 0.045]
Absorption correction	Semi-empirical from equivalents
Max. and min. transmission	1.0000 and 0.3500
Refinement method	Full-matrix least-squares on F^2
Data / restraints / parameters	5705 / 0 / 470
Goodness-of-fit on F^2	1.044
Final R indices [I>2sigma(I)]	R_1 = 0.0878, wR_2 = 0.2039
R indices (all data)	R_1 = 0.1005, wR_2 = 0.2066

Largest diff. peak and hole 0.350 and -0.360 e/Å^3

Table 2. Atomic coordinates (x 10^4) and equivalent isotropic displacement parameters (Å^2 x 10^3) for C60 H80 N22 O8 S6.

U_{eq} is defined as one third of the trace of the orthogonalized Uij tensor.

	Occ.	x	y	z	U_{eq}
C(1)	1	4891(5)	371(4)	4675(3)	52(1)
N(1)	1	4364(4)	2553(3)	2877(2)	49(1)
C(2)	1	5960(5)	963(4)	4557(3)	56(1)
C(3)	1	5791(5)	1649(4)	3934(3)	62(1)
C(4)	1	4548(5)	1799(4)	3466(3)	47(1)
C(5)	1	3477(5)	1247(4)	3595(3)	61(1)
C(6)	1	3658(5)	557(5)	4190(3)	71(2)
C(10)	1	4952(4)	2265(4)	2144(3)	47(1)
N(10)	1	7512(3)	408(3)	-88(2)	46(1)
C(11)	1	5310(5)	3154(4)	1801(3)	56(1)
N(11)	1	6622(3)	2138(3)	-513(2)	50(1)
C(12)	1	5871(4)	2838(4)	1074(3)	52(1)
N(12)	1	8033(4)	934(3)	-1328(2)	51(1)
C(13)	1	6164(4)	1650(4)	734(3)	51(1)
N(13)	1	7154(4)	2676(3)	-1664(2)	68(1)
C(14)	1	5850(4)	767(4)	1100(3)	49(1)
N(14)	1	8746(4)	-814(3)	-974(2)	59(1)
C(15)	1	5256(4)	1060(4)	1809(3)	50(1)
C(16)	1	6837(5)	1351(4)	-13(2)	47(1)
C(17)	1	7294(5)	1875(4)	-1175(3)	57(1)
C(18)	1	8068(5)	180(4)	-803(3)	53(1)
C(20)	1	3638(4)	3601(4)	3044(3)	46(1)
N(20)	1	1326(3)	7489(3)	3040(2)	48(1)
C(21)	1	2873(5)	4028(4)	2364(3)	50(1)
N(21)	1	1187(4)	7109(3)	4396(2)	56(1)
C(22)	1	2202(4)	5060(4)	2535(3)	43(1)
N(22)	1	311(4)	8895(3)	4010(2)	54(1)
C(23)	1	2272(4)	5708(4)	3430(3)	46(1)
N(23)	1	212(5)	8536(4)	5312(3)	93(2)
C(24)	1	2986(5)	5277(4)	4110(3)	49(1)
N(24)	1	421(4)	9182(3)	2679(2)	60(1)
C(25)	1	3677(4)	4241(4)	3935(3)	50(1)
C(26)	1	1518(4)	6845(3)	3619(3)	44(1)
C(27)	1	661(4)	8523(4)	3251(3)	50(1)
C(28)	1	558(5)	8155(4)	4535(3)	62(1)
S(30)	0.751(10)	7217(5)	6989(3)	3188(2)	98(2)
O(30)	1	7086(7)	6082(5)	2336(4)	187(3)
C(30)	1	5873(8)	6734(6)	3646(5)	152(3)
C(31)	1	6680(7)	8364(5)	2957(5)	126(2)
S(30)	0.249(10)	6349(15)	6524(10)	2853(7)	108(4)
S(40)	0.727(4)	9120(2)	6929(2)	587(1)	61(1)
O(40)	1	9248(3)	6950(3)	-276(2)	80(1)
C(40)	1	8484(7)	5538(6)	569(5)	134(3)

C(41)	1	7585(7)	7702(5)	666(4)	119(2)
S(41)	0.273(4)	8133(7)	6395(6)	-7(5)	98(3)
S(50)	0.498(5)	8794(3)	2606(2)	2671(2)	56(1)
O(50)	0.498(5)	9689(9)	1776(8)	2971(6)	87(4)
C(50)	0.498(5)	8155(10)	3881(7)	3325(6)	16(3)
C(51)	0.498(5)	9274(8)	3241(8)	1943(5)	47(2)
S(51)	0.502(5)	8335(8)	2528(8)	3175(6)	243(4)
O(51)	0.502(5)	9191(8)	926(8)	1852(6)	121(3)
C(52)	0.502(5)	8468(15)	3770(11)	3301(8)	21(3)
C(53)	0.502(5)	9066(12)	4104(11)	2522(8)	93(4)
O(60)	1	4818(4)	5773(3)	791(3)	104(1)
C(71)	0.297(4)	8910(20)	4016(18)	3552(13)	36(5)
C(72)	0.297(4)	9992(14)	3201(13)	3039(9)	44(4)
C(73)	0.297(4)	7171(12)	7743(12)	3728(9)	27(3)
C(74)	0.297(4)	9622(14)	4419(13)	4291(10)	49(4)
C(75)	0.297(4)	10163(16)	1869(13)	2979(10)	28(4)
C(76)	0.297(4)	9514(19)	4018(17)	3610(13)	54(6)

Table 3. Hydrogen coordinates ($x\ 10^4$) and isotropic displacement parameters ($Å^2\ x\ 10^3$) for C60 H80 N22 O8 S6.

	Occ.	x	y	z	U_{eq}
H(2)	1	6838	907	4907	67
H(3)	1	6553	2006	3843	74
H(5)	1	2595	1340	3269	73
H(6)	1	2889	193	4266	86
H(11)	1	5178	3988	2056	68
H(12)	1	6051	3453	813	62
H(13A)	1	7556	2578	-2092	82
H(13B)	1	6660	3299	-1557	82
H(14)	1	6039	-57	868	59
H(14A)	1	9140	-949	-1408	70
H(14B)	1	8800	-1335	-652	70
H(15)	1	5060	439	2061	60
H(21)	1	2812	3592	1760	60
H(22)	1	1690	5341	2055	51
H(23A)	1	-154	9237	5444	112
H(23B)	1	353	8082	5686	112
H(24)	1	3008	5693	4711	59
H(24A)	1	29	9871	2799	72
H(24B)	1	654	8934	2176	72
H(25)	1	4181	3957	4415	61
H(30A)	1	5012	6709	3204	227
H(30B)	1	5922	7403	4189	227
H(30C)	1	5952	5951	3794	227
H(31A)	1	7244	8629	2630	190
H(31B)	1	6753	9001	3521	190
H(31C)	1	5745	8228	2592	190
H(40A)	1	7626	5310	105	201
H(40B)	1	8344	5585	1153	201
H(40C)	1	9114	4919	437	201
H(41A)	1	7699	8544	633	179
H(41B)	1	7408	7722	1236	179
H(41C)	1	6829	7253	169	179
H(50A)	1	8399	3864	3950	24
H(50B)	1	7177	3831	3095	24
H(50C)	1	8539	4648	3287	24
H(51A)	1	10224	3537	2184	70
H(51B)	1	8736	3931	1863	70
H(51C)	1	9137	2621	1364	70

Table 4. Anisotropic parameters ($Å^2$ x 10^3) for C60 H80 N22 O8 S6.

The anisotropic displacement factor exponent takes the form:

$$-2\pi^2 [h^2 a^{*2} U_{11} + ... + 2 h k a^* b^* U_{12}]$$

	U11	U22	U33	U23	U13	U12
C(1)	81(3)	39(3)	32(2)	5(2)	19(3)	-10(2)
N(1)	77(3)	38(2)	35(2)	15(2)	16(2)	4(2)
C(2)	74(3)	53(3)	47(3)	28(2)	12(2)	-4(2)
C(3)	77(4)	53(3)	71(3)	34(3)	29(3)	7(3)
C(4)	69(3)	39(3)	30(2)	13(2)	9(2)	1(2)
C(5)	57(3)	73(3)	50(3)	35(3)	-8(2)	-21(3)
C(6)	77(4)	87(4)	54(3)	42(3)	2(3)	-29(3)
C(10)	65(3)	37(3)	33(2)	7(2)	8(2)	4(2)
N(10)	64(2)	47(2)	30(2)	17(2)	14(2)	-6(2)
C(11)	77(3)	55(3)	37(3)	16(2)	13(2)	3(2)
N(11)	63(2)	54(2)	36(2)	17(2)	15(2)	1(2)
C(12)	65(3)	50(3)	45(3)	23(2)	16(2)	-1(2)
N(12)	65(3)	48(2)	44(2)	25(2)	10(2)	1(2)
C(13)	73(3)	37(3)	35(2)	9(2)	4(2)	1(2)
N(13)	98(3)	75(3)	60(3)	44(2)	41(2)	28(2)
C(14)	75(3)	42(3)	30(2)	10(2)	13(2)	5(2)
N(14)	77(3)	51(2)	59(3)	30(2)	23(2)	4(2)
C(15)	68(3)	48(3)	35(2)	14(2)	13(2)	-7(2)
C(16)	79(3)	32(2)	28(2)	6(2)	11(2)	-5(2)
C(17)	73(3)	54(3)	43(3)	23(2)	4(3)	-6(3)
C(18)	65(3)	40(3)	48(3)	14(2)	2(2)	-8(2)
C(20)	65(3)	42(3)	31(2)	13(2)	11(2)	-11(2)
N(20)	65(2)	41(2)	44(2)	23(2)	11(2)	-2(2)
C(21)	74(3)	38(3)	41(3)	14(2)	18(2)	-4(2)
N(21)	90(3)	47(2)	39(2)	21(2)	24(2)	4(2)
C(22)	57(3)	39(3)	31(2)	15(2)	8(2)	-4(2)
N(22)	78(3)	50(2)	47(2)	22(2)	30(2)	5(2)
C(23)	58(3)	40(3)	40(2)	13(2)	9(2)	-9(2)
N(23)	171(5)	82(3)	69(3)	49(3)	76(3)	58(3)
C(24)	74(3)	38(3)	32(2)	10(2)	11(2)	2(2)
N(24)	90(3)	59(2)	53(2)	30(2)	40(2)	17(2)
C(25)	69(3)	46(3)	27(2)	15(2)	-5(2)	-10(2)
C(26)	57(3)	36(2)	37(2)	13(2)	8(2)	-7(2)
C(27)	52(3)	46(3)	56(3)	25(2)	9(2)	-6(2)
C(28)	104(4)	50(3)	43(3)	24(2)	28(3)	10(3)
S(30)	114(3)	93(2)	103(2)	39(2)	45(2)	-2(2)
O(30)	311(8)	122(4)	179(5)	5(4)	191(6)	-4(4)
C(30)	225(9)	127(6)	135(6)	24(5)	119(6)	-33(6)
C(31)	173(7)	81(5)	140(6)	33(4)	66(5)	29(5)
S(40)	77(1)	65(1)	38(1)	16(1)	7(1)	-5(1)
O(40)	98(3)	89(3)	55(2)	31(2)	14(2)	1(2)
C(40)	178(7)	120(6)	172(7)	99(5)	103(6)	66(5)
C(41)	174(7)	91(5)	143(6)	68(4)	92(5)	53(4)
S(50)	60(2)	57(2)	54(2)	32(1)	2(1)	-3(1)
O(60)	117(3)	96(3)	104(3)	29(2)	40(3)	14(2)

Table 5. Bond lengths [Å] and angles [°] for C60 H80 N22 O8 S6

C(1)-C(6)	1.363(6)	C(20)-N(1)-C(10)	121.0(3)
C(1)-C(2)	1.377(6)	C(4)-N(1)-C(10)	119.9(3)
C(1)-C(1)#1	1.490(8)	C(1)-C(2)-C(3)	122.1(4)
N(1)-C(20)	1.411(5)	C(4)-C(3)-C(2)	120.0(4)
N(1)-C(4)	1.422(4)	C(3)-C(4)-C(5)	118.5(4)
N(1)-C(10)	1.432(5)	C(3)-C(4)-N(1)	120.4(4)
C(2)-C(3)	1.409(5)	C(5)-C(4)-N(1)	121.1(4)
C(3)-C(4)	1.349(6)	C(4)-C(5)-C(6)	120.8(4)
C(4)-C(5)	1.364(6)	C(1)-C(6)-C(5)	123.0(4)
C(5)-C(6)	1.374(5)	C(11)-C(10)-C(15)	118.9(4)
C(10)-C(11)	1.369(5)	C(11)-C(10)-N(1)	121.8(4)
C(10)-C(15)	1.397(5)	C(15)-C(10)-N(1)	119.2(3)
N(10)-C(16)	1.276(5)	C(16)-N(10)-C(18)	113.6(3)
N(10)-C(18)	1.387(5)	C(10)-C(11)-C(12)	120.3(4)
C(11)-C(12)	1.408(6)	C(16)-N(11)-C(17)	112.7(4)
N(11)-C(16)	1.340(5)	C(13)-C(12)-C(11)	121.0(4)
N(11)-C(17)	1.393(5)	C(17)-N(12)-C(18)	115.0(4)
C(12)-C(13)	1.377(6)	C(14)-C(13)-C(12)	118.5(4)
N(12)-C(17)	1.323(5)	C(14)-C(13)-C(16)	121.6(4)
N(12)-C(18)	1.354(5)	C(12)-C(13)-C(16)	119.8(4)
C(13)-C(14)	1.372(5)	C(13)-C(14)-C(15)	121.2(4)
C(13)-C(16)	1.511(6)	C(10)-C(15)-C(14)	119.9(4)
N(13)-C(17)	1.343(5)	N(10)-C(16)-N(11)	129.3(4)
C(14)-C(15)	1.403(5)	N(10)-C(16)-C(13)	117.2(3)
N(14)-C(18)	1.334(5)	N(11)-C(16)-C(13)	113.6(4)
C(20)-C(21)	1.381(5)	N(12)-C(17)-N(13)	120.8(4)
C(20)-C(25)	1.412(5)	N(12)-C(17)-N(11)	124.7(4)
N(20)-C(26)	1.314(4)	N(13)-C(17)-N(11)	114.5(4)
N(20)-C(27)	1.370(5)	N(14)-C(18)-N(12)	116.4(4)
C(21)-C(22)	1.364(5)	N(14)-C(18)-N(10)	119.1(4)
N(21)-C(26)	1.344(5)	N(12)-C(18)-N(10)	124.4(4)
N(21)-C(28)	1.349(5)	C(21)-C(20)-N(1)	122.3(4)
C(22)-C(23)	1.414(5)	C(21)-C(20)-C(25)	118.1(4)
N(22)-C(28)	1.328(5)	N(1)-C(20)-C(25)	119.6(4)
N(22)-C(27)	1.329(5)	C(26)-N(20)-C(27)	114.9(4)
C(23)-C(24)	1.363(5)	C(22)-C(21)-C(20)	121.7(4)
C(23)-C(26)	1.512(6)	C(26)-N(21)-C(28)	111.8(3)
N(23)-C(28)	1.353(5)	C(21)-C(22)-C(23)	119.6(4)
C(24)-C(25)	1.381(6)	C(28)-N(22)-C(27)	115.9(4)
N(24)-C(27)	1.316(5)	C(24)-C(23)-C(22)	119.4(4)
S(30)-O(30)	1.447(6)	C(24)-C(23)-C(26)	120.9(4)
S(30)-C(31)	1.760(6)	C(22)-C(23)-C(26)	119.6(4)
S(30)-C(30)	1.799(7)	C(23)-C(24)-C(25)	120.7(4)
S(40)-O(40)	1.442(3)	C(24)-C(25)-C(20)	120.3(4)
S(40)-C(40)	1.700(6)	N(20)-C(26)-N(21)	127.6(4)
S(40)-C(41)	1.837(6)	N(20)-C(26)-C(23)	117.2(4)
S(50)-O(50)	1.413(9)	N(21)-C(26)-C(23)	115.1(3)
S(50)-C(51)	1.709(7)	N(24)-C(27)-N(22)	120.1(4)
S(50)-C(50)	1.785(8)	N(24)-C(27)-N(20)	116.9(4)
S(51)-C(52)	1.370(12)	N(22)-C(27)-N(20)	122.9(4)
C(6)-C(1)-C(2)	115.4(4)	N(22)-C(28)-N(21)	126.6(4)
C(6)-C(1)-C(1)#1	123.9(5)	N(22)-C(28)-N(23)	116.1(4)
C(2)-C(1)-C(1)#1	120.6(5)	N(21)-C(28)-N(23)	117.2(4)
C(20)-N(1)-C(4)	119.2(3)		

Symmetry transformations used to generate equivalent atoms:

#1 -x+1,-y,-z+1

Table 6. Torsion angles [°] for C60 H80 N22 O8 S6.

C(6)-C(1)-C(2)-C(3)	-3.9(7)	C(18)-N(12)-C(17)-N(11)	2.2(6)
C(1)#1-C(1)-C(2)-C(3)	178.6(5)	C(16)-N(11)-C(17)-N(12)	2.2(6)
C(1)-C(2)-C(3)-C(4)	3.7(7)	C(16)-N(11)-C(17)-N(13)	-177.1(4)
C(2)-C(3)-C(4)-C(5)	-1.8(7)	C(17)-N(12)-C(18)-N(14)	176.5(4)
C(2)-C(3)-C(4)-N(1)	176.1(4)	C(17)-N(12)-C(18)-N(10)	-6.8(6)
C(20)-N(1)-C(4)-C(3)	-118.3(5)	C(16)-N(10)-C(18)-N(14)	-177.0(4)
C(10)-N(1)-C(4)-C(3)	59.7(5)	C(16)-N(10)-C(18)-N(12)	6.4(6)
C(20)-N(1)-C(4)-C(5)	59.5(5)	C(4)-N(1)-C(20)-C(21)	-148.1(4)
C(10)-N(1)-C(4)-C(5)	-122.6(5)	C(10)-N(1)-C(20)-C(21)	34.0(6)
C(3)-C(4)-C(5)-C(6)	0.3(7)	C(4)-N(1)-C(20)-C(25)	31.4(6)
N(1)-C(4)-C(5)-C(6)	-177.5(4)	C(10)-N(1)-C(20)-C(25)	-146.5(4)
C(2)-C(1)-C(6)-C(5)	2.4(7)	N(1)-C(20)-C(21)-C(22)	-178.4(4)
C(1)#1-C(1)-C(6)-C(5)	179.8(5)	C(25)-C(20)-C(21)-C(22)	2.1(6)
C(4)-C(5)-C(6)-C(1)	-0.7(8)	C(20)-C(21)-C(22)-C(23)	-0.8(6)
C(20)-N(1)-C(10)-C(11)	26.1(6)	C(21)-C(22)-C(23)-C(24)	-1.5(6)
C(4)-N(1)-C(10)-C(11)	-151.8(4)	C(21)-C(22)-C(23)-C(26)	-179.5(4)
C(20)-N(1)-C(10)-C(15)	-158.5(4)	C(22)-C(23)-C(24)-C(25)	2.3(6)
C(4)-N(1)-C(10)-C(15)	23.6(6)	C(26)-C(23)-C(24)-C(25)	-179.7(4)
C(15)-C(10)-C(11)-C(12)	5.3(6)	C(23)-C(24)-C(25)-C(20)	-0.9(6)
N(1)-C(10)-C(11)-C(12)	-179.3(4)	C(21)-C(20)-C(25)-C(24)	-1.3(6)
C(10)-C(11)-C(12)-C(13)	-4.8(7)	N(1)-C(20)-C(25)-C(24)	179.2(4)
C(11)-C(12)-C(13)-C(14)	2.4(6)	C(27)-N(20)-C(26)-N(21)	-2.7(6)
C(11)-C(12)-C(13)-C(16)	-176.6(4)	C(27)-N(20)-C(26)-C(23)	-178.8(3)
C(12)-C(13)-C(14)-C(15)	-0.6(6)	C(28)-N(21)-C(26)-N(20)	1.8(6)
C(16)-C(13)-C(14)-C(15)	178.4(4)	C(28)-N(21)-C(26)-C(23)	177.9(4)
C(11)-C(10)-C(15)-C(14)	-3.5(6)	C(24)-C(23)-C(26)-N(20)	152.9(4)
N(1)-C(10)-C(15)-C(14)	-179.0(4)	C(22)-C(23)-C(26)-N(20)	-29.1(6)
C(13)-C(14)-C(15)-C(10)	1.1(7)	C(24)-C(23)-C(26)-N(21)	-23.6(6)
C(18)-N(10)-C(16)-N(11)	-1.2(6)	C(22)-C(23)-C(26)-N(21)	154.3(4)
C(18)-N(10)-C(16)-C(13)	178.4(3)	C(28)-N(22)-C(27)-N(24)	178.2(4)
C(17)-N(11)-C(16)-N(10)	-2.7(6)	C(28)-N(22)-C(27)-N(20)	-4.7(6)
C(17)-N(11)-C(16)-C(13)	177.6(3)	C(26)-N(20)-C(27)-N(24)	-178.6(4)
C(14)-C(13)-C(16)-N(10)	-23.7(6)	C(26)-N(20)-C(27)-N(22)	4.2(6)
C(12)-C(13)-C(16)-N(10)	155.3(4)	C(27)-N(22)-C(28)-N(21)	3.8(7)
C(14)-C(13)-C(16)-N(11)	156.0(4)	C(27)-N(22)-C(28)-N(23)	179.5(4)
C(12)-C(13)-C(16)-N(11)	-25.0(6)	C(26)-N(21)-C(28)-N(22)	-2.3(7)
C(18)-N(12)-C(17)-N(13)	-178.6(4)	C(26)-N(21)-C(28)-N(23)	-178.0(4)

Symmetry transformations used to generate equivalent atoms:

#1 -x+1,-y,-z+1

Table 7. Bond lengths [Å] and angles [°] related to the hydrogen bonding for C60 H80 N22 O8 S6.

D-H	..A	d(D-H)	d(H..A)	d(D..A)	<DHA
N(13)-H(13A)	N(20)#2	0.88	2.14	3.013(5)	173.8
N(13)-H(13B)	O(60)#2	0.88	2.30	3.075(5)	147
N(14)-H(14B)	O(40)#3	0.88	2.21	3.040(5)	157.4
N(23)-H(23B)	O(50)#4	0.88	2.14	2.865(10)	138.9
N(23)-H(23A)	N(22)#5	0.88	2.09	2.928(5)	159.7
N(24)-H(24A)	O(50)#6	0.88	2.15	2.986(10)	159.1
N(24)-H(24B)	N(12)#2	0.88	2.20	3.007(5)	151.6

Symmetry transformations used to generate equivalent atoms:

#1 -x+1,-y,-z+1 #2 -x+1,-y+1,-z #3 x,y-1,z
#4 -x+1,-y+1,-z+1 #5 -x,-y+2,-z+1 #6 x-1,y+1,z

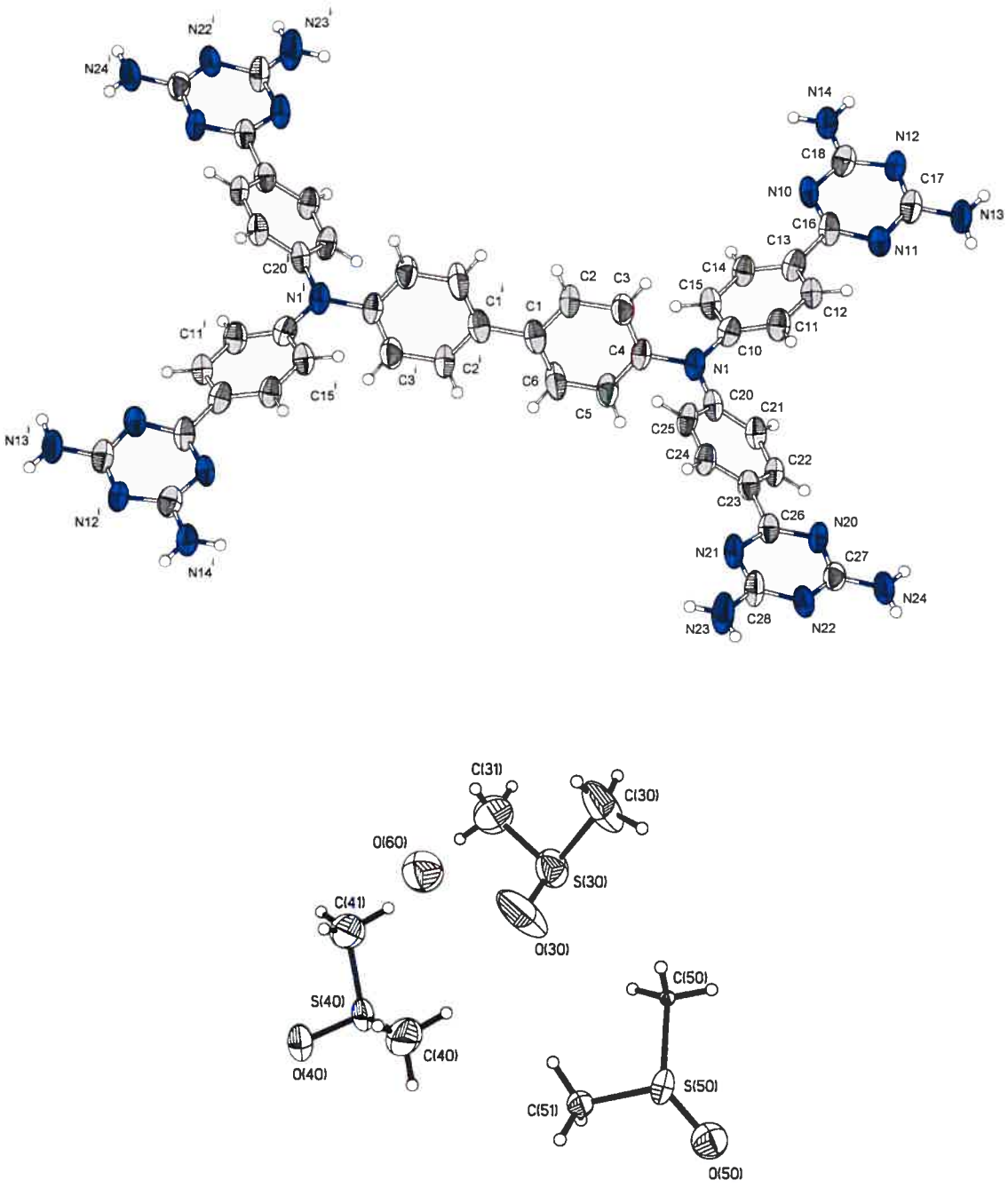

ORTEP view of the C60 H80 N22 O8 S6 compound with the numbering scheme adopted. Ellipsoids drawn at 30% probability level. Hydrogen atoms are represented by phere of arbitrary size.

REFERENCES

International Tables for Crystallography (1992). Vol. C. Tables 4.2.6.8 and 6.1.1.4, Dordrecht: Kluwer Academic Publishers.

SAINT (1999) Release 6.06; Integration Software for Single Crystal Data. Bruker AXS Inc., Madison, WI 53719-1173.

Sheldrick, G.M. (1996). SADABS, Bruker Area Detector Absorption Corrections. Bruker AXS Inc., Madison, WI 53719-1173.

Sheldrick, G.M. (1997). SHELXS97, Program for the Solution of Crystal Structures. Univ. of Gottingen, Germany.

Sheldrick, G.M. (1997). SHELXL97, Program for the Refinement of Crystal Structures. Univ. of Gottingen, Germany.

SHELXTL (1997) Release 5.10; The Complete Software Package for Single Crystal Structure Determination. Bruker AXS Inc., Madison, WI 53719-1173.

SMART (1999) Release 5.059; Bruker Molecular Analysis Research Tool. Bruker AXS Inc., Madison, WI 53719-1173.

Spek, A.L. (2000). PLATON, Molecular Geometry Program, 2000 version. University of Utrecht, Utrecht, Holland.

XPREP (1997) Release 5.10; X-ray data Preparation and Reciprocal space Exploration Program. Bruker AXS Inc., Madison, WI 53719-1173.

Université de Montréal

CRYSTAL AND MOLECULAR STRUCTURE OF

C35 H30.20 N4 O4 S0.20 COMPOUND (JW1032)

Equipe WUEST

Département de chimie, Université de Montréal,

C.P. 6128, Succ. Centre-Ville, Montréal, Québec, H3C 3J7 (Canada)

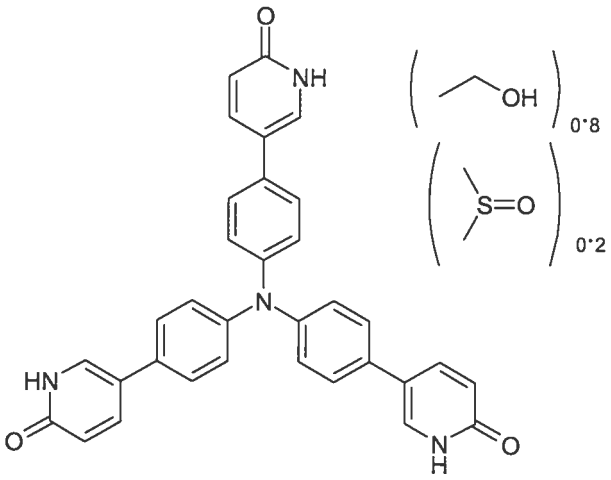

Structure solved and refined in the laboratory of X-ray diffraction Université de Montréal by Dr. Thierry Maris.

Table 1. Crystal data and structure refinement for C35 H30.20 N4 O4 S0.20.

Identification code	JW1032
Empirical formula	C35 H30.20 N4 O4 S0.20
Formula weight	577.24
Temperature	150(2)K
Wavelength	1.54178 Å
Crystal system	Monoclinic
Space group	P21/c
Unit cell dimensions	a = 13.8423(5) Å α = 90° b = 18.6565(6) Å β = 109.410(2)° c = 12.3250(4) Å γ = 90°
Volume	3002.01(17)Å^3
Z	4
Density (calculated)	1.277 g/cm^3
Absorption coefficient	0.809 mm^{-1}
F(000)	1214
Crystal size	0.10 x 0.10 x 0.05 mm
Theta range for data collection	3.39 to 68.84°
Index ranges	$-15 \leq h \leq 16$, $-22 \leq k \leq 22$, $-14 \leq \ell \leq 14$
Reflections collected	41436
Independent reflections	5438 [R_{int} = 0.036]
Absorption correction	Semi-empirical from equivalents
Max. and min. transmission	1.0000 and 0.8200
Refinement method	Full-matrix least-squares on F^2
Data / restraints / parameters	5438 / 5 / 372
Goodness-of-fit on F^2	1.094
Final R indices [I>2sigma(I)]	R_1 = 0.0790, wR_2 = 0.2308

R indices (all data) $R_1 = 0.1151$, $wR_2 = 0.2671$

Largest diff. peak and hole 0.731 and -0.292 e/Å^3

Table 2. Atomic coordinates (x 10^4) and equivalent isotropic displacement parameters (Å^2 x 10^3) for C35 H30.20 N4 O4 S0.20.

U_{eq} is defined as one third of the trace of the orthogonalized Uij tensor.

	Occ.	x	y	z	U_{eq}
C(1)	1	4874(4)	2202(2)	7328(4)	47(1)
N(1)	1	5721(3)	1731(2)	7508(3)	49(1)
O(1)	1	146(4)	5185(2)	6427(4)	89(1)
C(2)	1	4597(4)	2677(3)	6406(4)	50(1)
N(2)	1	1072(4)	4424(3)	5714(5)	78(2)
O(2)	1	6036(3)	-628(2)	532(3)	69(1)
C(3)	1	3785(4)	3138(3)	6243(4)	53(1)
N(3)	1	5449(4)	192(2)	1521(3)	60(1)
O(3)	1	9511(3)	692(2)	15600(3)	68(1)
C(4)	1	3229(4)	3153(3)	7013(4)	53(1)
N(4)	1	9206(3)	487(2)	13695(3)	53(1)
C(5)	1	3511(4)	2667(3)	7927(4)	52(1)
C(6)	1	4304(4)	2193(3)	8071(4)	49(1)
C(7)	1	2406(4)	3688(3)	6881(5)	59(1)
C(8)	1	1826(5)	3926(3)	5839(6)	72(2)
C(9)	1	858(5)	4718(3)	6619(6)	76(2)
C(10)	1	1438(5)	4458(3)	7731(6)	71(2)
C(11)	1	2183(5)	3968(3)	7839(5)	69(2)
C(12)	1	5839(4)	1354(2)	6558(3)	46(1)
C(13)	1	4980(4)	1195(3)	5615(4)	51(1)
C(14)	1	5088(4)	855(3)	4661(4)	52(1)
C(15)	1	6029(4)	663(2)	4610(4)	49(1)
C(16)	1	6891(4)	800(2)	5584(4)	50(1)
C(17)	1	6792(4)	1145(3)	6540(4)	49(1)
C(18)	1	6116(4)	320(3)	3561(4)	52(1)
C(19)	1	6846(4)	-205(3)	3567(4)	56(1)
C(20)	1	6854(5)	-531(3)	2568(4)	59(1)
C(21)	1	6109(5)	-339(3)	1488(4)	57(1)
C(22)	1	5438(4)	506(3)	2504(4)	56(1)
C(23)	1	6359(4)	1597(2)	8654(4)	46(1)
C(24)	1	6619(4)	2156(3)	9450(4)	48(1)
C(25)	1	7184(4)	2027(3)	10587(4)	49(1)
C(26)	1	7528(4)	1338(3)	10973(4)	48(1)
C(27)	1	7294(4)	791(3)	10166(4)	51(1)
C(28)	1	6724(4)	912(2)	9027(4)	50(1)
C(29)	1	8087(4)	1200(3)	12211(4)	51(1)
C(30)	1	7960(4)	1635(3)	13092(4)	57(1)
C(31)	1	8437(4)	1499(3)	14219(4)	59(1)
C(32)	1	9086(4)	885(3)	14576(4)	56(1)
C(33)	1	8729(4)	633(3)	12566(4)	51(1)
C(40)	0.40	1705(4)	1746(3)	5163(4)	137(8)
C(41)	0.40	863(4)	2250(3)	4199(4)	260(20)
O(42)	0.40	436(4)	2469(3)	3108(4)	309(18)
C(43)	0.40	1090(20)	3836(19)	2900(20)	344(2)

C(44)	0.40	790(20)	3132(19)	2580(20)	172(2)
O(45)	0.40	80(20)	2596(19)	2230(20)	509(2)
S(50)	0.20	899(8)	3571(6)	2859(9)	127(1)
O(50)	0.20	938(8)	3197(6)	1858(9)	357(1)
C(50)	0.20	-365(8)	3476(6)	2528(9)	63(1)
C(51)	0.20	1394(8)	2756(6)	3797(9)	27(4)

Table 3. Hydrogen coordinates (x 10^4) and isotropic displacement parameters ($Å^2$ x 10^3) for C35 H30.20 N4 O4 S0.20.

	Occ.	x	y	z	U_{eq}
H(2)	1	4972	2684	5885	60
H(2A)	1	706	4560	5015	94
H(3)	1	3596	3451	5599	64
H(3A)	1	5004	340	867	72
H(4)	1	9618	114	13874	63
H(5)	1	3148	2664	8460	63
H(6)	1	4465	1855	8682	59
H(8)	1	1944	3745	5173	86
H(10)	1	1301	4628	8393	85
H(11)	1	2572	3804	8587	82
H(13)	1	4318	1319	5625	61
H(14)	1	4493	752	4024	62
H(16)	1	7550	654	5587	60
H(17)	1	7383	1239	7187	59
H(19)	1	7345	-339	4277	67
H(20)	1	7356	-884	2595	71
H(22)	1	4945	869	2463	67
H(24)	1	6404	2631	9207	57
H(25)	1	7342	2414	11118	59
H(27)	1	7532	320	10402	61
H(28)	1	6579	526	8495	60
H(30)	1	7521	2040	12882	68
H(31)	1	8342	1814	14781	71
H(33)	1	8848	328	12005	61
H(40A)	0.40	1648	1832	5924	206
H(40B)	0.40	2398	1867	5178	206
H(40C)	0.40	1567	1239	4958	206
H(41A)	0.40	236	2111	4363	314
H(41B)	0.50	1045	2723	4577	314
H(42)	0.40	884	2662	2883	463
H(43A)	0.40	1830	3883	3068	516
H(43B)	0.40	917	3958	3587	516
H(43C)	0.40	730	4162	2271	516
H(44A)	0.40	1102	3083	1962	206
H(44B)	0.50	1284	2886	3243	206
H(45)	0.40	-200	2535	2730	763
H(50A)	0.20	-661	3309	1732	95
H(50B)	0.20	-670	3938	2610	95
H(50C)	0.20	-508	3125	3047	95
H(51A)	0.20	1345	2333	3308	40
H(51B)	0.20	983	2679	4298	40

H(51C)	0.20	2111	2833	4269	40

Table 4. Anisotropic parameters ($Å^2$ x 10^3) for C35 H30.20 N4 O4 S0.20.

The anisotropic displacement factor exponent takes the form:

$$-2\pi^2 [h^2 a^{*2} U_{11} + ... + 2 h k a^* b^* U_{12}]$$

	U11	U22	U33	U23	U13	U12
C(1)	60(3)	44(2)	33(2)	-1(2)	11(2)	7(2)
N(1)	67(3)	50(2)	27(2)	0(2)	10(2)	15(2)
O(1)	94(3)	75(3)	114(4)	32(3)	54(3)	32(3)
C(2)	65(3)	48(3)	38(2)	4(2)	19(2)	6(2)
N(2)	85(4)	73(3)	87(4)	30(3)	43(3)	30(3)
O(2)	105(3)	60(2)	42(2)	-10(2)	24(2)	6(2)
C(3)	65(3)	48(3)	46(3)	9(2)	17(2)	7(2)
N(3)	83(3)	56(3)	37(2)	-5(2)	14(2)	4(2)
O(3)	85(3)	78(3)	35(2)	9(2)	12(2)	21(2)
C(4)	59(3)	47(3)	51(3)	5(2)	17(2)	5(2)
N(4)	61(3)	60(3)	36(2)	8(2)	13(2)	13(2)
C(5)	63(3)	51(3)	43(3)	-1(2)	19(2)	0(2)
C(6)	65(3)	46(3)	34(2)	3(2)	13(2)	1(2)
C(7)	63(3)	53(3)	64(3)	5(2)	25(3)	1(3)
C(8)	76(4)	65(4)	81(4)	18(3)	36(3)	26(3)
C(9)	75(4)	62(4)	103(5)	16(3)	47(4)	12(3)
C(10)	65(4)	67(4)	83(4)	-5(3)	28(3)	5(3)
C(11)	65(4)	66(4)	74(4)	-6(3)	21(3)	5(3)
C(12)	67(3)	39(2)	28(2)	3(2)	11(2)	7(2)
C(13)	69(3)	45(3)	38(2)	2(2)	17(2)	1(2)
C(14)	66(3)	49(3)	35(2)	-1(2)	11(2)	2(2)
C(15)	76(4)	41(2)	30(2)	1(2)	17(2)	1(2)
C(16)	67(3)	46(3)	36(2)	3(2)	16(2)	8(2)
C(17)	67(3)	47(3)	29(2)	1(2)	11(2)	6(2)
C(18)	72(3)	44(3)	39(3)	-4(2)	19(2)	-5(2)
C(19)	72(3)	54(3)	39(3)	-4(2)	17(2)	-2(3)
C(20)	79(4)	51(3)	51(3)	-6(2)	25(3)	-2(3)
C(21)	80(4)	50(3)	41(3)	-6(2)	21(3)	-5(3)
C(22)	79(4)	52(3)	34(2)	-5(2)	16(2)	1(3)
C(23)	61(3)	45(3)	29(2)	5(2)	12(2)	9(2)
C(24)	63(3)	43(2)	35(2)	4(2)	14(2)	5(2)
C(25)	64(3)	46(3)	33(2)	-2(2)	10(2)	2(2)
C(26)	59(3)	50(3)	33(2)	5(2)	14(2)	7(2)
C(27)	70(3)	47(3)	34(2)	6(2)	16(2)	13(2)
C(28)	73(3)	42(2)	35(2)	0(2)	17(2)	7(2)
C(29)	66(3)	50(3)	35(2)	6(2)	16(2)	6(2)
C(30)	72(3)	56(3)	37(3)	5(2)	11(2)	14(3)
C(31)	77(4)	62(3)	36(3)	0(2)	15(2)	13(3)
C(32)	64(3)	66(3)	34(3)	3(2)	10(2)	7(3)
C(33)	60(3)	57(3)	32(2)	4(2)	12(2)	5(2)

Table 5. Bond lengths [Å] and angles [°] for C35 H30.20 N4 O4 S0.20

C(1)-C(2)	1.391(6)	S(50)-C(50)	1.6698
C(1)-C(6)	1.393(7)	S(50)-C(51)	1.8951
C(1)-N(1)	1.423(6)		
N(1)-C(23)	1.417(5)	C(2)-C(1)-C(6)	118.9(4)
N(1)-C(12)	1.422(5)	C(2)-C(1)-N(1)	120.7(4)
O(1)-C(9)	1.277(7)	C(6)-C(1)-N(1)	120.5(4)
C(2)-C(3)	1.375(7)	C(23)-N(1)-C(12)	122.0(4)
N(2)-C(9)	1.360(8)	C(23)-N(1)-C(1)	118.3(3)
N(2)-C(8)	1.367(7)	C(12)-N(1)-C(1)	119.4(4)
O(2)-C(21)	1.268(6)	C(3)-C(2)-C(1)	120.5(4)
C(3)-C(4)	1.407(7)	C(9)-N(2)-C(8)	123.2(5)
N(3)-C(22)	1.350(6)	C(2)-C(3)-C(4)	121.2(4)
N(3)-C(21)	1.358(7)	C(22)-N(3)-C(21)	123.5(4)
O(3)-C(32)	1.255(6)	C(5)-C(4)-C(3)	117.5(4)
C(4)-C(5)	1.396(7)	C(5)-C(4)-C(7)	121.6(5)
C(4)-C(7)	1.483(7)	C(3)-C(4)-C(7)	120.8(4)
N(4)-C(33)	1.355(6)	C(33)-N(4)-C(32)	124.0(4)
N(4)-C(32)	1.369(6)	C(6)-C(5)-C(4)	121.3(5)
C(5)-C(6)	1.375(7)	C(5)-C(6)-C(1)	120.6(4)
C(7)-C(8)	1.345(8)	C(8)-C(7)-C(11)	116.7(5)
C(7)-C(11)	1.415(8)	C(8)-C(7)-C(4)	121.4(5)
C(10)-C(11)	1.352(8)	C(11)-C(7)-C(4)	122.0(5)
C(9)-C(10)	1.424(9)	C(7)-C(8)-N(2)	121.5(6)
C(12)-C(17)	1.383(7)	C(11)-C(10)-C(9)	119.5(6)
C(12)-C(13)	1.390(7)	O(1)-C(9)-N(2)	119.3(6)
C(13)-C(14)	1.387(6)	O(1)-C(9)-C(10)	124.3(6)
C(14)-C(15)	1.372(7)	N(2)-C(9)-C(10)	116.4(5)
C(15)-C(16)	1.406(7)	C(10)-C(11)-C(7)	122.6(6)
C(15)-C(18)	1.483(6)	C(17)-C(12)-C(13)	118.8(4)
C(16)-C(17)	1.390(6)	C(17)-C(12)-N(1)	121.6(4)
C(18)-C(22)	1.373(7)	C(13)-C(12)-N(1)	119.6(4)
C(18)-C(19)	1.406(7)	C(14)-C(13)-C(12)	120.2(5)
C(19)-C(20)	1.376(7)	C(15)-C(14)-C(13)	121.9(5)
C(20)-C(21)	1.433(7)	C(14)-C(15)-C(16)	117.6(4)
C(23)-C(24)	1.395(6)	C(14)-C(15)-C(18)	120.4(5)
C(23)-C(28)	1.394(6)	C(16)-C(15)-C(18)	122.0(5)
C(24)-C(25)	1.380(6)	C(17)-C(16)-C(15)	120.8(5)
C(25)-C(26)	1.397(6)	C(12)-C(17)-C(16)	120.5(5)
C(26)-C(27)	1.387(7)	C(22)-C(18)-C(19)	116.4(4)
C(26)-C(29)	1.486(6)	C(22)-C(18)-C(15)	119.4(5)
C(27)-C(28)	1.381(6)	C(19)-C(18)-C(15)	124.2(4)
C(29)-C(33)	1.357(7)	C(20)-C(19)-C(18)	121.5(5)
C(29)-C(30)	1.412(7)	C(19)-C(20)-C(21)	120.3(5)
C(30)-C(31)	1.350(7)	O(2)-C(21)-N(3)	119.5(5)
C(31)-C(32)	1.432(7)	O(2)-C(21)-C(20)	124.6(5)
C(40)-C(41)	1.6543	N(3)-C(21)-C(20)	116.0(4)
C(41)-O(42)	1.3393	N(3)-C(22)-C(18)	122.3(5)
C(43)-C(44)	1.3941	C(24)-C(23)-C(28)	118.2(4)
C(44)-O(45)	1.3654	C(24)-C(23)-N(1)	119.9(4)
S(50)-O(50)	1.4333	C(28)-C(23)-N(1)	121.9(4)

C(25)-C(24)-C(23)	120.6(4)	C(30)-C(31)-C(32)	120.6(5)
C(24)-C(25)-C(26)	121.4(4)	O(3)-C(32)-N(4)	120.2(5)
C(27)-C(26)-C(25)	117.4(4)	O(3)-C(32)-C(31)	125.0(5)
C(27)-C(26)-C(29)	121.8(4)	N(4)-C(32)-C(31)	114.8(4)
C(25)-C(26)-C(29)	120.8(4)	N(4)-C(33)-C(29)	122.0(4)
C(28)-C(27)-C(26)	121.8(4)	O(42)-C(41)-C(40)	149.9
C(27)-C(28)-C(23)	120.5(4)	O(45)-C(44)-C(43)	153.1
C(33)-C(29)-C(30)	115.9(4)	O(50)-S(50)-C(50)	94.2
C(33)-C(29)-C(26)	121.9(4)	O(50)-S(50)-C(51)	91.4
C(30)-C(29)-C(26)	122.2(4)	C(50)-S(50)-C(51)	101.6
C(31)-C(30)-C(29)	122.6(5)		

Table 6. Torsion angles [°] for C35 H30.20 N4 O4 S0.20.

C(2)-C(1)-N(1)-C(23)	141.9(5)	C(15)-C(16)-C(17)-C(12)	0.8(7)
C(6)-C(1)-N(1)-C(23)	-38.3(6)	C(14)-C(15)-C(18)-C(22)	33.1(7)
C(2)-C(1)-N(1)-C(12)	-44.7(7)	C(16)-C(15)-C(18)-C(22)	-147.3(5)
C(6)-C(1)-N(1)-C(12)	135.1(5)	C(14)-C(15)-C(18)-C(19)	-145.6(5)
C(6)-C(1)-C(2)-C(3)	1.0(7)	C(16)-C(15)-C(18)-C(19)	33.9(7)
N(1)-C(1)-C(2)-C(3)	-179.2(4)	C(22)-C(18)-C(19)-C(20)	-2.1(8)
C(1)-C(2)-C(3)-C(4)	1.5(8)	C(15)-C(18)-C(19)-C(20)	176.6(5)
C(2)-C(3)-C(4)-C(5)	-2.0(8)	C(18)-C(19)-C(20)-C(21)	-0.1(8)
C(2)-C(3)-C(4)-C(7)	175.3(5)	C(22)-N(3)-C(21)-O(2)	176.8(5)
C(3)-C(4)-C(5)-C(6)	0.1(7)	C(22)-N(3)-C(21)-C(20)	-3.4(8)
C(7)-C(4)-C(5)-C(6)	-177.2(5)	C(19)-C(20)-C(21)-O(2)	-177.4(5)
C(4)-C(5)-C(6)-C(1)	2.4(7)	C(19)-C(20)-C(21)-N(3)	2.8(8)
C(2)-C(1)-C(6)-C(5)	-2.9(7)	C(21)-N(3)-C(22)-C(18)	1.2(8)
N(1)-C(1)-C(6)-C(5)	177.3(4)	C(19)-C(18)-C(22)-N(3)	1.7(8)
C(5)-C(4)-C(7)-C(8)	-150.2(6)	C(15)-C(18)-C(22)-N(3)	-177.1(5)
C(3)-C(4)-C(7)-C(8)	32.6(8)	C(12)-N(1)-C(23)-C(24)	146.4(5)
C(5)-C(4)-C(7)-C(11)	29.1(8)	C(1)-N(1)-C(23)-C(24)	-40.4(6)
C(3)-C(4)-C(7)-C(11)	-148.1(5)	C(12)-N(1)-C(23)-C(28)	-35.1(7)
C(11)-C(7)-C(8)-N(2)	1.1(9)	C(1)-N(1)-C(23)-C(28)	138.1(5)
C(4)-C(7)-C(8)-N(2)	-179.5(5)	C(28)-C(23)-C(24)-C(25)	-2.8(7)
C(9)-N(2)-C(8)-C(7)	0.8(1)	N(1)-C(23)-C(24)-C(25)	175.8(4)
C(8)-N(2)-C(9)-O(1)	179.3(6)	C(23)-C(24)-C(25)-C(26)	1.1(8)
C(8)-N(2)-C(9)-C(10)	-2.8(9)	C(24)-C(25)-C(26)-C(27)	1.0(7)
C(11)-C(10)-C(9)-O(1)	-179.4(6)	C(24)-C(25)-C(26)-C(29)	-176.6(5)
C(11)-C(10)-C(9)-N(2)	2.9(9)	C(25)-C(26)-C(27)-C(28)	-1.4(8)
C(9)-C(10)-C(11)-C(7)	-1.1(9)	C(29)-C(26)-C(27)-C(28)	176.2(5)
C(8)-C(7)-C(11)-C(10)	-0.9(9)	C(26)-C(27)-C(28)-C(23)	-0.2(8)
C(4)-C(7)-C(11)-C(10)	179.7(5)	C(24)-C(23)-C(28)-C(27)	2.3(7)
C(23)-N(1)-C(12)-C(17)	-34.8(7)	N(1)-C(23)-C(28)-C(27)	-176.1(5)
C(1)-N(1)-C(12)-C(17)	152.1(4)	C(27)-C(26)-C(29)-C(33)	26.0(8)
C(23)-N(1)-C(12)-C(13)	145.8(5)	C(25)-C(26)-C(29)-C(33)	-156.4(5)
C(1)-N(1)-C(12)-C(13)	-27.3(6)	C(27)-C(26)-C(29)-C(30)	-151.9(5)
C(17)-C(12)-C(13)-C(14)	-2.2(7)	C(25)-C(26)-C(29)-C(30)	25.6(8)
N(1)-C(12)-C(13)-C(14)	177.2(4)	C(33)-C(29)-C(30)-C(31)	-0.4(8)
C(12)-C(13)-C(14)-C(15)	0.2(7)	C(26)-C(29)-C(30)-C(31)	177.7(5)
C(13)-C(14)-C(15)-C(16)	2.3(7)	C(29)-C(30)-C(31)-C(32)	-1.6(9)
C(13)-C(14)-C(15)-C(18)	-178.2(4)	C(33)-N(4)-C(32)-O(3)	176.1(5)
C(14)-C(15)-C(16)-C(17)	-2.8(7)	C(33)-N(4)-C(32)-C(31)	-2.4(8)
C(18)-C(15)-C(16)-C(17)	177.7(4)	C(30)-C(31)-C(32)-O(3)	-175.5(5)
C(13)-C(12)-C(17)-C(16)	1.7(7)	C(30)-C(31)-C(32)-N(4)	2.9(8)
N(1)-C(12)-C(17)-C(16)	-177.7(4)	C(32)-N(4)-C(33)-C(29)	0.5(8)

C(30)-C(29)-C(33)-N(4)	1.0(8)	C(26)-C(29)-C(33)-N(4)	-177.1(5)

Table 7. Bond lengths [Å] and angles [°] related to the hydrogen bonding for C35 H30.20 N4 O4 S0.20.

D-H	..A	d(D-H)	d(H..A)	d(D..A)	<DHA
N(2)-H(2A)	O(1)#1	0.88	1.84	2.718(7)	175.5
N(3)-H(3A)	O(2)#2	0.88	1.92	2.799(6)	176.2
N(4)-H(4)	O(3)#3	0.88	1.9	2.779(5)	174.5

Symmetry transformations used to generate equivalent atoms:
#1 -x,-y+1,-z+1 #2 -x+1,-y,-z #3 -x+2,-y,-z+3

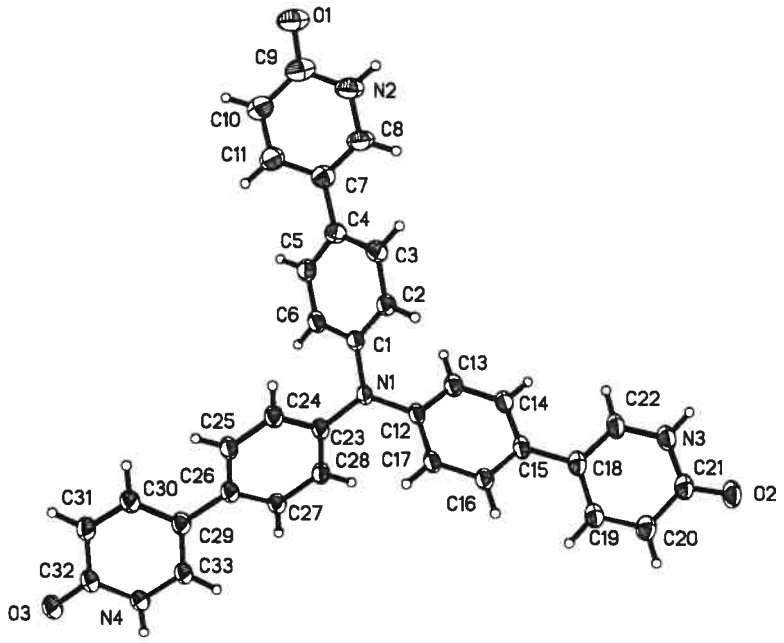

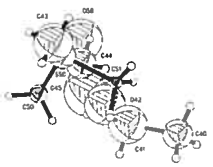

ORTEP view of the C35 H30.20 N4 O4 S0.20 compound with the numbering scheme adopted. Ellipsoids drawn at 30% probability level. Hydrogen atoms are represented by sphere of arbitrary size.

REFERENCES

SAINT (1999) Release 6.06; Integration Software for Single Crystal Data. Bruker AXS Inc., Madison, WI 53719-1173.

Sheldrick, G.M. (1996). SADABS, Bruker Area Detector Absorption Corrections. Bruker AXS Inc., Madison, WI 53719-1173.

Sheldrick, G.M. (1997). SHELXS97, Program for the Solution of Crystal Structures. Univ. of Gottingen, Germany.

Sheldrick, G.M. (1997). SHELXL97, Program for the Refinement of Crystal Structures. Univ. of Gottingen, Germany.

SHELXTL (1997) Release 5.10; The Complete Software Package for Single Crystal Structure Determination. Bruker AXS Inc., Madison, WI 53719-1173.

SMART (1999) Release 5.059; Bruker Molecular Analysis Research Tool. Bruker AXS Inc., Madison, WI 53719-1173.

Spek, A.L. (2000). PLATON, Molecular Geometry Program, 2000 version. University of Utrecht, Utrecht, Holland.

XPREP (1997) Release 5.10; X-ray data Preparation and Reciprocal space Exploration Program. Bruker AXS Inc., Madison, WI 53719-11

Université de Montréal

CRYSTAL AND MOLECULAR STRUCTURE OF

C19 H F15 COMPOUND (JIW843)

Equipe WUEST

Département de chimie, Université de Montréal,

C.P. 6128, Succ. Centre-Ville, Montréal, Québec, H3C 3J7 (Canada)

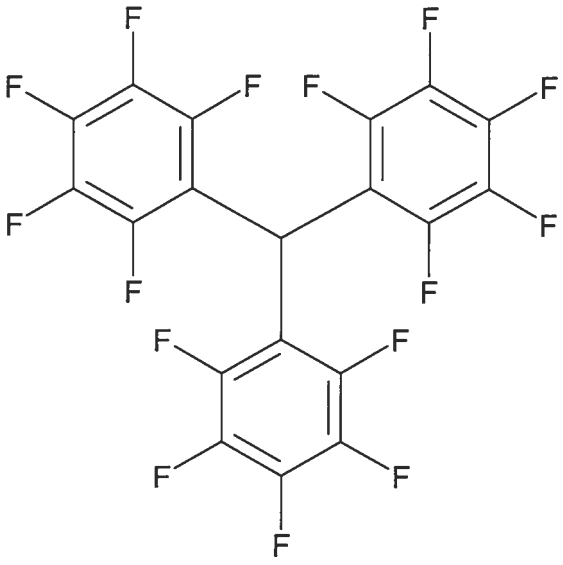

Structure solved and refined in the laboratory of X-ray diffraction, Université de Montréal by Dr. Thierry Maris.

Table 1. Crystal data and structure refinement for C19 H F15.

Identification code	JIW843
Empirical formula	C19 H F15
Formula weight	514.20
Temperature	100(2)K
Wavelength	1.54178 Å
Crystal system	Trigonal
Space group	R-3
Unit cell dimensions	a = 37.8257(5) Å α = 90° b = 37.8257(5) Å β = 90° c = 6.1199(2) Å γ = 120°
Volume	7583.1(3)Å^3
Z	18
Density (calculated)	2.027 Mg/m^3
Absorption coefficient	2.179 mm^{-1}
F(000)	4500
Crystal size	0.17 x 0.10 x 0.08 mm
Theta range for data collection	2.34 to 68.77°
Index ranges	$-45 \leq h \leq 45$, $-45 \leq k \leq 45$, $-7 \leq \ell \leq 7$
Reflections collected	25590
Independent reflections	3094 [R_{int} = 0.061]
Absorption correction	Semi-empirical from equivalents
Max. and min. transmission	1.0000 and 0.6900
Refinement method	Full-matrix least-squares on F^2
Data / restraints / parameters	3094 / 0 / 311
Goodness-of-fit on F^2	1.040
Final R indices [I>2sigma(I)]	R_1 = 0.0385, wR_2 = 0.1053
R indices (all data)	R_1 = 0.0485, wR_2 = 0.1111

Largest diff. peak and hole 0.302 and -0.338 e/Å^3

Table 2. Atomic coordinates (x 10^4) and equivalent isotropic displacement parameters (Å^2 x 10^3) for C19 H F15.

U_{eq} is defined as one third of the trace of the orthogonalized Uij tensor.

	x	y	z	U_{eq}
C(1)	2061(1)	1836(1)	2900(3)	17(1)
C(10)	1609(1)	1603(1)	2274(3)	18(1)
C(11)	1446(1)	1661(1)	366(3)	19(1)
F(11)	1689(1)	1933(1)	-1136(2)	24(1)
C(12)	1032(1)	1447(1)	-75(3)	20(1)
F(12)	892(1)	1509(1)	-1974(2)	27(1)
C(13)	766(1)	1167(1)	1405(3)	21(1)
F(13)	366(1)	955(1)	965(2)	29(1)
C(14)	914(1)	1100(1)	3328(3)	21(1)
F(14)	659(1)	829(1)	4784(2)	29(1)
C(15)	1330(1)	1315(1)	3715(3)	19(1)
F(15)	1463(1)	1234(1)	5589(2)	25(1)
C(20)	2298(1)	1620(1)	2270(3)	18(1)
C(21)	2248(1)	1406(1)	342(3)	19(1)
F(21)	1973(1)	1372(1)	-1147(2)	23(1)
C(22)	2475(1)	1221(1)	-134(3)	21(1)
F(22)	2416(1)	1020(1)	-2030(2)	27(1)
C(23)	2761(1)	1244(1)	1336(3)	23(1)
F(23)	2983(1)	1066(1)	878(2)	29(1)
C(24)	2820(1)	1452(1)	3275(3)	22(1)
F(24)	3099(1)	1479(1)	4706(2)	30(1)
C(25)	2589(1)	1635(1)	3711(3)	20(1)
F(25)	2658(1)	1834(1)	5617(2)	23(1)
C(30)	2279(1)	2288(1)	2283(3)	18(1)
C(31)	2507(1)	2453(1)	397(3)	18(1)
F(31)	2536(1)	2212(1)	-1117(2)	24(1)
C(32)	2712(1)	2868(1)	-20(3)	20(1)
F(32)	2925(1)	3014(1)	-1877(2)	26(1)
C(33)	2689(1)	3130(1)	1453(3)	19(1)
F(33)	2880(1)	3531(1)	1022(2)	26(1)
C(34)	2466(1)	2980(1)	3344(3)	20(1)
F(34)	2445(1)	3234(1)	4786(2)	27(1)
C(35)	2264(1)	2564(1)	3718(3)	18(1)
F(35)	2046(1)	2429(1)	5576(2)	24(1)
H(1)	2061(5)	1831(5)	4410(30)	18(5)

Table 3. Anisotropic parameters ($Å^2$ x 10^3) for C19 H F15.

The anisotropic displacement factor exponent takes the form:

$$-2\pi^2 [h^2 a^{*2} U_{11} + ... + 2 h k a^* b^* U_{12}]$$

	U11	U22	U33	U23	U13	U12
C(1)	16(1)	16(1)	20(1)	0(1)	1(1)	8(1)
C(10)	15(1)	15(1)	26(1)	-1(1)	0(1)	9(1)
C(11)	20(1)	15(1)	23(1)	1(1)	2(1)	9(1)
F(11)	21(1)	23(1)	26(1)	6(1)	1(1)	9(1)
C(12)	23(1)	19(1)	24(1)	-2(1)	-4(1)	14(1)
F(12)	27(1)	30(1)	28(1)	-1(1)	-8(1)	17(1)
C(13)	13(1)	19(1)	32(1)	-7(1)	-6(1)	9(1)
F(13)	14(1)	31(1)	40(1)	-2(1)	-5(1)	9(1)
C(14)	17(1)	16(1)	30(1)	2(1)	4(1)	8(1)
F(14)	18(1)	26(1)	36(1)	8(1)	5(1)	6(1)
C(15)	20(1)	18(1)	23(1)	1(1)	-2(1)	12(1)
F(15)	19(1)	25(1)	25(1)	5(1)	-2(1)	8(1)
C(20)	15(1)	12(1)	24(1)	1(1)	2(1)	5(1)
C(21)	15(1)	16(1)	24(1)	1(1)	-2(1)	6(1)
F(21)	21(1)	24(1)	26(1)	-4(1)	-6(1)	12(1)
C(22)	22(1)	15(1)	24(1)	-2(1)	2(1)	7(1)
F(22)	30(1)	23(1)	28(1)	-6(1)	2(1)	14(1)
C(23)	19(1)	18(1)	35(1)	2(1)	4(1)	11(1)
F(23)	32(1)	30(1)	37(1)	-2(1)	2(1)	24(1)
C(24)	19(1)	20(1)	28(1)	2(1)	-3(1)	10(1)
F(24)	27(1)	37(1)	34(1)	-3(1)	-8(1)	22(1)
C(25)	18(1)	14(1)	24(1)	-1(1)	0(1)	6(1)
F(25)	25(1)	25(1)	22(1)	-5(1)	-3(1)	15(1)
C(30)	11(1)	15(1)	25(1)	1(1)	-1(1)	6(1)
C(31)	17(1)	18(1)	22(1)	-3(1)	-1(1)	10(1)
F(31)	25(1)	19(1)	26(1)	-2(1)	5(1)	10(1)
C(32)	15(1)	20(1)	22(1)	3(1)	2(1)	7(1)
F(32)	26(1)	22(1)	26(1)	5(1)	9(1)	9(1)
C(33)	14(1)	13(1)	29(1)	3(1)	0(1)	5(1)
F(33)	27(1)	13(1)	35(1)	4(1)	5(1)	7(1)
C(34)	17(1)	17(1)	28(1)	-3(1)	-2(1)	10(1)
F(34)	29(1)	18(1)	33(1)	-3(1)	6(1)	12(1)
C(35)	13(1)	21(1)	19(1)	4(1)	2(1)	7(1)
F(35)	26(1)	20(1)	25(1)	2(1)	7(1)	10(1)

Table 4. Bond lengths [Å] and angles [°] for C19 H F15

C(1)-C(10)	1.527(2)	F(12)-C(12)-C(11)	119.71(15)
C(1)-C(30)	1.529(2)	C(13)-C(12)-C(11)	120.06(16)
C(1)-C(20)	1.532(2)	F(13)-C(13)-C(12)	120.11(16)
C(10)-C(11)	1.389(2)	F(13)-C(13)-C(14)	120.20(16)
C(10)-C(15)	1.390(2)	C(12)-C(13)-C(14)	119.68(16)
C(11)-F(11)	1.3420(19)	F(14)-C(14)-C(13)	120.33(15)
C(11)-C(12)	1.382(2)	F(14)-C(14)-C(15)	120.61(16)
C(12)-F(12)	1.3456(19)	C(13)-C(14)-C(15)	119.06(16)
C(12)-C(13)	1.375(2)	F(15)-C(15)-C(14)	117.22(15)
C(13)-F(13)	1.3389(18)	F(15)-C(15)-C(10)	119.66(14)
C(13)-C(14)	1.380(3)	C(14)-C(15)-C(10)	123.12(16)
C(14)-F(14)	1.336(2)	C(21)-C(20)-C(25)	115.83(15)
C(14)-C(15)	1.383(2)	C(21)-C(20)-C(1)	125.40(16)
C(15)-F(15)	1.3466(19)	C(25)-C(20)-C(1)	118.78(16)
C(20)-C(21)	1.390(2)	F(21)-C(21)-C(22)	117.08(15)
C(20)-C(25)	1.390(2)	F(21)-C(21)-C(20)	120.42(15)
C(21)-F(21)	1.3401(19)	C(22)-C(21)-C(20)	122.50(16)
C(21)-C(22)	1.383(2)	F(22)-C(22)-C(23)	120.22(15)
C(22)-F(22)	1.3433(19)	F(22)-C(22)-C(21)	119.99(15)
C(22)-C(23)	1.377(2)	C(23)-C(22)-C(21)	119.79(16)
C(23)-F(23)	1.3427(19)	F(23)-C(23)-C(22)	120.05(16)
C(23)-C(24)	1.378(2)	F(23)-C(23)-C(24)	120.14(16)
C(24)-F(24)	1.3352(19)	C(22)-C(23)-C(24)	119.81(16)
C(24)-C(25)	1.387(2)	F(24)-C(24)-C(23)	120.26(15)
C(25)-F(25)	1.3415(19)	F(24)-C(24)-C(25)	120.53(16)
C(30)-C(35)	1.388(2)	C(23)-C(24)-C(25)	119.20(16)
C(30)-C(31)	1.388(2)	F(25)-C(25)-C(24)	116.99(15)
C(31)-F(31)	1.3388(18)	F(25)-C(25)-C(20)	120.15(15)
C(31)-C(32)	1.384(2)	C(24)-C(25)-C(20)	122.87(16)
C(32)-F(32)	1.3423(19)	C(35)-C(30)-C(31)	116.09(15)
C(32)-C(33)	1.375(2)	C(35)-C(30)-C(1)	118.87(15)
C(33)-F(33)	1.3413(19)	C(31)-C(30)-C(1)	125.01(16)
C(33)-C(34)	1.376(2)	F(31)-C(31)-C(32)	116.97(15)
C(34)-F(34)	1.3361(19)	F(31)-C(31)-C(30)	120.94(15)
C(34)-C(35)	1.383(2)	C(32)-C(31)-C(30)	122.08(16)
C(35)-F(35)	1.3462(19)	F(32)-C(32)-C(33)	120.00(15)
		F(32)-C(32)-C(31)	120.18(15)
C(10)-C(1)-C(30)	113.95(13)	C(33)-C(32)-C(31)	119.81(16)
C(10)-C(1)-C(20)	114.45(13)	F(33)-C(33)-C(32)	119.64(15)
C(30)-C(1)-C(20)	113.56(13)	F(33)-C(33)-C(34)	120.32(15)
C(11)-C(10)-C(15)	115.77(15)	C(32)-C(33)-C(34)	120.03(15)
C(11)-C(10)-C(1)	125.24(15)	F(34)-C(34)-C(33)	120.25(15)
C(15)-C(10)-C(1)	118.97(15)	F(34)-C(34)-C(35)	120.72(16)
F(11)-C(11)-C(12)	117.15(15)	C(33)-C(34)-C(35)	119.03(16)
F(11)-C(11)-C(10)	120.56(14)	F(35)-C(35)-C(34)	117.27(15)
C(12)-C(11)-C(10)	122.29(16)	F(35)-C(35)-C(30)	119.79(15)
F(12)-C(12)-C(13)	120.22(15)	C(34)-C(35)-C(30)	122.95(16)

Table 5. Torsion angles [°] for C19 H F15.

C(30)-C(1)-C(10)-C(11)	38.5(2)	F(22)-C(22)-C(23)-C(24)	179.82(15)
C(20)-C(1)-C(10)-C(11)	-94.5(2)	C(21)-C(22)-C(23)-C(24)	0.2(3)
C(30)-C(1)-C(10)-C(15)	-139.98(17)	F(23)-C(23)-C(24)-F(24)	0.2(3)
C(20)-C(1)-C(10)-C(15)	87.0(2)	C(22)-C(23)-C(24)-F(24)	-179.63(15)
C(15)-C(10)-C(11)-F(11)	-179.98(14)	F(23)-C(23)-C(24)-C(25)	179.68(15)
C(1)-C(10)-C(11)-F(11)	1.5(3)	C(22)-C(23)-C(24)-C(25)	-0.1(3)
C(15)-C(10)-C(11)-C(12)	0.2(2)	F(24)-C(24)-C(25)-F(25)	-0.4(2)
C(1)-C(10)-C(11)-C(12)	-178.36(16)	C(23)-C(24)-C(25)-F(25)	-179.88(15)
F(11)-C(11)-C(12)-F(12)	1.6(2)	F(24)-C(24)-C(25)-C(20)	179.36(15)
C(10)-C(11)-C(12)-F(12)	-178.55(15)	C(23)-C(24)-C(25)-C(20)	-0.1(3)
F(11)-C(11)-C(12)-C(13)	-179.39(15)	C(21)-C(20)-C(25)-F(25)	-179.89(14)
C(10)-C(11)-C(12)-C(13)	0.4(3)	C(1)-C(20)-C(25)-F(25)	0.2(2)
F(12)-C(12)-C(13)-F(13)	-0.1(2)	C(21)-C(20)-C(25)-C(24)	0.3(3)
C(11)-C(12)-C(13)-F(13)	-179.04(15)	C(1)-C(20)-C(25)-C(24)	-179.57(15)
F(12)-C(12)-C(13)-C(14)	178.78(15)	C(10)-C(1)-C(30)-C(35)	85.7(2)
C(11)-C(12)-C(13)-C(14)	-0.2(3)	C(20)-C(1)-C(30)-C(35)	-140.83(16)
F(13)-C(13)-C(14)-F(14)	-1.2(2)	C(10)-C(1)-C(30)-C(31)	-96.29(19)
C(12)-C(13)-C(14)-F(14)	179.92(15)	C(20)-C(1)-C(30)-C(31)	37.2(2)
F(13)-C(13)-C(14)-C(15)	178.17(15)	C(35)-C(30)-C(31)-F(31)	-178.63(14)
C(12)-C(13)-C(14)-C(15)	-0.7(3)	C(1)-C(30)-C(31)-F(31)	3.3(3)
F(14)-C(14)-C(15)-F(15)	0.8(2)	C(35)-C(30)-C(31)-C(32)	0.7(2)
C(13)-C(14)-C(15)-F(15)	-178.60(15)	C(1)-C(30)-C(31)-C(32)	-177.30(16)
F(14)-C(14)-C(15)-C(10)	-179.22(15)	F(31)-C(31)-C(32)-F(32)	0.1(2)
C(13)-C(14)-C(15)-C(10)	1.4(3)	C(30)-C(31)-C(32)-F(32)	-179.25(15)
C(11)-C(10)-C(15)-F(15)	178.85(14)	F(31)-C(31)-C(32)-C(33)	178.88(15)
C(1)-C(10)-C(15)-F(15)	-2.5(2)	C(30)-C(31)-C(32)-C(33)	-0.5(3)
C(11)-C(10)-C(15)-C(14)	-1.1(3)	F(32)-C(32)-C(33)-F(33)	0.1(2)
C(1)-C(10)-C(15)-C(14)	177.54(15)	C(31)-C(32)-C(33)-F(33)	-178.61(15)
C(10)-C(1)-C(20)-C(21)	39.3(2)	F(32)-C(32)-C(33)-C(34)	179.24(15)
C(30)-C(1)-C(20)-C(21)	-93.87(19)	C(31)-C(32)-C(33)-C(34)	0.5(3)
C(10)-C(1)-C(20)-C(25)	-140.76(16)	F(33)-C(33)-C(34)-F(34)	-1.2(2)
C(30)-C(1)-C(20)-C(25)	86.0(2)	C(32)-C(33)-C(34)-F(34)	179.68(15)
C(25)-C(20)-C(21)-F(21)	179.47(15)	F(33)-C(33)-C(34)-C(35)	178.35(15)
C(1)-C(20)-C(21)-F(21)	-0.6(3)	C(32)-C(33)-C(34)-C(35)	-0.8(3)
C(25)-C(20)-C(21)-C(22)	-0.3(2)	F(34)-C(34)-C(35)-F(35)	0.2(2)
C(1)-C(20)-C(21)-C(22)	179.58(16)	C(33)-C(34)-C(35)-F(35)	-179.31(14)
F(21)-C(21)-C(22)-F(22)	0.6(2)	F(34)-C(34)-C(35)-C(30)	-179.39(15)
C(20)-C(21)-C(22)-F(22)	-179.57(14)	C(33)-C(34)-C(35)-C(30)	1.1(3)
F(21)-C(21)-C(22)-C(23)	-179.73(15)	C(31)-C(30)-C(35)-F(35)	179.35(14)
C(20)-C(21)-C(22)-C(23)	0.1(3)	C(1)-C(30)-C(35)-F(35)	-2.5(2)
F(22)-C(22)-C(23)-F(23)	0.0(3)	C(31)-C(30)-C(35)-C(34)	-1.0(2)
C(21)-C(22)-C(23)-F(23)	-179.67(15)	C(1)-C(30)-C(35)-C(34)	177.15(15)

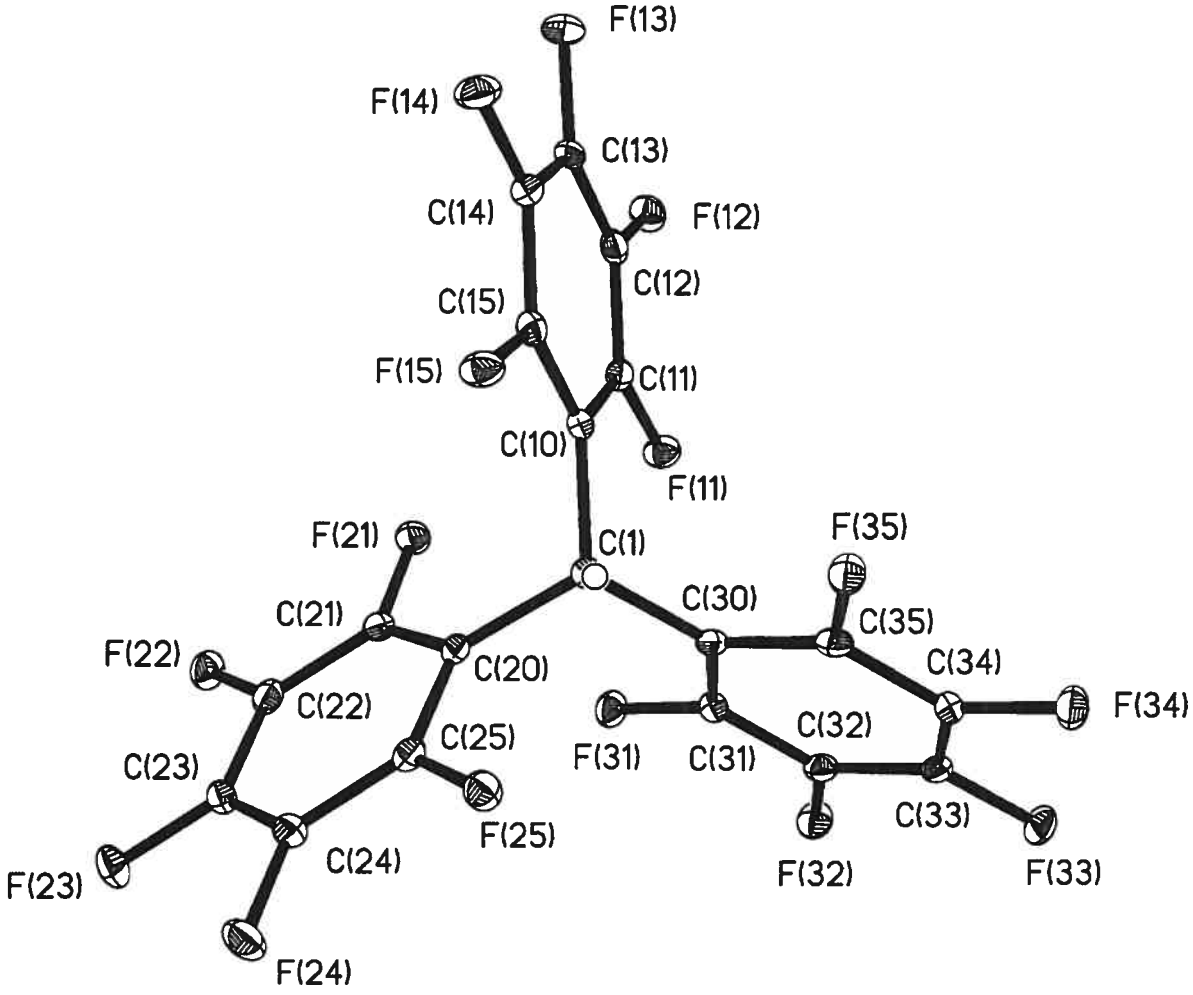

ORTEP view of the C19 H F15 compound with the numbering scheme adopted. Ellipsoids drawn at 30% probability level. Hydrogens represented by sphere of arbitrary size.

REFERENCES

SAINT (1999) Release 6.06; Integration Software for Single Crystal Data. Bruker AXS Inc., Madison, WI 53719-1173.

Sheldrick, G.M. (1996). SADABS, Bruker Area Detector Absorption Corrections. Bruker AXS Inc., Madison, WI 53719-1173.

Sheldrick, G.M. (1997). SHELXS97, Program for the Solution of Crystal Structures. Univ. of Gottingen, Germany.

Sheldrick, G.M. (1997). SHELXL97, Program for the Refinement of Crystal Structures. Univ. of Gottingen, Germany.

SHELXTL (1997) Release 5.10; The Complete Software Package for Single Crystal Structure Determination. Bruker AXS Inc., Madison, WI 53719-1173.

SMART (1999) Release 5.059; Bruker Molecular Analysis Research Tool. Bruker AXS Inc., Madison, WI 53719-1173.

Spek, A.L. (2000). PLATON, Molecular Geometry Program, 2000 version. University of Utrecht, Utrecht, Holland.

XPREP (1997) Release 5.10; X-ray data Preparation and Reciprocal space Exploration Program. Bruker AXS Inc., Madison, WI 53719-1173.

Université de Montréal

CRYSTAL AND MOLECULAR STRUCTURE OF

C22.50 H14 F12 N6 COMPOUND (JIW881)

Equipe WUEST

Département de chimie, Université de Montréal,

C.P. 6128, Succ. Centre-Ville, Montréal, Québec, H3C 3J7 (Canada)

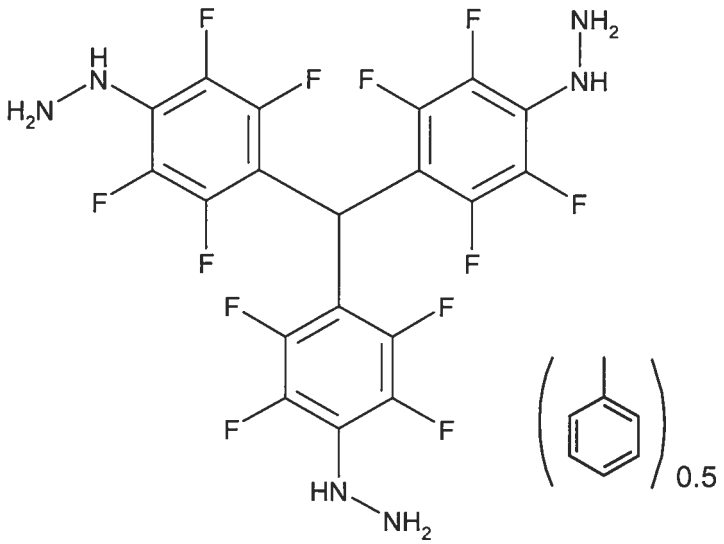

Structure solved and refined in the laboratory of X-ray diffraction Université de Montréal by Dr. Thierry Maris.

Table 1. Crystal data and structure refinement for C22.50 H14 F12 N6.

Identification code	JIW881
Empirical formula	C22.50 H14 F12 N6
Formula weight	596.40
Temperature	100(2)K
Wavelength	1.54178 Å
Crystal system	Monoclinic
Space group	P2/c
Unit cell dimensions	a = 13.9976(4) Å α = 90° b = 6.1918(2) Å β = 103.596(2)° c = 25.6809(7) Å γ = 90°
Volume	2163.40(11)Å^3
Z	4
Density (calculated)	1.831 Mg/m^3
Absorption coefficient	1.673 mm^{-1}
F(000)	1196
Crystal size	0.17 x 0.07 x 0.07 mm
Theta range for data collection	3.25 to 72.05°
Index ranges	$-17 \leq h \leq 16$, $-7 \leq k \leq 7$, $-31 \leq \ell \leq 31$
Reflections collected	12041
Independent reflections	4002 [R_{int} = 0.034]
Absorption correction	Semi-empirical from equivalents
Max. and min. transmission	1.0000 and 0.7600
Refinement method	Full-matrix least-squares on F^2
Data / restraints / parameters	4002 / 9 / 376
Goodness-of-fit on F^2	1.054
Final R indices [I>2sigma(I)]	R_1 = 0.0553, wR_2 = 0.1297
R indices (all data)	R_1 = 0.0578, wR_2 = 0.1302

Largest diff. peak and hole	0.431 and -0.404 e/Å^3

Table 2. Atomic coordinates (x 10^4) and equivalent isotropic displacement parameters ($Å^2$ x 10^3) for C22.50 H14 F12 N6.

U_{eq} is defined as one third of the trace of the orthogonalized Uij tensor.

	Occ.	x	y	z	U_{eq}
C(1)	1	2146(2)	6618(4)	6718(1)	17(1)
C(10)	1	1067(2)	5916(4)	6661(1)	20(1)
C(11)	1	752(2)	4038(4)	6846(1)	25(1)
C(12)	1	-237(2)	3454(4)	6739(1)	25(1)
C(13)	1	-970(2)	4735(4)	6437(1)	22(1)
C(14)	1	-640(2)	6688(4)	6265(1)	26(1)
C(15)	1	336(2)	7258(4)	6372(1)	24(1)
C(20)	1	2508(2)	6008(4)	6218(1)	21(1)
C(21)	1	2311(2)	4127(4)	5927(1)	20(1)
C(22)	1	2615(2)	3798(4)	5461(1)	20(1)
C(23)	1	3175(2)	5278(4)	5262(1)	20(1)
C(24)	1	3379(2)	7191(4)	5551(1)	19(1)
C(25)	1	3083(2)	7514(4)	6019(1)	21(1)
C(30)	1	2823(2)	6007(4)	7245(1)	20(1)
C(31)	1	2927(2)	7394(4)	7677(1)	26(1)
C(32)	1	3516(2)	6980(4)	8176(1)	23(1)
C(33)	1	4051(2)	5096(4)	8287(1)	23(1)
C(34)	1	3978(2)	3708(4)	7855(1)	22(1)
C(35)	1	3377(2)	4133(4)	7355(1)	21(1)
F(11)	1	1398(1)	2609(2)	7124(1)	33(1)
F(12)	1	-458(1)	1540(3)	6938(1)	36(1)
F(14)	1	-1326(1)	8045(2)	5966(1)	37(1)
F(15)	1	572(1)	9150(2)	6175(1)	38(1)
F(21)	1	1769(1)	2581(2)	6081(1)	29(1)
F(22)	1	2366(1)	1905(2)	5194(1)	29(1)
F(24)	1	3934(1)	8713(2)	5383(1)	30(1)
F(25)	1	3350(1)	9386(2)	6282(1)	26(1)
F(31)	1	2399(1)	9260(2)	7616(1)	33(1)
F(32)	1	3540(1)	8405(2)	8577(1)	33(1)
F(34)	1	4485(1)	1819(2)	7924(1)	33(1)
F(35)	1	3345(1)	2640(2)	6972(1)	32(1)
N(13)	1	-1975(1)	4332(4)	6314(1)	26(1)
N(14)	1	-2348(2)	2191(4)	6315(1)	33(1)
N(23)	1	3461(1)	4967(3)	4777(1)	21(1)
N(24)	1	4068(2)	3094(4)	4755(1)	24(1)
N(33)	1	4654(1)	4767(3)	8803(1)	20(1)
N(34)	1	4686(2)	2648(3)	9037(1)	23(1)
C(51)	0.50	88(12)	323(15)	5025(7)	250
C(52)	0.50	-637(12)	1240(20)	5242(7)	250
C(53)	0.50	-738(13)	3470(30)	5252(7)	250
C(54)	0.50	-112(16)	4787(15)	5045(8)	250
C(55)	0.50	613(15)	3870(20)	4828(8)	250
C(56)	0.50	714(11)	1640(30)	4817(7)	250
C(57)	0.50	198(18)	-2146(18)	5014(11)	250

Table 3. Hydrogen coordinates (x 10^4) and isotropic displacement parameters ($Å^2$ x 10^3) for C22.50 H14 F12 N6.

	Occ.	x	y	z	U_{eq}
H(1)	1	2131	8200	6719	20
H(13)	1	-2255(19)	4960(40)	6049(11)	28(6)
H(14A)	1	-2210(20)	1650(50)	6697(10)	47(6)
H(14B)	1	-1890(20)	1450(40)	6125(12)	47(6)
H(23)	1	3780(20)	5720(50)	4720(12)	28(6)
H(24A)	1	3688(17)	1840(30)	4645(10)	23(5)
H(24B)	1	4451(17)	2800(40)	5101(8)	23(5)
H(33)	1	4506(14)	5630(30)	9088(9)	6(5)
H(34A)	1	5138(15)	1890(30)	8940(10)	16(4)
H(34B)	1	4129(14)	1950(40)	8963(10)	16(4)
H(52)	0.50	-1056	359	5381	300
H(53)	0.50	-1223	4084	5398	300
H(54)	0.50	-180	6280	5052	300
H(55)	0.50	1032	4751	4689	300
H(56)	0.50	1199	1025	4672	300
H(57A)	0.50	-417	-2780	4834	375
H(57B)	0.50	386	-2684	5374	375
H(57C)	0.50	694	-2515	4826	375

Table 4. Anisotropic parameters ($Å^2$ x 10^3) for C22.50 H14 F12 N6.

The anisotropic displacement factor exponent takes the form:

$$-2\pi^2 [h^2 a^{*2} U_{11} + ... + 2 h k a^* b^* U_{12}]$$

	U11	U22	U33	U23	U13	U12
C(1)	15(1)	19(1)	17(1)	1(1)	4(1)	1(1)
C(10)	22(1)	25(1)	16(1)	-3(1)	10(1)	1(1)
C(11)	27(1)	33(2)	17(1)	1(1)	8(1)	4(1)
C(12)	23(1)	35(2)	20(1)	6(1)	8(1)	1(1)
C(13)	21(1)	25(1)	21(1)	-4(1)	8(1)	1(1)
C(14)	22(1)	32(2)	25(1)	-2(1)	6(1)	2(1)
C(15)	23(1)	27(1)	24(1)	3(1)	10(1)	-1(1)
C(20)	14(1)	37(2)	13(1)	-1(1)	3(1)	2(1)
C(21)	18(1)	22(1)	21(1)	2(1)	4(1)	-2(1)
C(22)	25(1)	21(1)	15(1)	-4(1)	9(1)	-4(1)
C(23)	15(1)	33(1)	13(1)	4(1)	6(1)	4(1)
C(24)	13(1)	27(1)	16(1)	3(1)	5(1)	-2(1)
C(25)	20(1)	22(1)	24(1)	-7(1)	12(1)	-2(1)
C(30)	13(1)	40(2)	10(1)	4(1)	7(1)	2(1)
C(31)	19(1)	43(2)	19(1)	4(1)	11(1)	5(1)
C(32)	23(1)	36(2)	13(1)	-3(1)	7(1)	1(1)
C(33)	18(1)	40(2)	11(1)	1(1)	8(1)	-1(1)
C(34)	17(1)	33(2)	18(1)	9(1)	8(1)	12(1)
C(35)	15(1)	38(2)	10(1)	-3(1)	2(1)	5(1)
F(11)	22(1)	40(1)	35(1)	16(1)	3(1)	2(1)
F(12)	26(1)	46(1)	36(1)	20(1)	6(1)	-4(1)
F(14)	21(1)	36(1)	49(1)	13(1)	1(1)	4(1)
F(15)	24(1)	32(1)	56(1)	14(1)	7(1)	-5(1)
F(21)	34(1)	33(1)	24(1)	-1(1)	17(1)	-9(1)
F(22)	34(1)	34(1)	21(1)	-6(1)	12(1)	-12(1)
F(24)	33(1)	30(1)	35(1)	-1(1)	23(1)	-8(1)
F(25)	28(1)	22(1)	31(1)	-9(1)	12(1)	-5(1)
F(31)	44(1)	36(1)	18(1)	1(1)	6(1)	16(1)
F(32)	55(1)	27(1)	16(1)	-3(1)	6(1)	8(1)
F(34)	33(1)	50(1)	15(1)	0(1)	2(1)	25(1)
F(35)	41(1)	36(1)	17(1)	-7(1)	3(1)	12(1)
N(13)	18(1)	35(1)	24(1)	3(1)	4(1)	-3(1)
N(14)	22(1)	36(1)	42(1)	6(1)	11(1)	-4(1)
N(23)	24(1)	24(1)	18(1)	3(1)	13(1)	-2(1)
N(24)	25(1)	33(1)	17(1)	-4(1)	8(1)	2(1)
N(33)	20(1)	28(1)	12(1)	2(1)	4(1)	0(1)
N(34)	28(1)	24(1)	19(1)	0(1)	10(1)	5(1)

Table 5. Bond lengths [Å] and angles [°] for C22.50 H14 F12 N6

C(1)-C(30)	1.506(3)	F(11)-C(11)-C(12)	116.5(2)
C(1)-C(20)	1.534(3)	C(10)-C(11)-C(12)	122.6(2)
C(1)-C(10)	1.546(3)	F(12)-C(12)-C(13)	120.6(2)
C(10)-C(11)	1.368(3)	F(12)-C(12)-C(11)	117.2(2)
C(10)-C(15)	1.389(3)	C(13)-C(12)-C(11)	122.3(2)
C(11)-F(11)	1.344(3)	C(12)-C(13)-N(13)	127.1(2)
C(11)-C(12)	1.393(3)	C(12)-C(13)-C(14)	114.5(2)
C(12)-F(12)	1.355(3)	N(13)-C(13)-C(14)	118.3(2)
C(12)-C(13)	1.382(3)	F(14)-C(14)-C(15)	119.2(2)
C(13)-N(13)	1.389(3)	F(14)-C(14)-C(13)	117.8(2)
C(13)-C(14)	1.403(3)	C(15)-C(14)-C(13)	123.0(2)
C(14)-F(14)	1.367(3)	F(15)-C(15)-C(14)	117.9(2)
C(14)-C(15)	1.375(3)	F(15)-C(15)-C(10)	120.4(2)
C(15)-F(15)	1.347(3)	C(14)-C(15)-C(10)	121.7(2)
C(20)-C(21)	1.377(3)	C(21)-C(20)-C(25)	115.0(2)
C(20)-C(25)	1.404(3)	C(21)-C(20)-C(1)	126.9(2)
C(21)-F(21)	1.338(2)	C(25)-C(20)-C(1)	118.1(2)
C(21)-C(22)	1.375(3)	F(21)-C(21)-C(22)	117.6(2)
C(22)-F(22)	1.361(3)	F(21)-C(21)-C(20)	120.0(2)
C(22)-C(23)	1.381(3)	C(22)-C(21)-C(20)	122.3(2)
C(23)-C(24)	1.392(3)	F(22)-C(22)-C(21)	118.1(2)
C(23)-N(23)	1.406(3)	F(22)-C(22)-C(23)	119.02(19)
C(24)-F(24)	1.355(2)	C(21)-C(22)-C(23)	122.9(2)
C(24)-C(25)	1.377(3)	C(22)-C(23)-C(24)	115.5(2)
C(25)-F(25)	1.349(3)	C(22)-C(23)-N(23)	122.8(2)
C(30)-C(31)	1.384(3)	C(24)-C(23)-N(23)	121.5(2)
C(30)-C(35)	1.387(3)	F(24)-C(24)-C(25)	119.4(2)
C(31)-F(31)	1.360(3)	F(24)-C(24)-C(23)	118.88(19)
C(31)-C(32)	1.374(3)	C(25)-C(24)-C(23)	121.6(2)
C(32)-F(32)	1.352(3)	F(25)-C(25)-C(24)	117.2(2)
C(32)-C(33)	1.379(3)	F(25)-C(25)-C(20)	120.25(19)
C(33)-C(34)	1.387(3)	C(24)-C(25)-C(20)	122.5(2)
C(33)-N(33)	1.409(3)	C(31)-C(30)-C(35)	114.1(2)
C(34)-F(34)	1.358(3)	C(31)-C(30)-C(1)	119.3(2)
C(34)-C(35)	1.385(3)	C(35)-C(30)-C(1)	126.6(2)
C(35)-F(35)	1.343(3)	F(31)-C(31)-C(32)	117.2(2)
N(13)-N(14)	1.425(3)	F(31)-C(31)-C(30)	118.9(2)
N(23)-N(24)	1.446(3)	C(32)-C(31)-C(30)	123.9(2)
N(33)-N(34)	1.439(3)	F(32)-C(32)-C(31)	119.4(2)
C(51)-C(52)	1.39	F(32)-C(32)-C(33)	118.6(2)
C(51)-C(56)	1.39	C(31)-C(32)-C(33)	121.9(2)
C(51)-C(57)	1.537(6)	C(32)-C(33)-C(34)	115.1(2)
C(52)-C(53)	1.39	C(32)-C(33)-N(33)	119.5(2)
C(53)-C(54)	1.39	C(34)-C(33)-N(33)	125.3(2)
C(54)-C(55)	1.39	F(34)-C(34)-C(35)	118.0(2)
C(55)-C(56)	1.39	F(34)-C(34)-C(33)	119.4(2)
		C(35)-C(34)-C(33)	122.5(2)
C(30)-C(1)-C(20)	115.37(17)	F(35)-C(35)-C(34)	117.2(2)
C(30)-C(1)-C(10)	114.19(18)	F(35)-C(35)-C(30)	120.40(19)
C(20)-C(1)-C(10)	110.97(18)	C(34)-C(35)-C(30)	122.4(2)
C(11)-C(10)-C(15)	115.9(2)	C(13)-N(13)-N(14)	121.2(2)
C(11)-C(10)-C(1)	126.4(2)	C(23)-N(23)-N(24)	115.89(19)
C(15)-C(10)-C(1)	117.6(2)	C(33)-N(33)-N(34)	118.47(19)
F(11)-C(11)-C(10)	120.8(2)	C(52)-C(51)-C(57)	119.9(8)

C(56)-C(51)-C(57)	120.1(8)

Table 6. Torsion angles [°] for C22.50 H14 F12 N6.

C(30)-C(1)-C(10)-C(11)	-37.5(3)	N(23)-C(23)-C(24)-C(25)	178.7(2)
C(20)-C(1)-C(10)-C(11)	95.0(3)	F(24)-C(24)-C(25)-F(25)	1.4(3)
C(30)-C(1)-C(10)-C(15)	145.8(2)	C(23)-C(24)-C(25)-F(25)	177.3(2)
C(20)-C(1)-C(10)-C(15)	-81.7(3)	F(24)-C(24)-C(25)-C(20)	-180.0(2)
C(15)-C(10)-C(11)-F(11)	179.1(2)	C(23)-C(24)-C(25)-C(20)	-4.1(4)
C(1)-C(10)-C(11)-F(11)	2.3(4)	C(21)-C(20)-C(25)-F(25)	-177.7(2)
C(15)-C(10)-C(11)-C(12)	2.1(3)	C(1)-C(20)-C(25)-F(25)	3.7(3)
C(1)-C(10)-C(11)-C(12)	-174.7(2)	C(21)-C(20)-C(25)-C(24)	3.7(3)
F(11)-C(11)-C(12)-F(12)	2.1(3)	C(1)-C(20)-C(25)-C(24)	-174.9(2)
C(10)-C(11)-C(12)-F(12)	179.2(2)	C(20)-C(1)-C(30)-C(31)	142.1(2)
F(11)-C(11)-C(12)-C(13)	-177.1(2)	C(10)-C(1)-C(30)-C(31)	-87.6(3)
C(10)-C(11)-C(12)-C(13)	0.1(4)	C(20)-C(1)-C(30)-C(35)	-38.2(3)
F(12)-C(12)-C(13)-N(13)	2.1(4)	C(10)-C(1)-C(30)-C(35)	92.1(3)
C(11)-C(12)-C(13)-N(13)	-178.8(2)	C(35)-C(30)-C(31)-F(31)	-178.55(19)
F(12)-C(12)-C(13)-C(14)	178.8(2)	C(1)-C(30)-C(31)-F(31)	1.2(3)
C(11)-C(12)-C(13)-C(14)	-2.0(3)	C(35)-C(30)-C(31)-C(32)	-0.4(3)
C(12)-C(13)-C(14)-F(14)	-179.6(2)	C(1)-C(30)-C(31)-C(32)	179.3(2)
N(13)-C(13)-C(14)-F(14)	-2.6(3)	F(31)-C(31)-C(32)-F(32)	0.5(3)
C(12)-C(13)-C(14)-C(15)	1.9(3)	C(30)-C(31)-C(32)-F(32)	-177.6(2)
N(13)-C(13)-C(14)-C(15)	179.0(2)	F(31)-C(31)-C(32)-C(33)	177.3(2)
F(14)-C(14)-C(15)-F(15)	-0.1(3)	C(30)-C(31)-C(32)-C(33)	-0.8(4)
C(13)-C(14)-C(15)-F(15)	178.3(2)	F(32)-C(32)-C(33)-C(34)	179.2(2)
F(14)-C(14)-C(15)-C(10)	-178.2(2)	C(31)-C(32)-C(33)-C(34)	2.4(3)
C(13)-C(14)-C(15)-C(10)	0.2(4)	F(32)-C(32)-C(33)-N(33)	-4.0(3)
C(11)-C(10)-C(15)-F(15)	179.7(2)	C(31)-C(32)-C(33)-N(33)	179.2(2)
C(1)-C(10)-C(15)-F(15)	-3.2(3)	C(32)-C(33)-C(34)-F(34)	179.48(19)
C(11)-C(10)-C(15)-C(14)	-2.2(3)	N(33)-C(33)-C(34)-F(34)	2.9(4)
C(1)-C(10)-C(15)-C(14)	174.9(2)	C(32)-C(33)-C(34)-C(35)	-2.9(3)
C(30)-C(1)-C(20)-C(21)	91.7(3)	N(33)-C(33)-C(34)-C(35)	-179.5(2)
C(10)-C(1)-C(20)-C(21)	-40.2(3)	F(34)-C(34)-C(35)-F(35)	-0.5(3)
C(30)-C(1)-C(20)-C(25)	-89.9(3)	C(33)-C(34)-C(35)-F(35)	-178.1(2)
C(10)-C(1)-C(20)-C(25)	138.2(2)	F(34)-C(34)-C(35)-C(30)	179.5(2)
C(25)-C(20)-C(21)-F(21)	-179.9(2)	C(33)-C(34)-C(35)-C(30)	1.8(4)
C(1)-C(20)-C(21)-F(21)	-1.5(3)	C(31)-C(30)-C(35)-F(35)	179.9(2)
C(25)-C(20)-C(21)-C(22)	-3.1(3)	C(1)-C(30)-C(35)-F(35)	0.2(3)
C(1)-C(20)-C(21)-C(22)	175.3(2)	C(31)-C(30)-C(35)-C(34)	-0.1(3)
F(21)-C(21)-C(22)-F(22)	-1.6(3)	C(1)-C(30)-C(35)-C(34)	-179.8(2)
C(20)-C(21)-C(22)-F(22)	-178.5(2)	C(12)-C(13)-N(13)-N(14)	-23.9(4)
F(21)-C(21)-C(22)-C(23)	179.8(2)	C(14)-C(13)-N(13)-N(14)	159.5(2)
C(20)-C(21)-C(22)-C(23)	3.0(4)	C(22)-C(23)-N(23)-N(24)	-61.2(3)
F(22)-C(22)-C(23)-C(24)	178.59(19)	C(24)-C(23)-N(23)-N(24)	123.8(2)
C(21)-C(22)-C(23)-C(24)	-2.9(3)	C(32)-C(33)-N(33)-N(34)	139.9(2)
F(22)-C(22)-C(23)-N(23)	3.3(3)	C(34)-C(33)-N(33)-N(34)	-43.7(3)
C(21)-C(22)-C(23)-N(23)	-178.1(2)	C(56)-C(51)-C(52)-C(53)	0
C(22)-C(23)-C(24)-F(24)	179.32(19)	C(57)-C(51)-C(52)-C(53)	-179.99(14)
N(23)-C(23)-C(24)-F(24)	-5.4(3)	C(57)-C(51)-C(56)-C(55)	179.99(14)
C(22)-C(23)-C(24)-C(25)	3.4(3)		

Table 7. Bond lengths [Å] and angles [°] related to the hydrogen bonding for C22.50 H14 F12 N6.

D-H	..A	d(D-H)	d(H..A)	d(D..A)	<DHA
N(13)-H(13)	N(23)#1	0.80(3)	2.38(3)	3.103(3)	150(3)
N(14)-H(14A)	F(31)#2	1.01(2)	2.36(2)	3.306(3)	154(2)
N(14)-H(14B)	F(14)#3	1.01(2)	2.32(3)	3.169(3)	141(2)
N(23)-H(23)	N(34)#4	0.69(3)	2.59(3)	3.204(3)	149(3)
N(24)-H(24A)	F(22)	0.945(19)	2.58(2)	2.959(2)	104.50(17)
N(24)-H(24B)	N(34)#5	0.942(19)	2.26(2)	3.194(3)	171(2)
N(33)-H(33)	N(24)#6	0.97(2)	2.10(2)	3.056(3)	168.00(18)
N(33)-H(33)	F(32)	0.97(2)	2.38(2)	2.723(2)	100.20(14)
N(34)-H(34B)	N(14)#7	0.872(18)	2.43(2)	3.195(3)	147(2)
N(34)-H(34B)	F(32)#3	0.872(18)	2.47(2)	3.158(3)	137(2)

Symmetry transformations used to generate equivalent atoms:

#1 -x,-y+1,-z+1 #2 -x,y-1,-z+3/2 #3 x,y-1,z
#4 x,-y+1,z-1/2 #5 -x+1,y,-z+3/2 #6 x,-y+1,z+1/2
#7 -x,y,-z+3/2

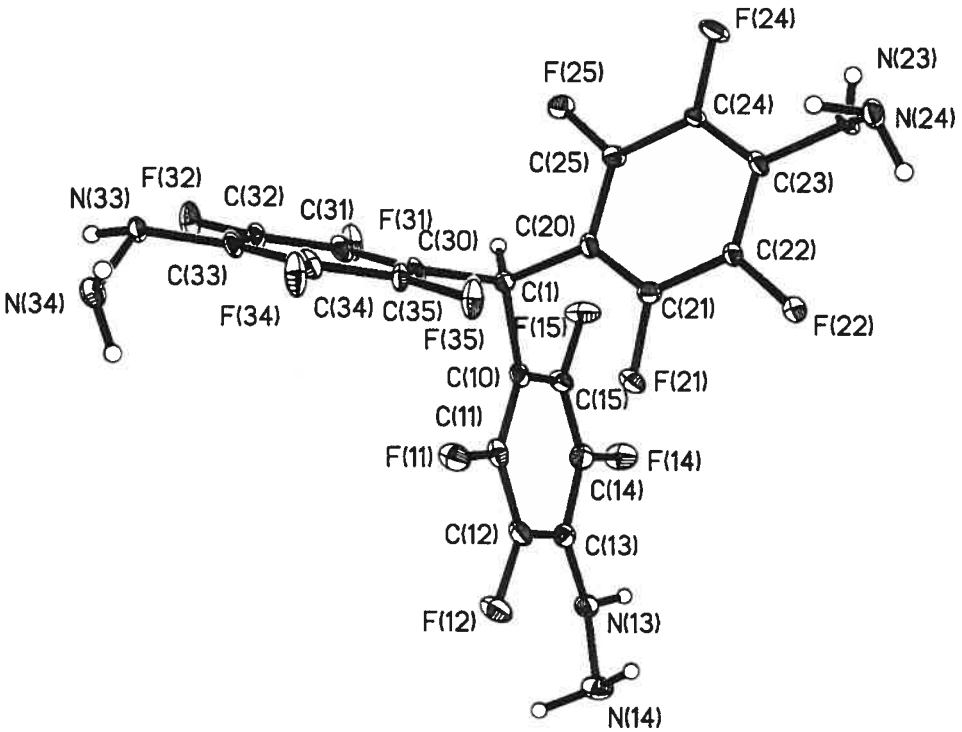

ORTEP view of the C22.50 H14 F12 N6 compound with the numbering scheme adopted. Ellipsoids drawn at 30% probability level. Hydrogens represented by sphere of arbitrary size.

REFERENCES

International Tables for Crystallography (1992). Vol. C. Tables 4.2.6.8 and 6.1.1.4, Dordrecht: Kluwer Academic Publishers.

SAINT (1999) Release 6.06; Integration Software for Single Crystal Data. Bruker AXS Inc., Madison, WI 53719-1173.

Sheldrick, G.M. (1996). SADABS, Bruker Area Detector Absorption Corrections. Bruker AXS Inc., Madison, WI 53719-1173.

Sheldrick, G.M. (1997). SHELXS97, Program for the Solution of Crystal Structures. Univ. of Gottingen, Germany.

Sheldrick, G.M. (1997). SHELXL97, Program for the Refinement of Crystal Structures. Univ. of Gottingen, Germany.

SHELXTL (1997) Release 5.10; The Complete Software Package for Single Crystal Structure Determination. Bruker AXS Inc., Madison, WI 53719-1173.

SMART (1999) Release 5.059; Bruker Molecular Analysis Research Tool. Bruker AXS Inc., Madison, WI 53719-1173.

Spek, A.L. (2000). PLATON, Molecular Geometry Program, 2000 version. University of Utrecht, Utrecht, Holland.

XPREP (1997) Release 5.10; X-ray data Preparation and Reciprocal space Exploration Program. Bruker AXS Inc., Madison, WI 53719-1173.

Université de Montréal

CRYSTAL AND MOLECULAR STRUCTURE OF

C45 H28 F24 N6 COMPOUND (JIW914)

Equipe WUEST

Département de chimie, Université de Montréal,

C.P. 6128, Succ. Centre-Ville, Montréal, Québec, H3C 3J7 (Canada)

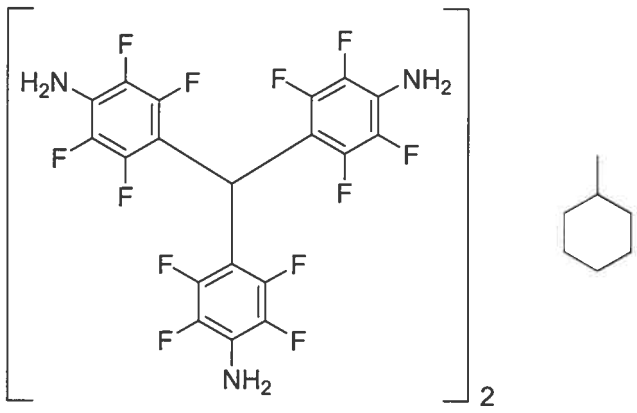

Structure solved and refined in the laboratory of X-ray diffraction Université de Montréal by Dr. Thierry Maris.

Table 1. Crystal data and structure refinement for C45 H28 F24 N6.

Identification code	JIW914
Empirical formula	C45 H28 F24 N6
Formula weight	1108.73
Temperature	100(2)K
Wavelength	1.54178 Å
Crystal system	Monoclinic
Space group	P2/n
Unit cell dimensions	a = 14.3870(15) Å α = 90° b = 7.7327(8) Å β = 96.617(4)° c = 19.596(2) Å γ = 90°
Volume	2165.5(4)Å^3
Z	2
Density (calculated)	1.700 g/cm^3
Absorption coefficient	1.575 mm^{-1}
F(000)	1112
Crystal size	0.12 x 0.06 x 0.06 mm
Theta range for data collection	3.62 to 68.30°
Index ranges	$-17 \leq h \leq 17$, $-9 \leq k \leq 9$, $-23 \leq \ell \leq 23$
Reflections collected	27609
Independent reflections	3947 [R_{int} = 0.038]
Absorption correction	Semi-empirical from equivalents
Max. and min. transmission	0.9100 and 0.7000
Refinement method	Full-matrix least-squares on F^2
Data / restraints / parameters	3947 / 0 / 375
Goodness-of-fit on F^2	1.051
Final R indices [I>2sigma(I)]	R_1 = 0.0423, wR_2 = 0.1166

R indices (all data)	R_1 = 0.0449, wR_2 = 0.1191
Largest diff. peak and hole	0.642 and -0.349 e/Å^3

Table 2. Atomic coordinates (x 10^4) and equivalent isotropic displacement parameters (Å^2 x 10^3) for C45 H28 F24 N6.

U_{eq} is defined as one third of the trace of the orthogonalized Uij tensor.

	Occ.	x	y	z	U_{eq}
C(1)	1	7783(1)	2733(2)	5899(1)	24(1)
C(10)	1	8137(1)	1295(2)	6395(1)	23(1)
C(11)	1	8849(1)	1651(2)	6915(1)	25(1)
F(11)	1	9211(1)	3267(1)	6975(1)	31(1)
C(12)	1	9209(1)	432(2)	7383(1)	26(1)
F(12)	1	9899(1)	867(1)	7880(1)	35(1)
C(13)	1	8893(1)	-1265(2)	7358(1)	26(1)
N(13)	1	9305(1)	-2535(2)	7782(1)	35(1)
C(14)	1	8173(1)	-1631(2)	6843(1)	25(1)
F(14)	1	7827(1)	-3259(1)	6797(1)	31(1)
C(15)	1	7811(1)	-392(2)	6382(1)	25(1)
F(15)	1	7112(1)	-879(1)	5902(1)	30(1)
C(20)	1	8337(1)	2920(2)	5284(1)	25(1)
C(21)	1	8694(1)	1578(2)	4923(1)	28(1)
F(21)	1	8557(1)	-77(1)	5100(1)	35(1)
C(22)	1	9179(1)	1862(2)	4366(1)	30(1)
F(22)	1	9506(1)	503(2)	4031(1)	40(1)
C(23)	1	9324(1)	3514(3)	4122(1)	31(1)
N(23)	1	9811(1)	3800(3)	3562(1)	41(1)
C(24)	1	8974(1)	4872(2)	4484(1)	29(1)
F(24)	1	9107(1)	6509(2)	4275(1)	40(1)
C(25)	1	8502(1)	4575(2)	5043(1)	26(1)
F(25)	1	8180(1)	5972(1)	5363(1)	30(1)
C(30)	1	6725(1)	2726(2)	5709(1)	24(1)
C(31)	1	6240(1)	2122(2)	5101(1)	27(1)
F(31)	1	6696(1)	1320(2)	4629(1)	37(1)
C(32)	1	5286(1)	2296(2)	4956(1)	29(1)
F(32)	1	4862(1)	1677(2)	4352(1)	38(1)
C(33)	1	4734(1)	3064(2)	5407(1)	27(1)
N(33)	1	3783(1)	3314(2)	5253(1)	35(1)
C(34)	1	5215(1)	3645(2)	6020(1)	28(1)
F(34)	1	4720(1)	4404(2)	6484(1)	37(1)
C(35)	1	6164(1)	3461(2)	6162(1)	25(1)
F(35)	1	6574(1)	4042(1)	6776(1)	30(1)
C(42)	1	2857(3)	2616(4)	7247(2)	83(1)
C(40)	1	2862(3)	-595(4)	7258(3)	92(1)
C(41)	1	2800(2)	1009(4)	6814(2)	64(1)
C(43)	0.50	2984(4)	-2402(7)	7043(3)	55(1)

Table 3. Hydrogen coordinates (x 10^4) and isotropic displacement parameters ($Å^2$ x 10^3) for C45 H28 F24 N6.

	Occ.	x	y	z	U_{eq}
H(1)	1	7906(13)	3830(30)	6152(10)	18(4)
H(13A)	1	9567(18)	-2180(30)	8105(14)	41(7)
H(13B)	1	8980(20)	-3490(40)	7798(14)	50(7)
H(23A)	1	9727(19)	4740(40)	3409(14)	44(7)
H(23B)	1	9818(19)	3120(40)	3322(14)	38(8)
H(33B)	1	3474(17)	3470(30)	5612(13)	37(6)
H(33A)	1	3540(20)	2700(40)	4961(15)	54(8)
H(42A)	1	2754	3640	6944	100
H(42B)	1	3491	2708	7500	100
H(40A)	1	3449	-385	7573	110
H(41A)	1	3318	1007	6522	77
H(41B)	1	2202	1002	6509	77
H(43A)	0.50	3069	-3150	7449	82
H(43B)	0.50	3537	-2484	6795	82
H(43C)	0.50	2429	-2773	6741	82
H(40B)	0.50	2650(50)	-1570(100)	6780(40)	80(20)

Table 4. Anisotropic parameters ($Å^2$ x 10^3) for C45 H28 F24 N6.

The anisotropic displacement factor exponent takes the form:

$$-2\pi^2 [h^2 a^{*2} U_{11} + ... + 2 h k a^* b^* U_{12}]$$

	U11	U22	U33	U23	U13	U12
C(1)	28(1)	19(1)	25(1)	-2(1)	-1(1)	-1(1)
C(10)	25(1)	21(1)	23(1)	0(1)	1(1)	-1(1)
C(11)	27(1)	20(1)	27(1)	-2(1)	1(1)	-5(1)
F(11)	34(1)	22(1)	34(1)	0(1)	-4(1)	-9(1)
C(12)	26(1)	28(1)	24(1)	-2(1)	-3(1)	-3(1)
F(12)	35(1)	33(1)	32(1)	-1(1)	-12(1)	-6(1)
C(13)	30(1)	25(1)	23(1)	2(1)	2(1)	0(1)
N(13)	46(1)	28(1)	28(1)	5(1)	-9(1)	-3(1)
C(14)	31(1)	19(1)	25(1)	-2(1)	3(1)	-5(1)
F(14)	41(1)	20(1)	32(1)	1(1)	-1(1)	-8(1)
C(15)	25(1)	25(1)	23(1)	-3(1)	-2(1)	-3(1)
F(15)	33(1)	24(1)	31(1)	-2(1)	-10(1)	-6(1)
C(20)	26(1)	22(1)	26(1)	1(1)	-3(1)	-2(1)
C(21)	31(1)	22(1)	31(1)	2(1)	-1(1)	-3(1)
F(21)	50(1)	19(1)	37(1)	0(1)	9(1)	-1(1)
C(22)	31(1)	28(1)	31(1)	-5(1)	2(1)	1(1)
F(22)	46(1)	34(1)	41(1)	-7(1)	12(1)	2(1)
C(23)	28(1)	34(1)	31(1)	1(1)	1(1)	-5(1)
N(23)	43(1)	39(1)	43(1)	5(1)	15(1)	-6(1)
C(24)	31(1)	24(1)	32(1)	4(1)	-2(1)	-5(1)
F(24)	50(1)	27(1)	44(1)	8(1)	8(1)	-6(1)
C(25)	27(1)	22(1)	29(1)	-2(1)	-3(1)	1(1)
F(25)	35(1)	20(1)	35(1)	0(1)	2(1)	2(1)
C(30)	29(1)	18(1)	25(1)	2(1)	-1(1)	-1(1)
C(31)	33(1)	23(1)	25(1)	-1(1)	2(1)	-1(1)
F(31)	35(1)	45(1)	30(1)	-13(1)	2(1)	-3(1)
C(32)	36(1)	24(1)	24(1)	1(1)	-7(1)	-5(1)
F(32)	39(1)	43(1)	28(1)	-4(1)	-8(1)	-7(1)
C(33)	29(1)	18(1)	33(1)	4(1)	-4(1)	-1(1)
N(33)	29(1)	30(1)	42(1)	-3(1)	-6(1)	1(1)
C(34)	31(1)	20(1)	33(1)	-2(1)	2(1)	0(1)
F(34)	31(1)	35(1)	44(1)	-14(1)	4(1)	2(1)
C(35)	31(1)	19(1)	24(1)	0(1)	-3(1)	-2(1)
F(35)	31(1)	31(1)	28(1)	-9(1)	-1(1)	-3(1)
C(42)	90(2)	47(2)	121(3)	13(2)	49(2)	-1(2)
C(40)	98(3)	43(2)	143(4)	-16(2)	52(3)	-10(2)
C(41)	59(2)	82(2)	53(2)	-9(1)	8(1)	-5(2)
C(43)	59(3)	46(3)	57(3)	-7(2)	-3(2)	1(2)

Table 5. Bond lengths [Å] and angles [°] for C45 H28 F24 N6

C(1)-C(30)	1.524(2)	F(12)-C(12)-C(13)	118.10(16)
C(1)-C(10)	1.525(2)	C(11)-C(12)-C(13)	121.90(16)
C(1)-C(20)	1.526(2)	N(13)-C(13)-C(12)	122.46(17)
C(10)-C(15)	1.386(2)	N(13)-C(13)-C(14)	121.82(17)
C(10)-C(11)	1.388(2)	C(12)-C(13)-C(14)	115.56(16)
C(11)-F(11)	1.353(2)	F(14)-C(14)-C(15)	119.64(15)
C(11)-C(12)	1.374(3)	F(14)-C(14)-C(13)	118.36(15)
C(12)-F(12)	1.351(2)	C(15)-C(14)-C(13)	121.99(16)
C(12)-C(13)	1.388(3)	F(15)-C(15)-C(14)	117.32(15)
C(13)-N(13)	1.376(2)	F(15)-C(15)-C(10)	119.95(15)
C(13)-C(14)	1.389(3)	C(14)-C(15)-C(10)	122.73(16)
C(14)-F(14)	1.353(2)	C(21)-C(20)-C(25)	115.19(17)
C(14)-C(15)	1.377(3)	C(21)-C(20)-C(1)	126.12(16)
C(15)-F(15)	1.348(2)	C(25)-C(20)-C(1)	118.69(16)
C(20)-C(21)	1.388(3)	F(21)-C(21)-C(22)	117.28(17)
C(20)-C(25)	1.394(2)	F(21)-C(21)-C(20)	120.35(16)
C(21)-F(21)	1.346(2)	C(22)-C(21)-C(20)	122.35(17)
C(21)-C(22)	1.380(3)	F(22)-C(22)-C(21)	119.73(17)
C(22)-F(22)	1.352(2)	F(22)-C(22)-C(23)	118.34(17)
C(22)-C(23)	1.388(3)	C(21)-C(22)-C(23)	121.91(17)
C(23)-N(23)	1.388(3)	N(23)-C(23)-C(22)	121.88(19)
C(23)-C(24)	1.392(3)	N(23)-C(23)-C(24)	121.90(19)
C(24)-F(24)	1.352(2)	C(22)-C(23)-C(24)	116.20(17)
C(24)-C(25)	1.372(3)	F(24)-C(24)-C(25)	119.94(17)
C(25)-F(25)	1.357(2)	F(24)-C(24)-C(23)	118.65(17)
C(30)-C(35)	1.388(3)	C(25)-C(24)-C(23)	121.41(17)
C(30)-C(31)	1.391(2)	F(25)-C(25)-C(24)	117.57(16)
C(31)-F(31)	1.346(2)	F(25)-C(25)-C(20)	119.50(16)
C(31)-C(32)	1.376(3)	C(24)-C(25)-C(20)	122.93(17)
C(32)-F(32)	1.355(2)	C(35)-C(30)-C(31)	114.44(16)
C(32)-C(33)	1.388(3)	C(35)-C(30)-C(1)	118.69(15)
C(33)-N(33)	1.380(3)	C(31)-C(30)-C(1)	126.80(16)
C(33)-C(34)	1.390(3)	F(31)-C(31)-C(32)	117.20(16)
C(34)-F(34)	1.352(2)	F(31)-C(31)-C(30)	120.50(16)
C(34)-C(35)	1.370(3)	C(32)-C(31)-C(30)	122.30(17)
C(35)-F(35)	1.354(2)	F(32)-C(32)-C(31)	118.91(17)
C(42)-C(41)	1.501(5)	F(32)-C(32)-C(33)	118.34(16)
C(42)-C(42)#1	1.508(6)	C(31)-C(32)-C(33)	122.75(17)
C(40)-C(43)	1.476(6)	N(33)-C(33)-C(32)	123.17(17)
C(40)-C(40)#1	1.486(7)	N(33)-C(33)-C(34)	121.67(18)
C(40)-C(41)	1.512(5)	C(32)-C(33)-C(34)	115.10(16)
		F(34)-C(34)-C(35)	119.94(16)
C(30)-C(1)-C(10)	113.79(14)	F(34)-C(34)-C(33)	118.26(16)
C(30)-C(1)-C(20)	113.90(14)	C(35)-C(34)-C(33)	121.80(17)
C(10)-C(1)-C(20)	113.90(15)	F(35)-C(35)-C(34)	117.84(16)
C(15)-C(10)-C(11)	114.84(16)	F(35)-C(35)-C(30)	118.58(16)
C(15)-C(10)-C(1)	126.01(15)	C(34)-C(35)-C(30)	123.57(16)
C(11)-C(10)-C(1)	119.15(15)	C(41)-C(42)-C(42)#1	112.0(2)
F(11)-C(11)-C(12)	117.59(15)	C(43)-C(40)-C(40)#1	107.3(3)
F(11)-C(11)-C(10)	119.45(15)	C(43)-C(40)-C(41)	127.8(4)
C(12)-C(11)-C(10)	122.95(16)	C(40)#1-C(40)-C(41)	111.6(3)
F(12)-C(12)-C(11)	120.00(16)	C(42)-C(41)-C(40)	111.0(3)

Symmetry transformations used to generate equivalent atoms:

#1 -x+1/2,y,-z+3/2

Table 6. Torsion angles [°] for C45 H28 F24 N6.

C(30)-C(1)-C(10)-C(15)	39.5(2)	N(23)-C(23)-C(24)-F(24)	0.8(3)
C(20)-C(1)-C(10)-C(15)	-93.3(2)	C(22)-C(23)-C(24)-F(24)	179.13(16)
C(30)-C(1)-C(10)-C(11)	-140.38(17)	N(23)-C(23)-C(24)-C(25)	-179.28(18)
C(20)-C(1)-C(10)-C(11)	86.8(2)	C(22)-C(23)-C(24)-C(25)	-0.9(3)
C(15)-C(10)-C(11)-F(11)	-179.56(15)	F(24)-C(24)-C(25)-F(25)	0.3(2)
C(1)-C(10)-C(11)-F(11)	0.3(3)	C(23)-C(24)-C(25)-F(25)	-179.62(16)
C(15)-C(10)-C(11)-C(12)	0.2(3)	F(24)-C(24)-C(25)-C(20)	179.75(16)
C(1)-C(10)-C(11)-C(12)	-179.91(16)	C(23)-C(24)-C(25)-C(20)	-0.2(3)
F(11)-C(11)-C(12)-F(12)	0.2(3)	C(21)-C(20)-C(25)-F(25)	179.96(15)
C(10)-C(11)-C(12)-F(12)	-179.61(16)	C(1)-C(20)-C(25)-F(25)	0.9(2)
F(11)-C(11)-C(12)-C(13)	-179.14(16)	C(21)-C(20)-C(25)-C(24)	0.6(3)
C(10)-C(11)-C(12)-C(13)	1.1(3)	C(1)-C(20)-C(25)-C(24)	-178.47(16)
F(12)-C(12)-C(13)-N(13)	-5.5(3)	C(10)-C(1)-C(30)-C(35)	81.0(2)
C(11)-C(12)-C(13)-N(13)	173.82(18)	C(20)-C(1)-C(30)-C(35)	-146.20(16)
F(12)-C(12)-C(13)-C(14)	179.08(16)	C(10)-C(1)-C(30)-C(31)	-102.4(2)
C(11)-C(12)-C(13)-C(14)	-1.6(3)	C(20)-C(1)-C(30)-C(31)	30.5(2)
N(13)-C(13)-C(14)-F(14)	5.3(3)	C(35)-C(30)-C(31)-F(31)	-177.39(15)
C(12)-C(13)-C(14)-F(14)	-179.23(15)	C(1)-C(30)-C(31)-F(31)	5.8(3)
N(13)-C(13)-C(14)-C(15)	-174.55(18)	C(35)-C(30)-C(31)-C(32)	2.0(3)
C(12)-C(13)-C(14)-C(15)	0.9(3)	C(1)-C(30)-C(31)-C(32)	-174.81(17)
F(14)-C(14)-C(15)-F(15)	0.4(2)	F(31)-C(31)-C(32)-F(32)	-0.7(3)
C(13)-C(14)-C(15)-F(15)	-179.76(16)	C(30)-C(31)-C(32)-F(32)	179.91(16)
F(14)-C(14)-C(15)-C(10)	-179.50(16)	F(31)-C(31)-C(32)-C(33)	178.55(16)
C(13)-C(14)-C(15)-C(10)	0.4(3)	C(30)-C(31)-C(32)-C(33)	-0.8(3)
C(11)-C(10)-C(15)-F(15)	179.21(15)	F(32)-C(32)-C(33)-N(33)	-3.8(3)
C(1)-C(10)-C(15)-F(15)	-0.6(3)	C(31)-C(32)-C(33)-N(33)	176.98(17)
C(11)-C(10)-C(15)-C(14)	-0.9(3)	F(32)-C(32)-C(33)-C(34)	179.11(15)
C(1)-C(10)-C(15)-C(14)	179.21(17)	C(31)-C(32)-C(33)-C(34)	-0.2(3)
C(30)-C(1)-C(20)-C(21)	-93.9(2)	N(33)-C(33)-C(34)-F(34)	3.0(3)
C(10)-C(1)-C(20)-C(21)	38.8(2)	C(32)-C(33)-C(34)-F(34)	-179.85(15)
C(30)-C(1)-C(20)-C(25)	85.00(19)	N(33)-C(33)-C(34)-C(35)	-177.34(17)
C(10)-C(1)-C(20)-C(25)	-142.25(16)	C(32)-C(33)-C(34)-C(35)	-0.1(3)
C(25)-C(20)-C(21)-F(21)	-178.43(15)	F(34)-C(34)-C(35)-F(35)	0.6(3)
C(1)-C(20)-C(21)-F(21)	0.5(3)	C(33)-C(34)-C(35)-F(35)	-179.08(15)
C(25)-C(20)-C(21)-C(22)	0.2(3)	F(34)-C(34)-C(35)-C(30)	-178.82(16)
C(1)-C(20)-C(21)-C(22)	179.18(17)	C(33)-C(34)-C(35)-C(30)	1.5(3)
F(21)-C(21)-C(22)-F(22)	-1.0(3)	C(31)-C(30)-C(35)-F(35)	178.26(15)
C(20)-C(21)-C(22)-F(22)	-179.70(16)	C(1)-C(30)-C(35)-F(35)	-4.7(2)
F(21)-C(21)-C(22)-C(23)	177.28(17)	C(31)-C(30)-C(35)-C(34)	-2.3(3)
C(20)-C(21)-C(22)-C(23)	-1.4(3)	C(1)-C(30)-C(35)-C(34)	174.75(16)
F(22)-C(22)-C(23)-N(23)	-1.6(3)	C(42)#1-C(42)-C(41)-C(40)	-53.5(5)
C(21)-C(22)-C(23)-N(23)	-179.92(19)	C(43)-C(40)-C(41)-C(42)	-169.4(4)
F(22)-C(22)-C(23)-C(24)	-179.99(16)	C(40)#1-C(40)-C(41)-C(42)	55.2(6)
C(21)-C(22)-C(23)-C(24)	1.7(3)		

Symmetry transformations used to generate equivalent atoms:

#1 -x+1/2,y,-z+3/2

Table 7. Bond lengths [Å] and angles [°] related to the hydrogen bonding for C45 H28 F24 N6.

D-H	..A	d(D-H)	d(H..A)	d(D..A)	<DHA
N(13)-H(13A)	F(32)#2	0.75(3)	2.46(3)	3.158(2)	155(3)
N(13)-H(13B)	F(35)#3	0.88(3)	2.26(3)	3.099(2)	159(2)
N(23)-H(23A)	F(11)#4	0.79(3)	2.35(3)	2.928(2)	130(2)
N(23)-H(23B)	N(13)#5	0.71(3)	2.67(3)	3.206(3)	135(3)
N(33)-H(33A)	F(15)#6	0.79(3)	2.31(3)	3.108(2)	178(3)

Symmetry transformations used to generate equivalent atoms:

#1 -x+1/2,y,-z+3/2 #2 x+1/2,-y,z+1/2
#3 -x+3/2,y-1,-z+3/2 #4 -x+2,-y+1,-z+1
#5 -x+2,-y,-z+1 #6 -x+1,-y,-z+1

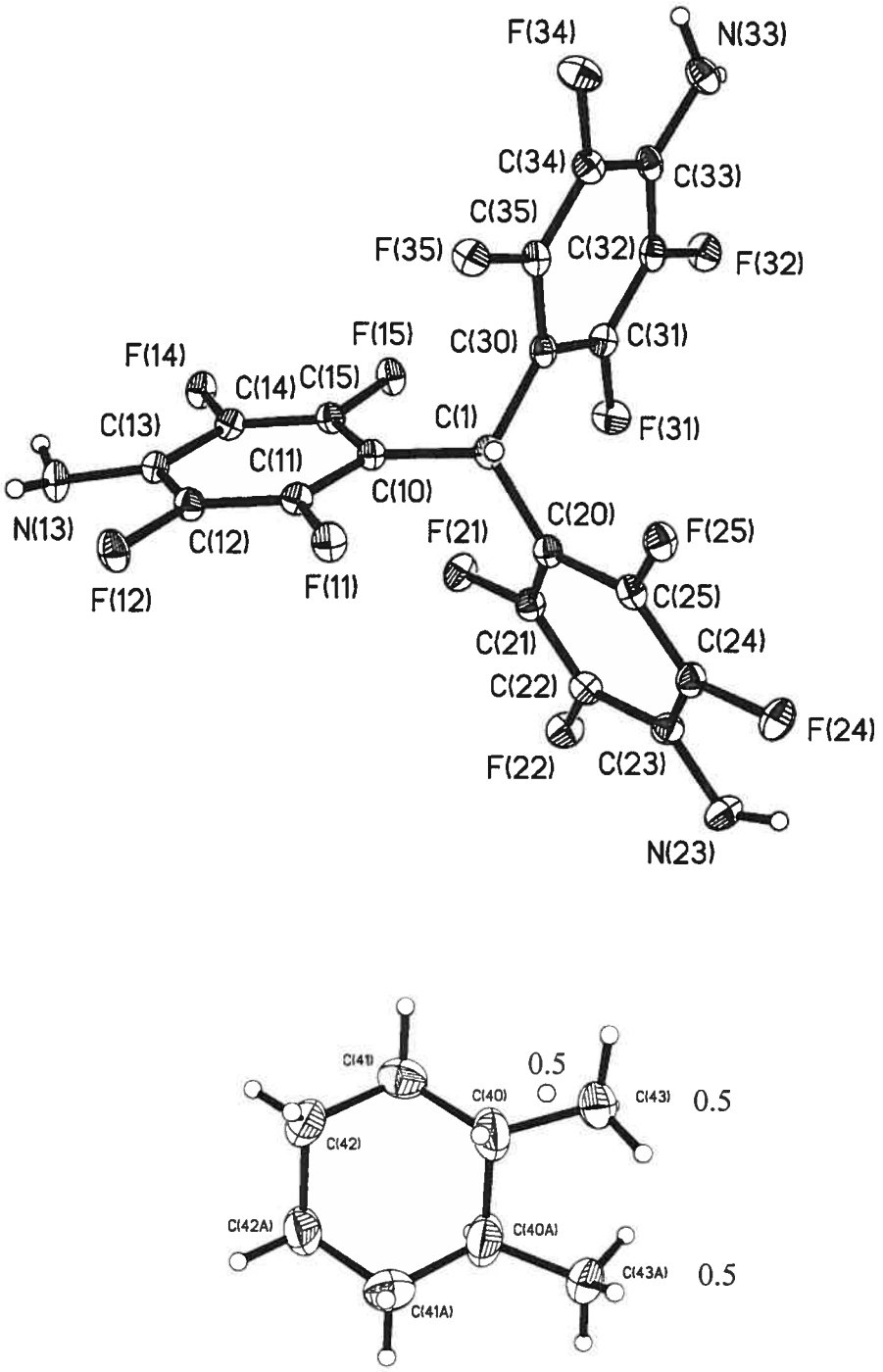

ORTEP view of the C45 H28 F24 N6 compound with the numbering scheme adopted. Ellipsoids drawn at 30% probability level. Hydrogen atoms are represented by sphere of arbitrary size.

REFERENCES

International Tables for Crystallography (1992). Vol. C. Tables 4.2.6.8 and 6.1.1.4, Dordrecht: Kluwer Academic Publishers.

SAINT (1999) Release 6.06; Integration Software for Single Crystal Data. Bruker AXS Inc., Madison, WI 53719-1173.

Sheldrick, G.M. (1996). SADABS, Bruker Area Detector Absorption Corrections. Bruker AXS Inc., Madison, WI 53719-1173.

Sheldrick, G.M. (1997). SHELXS97, Program for the Solution of Crystal Structures. Univ. of Gottingen, Germany.

Sheldrick, G.M. (1997). SHELXL97, Program for the Refinement of Crystal Structures. Univ. of Gottingen, Germany.

SHELXTL (1997) Release 5.10; The Complete Software Package for Single Crystal Structure Determination. Bruker AXS Inc., Madison, WI 53719-1173.

SMART (1999) Release 5.059; Bruker Molecular Analysis Research Tool. Bruker AXS Inc., Madison, WI 53719-1173.

Spek, A.L. (2000). PLATON, Molecular Geometry Program, 2000 version. University of Utrecht, Utrecht, Holland.

XPREP (1997) Release 5.10; X-ray data Preparation and Reciprocal space Exploration Program. Bruker AXS Inc., Madison, WI 53719-1173.

Université de Montréal

CRYSTAL AND MOLECULAR STRUCTURE OF

C19 H Br3 F12 COMPOUND (jw1064)

Equipe WUEST

Département de chimie, Université de Montréal,

C.P. 6128, Succ. Centre-Ville, Montréal, Québec, H3C 3J7 (Canada)

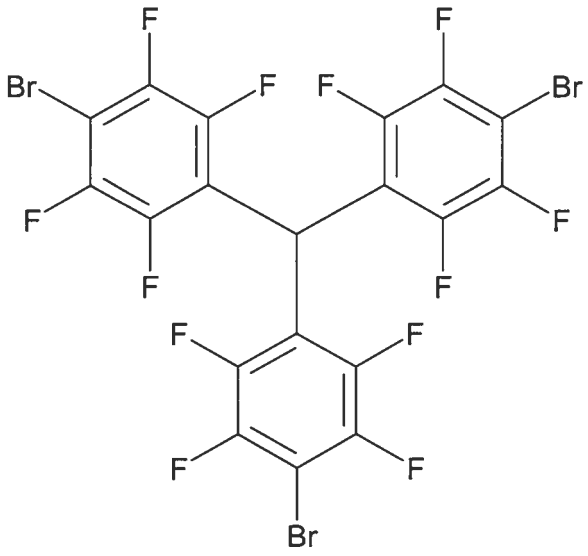

Structure solved and refined in the laboratory of X-ray diffraction Université de Montréal by Dr. Thierry Maris.

Table 1. Crystal data and structure refinement for C19 H Br3 F12.

Identification code	jw1064
Empirical formula	C19 H Br3 F12
Formula weight	696.93
Temperature	150(2)K
Wavelength	1.54178 Å
Crystal system	Monoclinic
Space group	C2/c
Unit cell dimensions	a = 18.448(9) Å α = 90° b = 16.573(8) Å β = 100.02(3)° c = 13.733(6) Å γ = 90°
Volume	4134(3)Å^3
Z	8
Density (calculated)	2.239 g/cm^3
Absorption coefficient	8.337 mm^{-1}
F(000)	2624
Crystal size	0.26 x 0.17 x 0.07 mm
Theta range for data collection	3.61 to 68.57°
Index ranges	$-22 \leq h \leq 22$, $-19 \leq k \leq 19$, $-16 \leq \ell \leq 16$
Reflections collected	28173
Independent reflections	3760 [R_{int} = 0.090]
Absorption correction	Semi-empirical from equivalents
Max. and min. transmission	1.0000 and 0.4300
Refinement method	Full-matrix least-squares on F^2
Data / restraints / parameters	3760 / 0 / 307
Goodness-of-fit on F^2	1.009
Final R indices [I>2sigma(I)]	R_1 = 0.0477, wR_2 = 0.1186
R indices (all data)	R_1 = 0.0627, wR_2 = 0.1288

Largest diff. peak and hole 0.535 and -0.772 e/Å^3

Table 2. Atomic coordinates (x 10^4) and equivalent isotropic displacement parameters (Å^2 x 10^3) for C19 H Br3 F12.

U_{eq} is defined as one third of the trace of the orthogonalized Uij tensor.

	x	y	z	U_{eq}
Br(1)	1400(1)	3682(1)	4716(1)	76(1)
Br(2)	251(1)	-2400(1)	5920(1)	119(1)
Br(3)	4442(1)	821(1)	10807(1)	78(1)
C(1)	1541(2)	852(2)	7728(3)	47(1)
C(10)	1542(2)	1524(3)	6959(3)	47(1)
C(11)	1368(2)	2306(3)	7217(3)	54(1)
C(12)	1337(3)	2940(3)	6569(3)	55(1)
C(13)	1470(2)	2827(3)	5620(3)	55(1)
C(14)	1642(2)	2054(3)	5353(3)	53(1)
C(15)	1677(2)	1418(2)	6007(3)	46(1)
C(20)	1276(2)	30(3)	7290(2)	45(1)
C(21)	587(2)	-11(3)	6692(3)	53(1)
C(22)	275(3)	-710(3)	6291(3)	59(1)
C(23)	651(3)	-1428(3)	6463(3)	62(1)
C(24)	1337(3)	-1416(3)	7056(3)	58(1)
C(25)	1638(2)	-701(3)	7456(3)	52(1)
C(30)	2263(2)	849(2)	8466(3)	46(1)
C(31)	2258(3)	945(3)	9466(3)	52(1)
C(32)	2905(3)	949(3)	10160(3)	56(1)
C(33)	3571(3)	856(3)	9877(3)	54(1)
C(34)	3590(3)	765(3)	8875(3)	55(1)
C(35)	2946(3)	768(3)	8201(3)	51(1)
F(11)	1221(2)	2442(2)	8145(2)	75(1)
F(12)	1148(2)	3682(2)	6857(2)	75(1)
F(14)	1771(2)	1910(2)	4428(2)	68(1)
F(15)	1832(1)	680(2)	5679(2)	57(1)
F(21)	185(1)	686(2)	6506(2)	62(1)
F(22)	-397(2)	-689(2)	5731(2)	81(1)
F(24)	1733(2)	-2103(2)	7240(2)	79(1)
F(25)	2307(1)	-755(2)	8027(2)	66(1)
F(31)	1607(2)	1038(2)	9799(2)	71(1)
F(32)	2847(2)	1035(2)	11119(2)	81(1)
F(34)	4232(2)	648(2)	8565(2)	74(1)
F(35)	2993(2)	654(2)	7243(2)	67(1)

Table 3. Hydrogen coordinates (x 10^4) and isotropic displacement parameters (Å^2 x 10^3) for C19 H Br3 F12.

	x	y	z	U_{eq}

H(1)	1160	1021	8124	56

Table 4. Anisotropic parameters ($Å^2$ x 10^3) for C19 H Br3 F12.

The anisotropic displacement factor exponent takes the form:

$$-2\pi^2 [h^2 a^{*2} U_{11} + ... + 2 h k a^* b^* U_{12}]$$

	U11	U22	U33	U23	U13	U12
Br(1)	80(1)	59(1)	84(1)	24(1)	-3(1)	-5(1)
Br(2)	101(1)	67(1)	166(1)	-35(1)	-40(1)	-9(1)
Br(3)	71(1)	79(1)	70(1)	-7(1)	-23(1)	6(1)
C(1)	51(3)	49(3)	39(2)	-2(2)	3(2)	1(2)
C(10)	50(3)	47(2)	41(2)	-2(2)	0(2)	-2(2)
C(11)	59(3)	54(3)	45(2)	-5(2)	0(2)	0(2)
C(12)	54(3)	44(2)	62(2)	-9(2)	-6(2)	2(2)
C(13)	55(3)	45(3)	59(2)	6(2)	-3(2)	-4(2)
C(14)	53(3)	58(3)	47(2)	1(2)	4(2)	-2(2)
C(15)	51(3)	40(2)	46(2)	1(2)	5(2)	0(2)
C(20)	42(2)	53(3)	40(2)	2(2)	6(2)	0(2)
C(21)	53(3)	53(3)	49(2)	3(2)	-1(2)	0(2)
C(22)	50(3)	71(3)	53(2)	-1(2)	-5(2)	-5(2)
C(23)	61(3)	56(3)	65(3)	-9(2)	-1(2)	-9(2)
C(24)	62(3)	49(3)	60(2)	1(2)	1(2)	2(2)
C(25)	52(3)	55(3)	43(2)	6(2)	-5(2)	-3(2)
C(30)	54(3)	41(2)	41(2)	-4(2)	-2(2)	-3(2)
C(31)	54(3)	54(3)	46(2)	-1(2)	3(2)	-5(2)
C(32)	70(3)	54(3)	40(2)	-2(2)	-3(2)	-4(2)
C(33)	58(3)	45(3)	55(2)	0(2)	-2(2)	-4(2)
C(34)	51(3)	50(3)	61(2)	1(2)	3(2)	-2(2)
C(35)	56(3)	55(3)	41(2)	0(2)	3(2)	-1(2)
F(11)	103(2)	61(2)	60(1)	-14(1)	7(1)	12(2)
F(12)	88(2)	47(2)	82(2)	-9(1)	-5(2)	6(1)
F(14)	83(2)	73(2)	49(1)	9(1)	15(1)	3(2)
F(15)	73(2)	49(1)	49(1)	-3(1)	9(1)	2(1)
F(21)	54(2)	61(2)	67(1)	3(1)	-2(1)	3(1)
F(22)	58(2)	84(2)	89(2)	-12(2)	-20(1)	-6(1)
F(24)	84(2)	51(2)	93(2)	-4(1)	-10(2)	8(2)
F(25)	60(2)	59(2)	68(1)	3(1)	-16(1)	3(1)
F(31)	63(2)	101(2)	46(1)	-2(1)	7(1)	-2(2)
F(32)	87(2)	114(3)	36(1)	-8(1)	-3(1)	-7(2)
F(34)	57(2)	86(2)	78(2)	-5(2)	5(1)	7(1)
F(35)	63(2)	93(2)	46(1)	-1(1)	11(1)	7(1)

Table 5. Bond lengths [Å] and angles [°] for C19 H Br3 F12

Br(1)-C(13)	1.874(4)	F(12)-C(12)-C(13)	119.7(4)
Br(2)-C(23)	1.872(5)	C(11)-C(12)-C(13)	121.0(4)
Br(3)-C(33)	1.872(4)	C(12)-C(13)-C(14)	117.5(4)
C(1)-C(30)	1.527(5)	C(12)-C(13)-BR1	121.4(3)
C(1)-C(20)	1.534(6)	C(14)-C(13)-BR1	121.1(3)
C(1)-C(10)	1.536(6)	F(14)-C(14)-C(15)	118.8(4)
C(10)-C(15)	1.383(5)	F(14)-C(14)-C(13)	119.8(4)
C(10)-C(11)	1.395(6)	C(15)-C(14)-C(13)	121.4(4)
C(11)-F(11)	1.367(5)	F(15)-C(15)-C(14)	117.5(4)
C(11)-C(12)	1.372(6)	F(15)-C(15)-C(10)	120.9(3)
C(12)-F(12)	1.355(5)	C(14)-C(15)-C(10)	121.6(4)
C(12)-C(13)	1.380(6)	C(25)-C(20)-C(21)	114.8(4)
C(13)-C(14)	1.386(6)	C(25)-C(20)-C(1)	126.9(3)
C(14)-F(14)	1.352(5)	C(21)-C(20)-C(1)	118.2(4)
C(14)-C(15)	1.379(6)	C(22)-C(21)-F(21)	117.5(4)
C(15)-F(15)	1.353(5)	C(22)-C(21)-C(20)	124.0(4)
C(20)-C(25)	1.384(6)	F(21)-C(21)-C(20)	118.5(4)
C(20)-C(21)	1.388(5)	F(22)-C(22)-C(21)	119.5(4)
C(21)-C(22)	1.365(6)	F(22)-C(22)-C(23)	120.5(4)
C(21)-F(21)	1.374(5)	C(21)-C(22)-C(23)	120.0(4)
C(22)-F(22)	1.342(5)	C(22)-C(23)-C(24)	118.1(4)
C(22)-C(23)	1.376(7)	C(22)-C(23)-BR2	121.6(3)
C(23)-C(24)	1.382(6)	C(24)-C(23)-BR2	120.2(4)
C(24)-F(24)	1.351(5)	F(24)-C(24)-C(25)	118.8(4)
C(24)-C(25)	1.381(6)	F(24)-C(24)-C(23)	120.5(4)
C(25)-F(25)	1.345(4)	C(25)-C(24)-C(23)	120.6(4)
C(30)-C(35)	1.378(6)	F(25)-C(25)-C(24)	116.0(4)
C(30)-C(31)	1.384(5)	F(25)-C(25)-C(20)	121.4(4)
C(31)-F(31)	1.365(5)	C(24)-C(25)-C(20)	122.5(4)
C(31)-C(32)	1.392(6)	C(35)-C(30)-C(31)	116.0(4)
C(32)-F(32)	1.347(5)	C(35)-C(30)-C(1)	123.9(4)
C(32)-C(33)	1.359(7)	C(31)-C(30)-C(1)	120.1(4)
C(33)-C(34)	1.390(6)	F(31)-C(31)-C(30)	120.2(4)
C(34)-F(34)	1.341(6)	F(31)-C(31)-C(32)	118.1(4)
C(34)-C(35)	1.373(6)	C(30)-C(31)-C(32)	121.7(4)
C(35)-F(35)	1.348(5)	F(32)-C(32)-C(33)	121.4(4)
		F(32)-C(32)-C(31)	117.6(5)
C(30)-C(1)-C(20)	116.1(3)	C(33)-C(32)-C(31)	120.9(4)
C(30)-C(1)-C(10)	110.7(3)	C(32)-C(33)-C(34)	118.4(4)
C(20)-C(1)-C(10)	114.3(3)	C(32)-C(33)-BR3	121.3(3)
C(15)-C(10)-C(11)	116.4(4)	C(34)-C(33)-BR3	120.3(4)
C(15)-C(10)-C(1)	125.5(4)	F(34)-C(34)-C(35)	119.7(4)
C(11)-C(10)-C(1)	118.1(4)	F(34)-C(34)-C(33)	120.4(4)
F(11)-C(11)-C(12)	119.0(4)	C(35)-C(34)-C(33)	119.9(5)
F(11)-C(11)-C(10)	118.8(4)	F(35)-C(35)-C(34)	117.6(4)
C(12)-C(11)-C(10)	122.2(4)	F(35)-C(35)-C(30)	119.3(3)
F(12)-C(12)-C(11)	119.3(4)	C(34)-C(35)-C(30)	123.1(4)

Table 6. Torsion angles [°] for C19 H Br3 F12.

C(30)-C(1)-C(10)-C(15)	100.8(5)	C(23)-C(24)-C(25)-F(25)	179.7(4)
C(20)-C(1)-C(10)-C(15)	-32.7(6)	F(24)-C(24)-C(25)-C(20)	178.8(4)
C(30)-C(1)-C(10)-C(11)	-81.6(5)	C(23)-C(24)-C(25)-C(20)	0.1(7)
C(20)-C(1)-C(10)-C(11)	144.9(4)	C(21)-C(20)-C(25)-F(25)	-179.5(4)
C(15)-C(10)-C(11)-F(11)	179.2(4)	C(1)-C(20)-C(25)-F(25)	-2.3(7)
C(1)-C(10)-C(11)-F(11)	1.4(6)	C(21)-C(20)-C(25)-C(24)	0.1(7)
C(15)-C(10)-C(11)-C(12)	-0.5(6)	C(1)-C(20)-C(25)-C(24)	177.2(4)
C(1)-C(10)-C(11)-C(12)	-178.3(4)	C(20)-C(1)-C(30)-C(35)	75.1(5)
F(11)-C(11)-C(12)-F(12)	-1.2(6)	C(10)-C(1)-C(30)-C(35)	-57.4(5)
C(10)-C(11)-C(12)-F(12)	178.4(4)	C(20)-C(1)-C(30)-C(31)	-105.9(5)
F(11)-C(11)-C(12)-C(13)	-178.9(4)	C(10)-C(1)-C(30)-C(31)	121.5(4)
C(10)-C(11)-C(12)-C(13)	0.8(7)	C(35)-C(30)-C(31)-F(31)	179.4(4)
F(12)-C(12)-C(13)-C(14)	-178.3(4)	C(1)-C(30)-C(31)-F(31)	0.4(6)
C(11)-C(12)-C(13)-C(14)	-0.6(6)	C(35)-C(30)-C(31)-C(32)	-0.7(7)
F(12)-C(12)-C(13)-BR1	0.4(6)	C(1)-C(30)-C(31)-C(32)	-179.7(4)
C(11)-C(12)-C(13)-BR1	178.0(3)	F(31)-C(31)-C(32)-F(32)	0.8(6)
C(12)-C(13)-C(14)-F(14)	179.4(4)	C(30)-C(31)-C(32)-F(32)	-179.2(4)
BR1-C(13)-C(14)-F(14)	0.8(6)	F(31)-C(31)-C(32)-C(33)	179.7(4)
C(12)-C(13)-C(14)-C(15)	0.2(6)	C(30)-C(31)-C(32)-C(33)	-0.2(7)
BR1-C(13)-C(14)-C(15)	-178.4(3)	F(32)-C(32)-C(33)-C(34)	179.6(4)
F(14)-C(14)-C(15)-F(15)	-0.6(6)	C(31)-C(32)-C(33)-C(34)	0.7(7)
C(13)-C(14)-C(15)-F(15)	178.6(4)	F(32)-C(32)-C(33)-BR3	1.2(6)
F(14)-C(14)-C(15)-C(10)	-179.2(4)	C(31)-C(32)-C(33)-BR3	-177.6(3)
C(13)-C(14)-C(15)-C(10)	0.0(7)	C(32)-C(33)-C(34)-F(34)	-178.1(4)
C(11)-C(10)-C(15)-F(15)	-178.4(4)	BR3-C(33)-C(34)-F(34)	0.3(6)
C(1)-C(10)-C(15)-F(15)	-0.7(6)	C(32)-C(33)-C(34)-C(35)	-0.2(7)
C(11)-C(10)-C(15)-C(14)	0.1(6)	BR3-C(33)-C(34)-C(35)	178.1(3)
C(1)-C(10)-C(15)-C(14)	177.8(4)	F(34)-C(34)-C(35)-F(35)	-0.2(6)
C(30)-C(1)-C(20)-C(25)	-3.4(6)	C(33)-C(34)-C(35)-F(35)	-178.1(4)
C(10)-C(1)-C(20)-C(25)	127.4(5)	F(34)-C(34)-C(35)-C(30)	177.1(4)
C(30)-C(1)-C(20)-C(21)	173.7(4)	C(33)-C(34)-C(35)-C(30)	-0.8(7)
C(10)-C(1)-C(20)-C(21)	-55.5(5)	C(31)-C(30)-C(35)-F(35)	178.5(4)
C(25)-C(20)-C(21)-C(22)	0.3(7)	C(1)-C(30)-C(35)-F(35)	-2.6(6)
C(1)-C(20)-C(21)-C(22)	-177.2(4)	C(31)-C(30)-C(35)-C(34)	1.2(7)
C(25)-C(20)-C(21)-F(21)	178.8(4)	C(1)-C(30)-C(35)-C(34)	-179.8(4)
C(1)-C(20)-C(21)-F(21)	1.3(6)		
F(21)-C(21)-C(22)-F(22)	0.8(7)		
C(20)-C(21)-C(22)-F(22)	179.3(4)		
F(21)-C(21)-C(22)-C(23)	-179.3(4)		
C(20)-C(21)-C(22)-C(23)	-0.8(8)		
F(22)-C(22)-C(23)-C(24)	-179.2(4)		
C(21)-C(22)-C(23)-C(24)	0.9(8)		
F(22)-C(22)-C(23)-BR2	0.5(7)		
C(21)-C(22)-C(23)-BR2	-179.4(4)		
C(22)-C(23)-C(24)-F(24)	-179.3(5)		
BR2-C(23)-C(24)-F(24)	1.0(7)		
C(22)-C(23)-C(24)-C(25)	-0.6(7)		
BR2-C(23)-C(24)-C(25)	179.7(4)		
F(24)-C(24)-C(25)-F(25)	-1.6(7)		

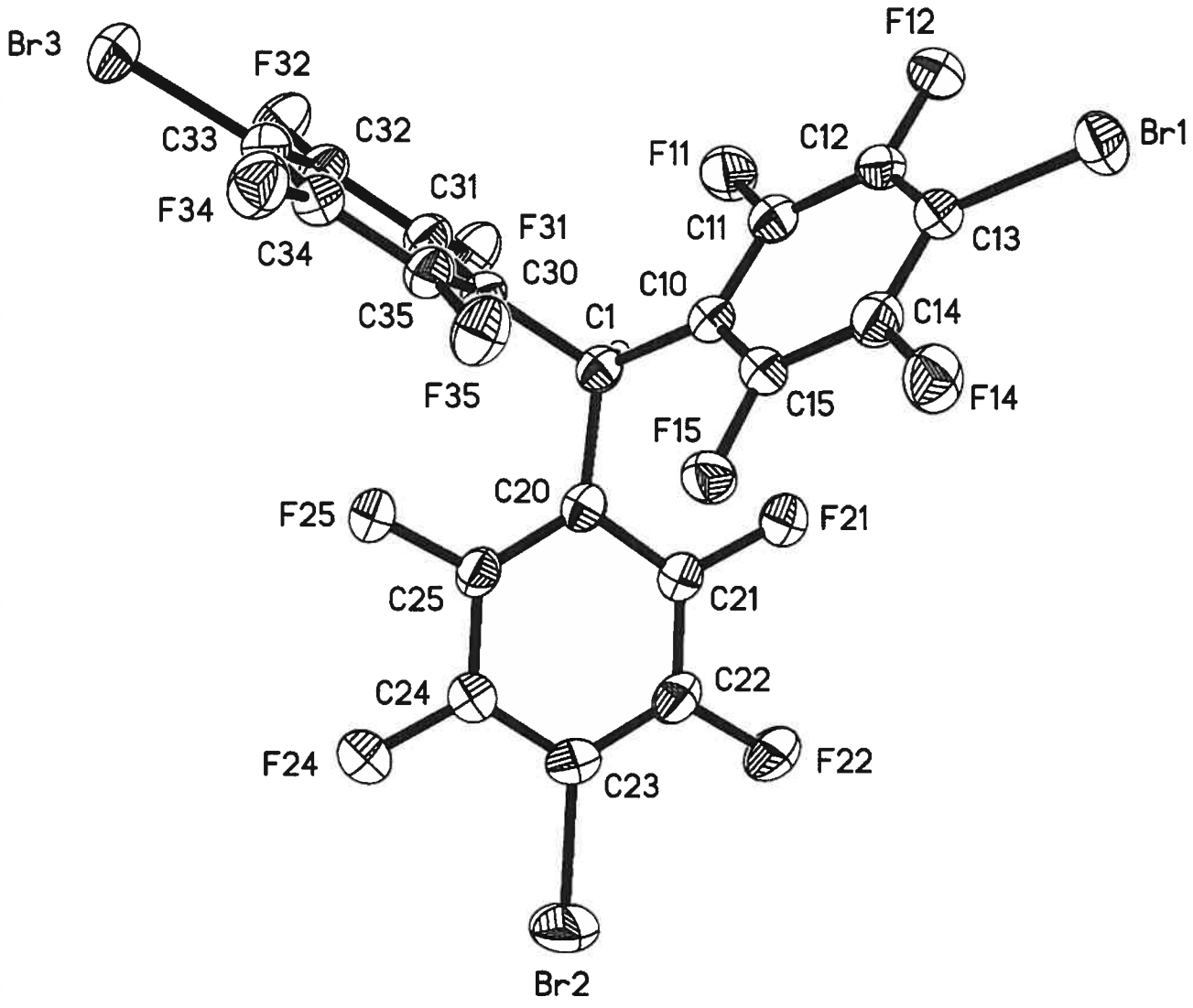

ORTEP view of the C19 H Br3 F12 compound with the numbering scheme adopted. Ellipsoids drawn at 30% probability level. Hydrogen atoms are represented by sphere of arbitrary size.

REFERENCES

SAINT (1999) Release 6.06; Integration Software for Single Crystal Data.
Bruker AXS Inc., Madison, WI 53719-1173.

Sheldrick, G.M. (1996). SADABS, Bruker Area Detector Absorption Corrections.
Bruker AXS Inc., Madison, WI 53719-1173.

Sheldrick, G.M. (1997). SHELXS97, Program for the Solution of Crystal Structures. Univ. of Gottingen, Germany.

Sheldrick, G.M. (1997). SHELXL97, Program for the Refinement of Crystal Structures. Univ. of Gottingen, Germany.

SHELXTL (1997) Release 5.10; The Complete Software Package for Single Crystal Structure Determination. Bruker AXS Inc., Madison, WI 53719-1173.

SMART (1999) Release 5.059; Bruker Molecular Analysis Research Tool.
Bruker AXS Inc., Madison, WI 53719-1173.

Spek, A.L. (2000). PLATON, Molecular Geometry Program, 2000 version.
University of Utrecht, Utrecht, Holland.

XPREP (1997) Release 5.10; X-ray data Preparation and Reciprocal space Exploration Program. Bruker AXS Inc., Madison, WI 53719-11

Annex 2
Electronic Resources

Electronic Resources

1. http://www.cnn.com/2004/TECH/01/07/hln.wired.oleds/index.html

2. http://www.kodak.com/global/en/service/products/ekn026716.jhtml?pq-path=971

3. http://www.sony.com.cn/electronics/walkman2005/ce/white/sony_CE-P.html